DEVELOPMENT OF 3D-PRINTED BIODEGRADABLE COMPOSITE SCAFFOLDS FOR TISSUE ENGINEERING APPLICATIONS

Author: Tiziano Serra

Universitat Politècnica de Catalunya, Barcelona, España

Director: Dr. Melba Navarro

UPC tutor: Dr. Elisabeth Engel

Programa de doctorat en Ciència i Enginyeria de Materials

Departament de Ciència dels Materials i Enginyeria Metal·lúrgica

Universitat Politècnica de Catalunya

Barcelona, Marzo, 2014

Tesi presentada per obtenir el títol de Doctor per la Universitat Politècnica de Catalunya

UNIVERSITAT POLITÈCNICA DE CATALUNYA

ibec Institute for bioengineering of Catalonia

Vol. 1

Abstract

The design of smart biodegradable scaffolds plays a crucial role in the regeneration of tissues and restoration of their functionality. Advances in material science and manufacturing and in the understanding on the effects of bio-chemical and bio-physical signals on cell behavior, are leading to a new generation of 3D scaffolds. Recent developments in additive manufacturing, also known as 3D-printing, open new exciting challenges in tissue/organ regeneration by means of the fabrication of complex and geometrically precise 3D structures. This thesis aimed the development and characterization of 3D scaffolds for tissue regeneration. For this, a nozzle-based rapid prototyping system was used to combine polylactic acid and a bioactive CaP glass (coded G5) to fabricate 3-D biodegradable scaffolds. Firstly, optimization of the printing conditions represents a key challenge for achieving high quality 3D-printed structures. Thus, we stress the importance of studying the outcome of the plasticizing effect of PEG on PLA-based blends used for the fabrication of 3D-printed scaffolds. Results indicated that the presence of PEG not only improves PLA processing but also leads to relevant surface, geometrical and structural changes including modulation of the degradation rate of PLA-based 3D printed scaffolds. Secondly, the obtained scaffolds were fully characterized from the physic-chemical point of view. Morphological and structural examinations showed that 3D scaffolds had completely interconnected porosity, uniform distribution of the glass particles, and a controlled and repetitive architecture. In addition, incorporation of G5 particles increased both roughness and hydrophilicity of the scaffolds. Compressive modulus was dependent on the scaffold geometry and the presence of glass. Cell study revealed that G5 glass improved mesenchymal stem cell adhesion after 4 h. Additional biological characterization in terms of the inflammatory response were also carried out. Novel studies have pointed towards a decisive role of inflammation in triggering tissue repair and regeneration, while at the same time it is accepted that an exacerbated inflammatory response may lead to rejection of an implant. Thus, understanding and having the capacity to regulate the inflammatory response elicited by 3D scaffolds aimed for tissue regeneration is crucial. In this context, cytokine secretion and cell morphology of human monocytes/macrophages in contact with biodegradable 3D-printed scaffolds (PLA, PLA/G5 and chitosan ones) with different surface properties, architecture and controlled pore geometry was reported. Results revealed that even though the material itself induced the biggest differences, scaffold geometry also affected on the secretion of cytokines. These findings strengthen the appropriateness of these 3D platforms to study modulation of macrophage responses by specific parameters (chemistry, topography, scaffold architecture). Finally, novel scaffolds composed by two phases (PLA and PLA/G5), for use in guided bone regeneration (GBR) were evaluated. Structural, morphological changes were observed during the in vitro degradation of both PLA and PLA/G5 structures. Although mechanical properties decreased, PLA/G5 scaffolds still showed higher compressive modulus than PLA ones, confirming the reinforcing effect of glass particles after immersion time. In vivo implantation was carried out subcutaneously in mice up to 30 days. Results showed that PLA scaffolds induced mononuclear cell without activating any relevant angiogenic process, while PLA/G5 induced higher presence of

multinucleated giant cells and consequently stimulated the vascularization process and further tissue regeneration. The technique/materials combination used in this PhD thesis led to the fabrication of promising fully degradable, mechanically stable, bioactive and biocompatible composite scaffolds with well-defined architectures valuable for TE applications.

Ai miei genitori Cosimo e Paola

Kublai Khan: "Why do you speak to me of the stones? It is only the arch that matters to me."
Marco Polo: "Without stones there is no arch."

Italo Calvino, Invisible Cities

Aknowledgements

"Farsi le ossa" is an Italian idiomatic expression that literally means “to build your bones”, but its real meaning is “to gain experience” in a specific field. By coincidence, I have been involved in the study of bone tissue regeneration during my PhD thesis. In a serendipity way, it gave me a deeper explanation of that expression. These years have been full of amazing and enjoyable experiences and I would like to express my sincere gratitude to those who have contributed to this thesis.

First of all, I would like to thank my PhD supervisor Dr. Melba Navarro for her support, patience, enthusiasm, and professionalism. Her guidance helped me during all these years and highly shaped and improved the present work. It has been a great pleasure to work and learn with her. I could not have imagined having a better mentor for my PhD study.

I would like to thank Prof. Planell and Dr. Elisabeth Engel for accepting me in their group at IBEC, and for their competences and suggestions. They have continuosly stimulated my curiosity and passion for research. Thanks for enlarging my vision of doing research and cultivating my scientific growth.

I would like to thank the institutions that welcomed me from the beginning and where I worked during my thesis: the Institute for Bioengineering of Catalonia (IBEC) and the BIBITE group at the Technical University of Catalonia (UPC). In particular, I would like to express my sincerest gratitude to Prof .Maria Pau Ginebra for her kindness, support and professionalism during these years.

I would like to thank the European Commission (ANGIOSCAFF 214402, FP7-NMP-2007-2.3-1), the Acción/Acções Integrada Spain-Portugal E22/11, and the Spanish Ministry of Economy and Competitiveness through the grant Personal Técnico de Apoyo (MINECO-PTA, 2011-11-14), for financing the research.

My most earnest gratitude to Prof. Mario Barbosa, Prof. Pedro Granja and all the members of the INEB (Instituto de Engenharia Biomédica) and IPATIMUP (Instituto de Patologia e Imunologia Molecular da Universidade do Porto) in Porto who welcomed me to their Research Centres and their wonderful city. In particular, I would like to thank Dr. Catarina Almeida, my supervisor during my stay at INEB. I am very grateful for her willingness in helping me.

I am indebted and thankful to Prof. Matteo Santin and to his collaborators, Steve, Valeria, and Gemi, for their encouragement, guidance and support during my stay at the School of Pharmacy & Biomolecular Sciences at the University of Brighton.

My sincere thanks also go to Dr. Shahram Ghanaati from the Repair-Lab at the Institute of Pathology, Johannes Gutenberg University (Mainz), for his significant contribution during the *in vivo* study.

I would like to thank my previous supervisor at the University of Salento in Lecce, Prof. Alessandro Sannino, for transmitting me his enthusiasm and passion for biomaterials and tissue engineering. Since I worked with him, I decided to start my way in this extraordinary field.

My appreciation to all the former and current members of the Biomaterials for Regenerative Therapies group at IBEC, Miguel, Oscar, Soledad, Johan, Aitor A., Xavi, Nadege, Aitor S., Riccardo, Arlyng, Zaida, Belén, Marta, Juan, Laura, Irene, Claudia, Joan, Pep Pau, it has been a real pleasure to share these years with you. I wish you all the best!

Special thanks also to all the members of BIBITE group at UPC for sharing enjoyable moments with me, in conferences, discussions, parties and travels.

I am grateful to the administration department for their efficiency, and help, and to all the research staff at IBEC, particularly the members of the Biomechanics and Mechanobiology group.

I am particularly grateful to all my friends: Gianni, Stefano, Marco, and Agnese from Italy; Hugo, Emilio, Luca and Solana from Porto; Antonio and Lorna from Brighton.

My warmest thanks to my friends Andrea, Asma, Andy, Riccardo, Aurelio, Nunzia, Alicia, Marta, Emiliano, Annalisa, Simon, Lucilla, Simone and Entela from Barcelona, they were an important part of my daily life, always present and helpful.

Finally, I owe my deepest gratitude to my family for giving me patience, passion and perseverance to achieve this goal. Thanks to all of them for their continuous support and encouragement, and in particular to my little niece Giulia.

Barcelona, March 2014 *Tiziano Serra*

Table of Contents

List of Figures

List of Tables

Glossary

3D – three dimensional

2D – two dimensional

PLA – polylactic acid

G5 – calcium phosphate glass

ECM – extracellular matrix

CAD/CAM - computer-aided design and manufacturing

CaP - Calcium Phosphate

GMP - good manufacturing practice

HSCs - hematopoietic stem cells

PPF – polypropylenefumarate

PHA – polyhydroxyalkanoates

PCL - polycaprolactone

PGA - polyglycolic acid

FDA - Food and Drug Administration

PEG - polyethylene glycol

PEO - polyethylene oxide

POE - polyoxyethylene

Tg – glass transition temperature

HCAp - hydroxycarbonate apatite

SBF - simulated body fluid

TCP - tricalcium phosphate

TIPS - thermally induced phase separation

AM - additive manufacturing

μCT - micro-computed tomography

RP - rapid prototyping

SFF - solid free form fabrication

SLA - Stereolithography

SLS - Selective Laser Sintering

FDM - Fused deposition modeling

SEM – scanning electron microscopy

FBGC - foreign body giant cells

MGCs - multinucleated giant cells

NK - natural killer cells

IL - interleukins

IFN - interferons

M1, M2 – macrophages polarization

S_a - surface roughness

S_{sk} - surface skewness

S_{sk} - surface kurtosis

AFM - atomic force microscopy

E - Young's modulus

QNM - Quantitative Mechanical Property Mapping at the Nanoscale

DSC – differential scanning calorimetry

Xc – fraction of crystallinity

ΔHm - heat of fusion

ΔHc - heat of crystallization

Xp - fraction of polymer

SD - standard deviation

ANOVA - one-way analysis of variance

σ40% - compressive strength at 40% deformation

ORTH - orthogonal layer configuration

DISPL – displaced double layer configuration

PBS - phosphate buffered saline

DMEM - Dulbecco's modified Eagle medium

MSCs - mesenchymal stem/stromal cells

CaRS - calcium sensing receptor

Ch - chitosan

TH – T helper cells

TNF - tumor necrosis factor

TGF - tumor growth factor

TCPS - tissue culture polystyrene

ELISA - enzyme-linked immunosorbent assay

GBR - Guided Bone Regeneration

GTR - Guided Tissue Regeneration

PTFE – polytetrafluoroethylene

VEGF – vascular endothelial growth factor

ARS - Alizarin Red S assay

Mw - molecular weight

GPC - gel permeation chromatography

H&E - haematoxylin and eosin staining

TRAP - Tartrate-resistant acid phosphatase

CD31 - cluster of differentiation 31

CBQCA - 3-(4-carboxybenzoyl) quinoline-2-carboxaldehyde

Micro BCA - Micro bicinchoninic acid

NHS - N-Hydroxysuccinimide

EDC - carbodiimide

LDH – lactate dehydrogenase

WST - Water soluble Tetrazolium

Aims and outline of the thesis

In previous years, different biodegradable materials based on PLA and calcium phosphate glass for bone tissue engineering applications have been developed within the biomaterials research group (Navarro 2005 and Charles-Harris 2007). In particular 3D porous composite scaffolds have been elaborated. Two scaffold processing methods, Solvent Casting and Thermally Induced Phase Separation were optimized and characterized. The surface degradation properties, and cellular behavior of the produced scaffolds were studied.

However, the fabrication of scaffolds using these methods lacks consistency and reproducibility. For these reasons it is interesting to study 3D-printing, a new technique able to design scaffold architecture that may not only improve mechanical performance but also cell growth. Scaffolds produced by 3D-printing technique have a high degree of interconnectivity and the porosity can be controlled to a great extent by optimizing the processing parameters and geometry. 3D- printing offers a unique opportunity to study the influence of the micro-architecture of the scaffold upon cell proliferation and ECM generation.

Furthermore, although PLA has been widely used for scaffolds fabrication, only few studies of nozzle-printed PLA have been reported. Up to now, setting the right materials composition and process parameters has represented a challenging task. **Therefore, in this thesis we propose the use of a low temperature 3D-printing process that guarantees scaffolds development without any thermal degradation of the PLA. In addition, this work aims at dissecting the right conditions such as plasticizer concentrations, together with the suitable polymer/solvent concentration and the appropriate set of printing parameters in order to fabricate PLA-based 3D direct-printing scaffolds with superior geometrical definition and mechanical properties. Thus, the general aim of this thesis is the development of three-dimensional PLA-based composite biodegradable scaffolds through an additive manufacturing technique and their physico-chemical and biological characterization.**

The main specific objectives are:

- Study of the effect of the incorporation of PEG in the PLA/CaP glass composite system and optimization of the protocols and parameters of the CAD/CAM system to produce well defined 3D structures.
- The design, fabrication and characterization of the 3D porous scaffolds fabricated by 3D-printing using a PLA/PEG blend and CaP glass particles.
- Evaluation of the *in vitro* behavior of human monocytes/macrophages on the developed scaffolds.
- Evaluation of the *in vitro* degradation of the developed scaffolds.
- Evaluation of the *in vivo* response of the developed scaffolds for maxillofacial applications.

In order to reach these objectives the thesis has been divided in the following chapters:

In **Chapter 1**, a review of the state of the art relevant to this thesis is presented.

In **Chapter 2**, the plasticizing effect of PEG on PLA-based blends used for the fabrication of 3D-direct-printed scaffolds for tissue engineering applications is studied. A comprehensive characterization (comprising structural, surface, mechanical and *in vitro* degradation studies) of the polymer blends and composite is done. The selection of a suitable PLA/PEG blend is assessed.

In **Chapter 3**, PLA-based composite scaffolds are developed via 3D-printing and characterized in terms of their structural, thermal, mechanical properties. Moreover an initial biological evaluation (adhesion, proliferation) of the developed scaffolds is presented.

In **Chapter 4**, the impact of four different 3-D printed PLA- and chitosan-based platforms (tuning on demand specific parameters: chemistry, topography, scaffold architecture) on human monocyte/macrophage responses and cytokine profiles is studied. A new protocol for the elaboration of 3D chitosan scaffolds is developed.

Chapter 5 presents an *in vivo* study of biphasic 3D-printed scaffolds for guided bone regeneration. In addition, the *in vitro* degradation behavior of the studied 3D structures has been investigated and related to the *in vivo* findings.

Chapter 6 presents the conclusions obtained out of this thesis.

In addition, three appendixes are included:

In **Appendix A**, technical specification of the additive manufacturing technique used in this thesis is described.

In **Appendix B**, the optimization of the parameters for the printing process via calibration curves is studied.

Appendix C is a commentary that stresses on the importance of tuning scaffolds parameters (materials, geometry, and surface properties) to develop versatile PLA-based scaffolds as a potential tool in regenerative medicine.

Chapter 1 - State of the Art

1.1. Introduction

The goal of this PhD thesis is the development and characterization of three-dimensional scaffolds for their application in tissue engineering. The thesis has been structured in various chapters devoted to: 1) optimization of the materials, 2) development and fabrication of three-dimensional scaffolds, 3) *in vitro* evaluation of the inflammatory response to the developed scaffolds, 4) *in vitro* degradation study of the developed scaffolds, and 5) *in vivo* tissue regeneration of biphasic scaffolds. This first introductory chapter has been divided in different sections to guide the reader through the main aspects and the state of the art in which the present work is involved. The first part describes the main tissue engineering strategies in the current scenario. In the following part, a comprehensive picture of the materials used in Tissue Engineering with focus on poly-lactic acid polymer and a calcium phosphate soluble glass has been done. In the same way a state of the art of scaffolds fabrication techniques have been shown, going from the traditional processes till additive manufacturing with particular focus on **3D-printing**. The following section introduces the main biological concepts with special attention to scaffold-based tissue engineering, going in more detail in the understanding of bone tissue engineering. Moreover, a brief presentation of the inflammatory response and foreign body reaction to biomaterials has been included.

1.2. Biomaterials, tissue engineering and regenerative medicine

Nowadays, there is a large demand of new available tissues and organs to replace the damaged ones after traumatic injuries or diseases. Lack of organs and tissues for transplantation and the necessity of immunosuppressive therapies represent onerous problems in human health care. In addition, the scientific community has shown a great interest for the concept of “healthy ageing” to enhance quality of life to the growing aged population in the world. Different surgical approaches have been adopted to address these problems and most of them are based on replacing the damaged tissue with xenografts, allografts or autografts.

Xenografts are organs or tissues of an organism of one species implanted in another individual of a different specie or family. A typical example is the transplantation of pig heart valve in human bodies [1]. Such strategy has shown quite high availability, but also strong risks of infections and immunological responses that could lead to the rejection of the graft from human body.

Allografts are grafts coming from human donors, usually after death, transplanted in other individuals having different genotype. The lack of human donors and the risk of immune response, as mentioned for the previous case, are strong limitations for this kind of transplants [2].

Autografts consist in tissues transplantation from one part to another of the same individuals, mostly used for tissue reconstruction e.g. skin or cartilage. On the one hand, these grafts show a faster healing without

triggering any immune response on the patients. Autografts can avoid the use of drugs to suppress the rejection and "foreign body reaction". On the other hand, this approach requires a double surgical treatment: firstly the tissue should be explanted and harvested with autologous cells and secondly such graft will be implanted in the damaged site. In addition, a large period after the surgery is necessary for the healing of the explanted zone.

In order to cover the large demand of new tissues and solve the problems and limitations related to the previous strategies, the fundamental concept of Tissue Engineering is to develop new engineered tissue with suitable biochemical and physicochemical cues in order to replace normal biological functionality into patients. In the last decades, Tissue Engineering has emerged as a multidisciplinary area involving fields such as engineering, biology and medical sciences and is expected to achieve a breakthrough in regenerative medicine.

In 1993 Langer and Vacanti gave the first definition of Tissue engineering: "an interdisciplinary field that applies the principles of engineering and life sciences towards the development of biological substitutes that restore, maintain, or improve tissue or organ functions" [3]. Since then, many other similar definitions have been given to define this emerging field. However, several approaches can be identified and summarized in three principal strategies: **cell therapy**, **cell instructive materials**, and **cell within matrix**.

- Cell therapy. This approach consists in treating damaged tissues by injecting cells previously isolated from the same patient or a compatible donor (Fig. 1.1a). Many processes via cells' transplantation e.g. stem cells, have been adopted and approved for human use in different operations. However, the main limitation of this method is the lack of fixation of cells in the injured area, indeed they move into the body and have been found also in many organs such as the liver, spleen and lungs [4].

- Cell within matrix. Also known as cell-scaffold engineered constructs, represent a method in which 3D matrices are associated with biochemical factors and cells previously explanted and expanded *in vitro* from the patient (Fig. 1.1b). It drives to the generation of an *in vitro* engineered tissue enabling continuity and faster cell fixation and attachment, once the implantation is done. The combination of cells with matrix currently represents one of the most used approaches in tissue engineering [5]. However, in spite of the great efforts made by researchers, currently there are only few cell-based products available in the market, mostly for the replacement of skin and cartilage. One explanation is the difficulty to overcome the gap between bench-scale research and clinical-scale, providing at the same time good manufacturing practice (GMP) qualifications. Moreover, the culturing process is quite complicated making the use of cell-constructs as a regular surgical procedure and obtaining a clinical license an enormous challenge.
- Cell-instructive materials. The development of the new generation of smart biomaterials, also called "Cell-Instructive Materials" containing chemical and physical cues able to restore and enhance the

function of healthy tissues is strongly required (Fig. 1.1c). This method represents a new option to the regeneration of tissues and organs. However, the development of a cells' free scaffold is one of the main challenges in the field. Once implanted in the injured site of the patient, such scaffolds should be able to direct and guide cell recruitment, homing, proliferation, differentiation of cells into the inner part of the structure [6]. A considerable challenge in the area of regenerative medicine is angiogenesis, the formation of new blood vessels that reach the inner part of new engineered complex constructs allowing blood delivering nutrients and oxygen to the cells [7,8]. In this context, tuning biochemical and physical cues of smart 3D scaffolds may trigger the angiogenic response. In addition, it is expected that such "smart devices" could be introduced easier in the market since they present fewer limitations than the cell-based constructs previously described.

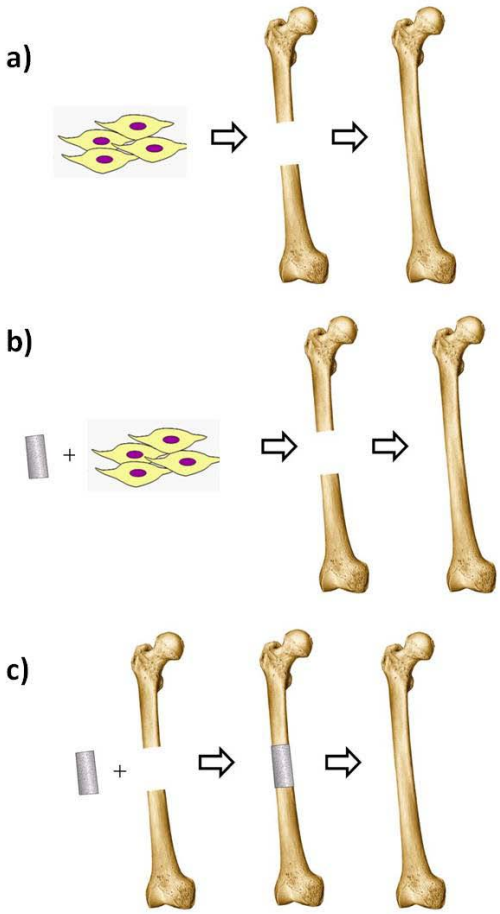

Figure 1. 1 Schematic representation of the three mainstrategies in tissue engineering. a) cell therapy, b) cell with matrix, c) cell instructive materials

Finally, the possibility to create three dimensional engineered structures able to simulate the in vivo scenario, with respect to the traditional 2D-approaches (tissue culture plate- based), open new possibilities in the application of Tissue engineering concepts. Indeed, during the last decade, scaffold-based investigation is starting to be used not only to regenerate damaged tissues but also for the *in vitro* examination of inflammatory reaction, drug screening, and development of disease models among others.

Synergistically coupling the state of the art in scaffolds fabrication techniques [9] with the advances in the field of developmental biology [10] lead to new strategies in tissue engineering such as the attainment of faster and cheaper high-throughput analysis systems and even the reduction of animal testing [10].

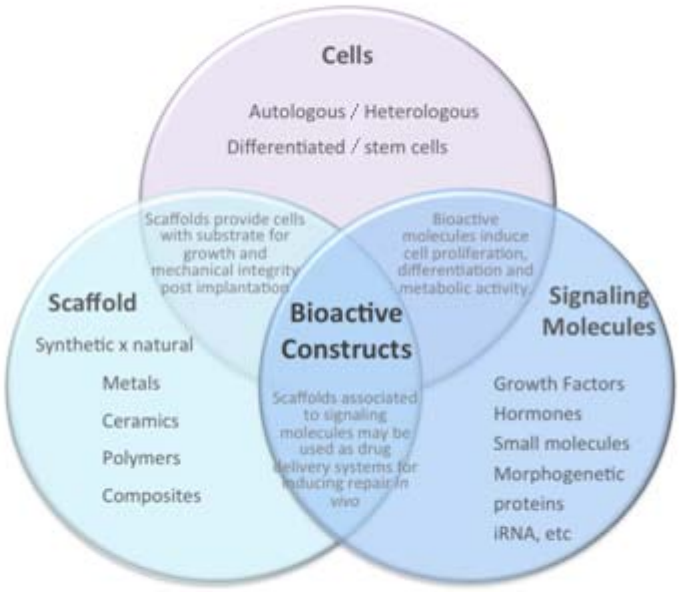

Figure 1. 2.Different Tissue engineering approaches. Adapted from [9].

As shown in Figure 1.2, mostly there are three components that opportunely combined can guide the process of regeneration of a damaged tissue: scaffolds, stem cells, biochemical signals. Undoubtedly, **scaffolds** development represents one of the main challenges in regenerative medicine. Such structures should exhibit adequate physicochemical properties, pore size, interconnectivity, and mechanical properties in order to trigger a cascade of cellular events leading to the regeneration of damaged tissue. **Stem cells** are the most encouraging source in the regeneration of aged and damaged tissues for their capacity to differentiate in specialized cell types [11]. In order to improve the effectiveness of cells, the scaffold should mimic as much as possible the natural environment of the extracellular matrix (ECM).
In this direction, a number of strategies have been used to modify surface properties from a physical and chemical point of view. Recapitulation of the biological complexity could be obtained by improving the **bioactivity** of the 3D scaffolds. Many studies have been done by introducing **biomolecules**, such as grow factors, hormones, and small molecules in the scaffold [6,10]. Other approach, mostly adopted for bone tissue engineering, consists in the inclusion of inorganic components (e.g. calcium phosphate glass particles among others) [12] able to improve bioactivity and to stimulate specific responses at molecular level [7].

Definition of biomaterial

During the last five decades, the definition of biomaterials has radically changed as much as the evolution of the field has been continuously evolving. Indeed, the rising of the biomaterials world and the related entry in the market has improved the quality of life for a growing number of people. Nowadays, biomaterials have been used in a wide range of applications such as hip prosthesis, contact lenses, heart valve, arterial prosthesis, dental implant, and skin. Along time, the development of fabrication technologies and knowledge in molecular biology is giving new concepts and adding more complexity to bypass undesirable effects of biomaterials implantation. Basically, the biomaterials have been defined and summarized in three generations:

- The first one consisting in **bioinert materials** that minimize the interaction with the biological environment in which they are implanted. This strategy leads to a lack of recognition of the material by the body and leads the formation of a surrounding fibrous capsule all around the prosthesis.

- The second one considering **biodegradable** and **bioactive materials.** A fundamental property of these materials is the capacity to progressively degrade in situ while the new tissue regenerates. Bioactivity consists in stimulating the interaction between the biological environment and the material itself in order to modify or activate specific responses from surrounding tissue. An example of bioactive materials in bone tissue engineering are bioactive glasses, ceramics and composite materials, ensuring the formation of hydroxyapatite nano-crystals on the surface and leading to higher fixation and replacement of the damaged bone.

- The third-generation of biomaterials was described by Hench and Polak: "biomaterials are meant to be new materials that are able to **stimulate specific cellular responses** at the molecular level" [13,14].

Certainly the previous classification is not strictly connected with a chronological evolution of the biomaterials world being each generation contained in the next one. Furthermore, the strong effort done in the last 10 years from a molecular and biological point of view push to refine the definition of third generation:

''A biomaterial is a substance that has been engineered to take a form which, alone or as part of a complex system, is used to direct, by control of interactions with components of living systems, the course of any therapeutic or diagnostic procedure, in human or veterinary medicine'' [15].

In other words, the new challenge in the development of biomaterials is to achieve the degree of complexity of the natural environment by mimicking the extracellular matrix (ECM). Designing scaffold with spatial and temporal distribution of mechanical and biochemical signals by using new micro and nanofabrication systems will allow the generation of dynamic environments able to tune cells response till

the remodeling of the new tissue [6].

Lastly, the scientific community is paying great attention to find new strategies for the translation of smart biomaterials concepts from the "bench to the bedside". It seems that the time is coming to transfer to the clinic the innovation and the reached maturity achieved in the biomedical labs [16,17].

1.3. Bone and Bone Tissue Engineering

Bone tissue is one of the most important connective tissues in the human body. Bone is basically formed by an organic phase and inorganic mineral phase. The organic material mainly constitutes the matrix of the tissue and it is mostly composed by collagen fibers and other noncollagenous proteins. Bone matrix occupies almost the totality of the bone tissue (90%) and collagen is the most abundant protein in the human body. The collagen molecule, also called "tropocollagen", is part of larger molecules called fibrils. Tropocollagen is approximately 300 nm long and 1.5 nm in diameter. It is formed by two left-handed and one right-handed helices arrangement of polypeptides chains in a way that stabilize the high number of hydrogen bonds. Polypeptides chains are composed by arrangement of specific amino acids, such as Glycine, Proline, Hydroxyproline and Arginine. The noncollagenous proteins indicated in Table 1.1, consist mostly in: osteonectin, osteopontin, osteocalcin, hyaluronan, thrombospondin, proteoglycans, growth factors, cytokines, phospholipids, and phosphoproteins.

Noncollagenous proteins	**Function**
Osteonectin	influence deposition of hydroxyapatite and cell-cycle antiadhesive protein; binds to growth factors
Osteocalcin	regulate activity of osteoclasts and precursors; tuning bone formation and resorption, balance mineral maturation
Osteopontin	cells binding, inhibition of mineralisation and nitric oxide synthase; regulation of cells proliferation, tissue repair, and mineralization
Alkaline Phosphatase	a phosphotransferase; potential Ca^{2+} carrier; hydrolyses inhibitors of mineral deposition such as pyrophosphates
Hyaluronan	unsulfated glycosaminoglycan, linked to osteoclast-mediated bone resorption
Thrombospondin	cell attachment, binds to heparin, platelets, type I and C collagen, thrombin, fibrogen, laminin, plasminogen, and plasminogen activator inhibitor
Fibronectin	binds to cells, fibrin, heparin, gelatine, collagen. Organises the intracellular cytoskeleton by means of receptors. Helps create a cross-linked network in the ECM by binding to other ECM components.
Vitronectin	cell attachment protein due to binding sites for integrins, binds to collagen and heparin, plasminogin, and plasminogen activator inhibitor
Bone sialoprotein	binds to cells, binds Ca^{2+}; may initiate mineralization

Table 1. 1. Noncollageneous proteins found in bone and their functions. **Adapted from [18].**

The other major component of bone is the mineral phase corresponding to the inorganic hydroxyapatite. It is a calcium orthophosphate containing water with the following chemical composition: $Ca_{10}(PO_4)_6(OH)_2$. The inclusion of hydroxyapatite crystals into the collagenous matrix gives the hardness and rigidity that is fundamentally important for bone function. However, bone function is not only restricted to support the body and organs that would collapse onto each other but also other important relevancies. Above all, bone is a dynamic and highly vascularized tissue acting in a continuous remodeling during the life of every individual [19].

Indeed, bones also act for: a) **protection** of the organs (ribs protect heart and lungs, skull protects the brain and vertebrae for spinal cord); b) **movement** (muscles, tendons and ligaments are connected to bones allowing allow for bending and movements in different directions); c) **mineral reserve of ions** (in particular Ca and P) which are crucial electrolytes in the blood and take part to every chemical reaction of the cells; d) **hematopoiesis**, that is the process of blood cells (erythrocytes, leukocytes, thrombocytes) production starting from hematopoietic stem cells (HSCs) contained in the marrow of long bones.

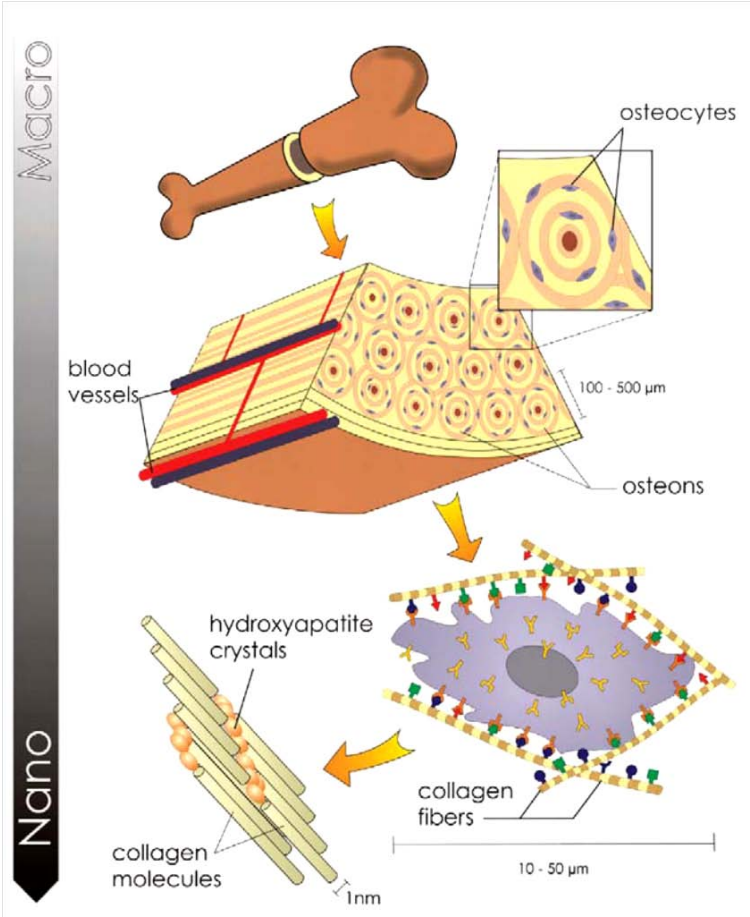

Figure 1. 3. Hierarchical bone structure [19].

As every biological tissue, bone (illustrated in Figure 1.3), has a complex hierarchical structure ranging from macro to nanoscale. As previously explained, at a nanoscopic level the collagen fibrils are

intimately connected with hydroxyapatite crystal forming such bright arrangement from a chemical and mechanical point of view. Bone extracellular matrix gives topographical and chemical signals to the cells in an intricate ultra porous geometry.

From a macroscopically point of view, bone tissue is arranged in mainly two conformations: cortical bone and spongious or trabecular bone [20]. Cortical bone represents the 80% of the bone mass in the body; it is very dense and contains only few microscopic channels. The remaining 20% of the mass is formed by trabecular bone consisting in an ultra-porous and interconnected structure with honeycombed or spongy appearance into the inner part of bone. The orientation and density of the trabeculae are strongly influenced toward stress directions.

1.3.1. Mechanical properties of bone

The mechanical properties of trabecular bone are strongly dependent on age [21]. Moreover, mechanical tests could be conducted on entire anatomic bone shape or by isolation of particular components of the structure. A number of techniques have been used to measure different mechanical properties such as uniaxial compressive and tensile assays, three and four-point bending, ultrasound atomic force microscopy (AFM) and nanoindentation techniques. In addition, different age, species, dry/wet conditions have been analyzed. Nevertheless, as shown in Table 1.2, a wide range of values is obtained when testing the mechanical properties. The elevated complexity of the bone microstructure and variation of data do not allow setting accurate mathematical models for the understanding of the properties.

Property	**Cortical bone**	**Trabecular bone**
Compressive strength (MPa)	100–230	2–12
Flexural, tensile strength (MPa)	50–150	10–20
Strain to failure (%)	1–3	5–7
Fracture toughness ($MPam^{1/2}$)	2–12	---
Young's modulus (GPa)	7–30	0.05–0.5

Table 1. 2. Mechanical properties of bone. **Adapted from [22].**

1.3.2. Bone cells

From a biological point of view, bone has a high regenerative capacity and it is able to heal without the help of relevant external intervention. This self-repairing and remodeling behavior is due to the presence of three different kinds of cells: osteoblasts, osteocytes and osteoclasts (Figure 1.4).

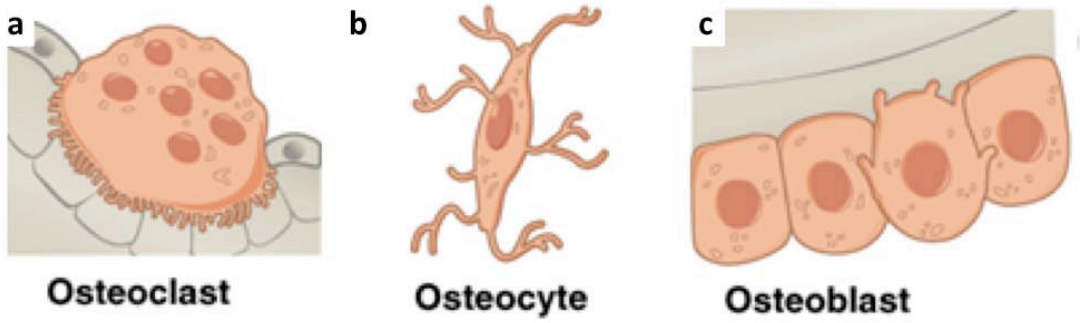

Figure 1. 4. Specific cells of bone tissue: (a) osteoclasts, (b) osteocytes, and (c) osteoblasts. Adapted from [23].

Osteoblasts

Osteoblasts are the cells responsible of the formation of bone tissue. They are mononuclear cells able to produce new bone matrix by secretion of collagen type I, osteocalcin sialoprotein, osteonectin, osteopontin, fibronectin, vitronectin, and other proteins of the bone extracellular matrix. Osteoblasts are polarized cells, with the nucleus at a boundary, and are deposited along the interface adjacent to bone formation such as the periosteum (external surface) and bone marrow (internal surface). They present a structurally complex apparatus of organelles (ample endoplasmic reticulum, a great number of ribosomes, important Golgi apparatus and mitochondria), characteristic of cells activity involved in protein synthesis. Moreover, they are able to influence the mineralization of the tissue by secretion of alkaline phosphatase enzyme. High values of alkaline phosphatase are expressed during the differentiation of osteoblasts.

Osteocytes

Osteocytes are modified osteoblasts that once surrounded by osteoid or demineralized bone matrix, reach their maturity. Osteocites represent the primary cells of mature bone and the most common among bone cells. They are entrapped in little pores into the bone matrix and show a stellate shape with a reduced endoplasmic reticulum and mitochondria and a single nucleum. Such morphology is particularly apt to fulfill the function of checking and maintaining mineral concentration in the matrix through thin channels within the bone matrix.

Osteoclasts

Osteoclasts are large multinucleated cells, mostly derived from monocytes/macrophage differentiation. They are specialized in bone resorption. They are located at the surface of bone and at sites of old, injured, or unneeded bone. In healthy bones the right equilibrium between the actions of osteoclasts (bone resorption) and osteoblasts (bone deposition) should exist. This constant process is responsible of bone growth and remodeling.

1.3.3. Bone tissue engineering

Bone tissue engineering represents one of the most important branches of regenerative medicine. It is particularly involved in the increasing demand of new therapies for significant clinical challenges such as osteoarthritis, cranial maxillofacial, dental, osteoporosis and bone cancer. Materials for bone regeneration have shown a great potential in clinical applications even with the launch of new strategies of patient-specific solution to the treatment of damaged tissue.

First and foremost, the materials suitable for bone tissue engineering should exhibit three essential conditions:

- osteoinduction: capacity of recruitment progenitor cells and the stimulation to differentiate in osteoblastic lineage;
- osteoconduction: aptitude to encourage bone growth and endorse the ingrowth of surrounding tissue
- osseointegration: potential to integrate both structurally and functionally the implanted material into the surrounding bone.

1.4. Materials for biomedical applications

A great number of materials have been used in the field of tissue engineering in order to fabricate three-dimensional scaffolds. As previously mentioned, it is well known that bone tissue is a composite material principally formed by an organic phase, consisting of a biological polymer (collagen), and an inorganic phase composed by a biological ceramic (natural apatite). Taking that into account, it is easy to explain why **polymers, ceramic** and their **composites** have been widely used to fabricate scaffolds for bone tissue engineering [2-4].

1.4.1. Biodegradable polymers

There are two kinds of biodegradable polymers:

- **Naturally derived polymers** include polysaccharides (chitosan, chondroitin sulfate, starch, alginate, hyaluronic acid, cellulose) or proteins (collagen, soy, fibrin gels, silk) [24-28].
- **Synthetic polymers** are the largest family of biodegradable polymers. They show commonly predictable and reproducible physical and mechanical properties (i.e. elastic modulus and degradation rate) as result of controlled conditions during the synthesis. An important advantage offered by this class of polymers is a high control of impurities with respect to the natural polymers. Thus, it decreases any possible risks of toxicity or immunogenicity.

A brief summary of biodegradable polymers is shown in Figure 1.5, while a list of the main advantages of different biodegradable polymer families is indicated in Table 1.3.

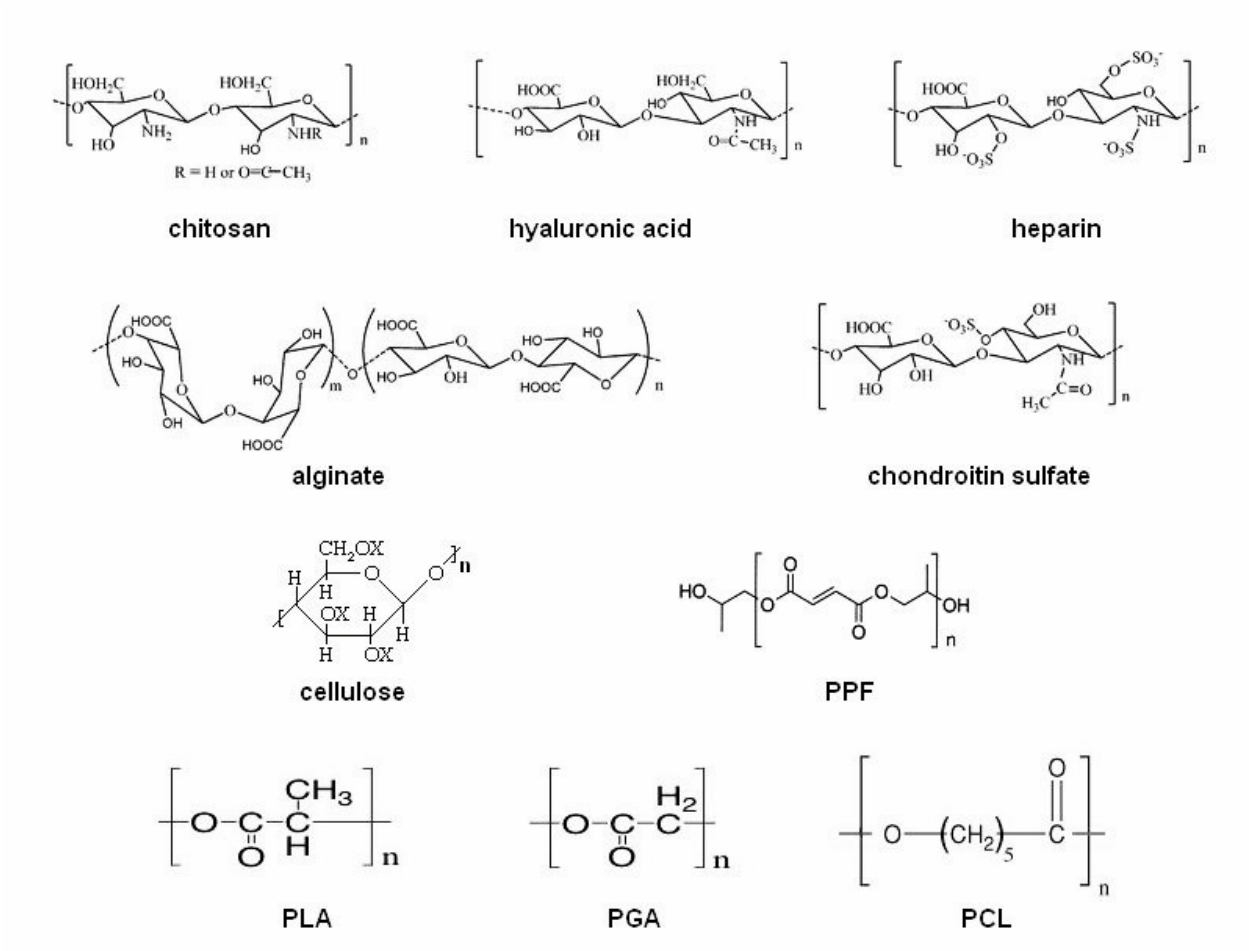

Figure 1. 5. Biodegradable polymers

Polyesters are the most common synthetic polymers for Tissue Engineering applications. They are basically divided in **unsaturated** and **saturated** depending on the final chemical structure.

Unsaturated polyesters

Among the unsaturated polyesters, polypropylenefumarate (PPF) and polyhydroxyalkanoates (PHA) are the most famous. The main advantage in using these polymers is the biocompatibility of their degradation products. The body can easily remove fumaric acid and propylene glycol upon hydrolysis. The limitation in using PPF consists in high viscosity at room temperature that makes it difficult to handle. PHA is produced by microorganisms under a particular reaction and is also degradable by hydrolysis [29]. PHA exhibits degradation by **surface erosion** mostly at the interface between polymer and water. This class of surface-eroding polymers has been intensively investigated for the development of drug-delivery carriers.

Saturated aliphatic polyesters

This class of polyesters is very well known for regenerative medicine applications and has been mostly used for the development of 3D scaffolds. In this group of saturated poly-α-hydroxy esters are included polycaprolactone (PCL), polylactic acid (PLA) and polyglycolic acid (PGA), as well as many copolymers such as polylactic-coglycolide (PLGA) [30-33]. These polymers are among the few synthetic polymers approved by the US Food and Drug Administration (FDA) for several medical devices for human clinical applications. However, these polymers withstand a **bulk erosion** process by absorption of water followed by ester bonds hydrolysis. In some case, a fast acidification of the surrounding environment can exacerbate the inflammatory response [34,35]. The choice of composite materials, mainly Calcium Phosphate based (CaP), has been largely used to solve this problem. In general, the degradation rate decrease with this order: PGA > PDLLA > PLLA > PCL [30]. Combining different polymers by a co-polymerization synthesis can also be tuned molecular weight (Mw), glass transition temperature (Tg), crystallinity, and degradation rate. In order to improve PLA degradation properties, PLA-based copolymers have been synthesized [36].

Polymer	Applications	Advantages	Disadvantages
Polyphosphazenes	Tissue Engineering Vaccine Adjuvant	Synthetic Flexibility Controllable Mechanical Properties	Complex Synthesis
Polyanhydrides	Drug Delivery Tissue Engineering	Significant Monomer Flexibility Controllable Degradation Rates	Low Molecular Weights Week Mechanical Properties
Polyacetals	Drug Delivery	Mild pH Degradation Products pH Sensitive Degradation	Low Molecular Weights Complex Synthesis
Poly(ortho esters)	Drug Delivery	Controllable Degradation Rates pH Sensitive Degradation	Week Mechanical Properties Complex Synthesis
Polyphosphoesters	Drug Delivery Tissue Engineering	Biomolecule Compatibility Highly Biocompatible Degradation Products	Complex Synthesis
Polycaprolactone	Tissue Engineering	Highly Processable Many Commercial Vendors Available	Limited Degradation
Polyurethanes	Prostheses Tissue Engineering	Mechanically Strong Handle Physical Stresses Well	Limited Degradation Require Copolymerization with Other Polymers
Polylactide	Tissue Engineering Drug Delivery	Highly Processable Many Commercial Vendors Available	Limited Degradation Highly Acidic Degradation Products
Polycarbonates	Drug Delivery Tissue Engineering Fixators	Chemistry-Dependent Mechanical Properties Surface Eroding	Limited Degradation Require Copolymerization with Other Polymers
Polyamides	Drug Delivery	Conjugatable Side Group Highly Biocompatible Degradation Products	Very Limited Degradation Charge Induced Toxicity

Table 1. 3. Summary of different polymeric families' applications: advantages and disadvantages. Adapted from [37].

Polylactic acid (PLA)

Polylactic acid is one of the most widely used synthetic polymers in biomedical products for drug delivery, barrier membranes, guided tissue regeneration (in dental applications), orthopedic, stents, sutures, and scaffolds for Tissue Engineering. PLA is a chiral molecule that gives rise to four polymers with different morphologies: P-DD-LA, P-LL-LA (also called PLLA), P-DL-LA (also called PDLA) and a P-meso-LA. By adjusting the ratio of such polymers, Mw, and fraction of crystallinity it is possible to modulate mechanical properties, degradation rate, Tg and many other factors in a desirable way for a specific application. The synthesis method of PLA is the ring-opening polymerization of the dimeric cyclic ester of lactic acid (or lactide). The polymerization requires heat and a metallic or an organometallic compound as catalyst (Figure 1.6).

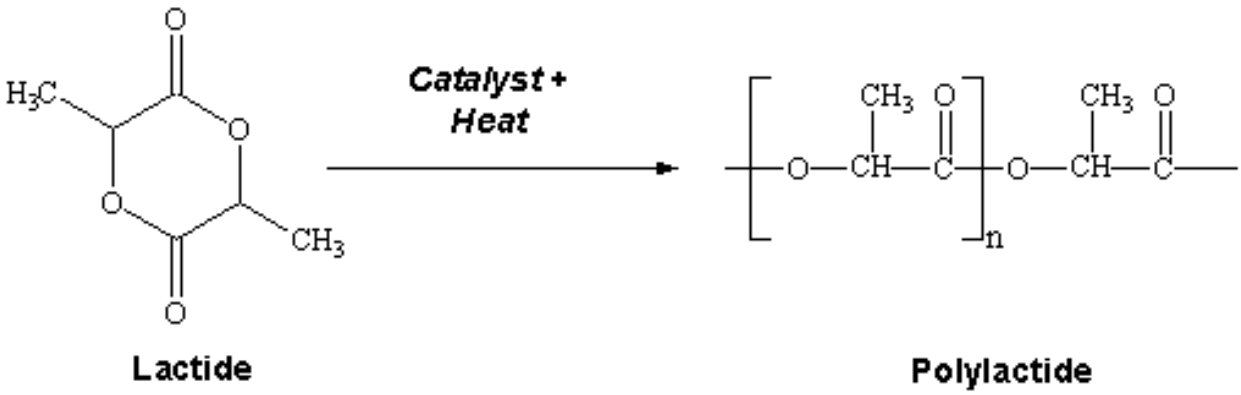

Figure 1. 6. Production route of polylactic acid.

Pure L-lactic acid or D-lactic acid, or mixtures of both components are needed for the synthesis of PLA. L-lactic acid and D-lactic acid, the two isomers of lactic acid, are shown in Figure 1.7.

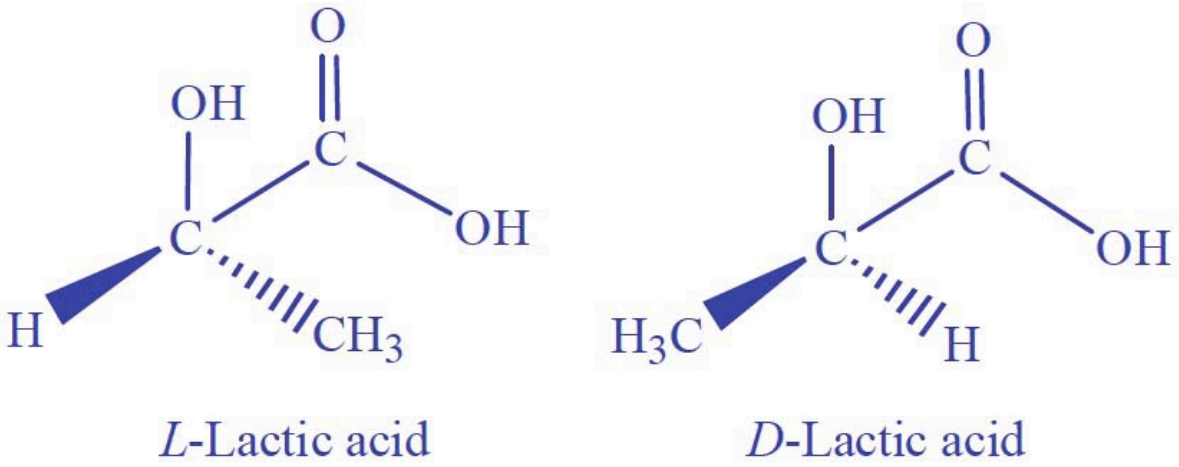

Figure 1. 7. Stereoisomers of lactide acid.

In particular, PLLA is the most used polylactic polymer because its degradation follows a hydrolytic process typical of the stereoisomer of lactic acid [38,39]. PLLA is semicrystalline and has a Tg in a range of 50-65ºC and a melting temperature (Tm) around 170-190ºC. On the other side, PDLA is an amorphous polymer with a Tg in a range of 50 - 60°C.

The polymer used in this thesis is a high molecular weight poly-95LL/5DL-lactic acid (PLA) from PURAC Biochem (Gorichem, The Netherlands). It is a copolymer of the LL and DL polylactic acids with 95% and 5% of each, respectively.

The material characteristics as given by the manufacturers are showed in Table 1.4:

Intrinsic viscosity	6.6 dl/g
Fusion range	163.4-172.4°C (DSC, 10°Cmin^{-1})
Heat of fusion	36.3 J/g (DSC, 10°Cmin^{-1})
Residual solvent	< 0.1%
Residual monomer	<3%

Table 1. 4. Properties of the P-LL/DL-LA used in this thesis.

The degradation of PLA consists in a non-enzymatic break of the ester bonds in it contained. The autocatalytic reaction finishes with the elimination of CO_2 and H_2O [38]. One of the main inconveniences of PLA degradation is the release of lactic acid (due to the cleavage of ester bonds) that causes the acidification of the surrounding environment [34,35].

Polyethylene glycol (PEG)

Poly(ethylene glycol) (PEG), also known as poly(ethylene oxide) (PEO), polyoxyethylene (POE) and under the trade name Carbowax is the most commercially important type of polyether (Figure 1.8). PEG, PEO or POE refers to an oligomer or polymer of ethylene oxide.

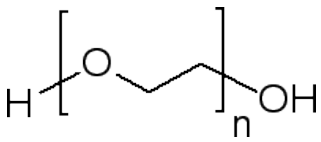

Figure 1. 8. Polyethylene glycol

PEGs are synthetized by polymerization of ethylene oxide and are commercially available over a wide range of molecular weights from 300 g/mol to 10,000,000 g/mol. PEGs are water-soluble liquids or waxy solids used in cosmetic and pharmaceutical preparations and in the manufacture of emulsifying or wetting agents and lubricants (FDA approved because of its low toxicity). Also, PEGs are good plasticizers due to their low glass transition temperature (Tg = -75 to -65°C).

1.4.2. Bioactive ceramics

Calcium phosphate ceramics and glasses are inorganic compounds that represent another relevant type of biomaterials [40]. They have been successfully used as biomaterials to replace hard connective tissues specifically for orthopedic and dental applications. This family of materials presents high bioactivity both *in vitro* and *in vivo. In vivo*, surface modification happens once implanted in host tissues, a thin layer of hydroxycarbonate apatite (HCAp) cauliflower-like shape is formed on the surface enhancing the integration of the implant with the surrounding tissues [30]. *In vitro*, this phenomenon has been observed when immersing the materials in simulated body fluid (SBF). SBF, developed by Kokubo and his colleagues [41], is an acellular solution that has inorganic ion concentrations comparable to those of human blood plasma. During immersion in SBF, a HCAp layer is also formed. The HCAp layer is chemically and structurally similar to the apatite found in bone tissue. It allows a good integration between the implanted material and the external body (surrounding tissue). Moreover, such HCAp phase improves the mechanical sustaining of the implant with stronger chemical bonds.

The most widely used bioceramics are Hydroxyapatite (HAp) and its related crystalline tricalcium phosphate α-TCP and β-TCP. They show excellent biological performance but their application in bone tissue engineering is limited due to low mechanical strength and slow degradation rate, typical of the crystalline materials.

Within the family of bioactive ceramics, bioactive glasses as well as glass ceramics and other calcium phosphate compounds are also included.

Bioactive glasses are one of the most studied bioceramics in the field of bone tissue engineering. They are mainly divided in two families: **silica-based** and **phosphate-based** glasses.

Silica-based glasses, such as Bioglass [42], are composed by SiO_2, Na_2O, CaO and P_2O_5, with SiO_2 less than 60% mol, high concentrations of Na_2O, CaO and ratio Ca/P higher than 1 in order to decrease acidification and solubility of the material [37]. A number of *in vitro* and in *vivo* assessments have proved cell attachment, proliferation and differentiation by using different cell sources such as osteoblasts and mesenchymal stem cells [43,44]. Nevertheless, due to the high content of silica, this type of glasses is stable to hydrolysis and only partially degradable.

Calcium phosphate glasses

Phosphate-based glasses are completely soluble in water and their degradation rate can be tuned depending on the application. Therefore, phosphate-based glasses offer an alternative to the silica-based glasses. This type of bioactive glasses is suitable for the development of temporary bioresorbable implants. With the aim of modifying the mechanical properties and solubility of these compounds, different oxides, such as magnesium, titania, sodium and fluorine among others have been used.

The biodegradable glass used in this thesis is a titania-stabilised, completely degradable, calcium phosphate glass named G5. This glass has the following molar composition (Table 1.5):

Molar composition	Compound
44.5%	CaO
44.5%	P_2O_5
6%	Na_2O
5%	TiO_2

Table 1. 5. Molar composition of the titania-stabilised calcium phosphate glass G5.

The addition of G5 [45,46], in particles shape to reinforce and improve bioactivity of PLA scaffolds has been explored [47]. It is known that G5 glass is highly hydrophilic (contact angle = 29.8°) [12]. Thus, addition of G5 particles contributes to decrease PLA contact angle. Previous studies have demonstrated a preferential attachment and spreading of cells on G5 glass particles than in the polymer matrix [12,31]. This soluble glass degrades along time while releasing different ions to the surrounding media [45]. It has been demonstrated that the presence of G5 glass particles not only increases cell attachment and spreading but also triggers angiogenesis and bone formation owing the Ca^{2+} release and stiffness of the glass [7,48]. Indeed, several studies have demonstrated the relevant role of ions on tissue regeneration [49,50].

The G5 glass was elaborated following a three-step procedure. All compounds were provided by Panreac Química S.A. First, $CaCO_3$ is calcinated at 900°C (Figure 1.9) in order to obtain CaO by reaction {1}:

$$CaCO_3 \xrightarrow{825^{\circ}C} CaO + CO_2 \quad \{1\}$$

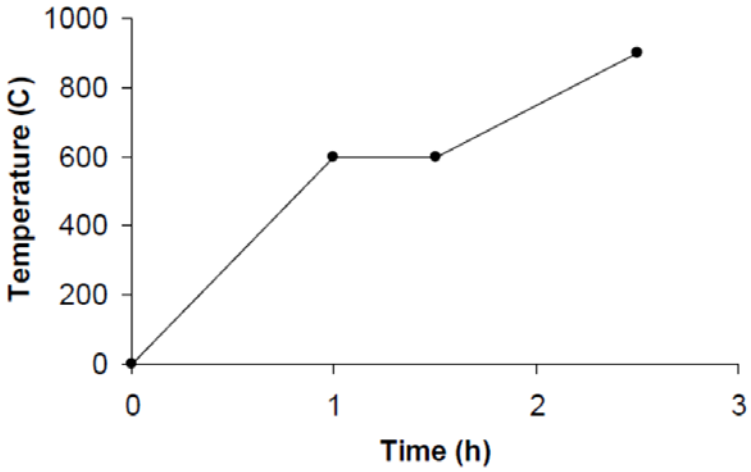

Figure 1. 9. Temperature cycle for the calcination of $CaCO_3$.

Next, the CaO is mixed with the other ingredients shown in Table 1.5, placed in a platinum crucible, and melted at 1350°C. The mixture remains at 1350°C for eight hours in order to ensure complete homogeneity of the molten matter. After eight hours, the molten glass is quenched on a stainless steel plate heated at 480°C, and is annealed at 533°C (the glass transition temperature of the G5 glass) for 30 minutes. The glass cools to form transparent slabs, which are then milled and sieved within a certain range. The properties of the G5 glass manufactured with this procedure can be seen in Table 1.6.

Density	2.903 gm^{-3}
Glass Transition Temperature	532.9 ^{o}C
Rate of dissolution	$3.2x10^{-7}$ g $cm^{-2}h^{-1}$
Vickers Hardness	431.1 kg mm^{-2}

Table 1. 6. Properties of the G5 glass used in this study**. Adapted from [51].**

Undoubtedly, mechanical properties of calcium phosphates strongly decrease by increasing microporosity or particle size. Moreover, in bone tissue a high tensile strength and fracture toughness are due to the presence of collagen fibres. Thus, the use of a calcium phosphate particles mixed with a biodegradable polymer is an available approach to enhance the mechanical behaviour of the material. The use of glass particles instead of a bulk system increases the degradation rate of the calcium phosphate phase. In addition, they act as filler opportunely introduced in the composite system in order to improve stiffness and compressive strength. In Table 1.7, the main properties of the PLA, calcium phosphate (CaP) glass and the composite PLA/CaP glass are briefly synthesized.

	Bioactivity	Degradation	Mechanical properties
PLA	Low	acidification of the surrounding environment, could be toxic, induce strong inflammatory response	high tensile strenght and fracture toughness, low stiffness: 300 kPa (solvent casting); 4.72 MPa (TIPS) scaffolds [31]
CaP glass	High	high mechanical stability, low degradation rate	low tensile strenght and fracture toughness, high stiffness: 66.6 - 75.95 GPa [45]
PLA/CaP glass	CaP glass particles increase bioactivity	CaP act as buffer for PLA decreasing acidification; the use of CaP particles instead bulk glass increase the degradation rate	stiffness: 190 kPa (solvent casting); 7.10 MPa (TIPS) scaffolds [31]

Table 1. 7. Bioactivity, degradation and mechanical properties of PLA, CaP glass and the relative ccomposite.

1.5. Scaffolds for Bone Tissue Engineering

As previously mentioned, the fundamental tesserae of the Tissue Engineering mosaic are scaffolds, cells, and signals. Every tissue presented in nature is composed by a matrix and one or more cells types. The *in vivo* matrix represents the ideal environment for cells providing a specific architecture with a precise spatial disposition of molecular signals. The design and development of a 3D construct is mainly a great challenge in every field of engineering and is the main objective of this thesis.

In case of Tissue Engineering, the production of temporary structures that provide the cells with the appropriate chemical and mechanical signals is crucial for the satisfactory growth of new tissue. To achieve this goal, scaffolds should also present bioactive signals and act as reservoir of water, nutrients, cytokines, and eventually growth factors. The optimal scaffold candidate for Tissue Engineering applications should accomplish a series of specifications [52]:

- The material used should be **biocompatible**. Once implanted in the body should perform its functions without inducing adverse immune response [52,53].

- The scaffold morphology should possess a **highly porous** configuration with a fully **interconnected pore network** to allow cells invasion and growth into the inner part of the structure. Porosity and interconnectivity are also important to consent flow transport of nutrients, oxygen and metabolic waste. Considering that the *in situ* distance between blood vessels and mesenchymal cells is not larger than 100 μm [53,54], the presence of meso and microporosity is also crucial for the neovascularization from the surrounding tissue. Thus, an interconnected porous scaffold with **pore size** in a range of 200-600 μm enhances the diffusion rates of nutrient, allowing the bone formation [55]. For the *in vitro* bone regeneration, some authors [56-59] proposed pore sizes ranging from 200 to 400 μm. Pore sizes between 20 and 125 μm have been used for regenerating adult mammalian skin [60] and 45–150 μm for liver regeneration [61]. Pores particularly small could cause pore occlusion [62] by cells, stopping the penetration and elaboration of new ECM inside the scaffolds.

- Two other factors having strong influence on the oxygen profile and permeability are **pores tortuosity** and **shape**. A suitable fabrication technique could modulate them, depending on the target tissue. Indeed, degree of porosity affects other properties of the scaffold such as its mechanical behaviour. Thus, a compromise should be found to achieve suitable features for the tissue that is going to be replaced.

- Scaffolds should be **bioresorbable**, and its degradation rate must be in tune with the growth of new tissue.

- Scaffolds' **mechanical properties** are one of the main aspects to take into account for the development of 3D matrices. They must be similar to those of the tissues at the site of implantation. In *in vitro* conditions, mechanical strength should be sufficient to compete with the hydrostatic pressure and the new ECM formation. *In vivo* the scaffold should resist to load-bearing site pledging the tissue regeneration by limiting pore occlusion. In other words, the structure should maintain its structural integrity during the first stages of the new bone formation [2].

- It is important that the designed structure has a high **surface/volume ratio** in order to enhance cell attachment.

- Scaffolds should possess **suitable surface properties** by tuning both topographical and chemical features in order to stimulate cell attachment, proliferation, and differentiation [63-65].

Scaffolds fabrication

From the material science point of view, native bone is a composite material that combines collagen, a natural polymer, with a biological hydroxyapatite. Thus, materials used for mimicking bone tissue should be mostly composed by a biopolymer matrix and an inorganic phase. Such materials should be organized into three-dimensional highly porous structures in which a particle-system of bioactive ceramic/glass is entrapped into a polymer matrix. The development of composite scaffold that synergistically combine the workability (shapeability) of polymers and fractions of a bioactive ceramic phase in order to reinforce mechanically the developed structure can be achieved.
To this end, a number of scaffold fabrication technologies have been successfully adopted, among others: solvent casting with and without particle leaching, thermally induced phase separation (TIPS) combined with freeze-drying, microsphere sintering, supercritical gas-foaming, and electrospinning have been applied successfully to the fabrication of polymer-ceramic composite scaffolds. In addition to this group of conventional techniques, recently, a new family of additive manufacturing techniques has emerged.

1.5.1. Conventional techniques for scaffolds fabrication

Solvent casting particulate-leaching

Solvent casting is one of the most largely used conventional techniques to produce scaffolds. It involves the dissolution of the polymer in an organic solvent and casting into a predesigned Teflon mould. In the same way, composite scaffolds have been produced by mixing the polymeric solution with bioactive CaP ceramic or glass granules (Figure 1.10). This approach is mostly associated with particulate-leaching in order to get highly porous three-dimensional structures. A porogen agent (such as salt or sugar) is added to the polymer solution. Then, after the evaporation of the solvent, the salt is dissolved in water leaving the pores behind.

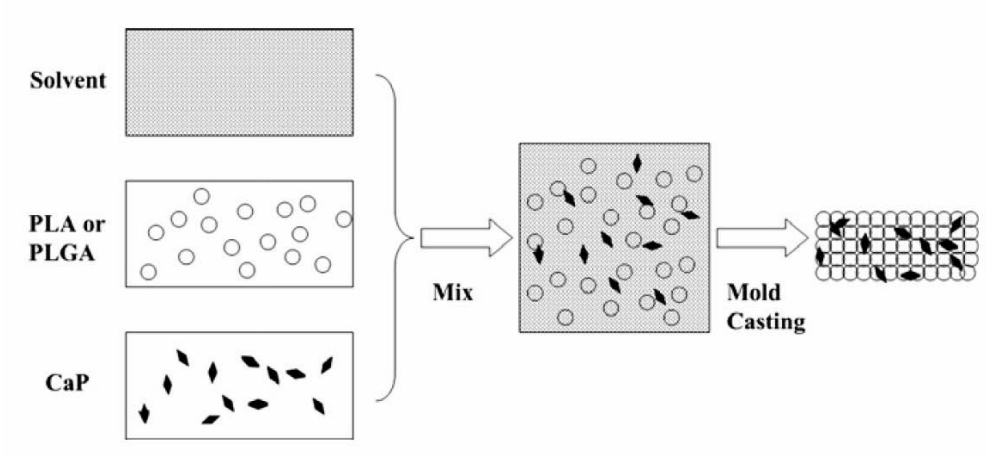

Figure 1. 10. Schematic description of a particle-leaching method. Adapted from [48].

The advantages of using this technique are its simplicity and low cost that allows scaffolds fabrication without the need of specialised equipment. The primary disadvantages of solvent casting are a) the possible retention of toxic solvent within the polymer and b) the limitation in the shapes (basically flat sheets and tubes). Furthermore, the use of organic solvent could lead to denaturation of the proteins and other biochemical signals incorporated into the polymer. Porosity can be controlled by varying salt particles size and the polymer/salt ratio. Nevertheless, control of pores shape and interconnectivity between adjacent pores is very low (Figure 1.11).

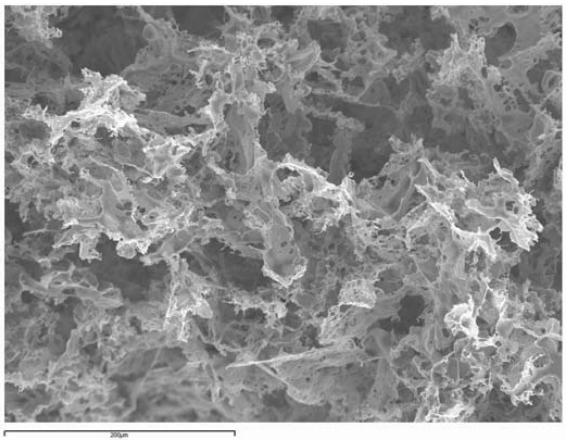

Figure 1. 11. Scanning electron microscopy micrograph of a PLA/Calcium phosphate scaffold by solvent casting-particle leaching [47].

Thermally induced phase separation (TIPS)

Porous scaffolds have been largely developed by thermally induced phase separation (TIPS) (Figure 1.12). Polymer and solvent are homogeneously mixed at low temperature. In the case of composites, inorganic particles are also included. Once the solvent solidifies, polymer and particles are forced into the interstitial spaces. The frozen mixture is then lyophilised using a freeze-dryer in which the iced solvent (and water) sublimates allowing the formation of homogeneous and highly porous scaffolds with anisotropic tubular morphology. TIPS process has been used to produce PLA/CaP glass scaffolds and its *in vitro* and *in vivo* response has been intensively studied [51]. Moreover, the attachment and spreading of osteoblast cells has been also confirmed [31].

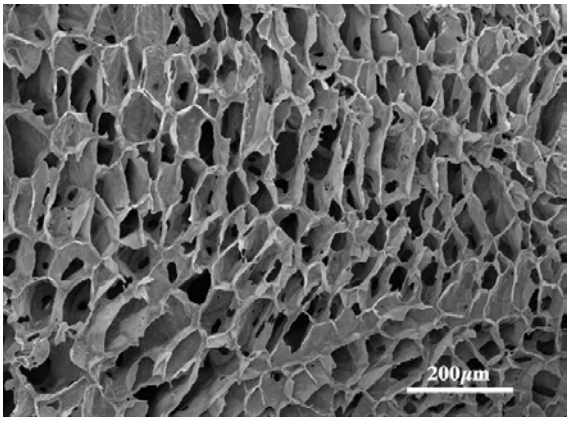

Figure 1. 12. Scanning electron micrograph of a PLLA scaffold fabricated using TIPS [66].

Microsphere sintering

This process consists in sintering polymer microspheres, previously produced by an emulsion/solvent evaporation technique. The sintering process can be thermally or chemically activated depending on the system used to attach and fuse the microspheres one to each other: heat or solvent vapour [67]. In the case of composites, inorganic particles have been encapsulated into the microspheres. Three-dimensional biodegradable and bioactive scaffolds have shown lower porosity of solvent casting or TIPS, but mechanical properties closer to cancellous bone.

Gas Foaming

This technique allows the production of macro-porous scaffolds from biodegradable polymers by using a process with high-pressure carbon dioxide at room temperature. After a melt-extrusion step, the ceramic/polymer mixture is exposed to high pressure of CO_2 gas in order to saturate the system. By reducing the CO_2 pressure to atmospheric levels, the solubility of the gas rapidly decreases causing thermodynamic instability in the network and the formation of pores. Open-pore foams using polyesters polymers have been fabricated [68].

Electrospinning

In the last years, electrospinning has attracted enormous attention in the scaffold fabrication community, particularly for reconstructive surgery application. It is a versatile and simple process to fabricate fibrous mats of biodegradable polymers. The dimension of the fibers, at the micro- nanoscale, gets particular interest in order to synthetically reproduce the extracellular matrix of living tissues. In the process, a polymer solution is forced in a capillary and forms a jet of solution at the tip. As shown in Figure 1.13, a high voltage is applied between the tip and the collector where the mat of thin fiber is deposited after the evaporation of a volatile solvent.

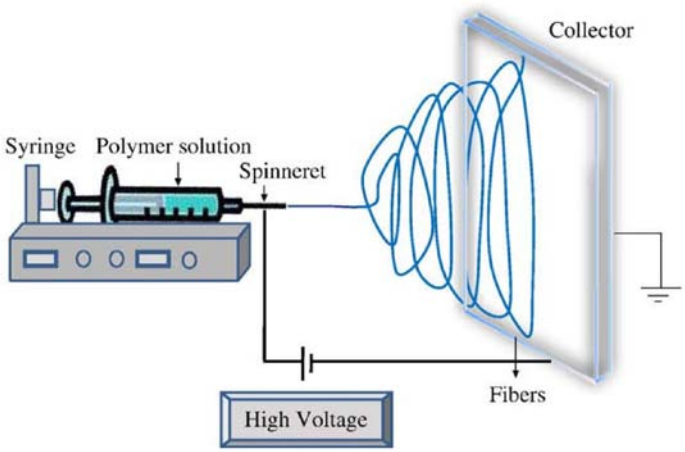

Figure 1. 13 .Schematic representation of electrospinning system. Adapted from [69].

Additionally, the easy incorporation of biochemical signals such as drugs, growth factors or enzymes, makes this approach attractive for tissue engineering applications. Nevertheless, significant drawbacks of this technique: are a) only few synthetic (PLA, PCL, PLGA) and natural (collagen, fibrinogen) polymers have been used to produce random fibers scaffolds; b) only thin layers have been produced, making difficult to fabricate geometrically complex three dimensional scaffold with controlled pores. Lastly, fiber diameter sometimes undergo in the micrometer range, which is not properly in the size of the natural extracellular matrix.

To conclude, Table 1.8 briefly shows a summary of the main advantages and limitations in using the conventional fabrication techniques.

Fabrication technique	Advantages	Disadvantages
Solvent casting / particulate-leaching	High porosity, quick and easy	Organic solvents are used
Thermally induced phase separation (TIPS)	High porosity, easily combined with other fabrication techniques	Shrinkage issues, organic solvents are used, anisotropic pores
Microsphere sintering	Gradient of pore size and complex shape are possible	Interconnectivity is an issue
Gas Foaming	Organic solvent and high temperature are not required	Low pore and geometry control
Electrospinning	Structural features similar to extracellular matrix, high aspect ratio and surface area	Organic solvent are used, low pore and geometry control

Table 1. 8. Main advantages and disadvantages in using conventional fabrication techniques.

1.5.2. Additive manufacturing techniques

Critical size bone defects, especially in the craniofacial region, are significant challenges in surgery and are strictly connected with patient's quality of life and high socio-economical costs. Therefore, new technologies should be adopted to achieve successful regenerative strategies. Additive manufacturing (AM) is changing radically implantology and regenerative therapies by adding new possibilities to reconstruct and regenerate tissues in a patient-specific way [9]. It also provides a tremendous tool to fabricate scaffolds on demand for the generation of *in vitro* platforms for preclinical drug development. Compared to the conventional fabrication technique, this new approach brings many advantages. First of all, a precise control and reproducibility of geometrically complex microstructures is achievable.

A fine control of pores size and shape allows tuning mechanical properties and permeability of the 3D structures. Honeycomb-like structures can be produced with morphological features similar to the natural structure of cancellous bone.

Overcoming low mechanical properties has always been a great challenge in the development of scaffolds for bone tissue engineering. By setting the design, pore volume, and eventually post processing

condition, the new scaffolds produced via AM technologies show higher mechanical properties in comparison with the ones produced by other conventional techniques. Moreover, precise selection of structural cues, eventually coupled with computational approaches like finite element analysis could give estimation of the scaffold behavior once implanted and during the tissue regrowth.

Such porous structures also provide higher pores interconnectivity and the interconnection area between pore volume results bigger and more suitable for cell migration. In the same way, permeability is also increased due to a decrease of tortuosity within the structure. Thus, oxygen and nutrients diffuse better into the inner part of the scaffold affecting positively the cell response and blood vessel infiltration [70].

From a technological point of view, this approach consists in a controlled robotic system connected to a CAD/CAM tool that allows the fabrication of 3D structures with well-defined geometries. A fundamental aspect to be highlighted is the capacity to produce patient-specific bone grafts. A new protocol based on medical imaging (such as computed tomography, CT) can be used. Once the CT data of the patient defect is treated in order to generate a 3D model, it can be imported into the software of the AM system. After a "slicing process" the three dimensional object is converted in a sum of thin horizontal layers having the specific informatics code requested (2D instructions). Afterwards, the code is used to instruct the robotic system in order to shape layer by layer the scaffold (Figure 1.14) [71].

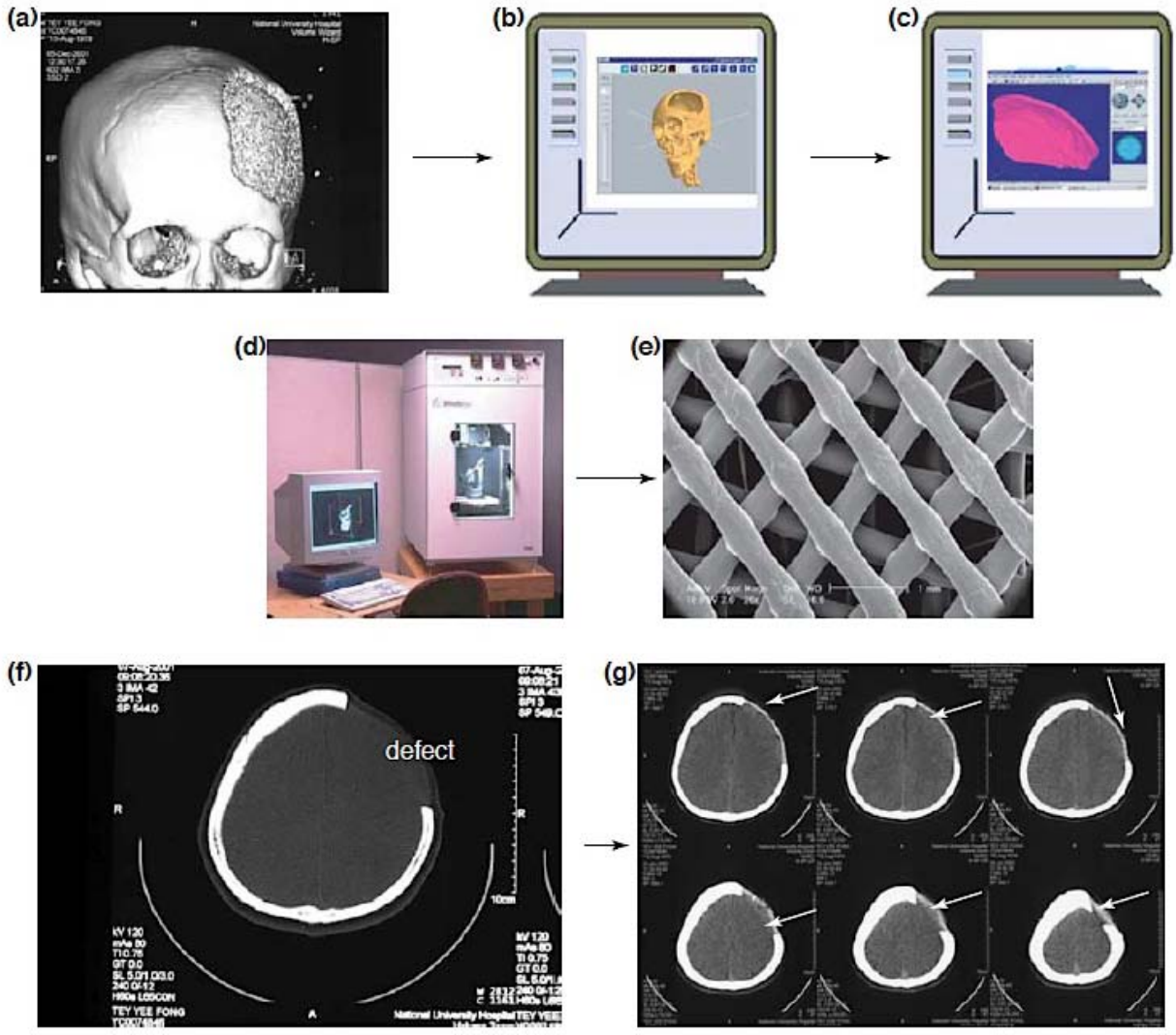

Figure 1. 14. Tissue Engineering of patient-specific bone grafts [71].

AM offers a new bottom-up philosophy, contrarily to most of the conventional fabrication approaches in which pores formation is due to the volume left by solvents or other agents randomly immersed in the bulk material (subtractive approach). As previously explained AM consists in building 3D structures by sequentially layering one material on top of another in a desired pattern in a precise and repeatable way. This aspect allows choice and spatial positioning of biophysical and biochemical signals (such as calcium phosphate glass particles or growth factors) all over the volume of the scaffolds, aiming to trigger specific biological responses.

Before entering a detailed exposition of the main AM used in the tissue engineering field, it is important to remark that such technology is still in its infancy [9]. Nowadays, the scientific community is doing a great effort in order to develop suitable biomaterials to be used for this aim. Indeed, biomaterials should have: a) adequate mechanical properties, b) fitted degradation rate while maintaining structural integrity, and c) appropriate rheological quality to be processed. Synergistically coupling suitable biomaterials with the extraordinary potential of the AM techniques will make possible the evolution of a new class of smarter scaffolds.

Moreover, due to the great number of recent publications, the nomenclature used to classify this emergent technology is quite confused. Additive manufacturing is also known as rapid prototyping (RP), solid free form fabrication (SFF), 3D-printing among many others. Trying to clarify between a great variety of categorization, the AM systems have been divided in three fundamental families: laser based, powder based, and nozzle based techniques.

Laser based systems

Stereolithography (SLA) is one of the most famous additive manufacturing techniques and one of the first to be commercialized. This laser based process basically consists in a photo-polymerization, in which a UV laser is used to build structures layer by layer (Figure 1.15a). A liquid photo-curable monomer resin that polymerize when exposed to UV light is used. The laser scans the top of a bath and polymerizes the resin creating a solid layer. The process is repeated on the sequent layers by moving down the table until the 3D structure is achieved. A post-process treatment could eventually be done by curing in a UV oven the obtained scaffold. Large porosity could be obtained with this method, with pore size in the range of 20-1000 μm. An accurate control over pore size and interconnectivity can be achieved. The layer-wise fashioned process allowed fabrication of complex and anatomically shaped structures. However, the machinery required are very expensive and only few polymers compatible with UV curing can be used. Figure 1.15b shows an example of SLA scaffold. A resin based on PDLLA monomers functionalized with methacrylate end-groups was photo-polymerized in the presence of ethyl lactate as a non-reactive diluent to obtain highly porous architectures [72].

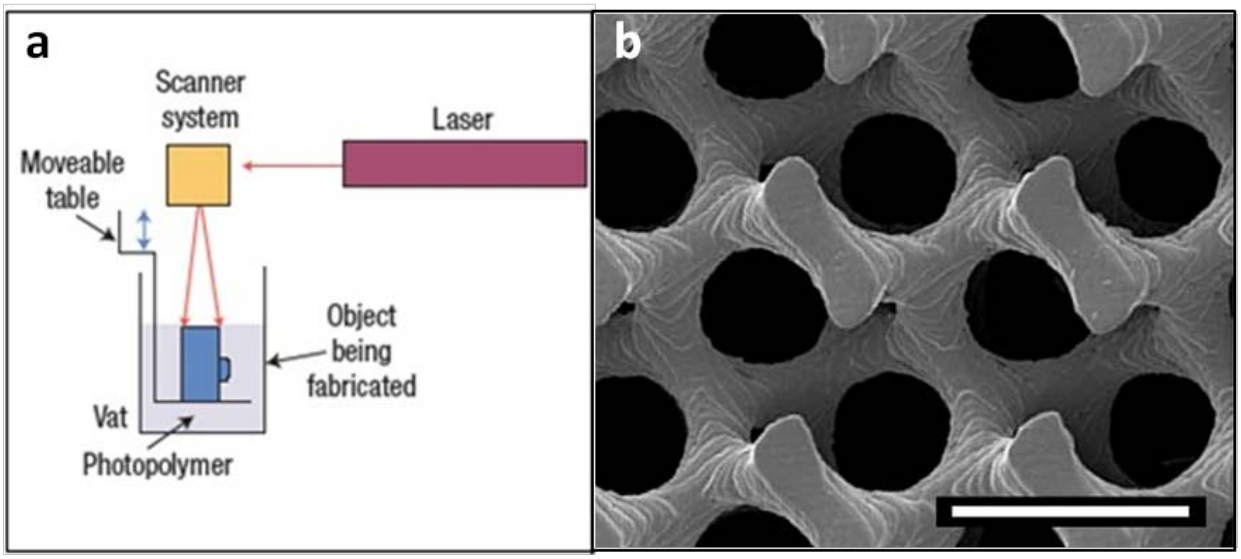

Figure 1. 15. (a) Schematic description of stereolitography method; (b) SEM micrographs of PLA scaffolds. Scale bars represent 500 μm. Adapted from [23,56].

Powder based systems

The first powder based system, named "3DP" or 3D-printer, was developed in the early 1990s at MIT (Cambridge, MA) by Sachs et al. [73]. Nowadays, the word 3D-printer has became one of the most common ways to state an additive manufacturing process.

This class of technology aims to the fabrication of layer by layer three-dimensional structures in which every 2D slide supplied by a computer model is printed on a new layer of powder by releasing a thin coating of binder [58]. A suitable binder (glue or solvent) should act as a plaster between adjacent powder microparticles. Crucial parameters such as powder packing density, wettability, flowability, layer thickness, binder drop volume, binder saturation should be optimized to improve the quality of the final architecture [59].

As shown in Figure 1.16a, successive 2D profiles are printed on a freshly prepared layer of powder until the whole model is completed. Once reached the final height of the designed structure, the next step consists in the removal of the entrapped unreacted powder. Finally, a suitable post-process is needed. In the case of ceramics powder deposition, a typical post-processing method involves high temperature sintering in order to promote binder removal and powder coalescence. A suitable alternative way to develop powder-based scaffold has been also the adoption of Selective Laser Sintering (SLS), in which the binder jet is replaced by a laser beam that melts selected patterns of powdered material [74]. Figure 1.16b shows the typical structural morphology of a calcium phosphate scaffold produced via 3D-printing technique. Layer thickness and powder particles size are the main factors influencing the final surface resolution of the scaffolds. Interconnected porous channels of about 800 μm and micro-porosities of 45–150 μm were achieved [75].

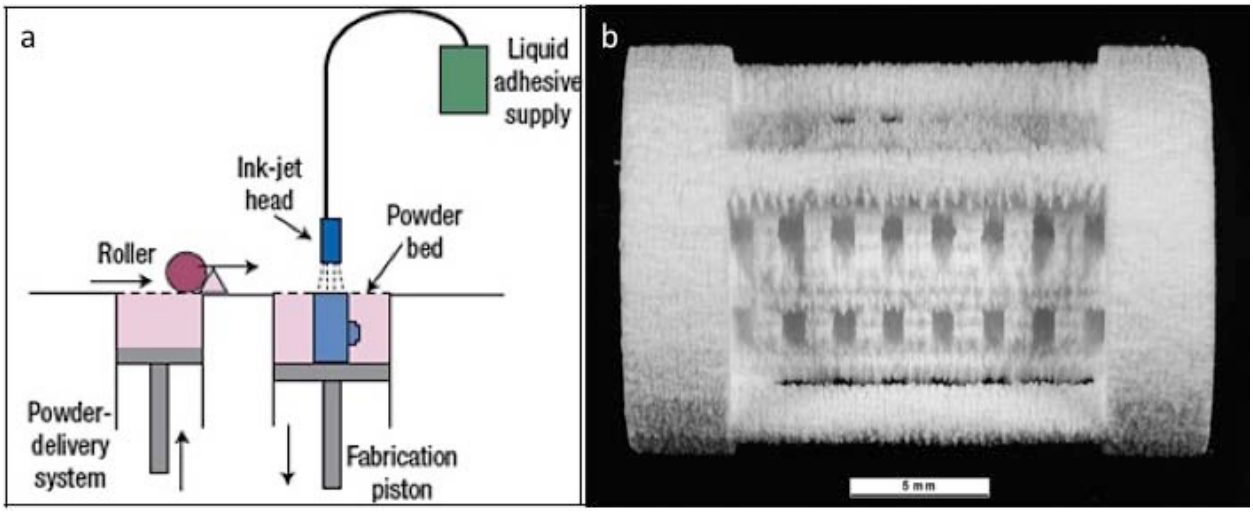

Figure 1. 16. (a) Schematic description of powder-based method; (b) calcium phosphate scaffold produced by a powder-based system. Adapted from [23, 58].

Nozzle based systems

The nozzle based system machines constitute the third family of additive manufacturing techniques. Fused deposition modeling (FDM) is one of the most popular rapid prototyping technologies. It was used to fabricate scaffolds with honeycomb-like pattern, fully interconnected porous network, and controllable porosity and channel size [32].

FDM is based on an extruder nozzle covered with a heating jacket that push out a thermoplastic polymer filament and dispense the melted polymer onto a table along a layer by layer process. The filament is forced by two rollers into the extruder and drives the flow out of the polymer. Once the layer is finished, the platform moves down and a new pattern is deposited (Figure 1.17a).

Also for this class of AM techniques, a preliminary optimization of the process parameters is strongly required. Fabrication condition such as speed of deposition, diameter of the nozzle, and the design of the 2D path are depending by the material properties and by the application aimed by the researcher.

Poly(e-caprolactone) (PCL) is the main used polymer used for this application, due to its low glass transition temperature of -60°C. PCL exists in a rubbery state at room temperature, and also has a low melting temperature of 60 °C, easily achievable by this kind of machines. Moreover, due to the high thermal stability, PCL can be strongly heated without degrading or losing its initial properties. Figure 1.17b shows the SEM micrograph of scaffold produced by FDM. PCL scaffolds with pore size in a range of 160–700 μm, strut diameter 260–370 μm and porosity 48–77% have been reported [32].

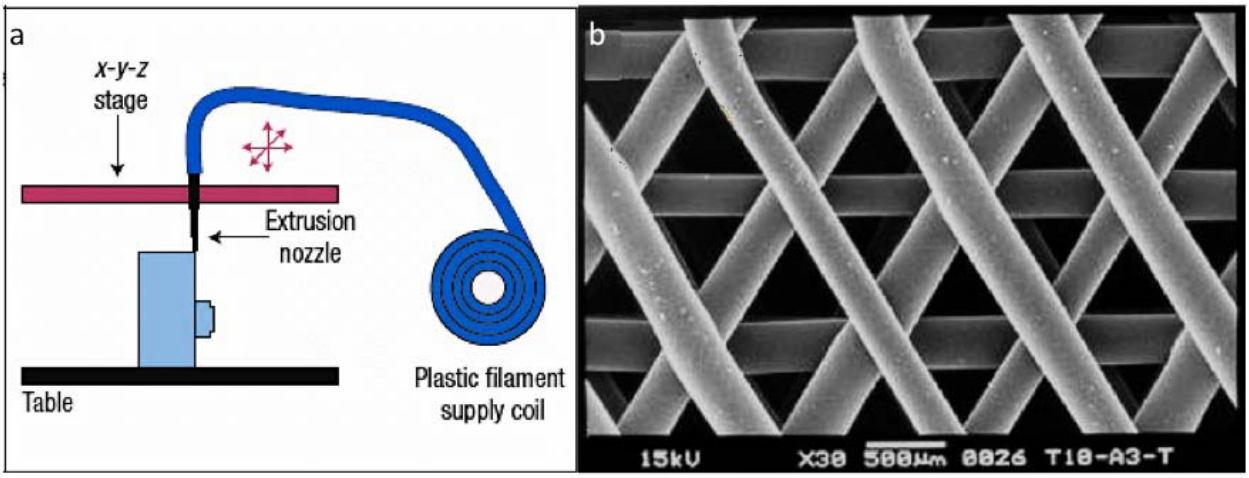

Figure 1. 17. (a) Schematic description of Fused Deposition Modeling method; (b) SEM micrograph of a PCL scaffold. Adapted from [23, 39].

Contrarily to the traditional 3D printer systems, in which powder based aliphatic polyesters required the use of organic solvents as binder [74], FDM is a solvent free method to produce scaffolds. Nevertheless, many are the limitations in using this technique to produce tissue engineering scaffolds. Among them, the resolution of the deposited struts is limited and strongly dependent on the diameter of both filament and needle tip.

Other important restriction to utilize a FDM system is the necessity to prepare polymeric filaments before starting the process. It makes the procedure longer and expensive. Moreover, the range of materials choice decreases and the eventual development of composite filaments containing CaP microparticles makes the printing process even harder to achieve. With the aim of eliminating the need of filaments and to enlarge the range of suitable materials, a number of novel technologies have been developed. Most of them are capable to melt and extrude raw polymer in pellets by connecting a heating jacket with a cylinder and plunging the materials by screw, coaxial metallic piston or compressed air systems.

Lastly, high temperatures required during the process do not match with the thermal stability of many biodegradable polymers. Biodegradable polymer such as collagen or chitosan, need to be printed at low temperatures to avoid denaturation that could lead to fast degradation both *in vitro* and *in vivo*.

This is also the case of polylactic acid, showing a lack in thermal stability at high processing temperature. Different mechanisms of degradation can affect the polymer, such as hydrolysis, thermolysis, and monomer reformation. It explains also why a number of studies employing nozzle based techniques presented in literature shows the use of PCL instead of PLA. **Being PLA the polymer used in this thesis, it represents a great issue to be taken into account during the implementation.**

Only few studies using PLA have been reported, and most of them were carried out with a laser based system approach as stereolithography [72]. An indirect approach to build 3D PLA scaffolds was used by Taboas and colleagues [76]. As can be observed in Figure 1.18a, PLA/porogen slurry was casted in a 3D printed wax mold containing global pore templates. After the evaporation of the solvent, the PLA structure solidified and the mold could be removed leaving a network of interconnected pores. Starting from a PLA/solvent solution, Xiong and colleagues developed PLA scaffolds (shown in Figure 1.18b) by combining nozzle-printing technology with a freeze-drying system [77]. However, published studies have shown a low resolution in term of design, pore size and shape and a great effort should be done to improve the complexity and repeatability of PLA microporous structures.

Thus, this thesis proposes a novel low temperature nozzle-based system in order to avoid the thermal degradation of PLA. Moreover, addition of PEG to a PLA/solvent solution will allow the fabrication of precise and reproducible 3D structures with higher resolution than the ones obtained by currently (nozzle-based) methods.

To conclude, Table 1.9 briefly shows a summary of the advantages and limitations in using additive manufacturing systems to develop Tissue Engineering scaffolds.

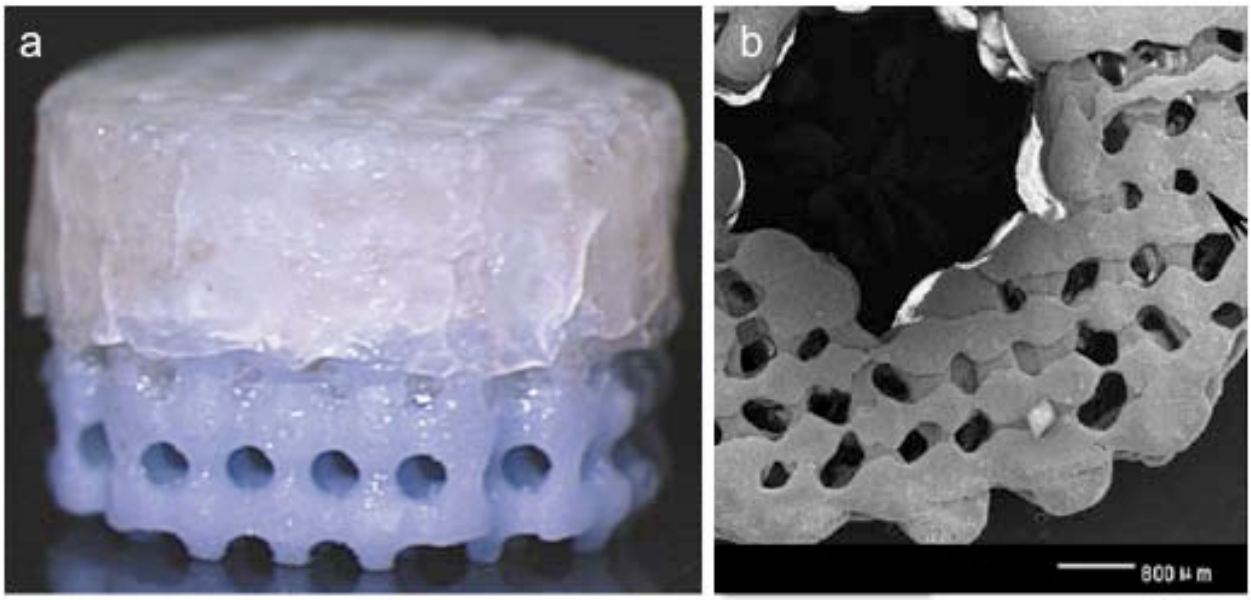

Figure 1. 18. 3D printed PLA scaffolds by (a) indirect approach and (b) low temperature deposition. Adapted from [60,61].

AM family	Advantage	Disadvantage
Laser based system	Hydrogel, high-resolution and accuracy liquid build material can be easily removed from within complex scaffolding	Limited choice of materials, may require furnace post processing (e.g. bioceramics), high material cost, complex and expensive equipment
Powder based system	Wide range of material choice, low cost, quick process, multimaterial capabilities through multiprint-heads	Hard to remove trapped materials, low to medium resolution, powder particles may not bind well, binders are always necessary to bind powders
Nozzle based system	No trapped materials, minimal material waste, low cost	Materials may thermally degrade during the process, lower range of material choice, medium resolution

Table 1. 9. Brief summary of advantages and disadvantages of using AM technologies.

Finally, to have an idea of the ambitious growth of the additive manufacturing scenario, it should be mentioned that a new society and journal (Biofabrication) focused on this topic, have been recently established. Moreover, a first generation of FDM PCL-based scaffold has been FDA approved and commercialized (http://www.osteoporeinternational.com) after clinical trials. Furthermore, new *bioprinting* strategies are being developed due to the possibility to print living cells solutions. Among others, Mironov and collegues, by means of an automated modular approach for cell printing opens new possibilities to regrowth tissues and to build engineered tissue construct for better *in vitro* simulation of the *in vivo* milieu [78].

1.6. Inflammatory response to biomaterials

The inflammatory reaction triggered at the time of implantation by the invasive intervention and as part of the host response to the foreign body being implanted influences the behavior of different cell populations involved in the regenerative process, and therefore the success of the implanted materials [79].

In the materials section of this introduction it was mentioned that one of the main drawbacks of PLA degradation is the generation of acidic products that decrease the pH of the surrounded environment. It provokes autocatalytic degradation that causes an intense inflammatory response [34,35]. The addition of CaP glass particles to PLA, activating a pH buffering mechanism, hinders the acidic degradation and is expected to modify the related inflammation [30,81].

Moreover, though it is commonly known that an acute inflammatory response could lead to the rejection of an implant, it is also recognized that inflammation may also be essencial in tissue regeneration. Thus, a deeper understanding of the biological response to the implanted biomedical devices is a paramount issue in the tissue engineering field. Moreover, Anderson and colleagues in 2008 said, “the chemical, physical, and morphological characteristics of the synthetic surface are considered to play a role in modulating cellular events” [79]. Thus, it is currently accepted that a comprehensive understanding of cell/material interactions may lead to a better control of the inflammatory response in the direction of tissue regeneration.

Nowadays, the scientific community is doing a strong effort in order to understand the complex interaction between cells and materials with the aim of developing a new type of biomaterials and medical devices. Modulating the biochemical and biophysical cues of biomaterial surfaces will impact inflammatory reaction by tuning macrophages behavior such as adhesion, apoptosis, fusion, and cytokine secretion.

Up to now, most of the traditional studies stress on the need to diminish inflammatory response to implanted biomaterials. In spite of this, recently, researchers are considering the positive aspects and potentialities of this phenomenon. Indeed, inflammation and the mechanism behind the foreign body response are relevant factors to enhance tissue repair and remodeling, in particular bone [80].

Foreign body reaction

The foreign body reaction is basically an inflammatory response that persists as long as there is a foreign body present to respond to. It comprises a sequence of interconnected events concluded with the fibrous encapsulation of the implant [79]. Such isolation from the surrounding tissue provokes the loss of functionality and then the failure of the device.

An inflammatory response involves the migration of neutrophils and monocytes/macrophages to the injury site by chemotaxis of different cytokines in order to phagocytose all the material labelled as foreign and cellular debris. Neutrophils disappear after finishing their task, leaving place to macrophages. A sustained macrophage response is typical of a chronic inflammatory reaction and is common in most

implants. The numerous presences of macrophages lead the formation of multinucleated giant cells or foreign body giant cells (FBGC), also called multinucleated giant cells (MGCs), as a response to the effort to overcome the frustrated phagocytosis process experienced by single cells [79].

In other words, macrophages are not able to phagocyte the surrounding materials thus they fuse one in each other forming multinucleated giant cells.

At this stage, macrophages and also fibroblasts release chemotactic factors for the recruitment of more fibroblasts. Macrophages inactivate their attack mechanisms and fibroblasts become the main cell line. At this time, fibroblasts start secreting a collagen I and III-based extracellular matrix that will encapsulate the material. The thickness of the collagenous capsule varies depending on the movement of the implanted device [22], and will isolate the material from the host tissue.

The foreign body reaction is a serious limitation; it can lead to chronic pain and eventual device rejection and failure. The result of all the previous considerations is that the implant or medical device surface plays the leading role in its interaction with the biological environment. Consequently, the study and characterization, modification and functionalization of the biomaterials surfaces are probably the main strategies for success of implants and the tissue regeneration.

To summarize, Figure 1.19 shows the different steps of the monocytes route from blood to tissue and in contact with biomaterial.

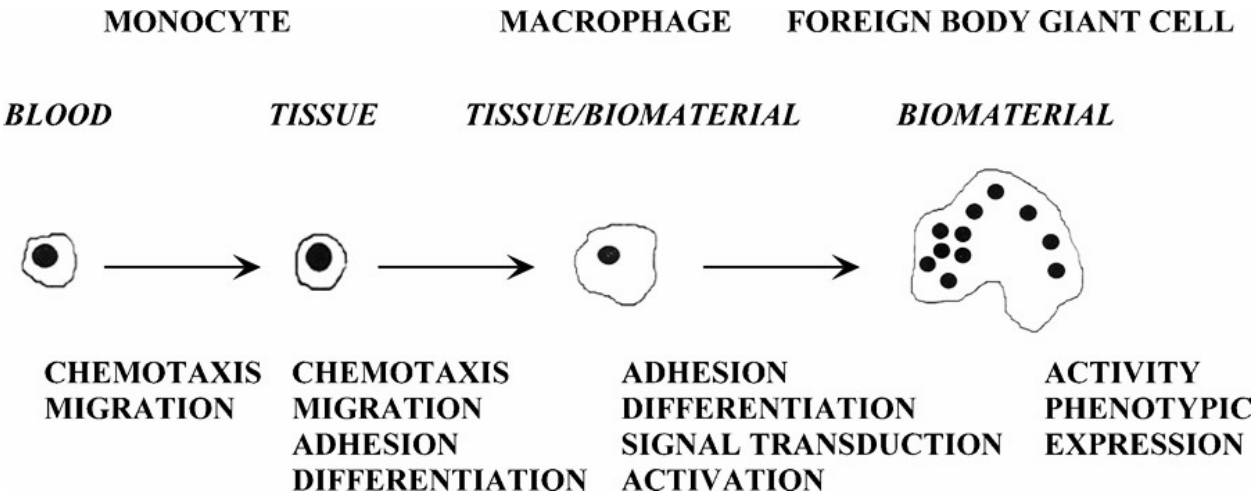

Figure 1. 19. Schematic of the *in vivo* transition from blood derived monocyte to biomaterial adherent monocyte/macrophage to multinuclear giant cell at the tissue/biomaterial interface. Adapted from [79].

In order to understand better the complex mechanisms involved in inflammation and foreign body reaction, some concepts should be introduced: monocytes/macrophages cells, cytokines, macrophages polarization.

Monocytes/macrophages cells

Monocytes derived from the bone marrow, migrate through the peripheral blood stream and reach the tissue surrounding the biomaterial where the inflammation phenomenon takes place. Once adhered on the biomaterial surface and releasing/exchanging cytokines signals, they differentiate into macrophages. Macrophages are a fundamental element in the immune system giving a crucial contribution to inflammation and host protection [82]. Furthermore, they are able to secret both angiogenic and growth factors that are particularly important for new blood vessel formation and tissue remodeling [68]. Such cells are strictly interacting with lymphocytes, another kind of white blood cell, involved in specific immune response. Lymphocytes are mainly classified in large granular ones (natural killer cells, NK) and small ones (T cells and B cells) that play an important role in cell-mediated immunity.

Cytokines

The response of the body to foreign agents or pathogens is managed by a great number of complex interactions between different kinds of cells involved in the immune system. Such cells interact with one another by delivering and replying to chemical signals called cytokines.

Cytokines (from the greek cyto- cell; and –kinos, movement) are a wide group of small proteins (but also exist in peptide and glycoprotein form) released by immune cells. They are very specific chemical messengers capable to interact with other cells via specific receptors of the target cell membrane in order to coordinate the immune response. Hence, together with mitogens, chemoattractants and growth factors, they provide the generation of natural drug delivery systems acting on the sustained release of biochemical signals to control wound healing [79].

The large family of cytokines includes a diverse collection of interleukins (IL), interferons (IFN) and growth factors. However, they are also classified in lymphokines, monokines, chemokines, and interleukins, depending from the supposed function or cell of secretion:

- Lymphokines - produced by lymphocytes;
- Monokines - produced by monocytes;
- Chemokines - chemotactic activities;
- Interleukins - manufactured by one leukocyte to act on other leukocytes.

Cytokines are mainly involved in the following actions:

- regulation of the expression of membrane proteins (including cytokine receptors);
- release of effector molecules: histamine release; antibody secretion - IgA, IgG1, and IgE synthesis; IL-1 synthesis; cytokine production; MHC Class II; and CAM expression;
- cell proliferation and differentiation;
- chemotaxis of neutrophils, monocytes, and T cells;
- inflammation;

- phagocytosis;
- death of tumor cells;
- elimination of pathogens.

Some of them, acting as chemical switches, are capable to turn specific immune cell types on and off. Chemokines are an interesting group of cytokines, which possess chemoattractant properties for specific cell types. Released by cells, they are capable to recruit other immune cells to the injury site for repairing the damaged zone. For this reason, they are recently studied for the formulation of new drugs to regulate the immune response. In particular, chemokines comprise four major families: CC, CXC, C, and CX3C [66]. In addition they are also involved in other processes such as hematopoiesis, angiogenesis, tumor metastasis, homing and differentiation of lymphocyte [80,82].
Some points regarding cytokines should be mentioned before continuing. Firstly, cytokines activity is redundant and different cytokines can trigger similar functions. They are produced in cascades; indeed cytokines are targets for other cells that will secrete other cytokines. Moreover, there could be synergistic and antagonistic effects between two or more cytokines acting contemporarily. Finally, many cell types can produce the same cytokines or each cytokine could stimulate many different cell types behavior.

Macrophages polarization

Among the myelomonocytic cells, macrophages show a relevant diversity and plasticity. Due to a high capacity to identify and interchange signals with lymphocytes, they are able to switch their phenotype functions going through a response modification [83-85]. Thus, depending on various stimuli, macrophages can undergo M1 or an alternative M2 activation [84,85]. Such phenotype shift, particularly relevant in macrophages, is called polarization. Briefly:

- M1 stimulated by toll-like receptors (TLR) and IFN-γ;
- M2 stimulated by IL-4/IL-13;
- They show a similar behavior with T cells that polarize in Th1 and Th2;
- M1 and M2 phenotypes show a quite different chemokine profiles.

The phenotype of M1 macrophages could be identified by a strong release of proinflammatory cytokines, a high microbicidal and tumoricidal activity, and a stimulation of Th1 cells response.
On the other hand, M2 phenotypes are characterized by immunoregulatory functions. They are particularly active on parasites control and encapsulation thanks to high phagocytic skills. M2 are mainly involved in tissue remodeling and repair, tumor progression, angiogenesis promotion [84,85]. The different properties of M2 are emphasized by three different versions of this phenotype: M2a, M2b, M2c. M2a is stimulated by interleukins IL-4 and IL-13 and promote Th2 response. Among M2 macrophages, M2a are the main involved in killing and encapsulation of parasites. M2b is stimulated by exposure to immune complexes and TLR or IL-1R. Together with M2c is the main phenotype involved in immunoregulation process. Finally M2c phenotype, stimulated by IL-10 interleukin, is essentially

associated to matrix deposition and tissue remodeling activities [85]. A schematic representation of the macrophages polarization is described in Figure 1.20.

M1-M2 polarization is reversible both *in vitro* and *in vivo* [86]. Furthermore, M1-M2 polarization switch often happens in pathologies where M1 activation leads to a continuous inflammation (proinflammatory properties) while M2 drives to soften an acute inflammation (anti-inflammatory properties).

Therefore, the scientific community is paying great attention to understand mechanisms and molecules associated with macrophage plasticity and polarization in order to develop new macrophage-focused therapeutic strategies [84]. In particular, from a Tissue Engineering point of view, it is enormously important to find suitable strategy to boost the M2 anti-inflammatory polarization with the aim of reducing the acute inflammation generated by biomaterial implantation [87].

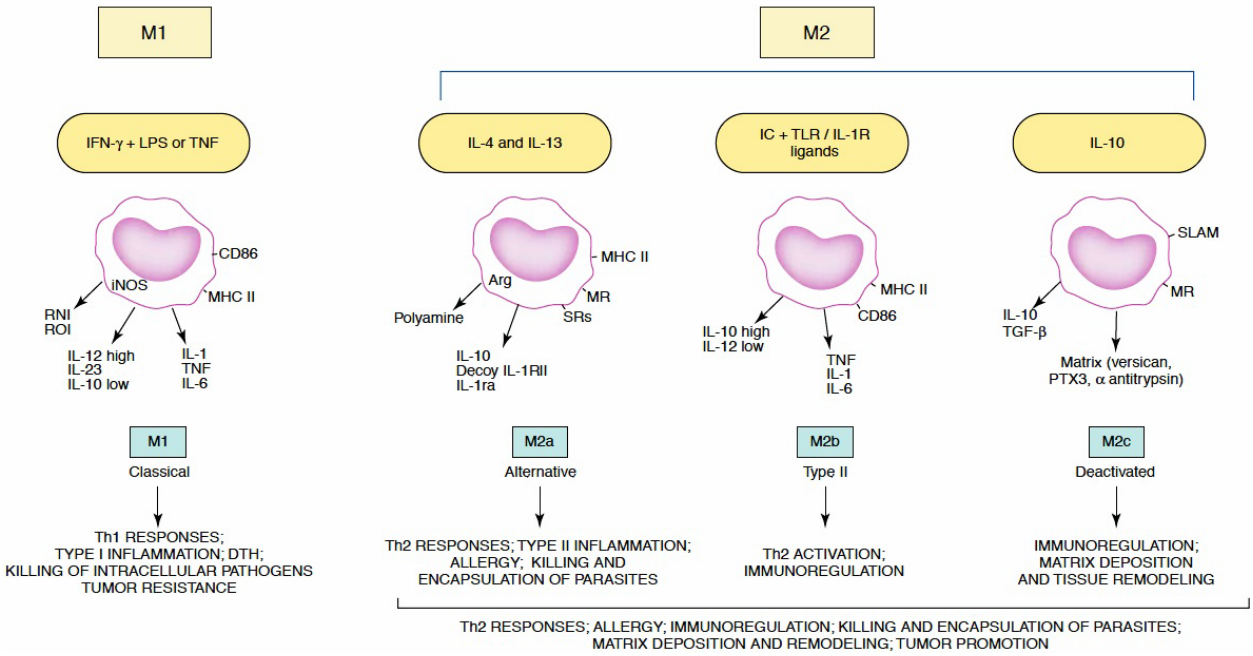

Figure 1. 20. Schematic representation of macrophages polarization. Adapted from [85].

1.7. References

[1]. Manji RA, Zhu LF, Nijjar NK, Rayner DC, Korbutt GS, Churchill TA, Rajotte RV, Koshal A, Ross DB. Glutaraldehyde-fixed bioprosthetic heart valve conduits calcify and fail from xenograft rejection. Circulation. 2006 Jul 25;114(4):318-27.

[2]. Song JJ, Ott HC. Organ engineering based on decellularized matrix scaffolds. Trends in Molecular Medicine 2011;17(8):424-32.

[3]. Langer R, Vacanti JP. Tissue Engineering. Science 1993;260:920-926.

[4]. Assis AC, Carvalho JL, Jacoby BA, Ferreira RL, Castanheira P, Diniz SO, Cardoso VN, Goes AM, Ferreira AJ. Time-dependent migration of systemically delivered bone marrow mesenchymal stem cells to the infarcted heart. Cell Transplantation 2010;19(2) 219-30.

[5]. Ross JM. Cell-Extracellular Matrix Interactions. In: Patrick CW, Mikos AG, Mc.Intre L, editors. Frontiers in Tissue Engineering. Oxford: Elsevier Science Ltd., 1998: 15-27.

[6]. Patterson J, Martino MM, Hubbell JA. Biomimetic materials in tissue engineering. Mater Today 2010;13:14–22.

[7]. Aguirre A, González A, Navarro M, Castaño O, Planell JA, Engel E. Control of microenvironmental cues with a smart biomaterial composite promotes endothelial progenitor cell angiogenesis. Eur Cell Mater. 2012 Jul 24;24:90-106; discussion 106.

[8]. d'Angelo I, Oliviero O, Ungaro F, Quaglia F, Netti PA. Engineering strategies to control vascular endothelial growth factor stability and levels in a collagen matrix for angiogenesis: The role of heparin sodium salt and the PLGA-based microsphere approach. Acta Biomaterialia 9 (2013) 7389–7398.

[9]. Melchels FPW, Domingos MAN, Klein TJ, Malda J, Bartolo PJ and Hutmacher DW. Additive manufacturing of tissues and organs Prog. Polym. Sci. 37 (2012) 1079–1104.

[10]. Lutolf MP, Gilbert PM, Blau HM. Designing materials to direct stem-cell fate. Nature. 2009 Nov 26;462(7272):433-41.

[11]. Daher JD, Chahine NO, Greenberg AS, Sgaglione NA, Grande DA. New methods to diagnose and treat cartilage degeneration. Nature Reviews Rheumatology 2009; 5 599-607.

[12]. Navarro M, Engel E, Planell JA, Amaral I, Barbosa M, Ginebra MP. Surface characterization and cell response of a PLA/CaP glass biodegradable composite material. J Biomed Mater Res A 2008;85:477–86.

[13]. Hench LL, Polak JM. Third-generation biomedical materials. Science. 2002 Feb 8;295(5557):1014-7.

[14]. Navarro M, Michiardi A, Castaño O,Planell JA. Biomaterials in orthopaedics. J R Soc Interface. 2008 October 6; 5(27): 1137–1158.

[15]. Williams DF. On the nature of biomaterials, Biomaterials 30 (2009) 5897–5909.

[16]. Holzapfel BM, Reichert JC, Schantz JT, Gbureck U, Rackwitz L, Nöth U, Jakob F, Rudert M, Groll J, Hutmacher DW. How smart do biomaterials need to be? A translational science and clinical point of view. Adv Drug Deliv Rev. 2013 Apr;65(4):581-603.

[17]. Woodruff, M. A.; Lange, C.; Reichert, J.; Berner, A.; Chen, F. L.; Fratzl, P.; Schantz, J. T.; Hutmacher, D. W. Bone tissue engineering: from bench to bedside. Materials Today. Oct 2012 15(10):430–435.

[18]. Jee WSS. Integrated Bone Tissue Physiology: Anatomy and Physiology. In: Cowin SC, editor. Bone Mechanics HANDBOOK. Boca Raton: CRC Press LLC, 2001: 1-1-1-68.

[19]. Stevens MM. Biomaterials for bone tissue engineering. Mat Today. 2008, 11,5,18-25.

[20]. Ackerman LV, Spjut HJ, Abell MR. Bones and joints. International academy of pathology monograph. Williams and Wilkins, Baltimore 1976, 236-299.

[21]. McCalden RW, McGeough JA, Court-Brown CM. 1997; Age-related changes in the compressive strength of cancellous bone. The relative importance of changes in density and trabecular architecture. J Bone Jt Surg 79: 421–427.

[22]. Hench LL, Wilson J. An Introduction to Bioceramics. Singapore: World Scientific; 1993; 25-40.

[23]. http://cnx.org/content/m46281/latest/

[24]. Reis RL, Cunha AM, Allan PS, Bevis MJ. Mechanical behavior of injection-molded starch-based polymers. Polym Adv Technol 1996;7:784–90.

[25]. Seal BL, Otero TC, Panitch A. Polymeric biomaterials for tissue and organ regeneration. Mater Sci Eng: R: Rep 2001;34:147–230.

[26]. Di Martino A, Sittinger M, Risbud MV. Chitosan: a versatile biopolymer for orthopaedic tissue-engineering. Biomaterials 2005; 26:5983–90.

[27]. Lee SB, Kim YH, Chong MS, Hong SH, Lee YM. Study of gelatincontaining artificial skin V: fabrication of gelatin scaffolds using a salt-leaching method. Biomaterials 2005;26:1961–8.

[28]. Mohanty AK, Misra M, Hinrichsen G. Biofibres, biodegradable polymers and biocomposites: an overview. Macromol Mater Eng 2000;276–277:1–24.

[29]. Doi Y, Kitamura S, Abe H. Microbial synthesis and characterization of poly(3-hydroxybutyrate-co-3-hydroxyhexanoate). Macromolecules 1995;28:4822–8.

[30]. Rezwan K, Chen QZ, Blaker JJ, Boccaccini AR. Biodegradable and bioactive porous polymer/inorganic composite scaffolds for bone tissue engineering. Biomaterials. 2006;27:3413-31.

[31]. Charles-Harris M, Koch MA, Navarro M, Lacroix D, Engel E, Planell JA. A PLA/calcium phosphate degradable composite material for bone tissue engineering: An in vitro study. J Mater Sci Mater Med. 2008;19:1503-1513.

[32]. Zein I, Hutmacher DW, Tan KC, Teoh SH. "Fused deposition modeling of novel scaffold architectures for tissue engineering applications", Biomaterials, 23:4, 1169-1185, 2002.

[33]. Ashammakhi N, Rokkanen P. Absorble polyglycolide devices in trauma and bone surgery. Biomaterials 1997;18:3–9.

[34]. Bergsma EJ, Rozema FR, Bos RRM, Debruijn WC. Foreign body reaction to resorbable poly(L-lactic) bone plates and screws used for the fixation of unstable zygomatic fractures. J Oral Maxillofac Surg 1993; 51:666–70.

[35]. Martin C, Winet H, Bao JY. Acidity near eroding polylactidepolyglycolide in vitro and in vivo in rabbit tibial bone chambers. Biomaterials 1996;17(24):2373–80.

[36]. Miller RA, Brady JM, Cutright DE. Degradation rates of oral resorbable implants (polylactates and polyglycolates): rate modification with changes in PLA/PGA copolymer ratios. J Biomed Mater Res. 1977 Sep;11(5):711-9.

[37]. Ulery BD, Nair LS, Laurencin CT. Biomedical Applications of Biodegradable Polymers. J Polym Sci B Polym Phys. 2011:15; 49(12): 832–864.

[38]. Pachence JM, Kohn J. Biodegradable Polymers. In: Lanza RP, Langer R, Vacanti JP, editors. Principles of Tissue Engineering. San Diego: Academic Press, 2000: 263-274.

[39]. Grizzi I, Garreau H, Li S, Vert M. Hydrolytic degradation of devices based on poly(DL-lactic acid) size-dependence. Biomaterials 1995; 16(4):305-311.

[40]. Hench LL, "Bioceramics," J Am Ceram Soc, 81(7):1705–28 (1998).

[41]. Kokubo T, Kushitani H, Sakka S, Kitsugi T, Yamamuro T. Solutions able to reproduce in vivo surface-structure changes in bioactive glass-ceramic A-W. J Biomed Mater Res. 1990;24(6):721–34.

[42]. Hench LL, Splinter RJ, Allen WC. Bonding mechanisms at the interface of ceramic prosthetic materials. J Biomed Mater Res Symp 1971;2:117–41.

[43]. Schepers E, de Clercq M, Ducheyne P, Kempeneers R. Bioactive glass particulate material as filler for bone lesions. J Oral Rehab 1991;18:439–52.

[44]. Gatti AM, Valdre G, OH A. Analysis of the in vivo reactions of a bioactive glass in soft and hard tissue. Biomaterials 1994;15:208–12.

[45]. Navarro M, Ginebra MP, Clement J, Martinez S, Avila G, Planell JA. Physico-chemical degradation of resorbable phosphate glasses stabilized with TiO2. J Am Ceram Soc 2003; 86:1345-52.

[46]. Navarro M, Ginebra MP, Planell JA. Cellular response to calcium phosphate glasses with controlled solubility. J Biomed Mater Res A 2003; 67:1009- 15.

[47]. Navarro M, Aparicio C, Charles-Harris M, Ginebra MP, Engel E, Planell JA. Development of a biodegradable composite scaffold for bone tissue engineering: physicochemical, topographical, mechanical, degradation, and biological properties. Adv Polym Sci 2006; 200:209-31.

[48]. Vila OF, Bag. JR, Navarro M, Alieva M, Aguilar E, Engel E, Planell JA, Rubio N, Blanco J. Calcium phosphate glass improves angiogenesis capacity of poly(lactic acid) scaffolds and stimulates differentiation of adipose tissue-derived mesenchymal stromal cells to the endothelial lineage. J Biomed Mater Res A 2013; 101:932-41.

[49]. Mouri.o V, Cattalini JP, Boccaccini AR. Metallic ions as therapeutic agents in tissue engineering scaffolds: an overview of their biological applications and strategies for new developments. J R Soc Interface 2012; 9:401-19.

[50]. Martin RA, Yne S, Hanna JV, Lee PD, Newport RJ, Smith ME, Jones JR. Characterizing the hierarchical structures of bioactive sol-gel silicate glass and hybrid scaffolds for bone regeneration. Philos Transct A Math Phys Eng Sci 2012; 370:1422-43.

[51]. Charles-Harris M. Development and Characterisation of Completely Degradable Composite Tissue Engineering Scaffolds. PhD Thesis ISBN: 9788469103852.

[52]. Hutmacher DW. Scaffolds in tissue engineering bone and cartilage. Biomaterials. 2000 Dec;21(24):2529-43.

[53]. Yang S, Leong KF, Du Z, Chua CK.The Design of Scaffolds for Use in Tissue Engineering. Part I. Traditional Factors‖, Tissue Eng, 7:6, 679 -689, 2001.

[54]. Vander AJ, Shermann JH, Luciano DS. Human physiology. New York: McGraw-Hill, 1985. p. 341}66.

[55]. Leong KF, Cheah CM, Chua CK. Solid freeform fabrication of three-dimensional scaffolds for engineering replacement tissues and organs. Biomaterials. 2003 Jun;24(13):2363-78.

[56]. Robinson B, Hollinger JO, Szachowicz E, Brekke J. Calvarial bone repair with porous d,l-polylactide. Otolaryng Head Neck 1995;112(6):707–13.

[57]. Boyan BD, Hummert TW, Dean DD, Schwartz Z. Role of material surfaces in regulating bone and cartilage cell response. Biomaterials 1996;17(2):137–46.

[58]. Hollister SJ. Porous scaffold design for tissue engineering. Nat Mater 2005;4:518–24.

[59]. Karageorgiou V, Kaplan D. Porosity of 3D biomaterial scaffolds and osteogenesis. Biomaterials 2005;26:5474–91.

[60]. Yannas IV, Lee E, Orgill DP, Skrabut EM, Murphy GF. Synthesis and characterization of a model extracellular matrix that induces partial regeneration of adult mammalian skin. Proc Natl Acad Sci USA 1989;86:933.

[61]. Kim SS, Utsunomiya H, Koski JA, Wu BM, Cima MJ, Sohn J, Mukai K, Griffith LG, Vacanti JP. Survival and function of hepatocytes on a novel three-dimensional synthetic biodegradable polymer scaffold with an intrinsic network of channels. Ann Surg 1998;228(1):8–13.

[62]. Rout PGJ, Tarrant SF, Frame JW, Davies JE. Interaction between primary bone cell cultures and biomaterials. Part 3: a comparison of dense and macroporous hydroxyapatite. In: Pizzoferratto A, Ravaglioli PG, Lee AJC, editors. Bioceramics and clinical applications. Amsterdam: Elsevier, 1988. p.591–6.

[63]. Lange R, Luthen F, Beck U, Rychly, Baumann J A, Nebe B. Cell-extracellular matrix interaction and physico-chemical characteristics of titanium surfaces depend on the roughness of the material. Biomol. Eng. 19:2-6 255-261, 2002.

[64]. Cassinelli, C, Morra M, Bruzzone G, Carpi A, Di Santi G, Giardino R, Fini M. Surface chemistry effects of topographic modification of titanium dental implant surfaces: 1. Surface analysis, Int. J. Oral & Maxillofac. Impl. 18:1, 46-50, 2003.

[65]. Ventre M, Causa F, Netti PA. Determinants of cell–material crosstalk at the interface: towards engineering of cell instructive materials. J R Soc Interface 2012;9(74):2017–32.

[66]. Ma PX, Zhang R, Xiao G, Franceschi R. Engineering new bone tissue in vitro on highly porous poly(alpha-hydroxyl acids)/hydroxyapatite composite scaffolds. J Biomed Mater Res. 2001 Feb;54(2):284-93.

[67]. Luciani A, Guarino V, Ambrosio L, Netti PA. Solvent and melting induced microspheres sintering techniques: a comparative study of morphology and mechanical properties. J Mater Sci Mater Med. 2011 Sep;22(9):2019-28.

[68]. Salerno A, Guarnieri D, Iannone M, Zeppetelli S, Netti PA. Effect of micro- and macroporosity of bone tissue three-dimensional-poly(epsilon-caprolactone) scaffold on human mesenchymal stem cells invasion, proliferation, and differentiation in vitro. Tissue Eng Part A. 2010 Aug;16(8):2661-73.

[69]. Bhardwaj N, Kundu SC. Electrospinning: A fascinating fiber fabrication technique. Biotechnology Advances 2010 May-Jun;28(3):325-347.

[70]. Dias MR, Fernandes PR, Guedes JM, Hollister SJ. Permeability analysis of scaffolds for bone tissue engineering.

[71]. Hutmacher DW, Sittinger M, Risbud MV. Scaffold-based tissue engineering: rationale for computer-aided design and solid free-form fabrication systems. Trends Biotechnol. 2004 Jul;22(7):354-62.

[72]. Melchels FP, Feijen J, Grijpma DW. A poly(D,L-lactide) resin for the preparation of tissue engineering scaffolds by stereolithography. Biomaterials. 2009 Aug;30(23-24):3801-9.

[73]. Sachs EM, et al., Three-dimensional printing techniques, US Patent # 5,204,055.

[74]. Butscher A, Bohner M, Hofmann S, Gauckler L, Müller R. Structural and material approaches to bone tissue engineering in powder-based three-dimensional printing. Acta Biomater. 2011 Mar;7(3):907-20.

[75]. Lam CX, Mo XM, Teoh SH and Hutmacher DW. Scaffold development using 3D printing with a starch-based polymer. Mater Sci Eng: C 2002; 20(1-2):49-56.

[76]. Taboas JM, Maddox RD, Krebsbach PH, Hollister SJ. Indirect solid free form fabrication of local and global porous, biomimetic and composite 3D polymer–ceramic scaffolds. Biomaterials 2003;24:181-94.

[77]. Xiong Z, Yan Y, Wang S, Zhang R, Zhang C. Fabrication of porous scaffolds for bone tissue engineering via low-temperature deposition, Scripta Mater 2002; 46 (11):771–776.

[78]. Mironov V, Kasyanov V, Drake C, Markwald RR. Organ printing: promises and challenges. Regen Med 2008;3:93–103.

[79]. Anderson JM, Rodriguez A, Chang DT. Foreign body reaction to biomaterials. Semin Immunol. 2008; 20(2): 86–100.

[80]. Mountziaris PM, Spicer PP, Kasper FK, Mikos AG. Harnessing and modulating inflammation in strategies for bone regeneration. Tissue Eng Part B Rev 2011;17:393-402.

[81]. Zhou H, Lawrence JG, Bhaduri SB. Fabrication aspects of PLA-CaP/PLGA-CaP composites for orthopedic applications: a review. Acta Biomater. 2012,8(6):1999-2016.

[82]. Gordon S, Martinez FO. Alternative activation of macrophages: mechanism and functions. Immunity. 2010;32(5):593–604.

[83]. Biswas SK, Mantovani A. Macrophage plasticity and interaction with lymphocyte subsets: cancer as a paradigm. Nat Immunol. 2010 Oct;11(10):889-96.

[84]. Sica A, Mantovani A. Macrophage plasticity and polarization: in vivo veritas. J Clin Invest. 2012;122(3):787–795.

[85]. Mantovani A, Sica A, Sozzani S, Allavena P, Vecchi A, Locati M. The chemokine system in diverse forms of macrophage activation and polarization. Trends Immunol. 2004 Dec;25(12):677-86.

[86]. Saccani A, Schioppa T, Porta C, Biswas SK, Nebuloni M, Vago L, Bottazzi B, Colombo MP, Mantovani A, Sica A. p50 nuclear factor-kappaB overexpression in tumor-associated macrophages inhibits M1 inflammatory responses and antitumor resistance. Cancer Res. 2006;66(23):11432–11440.

[87]. Vasconcelos DP, Fonseca AC, Costa M, Amaral IF, Barbosa MA, Águas AP, Barbosa JN. Macrophage polarization following chitosan implantation. Biomaterials. 2013 Dec;34(38):9952-9.

Chapter 2 - Relevance of PEG in PLA-based blends for Tissue Engineering 3D-printed scaffolds

2.1. Introduction

Understanding the impact of materials on the fabrication of 3D structures, and dissecting the right fabrication technique and conditions is of paramount importance to optimize both 3D scaffolds' production and performance. Rapid prototyping (RP) techniques, in particular, low temperature nozzle-based dispensing systems are an interesting option that allows scaffolds production under non-aggressive processing conditions. Nozzle-based dispensing systems enable the fabrication of scaffolds with well defined and reproducible architectures, and ultimately, the production of customized scaffolds adapted to patient-specific needs [1-3]. These direct printing systems build 3D structures following a layer-by-layer approach, dispensing the material solution or slurry accordingly to a previously designed geometry and internal architecture [1-7].

Curiously, although direct printing techniques have been widely used to fabricate 3D porous polymer structures [4-7], printing of polylactic acid (PLA), a well-known and currently used biodegradable polymer for the development of 3D scaffolds [8,9], has been barely reported [10,11]. In the case of PLA, keeping the right solution viscosity at low temperature during the entire printing process is of paramount importance and most of the times it represents a challenging task.

In order to maintain the right viscosity of the PLA-printing ink, two methods are mainly acknowledged: a) increasing the processing temperature or b) using a plasticizer. Using the right plasticizer is most advantageous since it enables working at low temperatures without causing any thermal degradation to the polymer. Different biodegradable as well as non-biodegradable plasticizers have been used to lower the glass transition temperature, increase ductility, and improve processing of PLA [12]. Among them, polyethylene glycols (PEG), especially low molecular weight PEG, has been reported as one of the most efficient plasticizers for PLA. Furthermore, PEG is a hydrophilic, biocompatible polymer that has been used for many applications from industrial manufacturing to biotechnology [13,14]. Similarly to PLA, PEGs are also soluble in chloroform. Thus, it is possible to obtain homogeneous PLA/PEG blends for the fabrication of 3D porous scaffolds, in particular by low temperature nozzle based 3D printing.

Incorporation of PEG in the PLA solution not only facilitates scaffolds printing process by means of its plasticizing effect but also introduces structural and physico-chemical changes to the resultant scaffolds. Various studies on the structural/thermal and mechanical properties of PLA/PEG blends and block copolymer systems of PLA with PEG have been reported [15-17]. However, the effect of PEG on the final structural, surface and mechanical properties of 3D scaffolds processed by RP has not been fully explored. This work aims to study the effect of PEG concentration on PLA/PEG blends and its relevance on the development of porous scaffolds by 3D printing, especially on their final structural and surface

features. Furthermore, owing to PLA's lack of bioactivity, it was also combined with a calcium phosphate based biodegradable and bioactive glass [18-20] in order to develop PLA/PEG/glass bioactive composite scaffolds. The effect of PEG on the distribution of the glass particles in the PLA matrix, and the polymer/particle interface was also studied in this work.

2.2. Materials and Methods

2.2.1. Materials

Poly(95L/5DL)lactic acid (Purasorb, PURAC) and PEG (Mw=400 Da; Sigma Aldrich) were dissolved in chloroform (5%w/v) with various PEG concentrations (0, 5, 10, 20% w/w) on an orbital mixer during 48h and combined to obtain a homogeneous polymer blend solution. A completely degradable, calcium phosphate glass with the following molar composition: $44.5P_2O_5$-$44.5CaO$-$6Na_2O$-$5TiO_2$, coded G5 was used in the form of particles (< 40 μm) to elaborate the PLA/PEG/G5 composite materials [9,18] G5 is a bioactive glass that has shown outstanding in vitro and in vivo results and has successfully improved PLA biological response [19, 20].

2.2.2. Scaffolds fabrication

A nozzle-deposition system also known as a direct-print tool (Tissue Engineering 3Dn-300, Sciperio/nScrypt Inc. Orlando, Florida; available in the Rapid Prototyping service of the Biomedical Networking Center, CIBER-BBN and IBEC www.ibecbarcelona.eu/biomaterials) was used to fabricate the 3D scaffolds. It utilizes a computer-aided design/computer-aided-manufacturing (CAD/CAM) approach to build layer-by-layer three-dimensional structures. Orthogonal displaced doubled layer scaffolds with distance between struts D=375 ± 25 μm were fabricated. Polymer blends containing 5, 10 and 20% (w/w) of PEG and a PLA/PEG/G5 composite as described in Table 2.1 were used. A printing pressure in a range between 40-80 psi, a motor speed of 7-10 mm/sec, and a G27 (200 μm) nozzle were used to print the polymer solutions. Both pressure and motor speed were tuned accordingly to the viscosity of each blend solution. The syringe temperature was set at 40±5ºC by using a heating jacket, and room temperature was kept at 25±2ºC.

Material	Polymer matrix (w/w%)		G5 particles (w/w%)
	PLA	PEG	
PLA/PEG 95/5	95	5	---
PLA/PEG90/10	90	10	---
PLA/PEG80/20	80	20	---
PLA/G5 [a]	100	---	50
PLA/PEG/G5 [a]	95	5	50

Table 2. 1. Composition of the studied materials. [a]The percentages shown for the polymer matrix of PLA/G5 and PLA/PEG/G5 corresponds to 50% of the total weight of the scaffold.

2.2.3. Scaffolds characterization

Materials characterization was conducted on both three dimensional RP structures and films in order to better analyze the surface properties. Films were made by solvent casting in an attempt to recreate the procedure followed to print the struts of 3D scaffolds by nozzle-based rapid prototyping. Materials were combined according to the compositions shown in Table 2.1.

2.2.3.1. Morphological SEM study

Scaffolds and films morphological observation was carried out by scanning electron microscopy (SEM, JEOL JSM 6400, Tokyo, Japan). In both cases, surface morphology of the polymer matrix as well as glass distribution was observed. In the case of scaffolds, SEM observation permitted a qualitative evaluation of the effect of PEG on the geometrical parameters of the final structures. Image J software was used to measure struts and pores size. In the case of the polymer films, SEM observation after t= 0, 2, 4, 6 and 8 weeks was carried out to visualize possible surface changes during degradation.

2.2.3.2. Porosity

The theoretical volume porosity percentage ($\%Vol_{theoretical}$) was calculated for each scaffold using the initially designed geometries based on a unit cube, whereby the strut diameter and spacing between layers were equal (i.e., no overlapping due to the fusion between struts from one layer to the adjacent one was assumed).

$$\%Vol_{theoretical} = (Va - Vt) / Va \times 100\% \quad (1)$$

where V_t is the true volume (mm^3) ($=V_cN_cN_l = (Ø^2/4)\ \pi\ LN_cN_l$); V_c is the cylinder volume (mm^3); and Va is the apparent volume (mm^3) = Lwh; L = ØNc + D(Nc - 1); D is the distance between struts; $h = ØN_l$. Therefore,

$$\%Vol_{theoretical} = (1 - (Ø^2/4)\ \pi N_cN_l /(wh)) \times 100\% \quad (2)$$

where Ø, L, w and h refer to the strut diameter, strut length, scaffold width and scaffold height in millimeters, respectively. Furthermore, N_c represents the number of cylinders (struts) per layer, while N_l represents the number of layers per scaffold.

2.2.3.3. Mechanical properties of the 3D-scaffolds

A universal testing machine (Zwick-Roell, Zwicki-Line Z0.5TN) with a 200N load cell was used to evaluate the compressive mechanical properties of the developed scaffolds. Cylindrical scaffolds (4 mm

diameter x 2 mm height) were cored from larger 3D printed blocks. The real dimensions of the specimens were measured before test. For each material composition, three samples were tested. A speed of 1 mm min-1 was used and a preloading of 0.5N was applied. Stress-strain data were computed from load displacement measurements. The compressive strength at 40% deformation (σ40%) was reported.

2.2.3.4. Surface Topography

Surface topography as well as glass distribution at the surface of the composite material were observed by optical interferometry (WYCO NT1100, Veeco), a non-destructive technique that allows measuring surface topography in 3D. The studied parameters were: surface roughness (S_a), and skewness (S_{sk}), or the asymmetry of the surface about the mean plane. The study was carried out in films as previously mentioned. Three samples of each material (PLA/PEG 95/5, 90/10, 80/20, PLA/G5 and PLA/PEG/G5 films) with the following dimensions (2 x 2 x 0.1 cm^3) were used for the study. Three different zones (124 × 96 μm^2) were analyzed for each material.

2.2.3.5. Mechanical properties by atomic force microscopy (AFM)

Evaluation of the surface mechanical properties at the nanoscale was carried out by atomic force microscopy (AFM) using a force mapping method. The surface morphology and mapping of the Young's modulus (E) of the PLA/PEG blends and composites at the nanoscale were explored using an innovative AFM technique, Peak Force QNM (Quantitative Mechanical Property Mapping at the Nanoscale) [21].
Samples with the following dimensions (10 x 10 x 1 mm^3) were sticked onto Teflon discs with epoxy glue and images were captured under ambient condition. For the polymeric materials a silicon oxide tip (VistaProbes T300R-W with 40nN/nm nominal spring constant) mounted on a stainless steel cantilever (Bruker Corporation, CA, USA) was used, while a diamond one was used to analyze the composite material. Tip radius of 2 nm and 18 nm for the polymeric and the composite materials respectively were used. Probe calibration was carried out by thermal noise method and 40x40 μm^2 modulus images were achieved. All AFM data analysis and image processing were carried out with NanoScope software version 8.10 (Veeco Instruments Inc.).

2.2.3.6. Wettability

Contact angle measurements were performed to evaluate the materials wettability. The sessile drop method was used to measure the contact angle by depositing ultrapure water (3µl; Milli-Q; Millipore, USA) on the surfaces of the polymer films using a contact angle measurement system (OCA 20; Dataphysics, GmbH, Germany). As in the case of interferometry and AFM, polymer films were used to perform the measurements. Three samples of each material (PLA/PEG 95/5, 90/10, 80/20, PLA/G5 and PLA/PEG/G5) with the following dimensions (3 x 1 x 0.1 cm^3) were used for the study. Three

measurements were performed in each specimen, and independent experiments were conducted on three different samples.

2.2.4. In vitro degradation study

In vitro degradation studies were performed by immersing the films in simulated body fluid (SBF), an acellular solution whose chemical composition is similar to that of blood plasma [22]. Samples were immersed in SBF at 37ºC keeping a volume/mass ratio of 250/1 for 8 weeks. The degradation of the materials was evaluated by means of weight loss measurements, DSC and SEM analysis.

2.2.4.1. Weight loss

Materials' weight loss during degradation was calculated from the changes in the specimens' dry weight before and after the incubation time periods. After 2, 4, 6 and 8 weeks of immersion in SBF, the samples were removed from the fluid, rinsed with distilled water and dried in a furnace at 37°C for 12h or until complete weight stabilization. The percentage of weight loss was computed according to the following equation:

$$\%W = 100 \times (Wo - Wt)/Wo,$$

where Wo is the initial dry weight and Wt is the dry weight of the specimen at different degradation times. Values are expressed as the average of three replicates.

2.2.4.2. Differential Scanning Calorimetry

A differential scanning calorimeter (DSC-2910, TA Instruments) was used to determine the thermal properties of the materials after 0, 4 and 8 weeks of degradation. Samples (5-10 mg) from PLA/PEG and PLA/PEG/G5 films, were firstly heated from 10ºC to 200ºC then cooled to -25ºC and heated up to 200ºC, at a heating rate of 10ºC/min in aluminum pans with nitrogen as a purge gas. The resulting DSC curves were analyzed to determine the glass transition (Tg) temperature, and the crystallinity (Xc) of the polymer. Tg values were taken from the thermograms corresponding to the second heating cycle whereas for the Xc calculation enthalpy values were taken from the first cycle. The crystallinity percentage was calculated using the reference heat of enthalpy (93.1 J/g) for theoretically 100% crystalline PLA [23]. In the case of the composite materials, the heat of fusion (ΔHm) and the heat of crystallization (ΔHc) of the samples were recalculated according to the amount of inorganic phase present at each time. The new heats of fusion and crystallization ($\Delta H'f$ and $\Delta H'c$) were calculated as:

$$\Delta H' = \Delta H/Xp,$$

where Xp is the fraction of polymer matrix present at each time. This fraction was determined by means of a standard ash method (data not shown). The specimens were heated in an electric furnace at 600 ºC for 3 h to burn out the organic matrix and then reweighed in order to calculate the inorganic fraction.

2.2.5. Statistical analysis

All the results are described as means ± standard deviation (SD). The statistical significance was determined by the one-way analysis of variance (ANOVA) at a significance level of less than 0.05 ($p < 0.05$).

2.3. Results

2.3.1. Morphological evaluation

Figure 1 shows the morphology and geometrical accuracy of the different 3D structures. It reveals clear differences between pore size and strut thickness of the three scaffolds depending on PEG concentration. Indeed, by increasing PEG concentration the originally designed squared pores (Figure 2.1a) turned into slightly rounded ones (Figure 2.1c). Figure 1e summarizes differences found on struts and pores size according to the amount of PEG added in the blend. Strut size increased from 52.09 ± 6.39 μm to 80.32 ± 23.13 μm while pore area decreased from 161.16±5.19 mm^2 to 121.8 ±3.25 mm^2 for the 5 and 20% blends respectively. A noteworthy increase of the SD in the strut thickness of 20% blends due to their non-uniformity was observed. In the case of the PLA/PEG/G5 material (Fig. 1d), the plasticizing effect of PEG allowed a good distribution and embedment of the glass particles in the polymer matrix. Also, it was observed that the theoretical design was reproduced properly showing well-defined orthogonal pores.

Figures 2a and c show SEM images of PLA and PLA/PEG 80/20 films before the degradation process. Remarkable differences in terms of their surface morphology were observed. PLA showed a smooth and flat surface whereas the blend with 20% of PEG showed a rather bumpy and rough surface with irregular coarse protuberances. After 8 weeks of immersion in SBF, PLA surface (Fig. 2.2b) did not show any degradation sign and remained similar to the one observed before immersion in the fluid; conversely, the PLA/PEG 80/20 showed clear signs of intense degradation such as numerous cracks at the surface (indicated with white arrows in Fig. 2.2d). After 8 weeks PLA/PEG 80/20 samples were significantly damaged and broken into pieces.

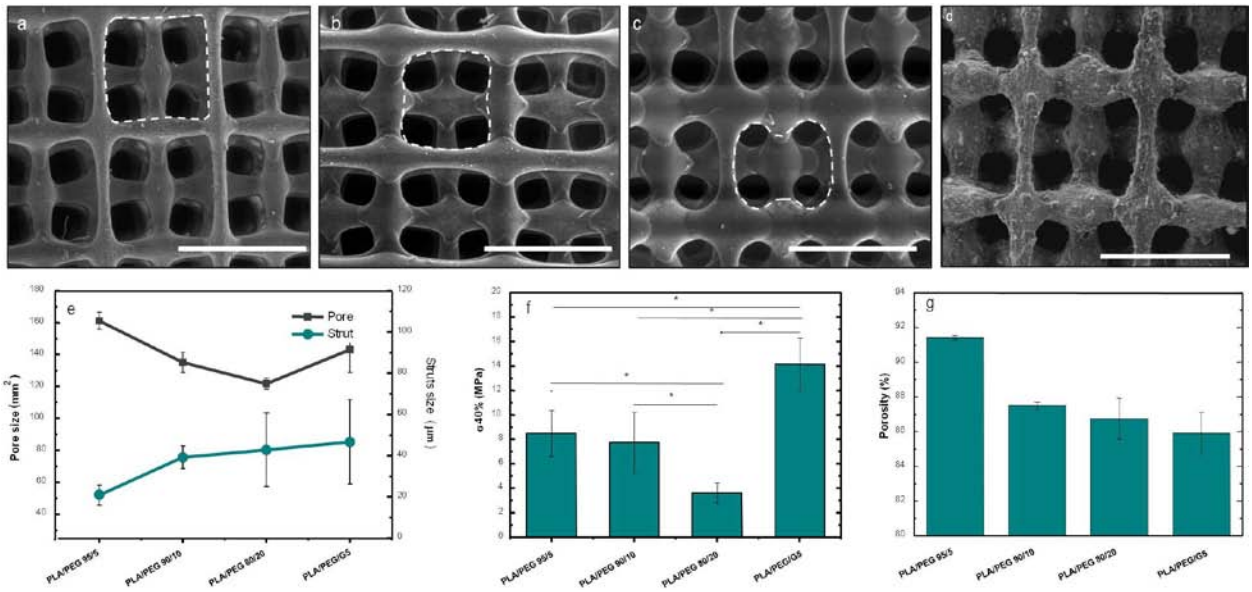

Figure 2. 1. SEM images of 3D-printed scaffolds. Axial view of a) PLA/PEG 95/5, b) PLA/PEG 90/10, c) PLA/PEG 80/20, d) PLA/PEG/G5 structures. Higher concentrations of PEG led to thicker struts and smaller rounded pores. Scale bar indicates 500µm. e) **Variation of struts and pore size** of 3D scaffolds printed with the studied PLA/PEG blends (5, 10 and 20% PEG) and PLA/PEG/G5; f) **Compressive strength at 40% deformation** (σ40%) for PLA/PEG (5, 10, 20% of PEG and PLA/PEG/G5); g) **theoretical volume porosity percentage** of the 3D-printed scaffolds with the different PLA/PEG blends and PLA/PEG/G5. The values marked with an asterisk (*) showed statistical significant differences ($p \leq 0.05$).

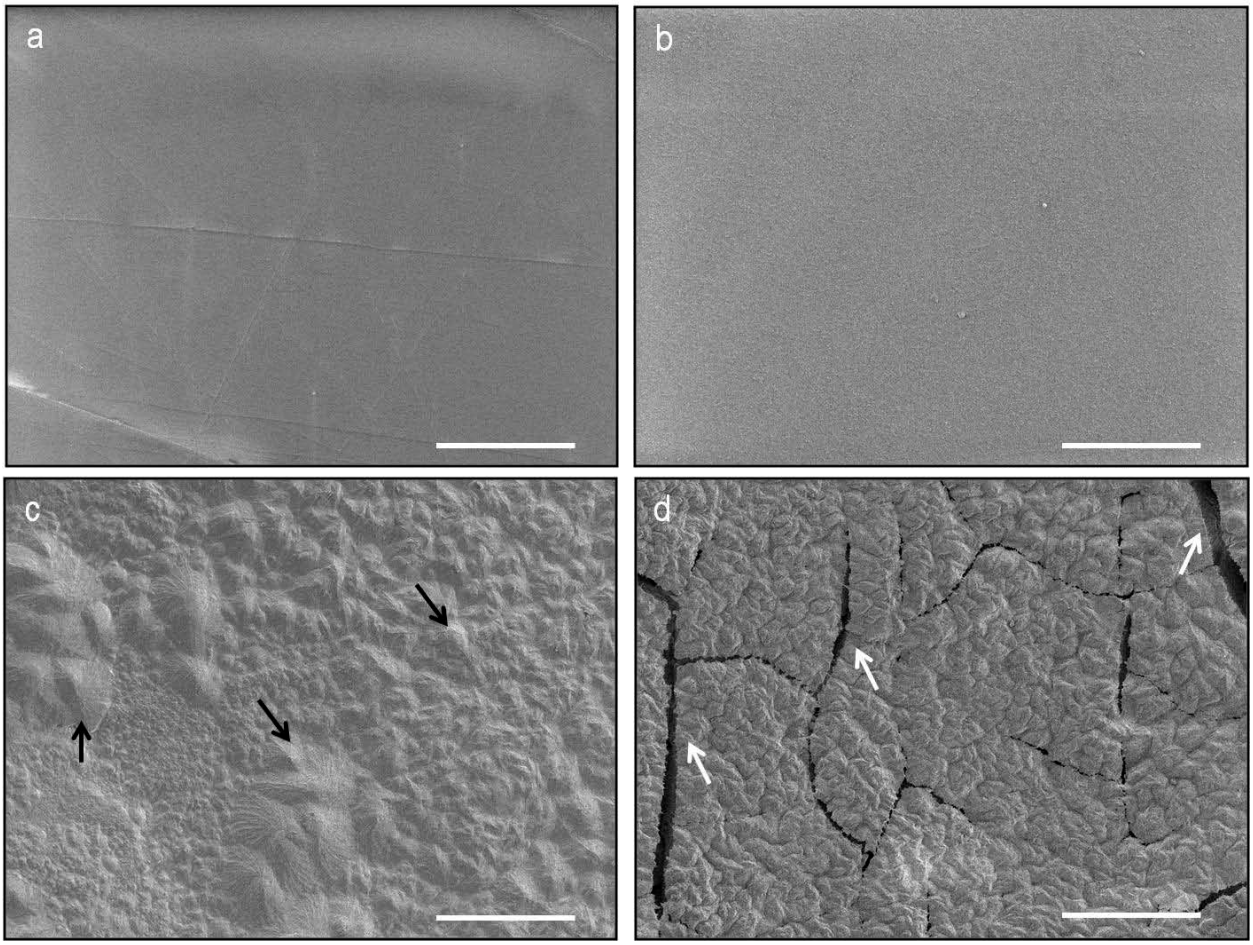

Figure 2. 2. SEM images of PLA films a) before and b) after 8 weeks of degradation. PLA/PEG 80/20 films c) before and d) after 8 weeks of degradation. Black arrows indicate the presence of PLA spherulites while white arrows show the cracks formed between spherulites peaks due to material degradation. Scale bar indicates 50 µm.

2.3.2. Porosity evaluation

Figure 1g shows the theoretical volume porosity percentages of the 3D-printed structures fabricated with the different PLA/PEG blends. As observed scaffolds porosity decreased from 91.4% to 86.75% as PEG concentration increased from 5 to 20% (w/w), while the composite scaffold PLA/PEG/G5 shows a value of 85.91%.

2.3.3. Scaffolds' Mechanical Properties

Figure 2.1f shows the data corresponding to the compressive strength at 40% deformation (σ40%) for the polymeric scaffolds with 5, 10 and 20%w/w of PEG and for the composite one (PLA/PEG/G5). Compressive strength values decreased from 9.11 ± 1.19 MPa to 3.63 ± 0.82 MPa for the scaffolds with 5 and 20% PEG respectively. The composite scaffold PLA/PEG/G5 showed the highest compressive strength.

2.3.4. Surface Topography

As seen in Figure 2.3, interferometry provided a qualitative morphological evaluation of the surface of the studied materials. PLA showed the smoothest topography (Fig. 2.3a). Figure 2.3 a-d shows the influence of the different PEG concentrations on PLA surface topography. Addition of PEG induced the formation of spherulites as indicated by the arrows. Moreover, by increasing the concentration of PEG, the number of peaks increased while the distance between them and their height decreased. Figures 2.3a and d, showing the surface of PLA and PLA/PEG 80/20, are in good agreement with the SEM images shown in Figure 2.2.

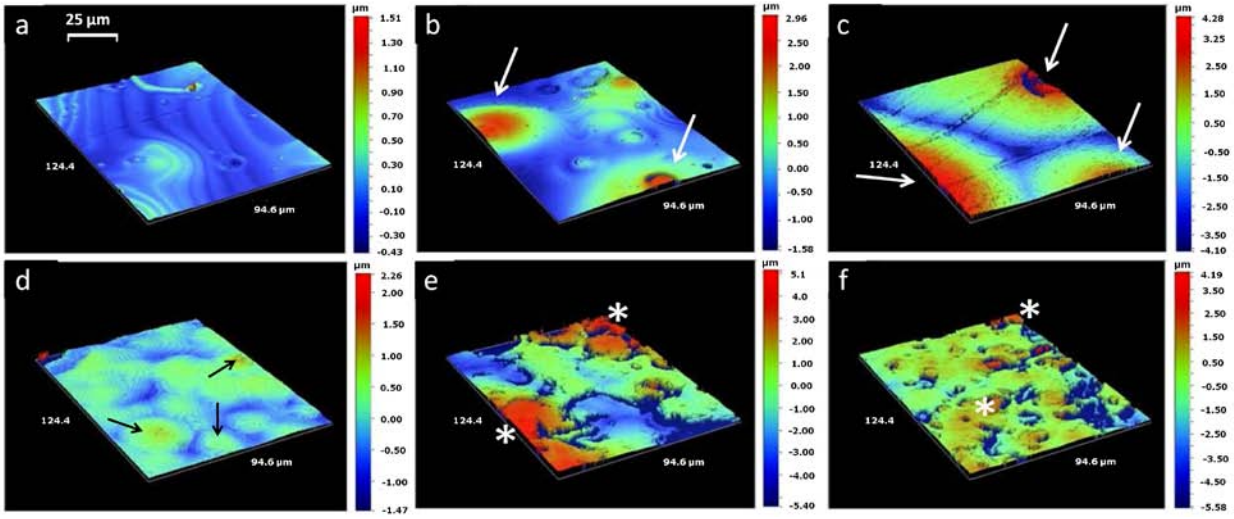

Figure 2. 3. Interferometry images of the surface of a) PLA, b) PLA/PEG 95/5, c) PLA/PEG 90/10, d) PLA/PEG 80/20, e) PLA/G5, f) PLA/PEG/G5 films. Arrows indicate spherulites domains in b) PLA/PEG 95/5, c) PLA/PEG 90/10 d) PLA/PEG 80/20. Asterisks indicate the presence of glass particles in e) PLA/G5, f) PLA/PEG/G5.

Composite materials (PLA/G5 and PLA/PEG/G5) displayed in Figures 3e and f, exhibited a significantly rougher topography. PLA/G5 seemed to be more wrinkled than its PLA/PEG/G5 counterpart. Asterisks in Figures 2.3e, f show the presence of G5 particles distributed and embedded in the polymer matrix. PLA/G5 showed the highest peaks.

Table 2.2 displays the values obtained for the topography study. Interferometry measurements showed that the average roughness of PLA (117.72 ± 60.50 nm) increased significantly with the addition of G5 glass particles and PEG (PLA/G5=1401.81±570.59 nm and PLA/PEG/G5=1003.89±228.45 nm). The polymeric blends showed an increase of their surface roughness (S_a) values with PEG concentration. Nevertheless, PLA/PEG 80/20, the material with highest PEG concentration showed the lowest Sa value. S_{sk} values indicated a higher surface asymmetry when 5% PEG was added to PLA, while both composite materials (PLA/G5 and PLA/PEG/G5) revealed negative S_{sk} values.

Material	S_a (nm)	S_{sk}	Young modulus by AFM (GPa)	Distilled and Deionized Water (°)
PLA	117.72±60.50	0.79±0.66	0.87	83.77±0.77*
PLA/PEG 95/5	147.12±29.11	1.08±0.55	2.5§ and 6.2	76.56±1.61*
PLA/PEG 90/10	377.96±121.22	0.37±0.71	5.6§ and 6.9	79.±8.2
PLA/PEG 80/20	296.22±34.58	0.34±0.42	18.3	68.±13.4
PLA/G5	1401.81±570.59	-0.5±0.17	16.2	77.57±7.58
PLA/PEG/G5	1003.89±228.45	-0.03±0.52	20	60.33±8.57*

Table 2. 2. Surface properties for the studied materials. S_a = average roughness, S_{sk} = skewness. The values marked with the § correspond to the Young modulus calculated in the dark zones as indicated in Figure 4. The values marked with the asterisk (*) showed statistical significant differences between them ($p \leq 0.05$).

2.3.5. Mechanical evaluation by AFM

Surface Young's modulus values for the studied blends are shown in Table 2.2. It can be appreciated that the Young's modulus increased by increasing the concentration of PEG. In particular the Young's modulus value for pure PLA samples was 0.87 GPa while for PLA/PEG 80/20 a modulus of 18.3 GPa was obtained. The presence of 50% of G5 particles into the polymer matrix increased the Young's modulus to 16.2 GPa.

Moreover, the addition of both PEG and G5 led to a synergistic effect as observed in the case of the PLA/PEG/G5 composite (E = 20 GPa). According to AFM results, the blends containing 5 and 10% of PEG showed a "bimodal distribution" of the Young's modulus. A Peak Force QNM-modulus image (scanning area 40 μm × 40 μm) of PLA/PEG 90/10 blend is shown in Figure 2.4. In this case, the presence of two different E values was observed, a high modulus corresponding to bright (light-colored) and a low modulus for the dark (dark-colored) regions which are intercalated and are indicated by white arrows.

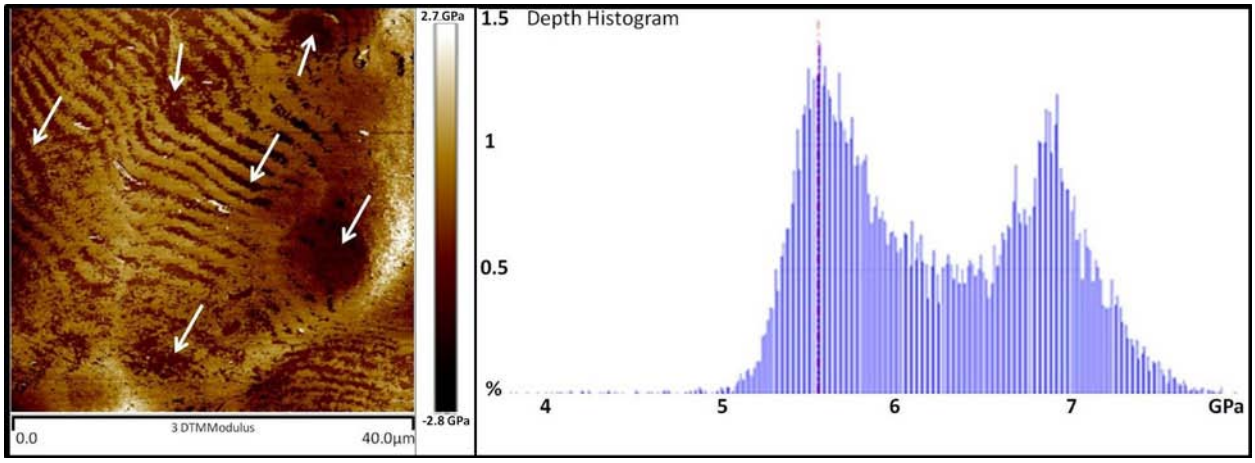

Figure 2. 4. Mechanical evaluation by AFM. Image showing a bimodal distribution of the Young modulus (on the left); white arrows indicate the regions with lower E (darker regions). Histogram for the PLA/PEG 90/10 sample (on the right). E value histogram shows two very well defined peaks corresponding to the two "phases" that appear in the image. In this case, the mean values for the dark and the bright coloured regions were 5.6 GPa and 6.9 GPa respectively.

2.3.6. Contact angle evaluation

Contact angle values for the studied materials are shown in Table 2.2. Overall, the presence of PEG decreased the contact angle values of the polymer blends in comparison to pure PLA. As observed, the presence of G5 increased the wettability of the PLA surface. Furthermore, the combination of PEG and G5 glass into the PLA matrix also led to a clear decrease of the contact angle.

2.3.7. Weight loss

Weight loss percentages of the studied samples along in vitro degradation are recorded in Figure 2.5a. Overall, the weight loss curves showed the effect of both PEG and G5 particles on the degradation of PLA/PEGs and PLA/PEG/G5 materials. In the case of the materials with PEG, a visible weight loss was observed after the first two weeks of immersion in SBF. The concentration of PEG in the polymer blends clearly influenced the samples weight loss showing higher degradation rates at higher PEG concentrations.

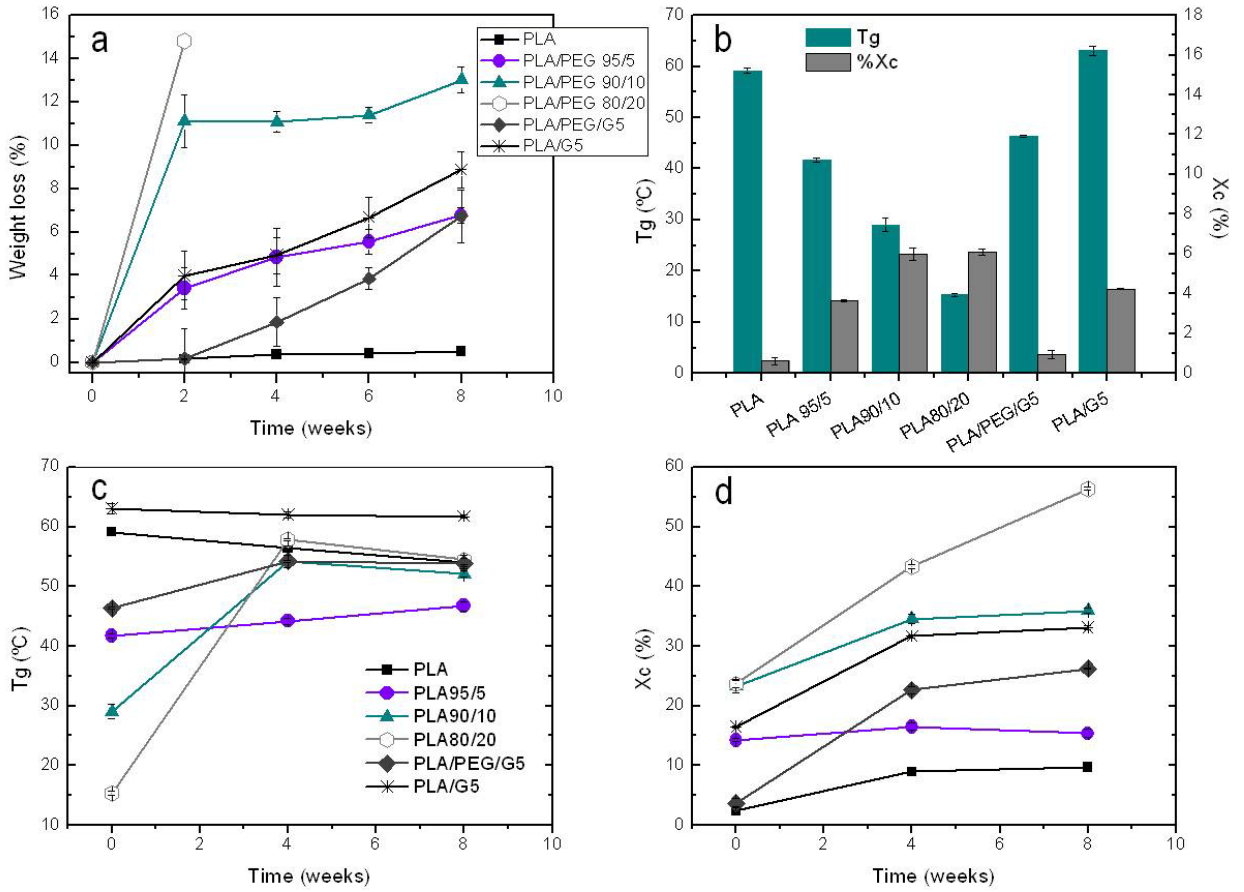

Figure 2. 5. (a) **Evolution of the percentage of weight loss** underwent by the studied PLA/PEG and PLA/PEG/G5 films along degradation in SBF at 37ºC. PLA and PLA/G5 films were used as control (n=3); (b) **Initial thermal properties** (Tg, %Xc) of the studied materials. **Evolution of (c) glass transition temperature (Tg) and (d) Crystalline fraction (%Xc) along the degradation time** in SBF at 37ºC. Error bars not shown if smaller than symbols.

In particular, the PLA/PEG 80/20 blend underwent a prompt weight loss after only two weeks of degradation. This abrupt degradation hampered further weight measurements due to difficulties to manipulate the sample pieces. Though the incorporation of the glass particles into the polymer matrix (PLA/G5) increased the weight loss in comparison to PLA, PLA/PEG/G5 showed a higher weight loss starting from the second week of degradation as in the case of the other PLA/PEG blends. Indeed, PLA/PEG/G5 showed a similar tendency to that of PLA/PEG 95/5.

2.3.8. Thermal characterization

Figure 2.5b, c and d shows a summary of the thermal properties obtained by DSC for the set of studied materials throughout the degradation period. A decrease in the glass transition temperature (Tg) values was observed before degradation (t = 0) when increasing the concentration of PEG in the polymer blend. In particular Tg values decreased from a value of 59.15 ºC to 15.34 ºC by increasing PEG concentration from 0% to 20% (w/w) respectively. Incorporation of G5 particles did not influence Tg values. In fact, PLA/G5 and PLA/PEG/G5 showed quite similar values to PLA and PLA/PEG 95/5 respectively.

The percentage of crystallinity (Xc) significantly increased from 2.41% to 30.57% when different amounts of PEG were added to the blend. It appeared to achieve its highest value with 5% of PEG (30.57%) and then decrease and undergo further stabilization at Xc around 23% at higher PEG concentrations (10 and 20% (w/w)).

In general, the behaviour of the materials during degradation was strongly influenced by the presence of PEG. A progressive increase of Tg values along the degradation time was revealed, especially for the materials with higher concentration of PEG. With respect to the evolution of the crystallinity percentage during the degradation period, a general increase was observed for the materials with and without PEG. In the case of PLA, Xc underwent a gradual increase whereas in the case of PLA/G5 a steeper increase was displayed, especially after the first 4 weeks of degradation. Crystallinity was also increased in the PLA/PEG blends. However, the blend with 5% of PEG showed a different behaviour. In this particular case, Xc values decreased along the degradation time. Blends with 10 and 20% (w/w) of PEG showed a significant increase being it more obvious in the PLA/PEG 80/20 material. Regarding the composite materials, PLA/G5 showed an increase of the crystallinity fraction, as expected from previous studies [24], while in PLA/PEG/G5 95/5 the percentage of crystallinity was rather constant.

2.4. Discussion

Polyethylene glycol, in particular low molecular weight one has been widely acknowledged as an efficient plasticizer for PLA [12,16,17]. Thus, it is expected that the use of PLA/PEG blends may facilitate the fabrication process of 3D structures for tissue engineering. In particular, in rapid prototyping structures where the nozzle-based printing process is highly dependent on the polymer solution viscosity and flow, the plasticizing effect of PEG is of great help to ease and optimize the fabrication process at low temperature [25]. Besides affecting PLA processing, it is anticipated that PLA/PEG combination lead to various changes in scaffolds properties including its structural, surface, and mechanical properties as well as its in vitro degradation. Therefore, knowing the effect of PEG's concentration on the blends properties and their degradation behavior, it is of main importance to find the right interplay between PEG concentration, material performance and fabrication process.

In this work, the effect of PEG concentration on the structural and surface properties of PLA/PEG based 3D scaffolds as well as in their in vitro degradation was studied. A set of materials with different PEG concentration was investigated by means of various characterization techniques.

Overall, the results obtained in this study showed a clear effect of PEG on both, the morphology and mechanical properties of the 3D structures as well as in their surface properties and the degradation behavior of the polymer blends with the different concentrations of PEG.

With respect to the 3D structures, both SEM examination and mechanical compression tests indicated structural changes due to PEG incorporation into the polymer matrix. In fact, it was observed that though all the blends followed the predetermined geometry, there were clear variations on struts' diameter and an increase in pores roundness owed to PEG addition. The effect of PEG was particularly obvious in the case

of the 20% PEG blend. These changes in struts and pores size and geometry are attributed to the important decrease of viscosity experienced by the polymer blends due to the addition of PEG. Lower viscosities led to a faster and easier polymer flow out of the tip during printing and therefore to less defined and less uniform struts.

Furthermore, a clear decrease of compressive strength was observed by increasing PEG concentration (Figure 2.1f). Despite the structural changes induced by the addition of PEG in the blend, variations in mechanical properties were mainly attributed to its plasticizing effect. In the case of the PLA/PEG/G5 composite scaffolds, G5 glass reinforcing effect was more evident than the plasticizing effect of PEG.

With respect to the surface properties, morphological differences were observed at the surface of the different blends. Both SEM and interferometry images displayed evident differences in the samples with PEG and glass particles in comparison to pure PLA (Figures 2.2 and 2.3). Incorporation of PEG into the PLA matrix led to different chain arrangements during the solvent evaporation process of the films. It is known that the plasticizing effect of PEG increases chain mobility and also acts as nucleating agent accelerating the creation of crystalline domains and therefore, increasing their density on the surface [26,27]. This in turn, affects the crystallinity, topography (due to the formation of spherulites), and other surface properties of the material. In fact, thermal analysis of the different blends showed a progressive decrease of the Tg and an increase of the crystallinity values with higher concentrations of PEG (Figure 2.5b). Lower Tg values suggested higher chain mobility allowing chain arrangement and the nucleation process described above.

In this study, a significant increase of surface roughness values (S_a) was observed when adding PEG into the system. The formation of spherulites with different morphologies, size and distribution in the PLA/PEG blends (Figure 2.3) led to higher S_a values than in PLA, especially in the films with 10 and 20% of PEG. Though, no statistically significant differences were observed between the Sa values of both surfaces, interferometry images showed clear differences in the peaks' shape and distribution on the surfaces. The blend with 10% PEG showed an elevated standard deviation owing to the presence of a combination of high and low mounds with large diameter and well separated from each other; whereas the blend with 20% PEG displayed a higher amount of mounds with lower diameter and height but more homogeneous and almost no separation between them. In the case of PLA/G5 composite materials, a substantial increase of S_a was observed in both PLA/G5 and PLA/PEG/G5 ($S_{aPLA/G5}$ =1401.81 nm and $S_{aPLA/PEG/G5}$ =1003.89 nm respectively). Again, the plasticizing effect of PEG was present as revealed by the S_{sk} values. Negatively skewed surfaces were obtained for the composite materials (PLA/G5 and PLA/PEG/G5) indicating the predominance of valleys due to the glass/polymer interface. Nonetheless, the S_{sk} value obtained for PLA/PEG/G5 (S_{sk} = -0.03 ± 0.52) was significantly lower than the one obtained for PLA/G5 (S_{sk}=-0.5 ± 0.17) indicating that the plasticizing effect of PEG smoothed the material surface.

Surface wettability was also affected by the addition of PEG. Though contact angle values decreased in comparison to pure PLA, no statistically significant differences were observed between the studied blends. As anticipated, composites including G5 revealed lower contact angle values [25,28].

Hydrophilicity of both G5 and PEG contributed to improve samples wettability, in particular, in the case of the PLA/PEG/G5.

The effect of PEG distribution on the films obtained from the different polymer blends was also translated in differences in the surface Young's modulus of the studied blends. AFM analysis allowed determining surface Young's modulus of the blends at the nanoscale. It is known that mechanical behaviour of materials at the nanoscale is different from that at macroscopic scale, and this phenomenon is mainly attributed to the increasing surface/volume ratio. In general, an improvement of the Young's modulus with PEG incorporation was observed. Of particular interest were the blends containing 5 and 10% of PEG (shown in Figure 2.4). In these cases, AFM analysis permitted the identification of a bimodal distribution of the Young's modulus corresponding to areas with higher and lower crystallinity. The blend with 20% PEG presented only one E value, remarkably higher in comparison to the other blends. The high density of spherulites on the PLA/PEG 80/20 blend provided certain uniformity to the material surface leading to only one E value. The mechanism responsible for such an elevated Young's modulus is not well known; however, it is most likely that these differences respond to the roughness differences between surfaces. In fact, it has been reported that surface Young's modulus is highly dependent on surface roughness [29].

A key issue when choosing a material for temporary tissue engineering templates is its degradation rate. Therefore, a preliminary in vitro degradation study was carried out as an additional parameter for the evaluation of the role of PEG in PLA-based structures.

The presence of PEG in the polymer blend also affected the material behaviour in simulated physiological conditions. Weight loss results indicated that presence of PEG strongly influenced the degradation rate of the blends (Figure 2.5a). This phenomenon became more relevant at higher concentrations of plasticizer; indeed a striking degradation was observed in the case of the blend with 20% PEG after two weeks of immersion in SBF (Figure 2.5a). The hydrophilic PEG domains in the films surface led to a faster degradation when in contact with the fluid. Addition of G5 also accelerated the degradation of the material in agreement with previous studies [24]. However, presence of PEG elicited a more determinant effect. In fact, the mass loss underwent by PLA/PEG/G5 was considerably higher than the one experienced by PLA/G5 after the first 2 weeks of degradation (Figure 2.5a).

Important differences were also observed along the degradation time in terms of the thermal properties of the studied polymer blends with the different percentages of PEG (Figure 2.5c,d). Overall, both glass transition temperature and crystallinity percentage values obtained for the PLA/PEG blends increased during the degradation period. Again, the increase of Tg and %Xc values was more evident in the case of blends with higher PEG concentration. In fact, $Tg_{PLA/PEG80/20}$ increased from 15.34ºC to 54.5ºC while $Tg_{PLA/PEG95/5}$ increased from 41.67 ºC to 46.72 ºC. This important increase of Tg suggested a significant loss of PEG from the polymer blends due to hydrolytic degradation. In fact, after 8 weeks of immersion in SBF, PLA/PEG blends with 10 and 20% of PEG displayed Tg values similar to the one obtained for PLA. It is worth mentioning that this substantial increase of Tg took place after the first 4 weeks of degradation

for all the PEG-containing blends. According to the weight loss curves, an analogous behavior was observed after the first two weeks of immersion in SBF, when PEG-containing samples also exhibited an important mass loss.

With respect to Xc, an important boost of crystallinity was revealed for the polymeric matrix of both PLA/G5 and PLA/PEG/G5 composites after the first 4 weeks of in vitro degradation. As previously described by Navarro et al. [24], a hydrolysis process initiated at the interface between the polymer and G5 particles drove to a faster molecular packing and degradation of the polymer matrix, in particular of the PEG and amorphous domains leading to a higher fraction of crystallinity.

2.5. Conclusion

Finding the right processing conditions is crucial in the fabrication of 3D structures by rapid prototyping. Addition of PEG has shown to be advantageous to produce high-resolution PLA-based scaffolds at low temperature. Thus, knowing the effect of PEG in the final scaffolds properties is of great importance not only from the fabrication point of view but also from the structural and physico-chemical one as it is known that scaffolds success is ruled by their surface, structural and degradation properties. This chapter provides a full-scale study on the effect of PEG in PLA-based blends used to fabricate 3D-printed scaffolds. Results obtained from this work make evident that the incorporation of different percentages of PEG leads to significant changes in PLA/PEG structures and also accelerates their degradation rate. In fact, it was shown that addition of PEG increased surface roughness and wettability, led to non-uniform struts, and decreased mechanical properties of the 3D structures. Thus, in addition to improving scaffolds processing, incorporation of PEG is an effective method for tailoring both surface and structural properties, and modulating scaffold degradation. The outcomes of this work suggest that addition of 5% (w/w) of PEG in the PLA matrix allows the fabrication of 3D structures with a fair balance between their structural/mechanical properties and degradation rate [25].

2.6. References

[1] D.W. Hutmacher, J.T. Schantz, C.X.F. Lam, K.C. Tan, T.C. Lim. State of the art and future directions of scaffold-based bone engineering from a biomaterials perspective. J. Tissue Eng. Regen. Med. 2007;1:245-260.

[2] D.W. Hutmacher. Scaffolds in tissue engineering bone and cartilage. Biomaterials. 2000;21:2529–2543.

[3] S.J. Hollister. Porous scaffold design for tissue engineering. Nature Materials. 2005;4:518–524.

[4] L. Moroni, J. Elisseeff. Biomaterials engineered for integration. Materials Today. 2008;11: 44-51.

[5] W.Y. Yeong, C.K. Chua, K.F. Leong, M. Chandrasekaran. Rapid prototyping in tissue engineering: challenges and potential. Trends Biotechnol. 2004; 22 : 643–652.

[6] I. Zein, D.W. Hutmacher, K.C. Tan, S.H. Teoh. Fused deposition modeling of novel scaffold architectures for tissue engineering applications. Biomaterials 2002;23:1169–1185.

çeri, X. Wen, M. Gandhi, W. Sun. Fabrication of three-dimensional polycaprolactone/hydroxyapatite tissue scaffolds and osteoblast-scaffold interactions in vitro. Biomaterials. 2007;28:5291-5297.

[8] K. Rezwan, Q.Z. Chen, J.J. Blaker, A.R. Boccaccini. Biodegradable and bioactive porous polymer/inorganic composite scaffolds for bone tissue engineering. Biomaterials. 2006;27:3413-31.

[9] M. Navarro, C. Aparicio, M. Charles-Harris, M.P. Ginebra, E. Engel, J.A. Planell. Development of a Biodegradable Composite Scaffold for Bone Tissue Engineering: Physicochemical, Topographical, Mechanical, Degradation, and Biological Properties. Advances in Polymer Science 2006; 200 (1):209-231.

[10] J.M. Taboas, R.D. Maddox, P.H. Krebsbach, S.J. Hollister. Indirect solid free form fabrication of local and global porous, biomimetic and composite 3D polymerceramic scaffolds. Biomaterials. 2003;24:181–94.

[11] Z. Xiong, Y. Yan, S. Wang, R. Zhang, C. Zhang. Fabrication of porous scaffolds for bone tissue engineering via low-temperature deposition, Scripta Materialia 46 (11):771–776.

[12] R.M. Rasal, A.V. Janorkar, D.E. Hirt. Poly(lactic acid) Modifications, Prog Polym Sci. 2010;35:338-356.

[13] S. Zalipsky, J.M. Harris. Introduction to chemistry and biological applications of poly(ethylene glycol). In: J.M. Harris, S. Zalipsky editors. Poly(ehtylene glycol): Chemistry and Biological Applications. Vol. 680. ACS Symposium Series. American Chemical Society. Washington, DC; 1997, 1–13.

[14] Y. Inada, M. Furukawa, H. Sasaki, Y. Kodera, M. Hiroto, H. Nishimura, A. Matsushima. Biomedical and biotechnological applications of PEG- and PM-modified proteins, Trends Biotechnol. 1995;13(3):86-91.

[15] Y. Hu, Y.S. Hu, V. Topolkaraev, A. Hiltner, E. Baer. Crystallization and phase separation in blends of high stereoregular poly(lactide) with poly(ethylene glycol), Polymer. 2003;44(19):5681–5689.

[16] Z. Kulinski, E. Piorkowska. Crystallization, structure and properties of plasticized poly(L-lactide). Polymer. 2005,46:10290–10300.

[17] H. Li, M.A. Huneault. Effect of nucleation and plasticization on the crystallization of poly(lactic acid). Polymer. 2007,48:6855-6866.

[18] M. Navarro, M.P. Ginebra, J. Clement, S. Martinez, G. Avila, J.A. Planell. Physicochemical degradation of resorbable phosphate glasses stabilized with TiO2. J. Amer.
Ceram. Soc. 2003; 86:1345-52.

[19] M. Navarro, M.P. Ginebra, J.A. Planell. Cellular response to calcium phosphate glasses with controlled solubility. J. Biomed. Mater. Res. 2003; 67:1009-1015.

[20] E.S. Sanzana, M. Navarro, F. Macule, S. Suso, J.A. Planell, M.P. Ginebra. Of the in vivo behaviour of calcium phosphate cements and glasses as bone substitutes. Acta Biomaterialia. 2008;4:1924-1933.

[21] A.N. Frone, S. Berlioz, J.F. Chailan, D.M. Panaitescu. Morphology and thermal properties of PLA-cellulose nanofibers composites. Carbohydr Polym. 2013;91(1):377-84.

[22] T. Kokubo, H. Kushitani, S. Sakka, T. Kitsugi, T. Yamamuro. Solutions able to reproduce in vivo surface-structure changes in bioactive glass-ceramic A-W. J Biomed Mater Res. 1990;24(6):721–34.

[23] E.W. Fischer, H.J. Sterzel, G. Wegner. Investigation of the structure of solution grown crystals of lactide copolymers by means of chemical reactions. Kolloid- Zeitschrift and Z Polymere. 1973;251:978–90.

[24] M. Navarro, M.P. Ginebra, J.A. Planell, C.C. Barrias, M.A. Barbosa. In vitro degradation behavior of a novel bioresorbable composite material based on PLA and a soluble CaP glass. Acta Biomater. 2005;1(4):411-9.

[25] T. Serra, J.A. Planell, M. Navarro. High-resolution PLA-based composite scaffolds via 3-D printing technology. Acta Biomater. 2013;9(3):5521-30.

[26] S. Rathi, X. Chen, E.B. Coughlin, S.L. Hsu, C.S. Golub, M.J. Tzivanis. Toughening semicrystalline poly(lactic acid) by morphology alteration. Polymer. 2011,52(19):4184-4188.

[27] S. Saeidlou, M.A. Huneault, H. Li, C.B. Park. Poly(lactic acid) crystallization. Prog Polym Sci. 2012;37(12):1657-1677.

[28] M. Navarro, E. Engel, J.A. Planell, I. Amaral, M. Barbosa, M.P. Ginebra. Surface characterization and cell response of a PLA/CaP glass biodegradable composite material. J Biomed Mater Res A. 2008;85(2):477-86.

[29] P. Mohammadi, L.P. Liu, P. Sharma, R.V. Kukta. Surface energy, elasticity and the homogenization of rough surfaces. J Mech Phys Solids. 2013;61(2):325-340.

Chapter 3 - High-resolution PLA-based composite scaffolds via 3-D printing technology

Chapter 2 stressed the importance of developing suitable biomaterials and blends for scaffolds fabrication via computer-aided design and manufacturing (CAD/CAM) techniques, specifically nozzle-based systems. Indeed, ideal materials should fit a number of requirements such as having good rheological properties to ease the fabrication processes while preserving structural integrity, providing adequate mechanical properties to the final structures, and tuning degradation throughout tissue development. Thus, in the previous chapter, a first step was taken in order to determine the most suitable PLA/PEG blend for scaffolds fabrication. To this end, a comprehensive study on the effect of PEG in PLA-based blends was done. The objective of the present chapter is the fabrication and characterization of 3D-printed composite scaffolds using the PLA-based blend optimized in chapter 2 (PLA/PEG 95/5).

3.1. Introduction

Rapid prototyping (RP), also known as additive manufacturing (AM), has emerged in the biomaterials field as a new tool for the fabrication of scaffolds with well-defined and reproducible architectures. RP techniques open the possibility of building custom-made scaffolds based on patient-specific tissue defects. These techniques combine computer design together with automated printing technology. In addition, temporary, tailor-made scaffolds fabricated by RP provide an excellent in vitro platform for the study of the effect of geometry/architecture on cell response, and for computer modeling of the scaffold's behavior. It also allows three-dimensional (3-D) structures with improved mechanical performance to be obtained. In fact, RP structures show mechanical properties significantly higher than those of structures fabricated by other well-known techniques such as solvent-casting and particle leaching, thermal-induced phase separation and gas foaming, among others [1–4].

Several RP techniques have been developed in recent decades. The elaboration of different polymer and ceramic scaffolds with different geometries has been reported [1–8]. Of remarkable interest are the nozzle-deposition-based techniques, particularly the approach consisting in a dispensing system integrated with pumping technology and a CAD/CAM tool. This is a versatile technique that allows the building of 3-D structures and complex geometry models with precise control and reproducibility, using a large variety of materials [5]. Reviewing the literature on RP fabricated scaffolds reveals that numerous degradable polymers such as polycaprolactone, polylactic acid (PLA), polyglycolic acid, chitosan and their copolymers have been used to fabricate 3-D scaffolds [2,6,8–11]. In particular, PLA is a currently used biodegradable polymer that has been approved by the FDA for various biomedical applications. Though this polymer has been extensively studied, its use in the fabrication of RP scaffolds and

specifically those elaborated through nozzle-based systems has been limited and scarcely reported. At present, most of the reported PLA-based scaffolds fabricated by RP require the molecular modification of the PLA matrix, the use of temperature during printing or further processing of the structure by freeze-drying [12,13]. The RP tool used in the present study allows the fabrication of PLA 3-D structures without modifying the polymer structure with specific chemical groups, without melting the polymer and without using any subsequent process to remove the solvent from the final structure.

One of the strategies to improve the bioactivity and mechanical integrity of polymer scaffolds is the incorporation of an inorganic phase such as calcium phosphate (CaP) particles [14]. Indeed, several studies combining biodegradable polymers with different CaP ceramics have been reported [15–17]. In this area, CaP-based glasses are an interesting option, given their controlled biodegradability and bioactive potential [18]. In particular, CaP glasses in the system P_2O_5–CaO–Na_2O–TiO_2 have shown excellent biocompatibility both in vitro and in vivo [19,20]. This work describes the fabrication of PLA-based 3-D scaffolds by RP. Both polyethylene glycol (PEG) and G5 glass particles were combined with the PLA matrix to obtain 3-D fully biodegradable porous composite structures with superior mechanical and bioactive properties. The structures obtained were characterized in terms of their processing effect, final architecture, mechanical behavior, surface properties and biological response.

3.2. Materials and methods

3.2.1. Material

The materials used have been described in the previous chapter (2.2.1). From now on, a PLA-blend containing 5% (w/w) of PEG is used. Materials were combined according to the compositions shown in Table 3.1.

Material	**Polymer matrix (w/w %)**		**G5 particles (w/w%)**
	PLA	PEG	
PLA/PEG	95	5	-
PLA/PEG/G5	95	5	50

Table 3. 1. Composition of the studied materials

3.2.2. Scaffolds design and fabrication

Scaffold fabrication has been conducted following the protocol described in 2.2.2. In order to study the influence of pore size and pore distribution in the axial and transversal direction, two different architectures were designed and fabricated (see Fig. 3.1): (a) an orthogonal layer configuration (ORTH) with distance between struts axes (d1) of 500 μm and diameter of the struts (Ø) ~200 μm, and (b) a

displaced double-layer design (DISPL) [22] with distance between struts d2 = d1/2 dispensing a double layer in each direction.

Three-dimensional structures were built accordingly to the created designs by means of the layer-by-layer deposition of the material using the pumping equipment. A printing pressure in a range between 40 and 80 psi and a motor speed of 3 mm s^{-1} were used to enable the material flow through a G27 (200 μm) nozzle. The syringe temperature was set at 40 ± 5 °C using a heating jacket, and room temperature was kept at 25 ± 2 °C.

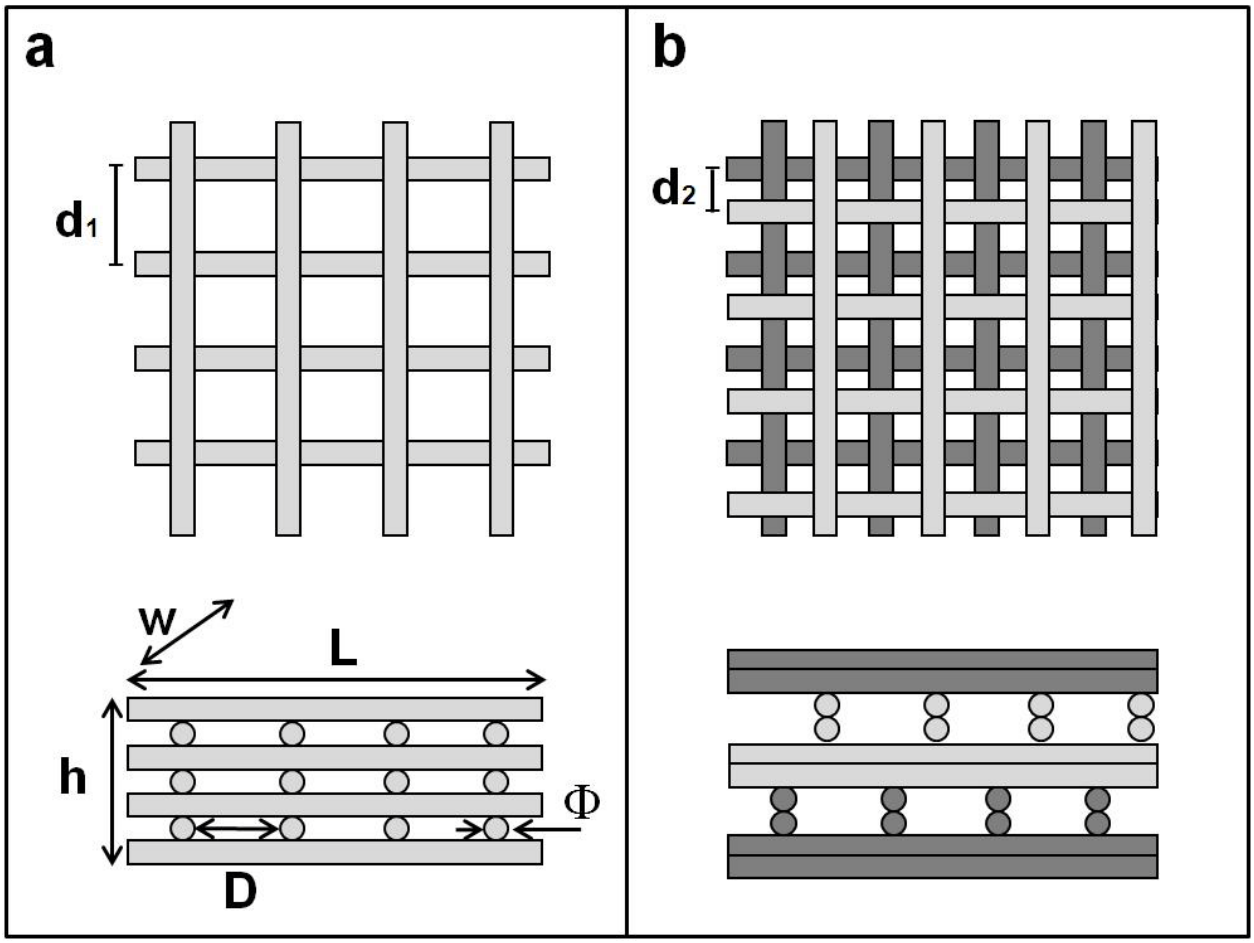

Figure 3. 1. Axial and cross-section view of the theoretical 3D structures of (a) ORTH and (b) DISPL scaffolds: d_1 = 500 μm; d_2 = 250 μm; Ø = 200 μm.

3.2.3. Scaffold characterization

3.2.3.1. Differential scanning calorimetry

Differential scanning calorimetry (DSC; DSC-2910, TA Instruments) was used to determine the effect of PEG in the thermal properties of the polymer blend, and the thermal properties of the material pre- and post-processing. Samples of the PLA/PEG 3-D-deposited scaffolds were analyzed following the protocol exposed in chapter 2 (2.2.4.2.).

3.2.3.2. Morphological scanning electron microscopy study

Morphological analysis of the 3-D structures was carried out by scanning electron microscopy to visualize and evaluate the architecture of the 3-D scaffolds, surface morphology and structural stability of the deposited struts and layers. SEM observation allowed qualitative evaluation of the differences between the theoretically defined pore geometry and size and those obtained after processing. The protocol used is detailed in chapter 2 (2.2.3.1). It also allowed verification of the distribution of glass particles within the polymer matrix and the final 3-D scaffold.

3.2.3.3. Porosity

The theoretical volume porosity percentage ($\%Vol_{theoretical}$) was calculated for each scaffold using the initially designed geometries based on a unit cube (Fig. 3.1) and following the protocol described in chapter 2 (2.2.3.2). It was also considered that, when changing the design from the ORTH to the DISPL configuration, the value of volume porosity was not changed.

$$\%Vol_{theoretical} = (1 - (Ø^2/4)\,\pi N_c N_l /(wh)) \times 100\%.$$

3.2.3.4. Microstructure analysis and 3-D reconstruction by microcomputer tomography

Three scaffolds (for each material composition) were scanned using a micro-computer tomography (μCT) X-Tek HMX225 (Digisens) instrument with a voxel resolution of $8 \times 8 \times 8\ \mu m^3$. Computer 3-D reconstruction of the scaffolds was made using Mimics 14.0 software (Materialise, Leuven, Belgium) to determine the porosity as well as the percentage and distribution of the glass particles within the 3-D composite structures.

3.2.3.5. Mechanical properties of scaffolds

A Universal Testing Machine (MTS-Bionix 858, MTS Systems Corporation, Eden Prairie, USA) with a 2.5 KN load cell was used to evaluate the mechanical properties of the scaffolds. The samples were tested at a speed of 1 mm min^{-1} without preloading. Stress–strain data were computed from load–displacement

measurements. The compressive modulus was determined based on the slope of the stress–strain curve in the elastic region. For each material composition, three cubic scaffolds ($5 \times 5 \times 5 mm^3$) were tested. Cubic samples were cored from larger 3-D printed blocks initially designed in the CAD software. The real accurate dimensions of the specimens were measured before the test.
An ANOVA test was performed to determine the statistical significance ($p \leq 0.05$) of the differences in the values of compressive modulus.

3.2.3.6. Topography

Surface topography as well as glass distribution at the surface of the composite material were observed by optical interferometry following the protocol described in chapter 2 (2.2.3.4). The studied parameters were: surface roughness (S_a), skewness, or the asymmetry of the surface about the mean plane (S_{sk}) and kurtosis, or peakedness of the surface about the mean plane (S_{ku}).

3.2.3.7. Wettability

Contact angle measurements were performed to evaluate the material's wettability. The protocol used is detailed in chapter 2 (2.2.3.6).

3.2.3.8. Cell cultures

Rat mesenchymal stem cells (rMSC) isolated from bone marrow were employed for cell culture studies. Cells were plated in culture flasks with Advanced Dulbecco's modified Eagle medium (DMEM, Invitrogen) supplemented with 15% fetal bovine serum, 1% penicillin/ streptomycin, 1% L-glutamine, and 1% pyruvate (all supplements from Invitrogen) at 37 °C in a humidified atmosphere of 5% CO_2 in air. The culture medium was changed every 2 days. At the fifth passage, cells were rinsed with phosphate buffered saline (PBS) and trypsinized with trypsin–EDTA (0.25%) in an incubator for 5 min at 37 °C. The cells were replated according to the conditions for the WST test.

3.2.3.9. Adhesion test

Cell adhesion was investigated by WST assay (Roche, Germany), which quantified the formazan released from cells into the supernatant by viable cells. The WST assay measures the reduction of the tetrazolium salt to formazan by mitochondrial succinate dehydrogenase. The increase in the supernatant formazan was directly correlated to the amount of viable cells. The 3-D PLA/PEG and PLA/PEG/G5 structures (10 mm diameter, 3 mm high) previously sterilized by ethanol were located in a 48-well polystyrene standard culture plate. A concentration of 1×10^5 cells was seeded in the scaffolds with 300 µl of medium per well. Polystyrene microplate wells were used as control. Cell adhesion was studied at 4 and 24 h. After each adhesion time point, scaffolds were replaced in new culture plates with 300 µl of fresh medium. For

the assay, 30 µl of WST reagent were added to each sample including the polystyrene controls. The plate was incubated at room temperature for 1 h, and absorbance values were read in the spectroscopic microplate reader at 450 nm using a Power-Wave X, Bio-Tek spectrophotometer. The results are expressed as the averaged absorbance levels of three replicates.

An ANOVA between groups test was performed to determine the statistical significance ($p \leq 0.05$) of the differences in the absorbance values.

3.2.3.9.1. Immunofluorescence study

In order to observe the morphology of the cells attached to the studied surfaces, an immunofluorescence study was performed. After 4 h of culturing, the cells were fixed by immersion in 3% paraformaldehyde in 10 mM PBS at room temperature for 15 min. The cells were rinsed with a mixture of 10 mM PBS and 20 mM glycine. Subsequently, the cells were permeabilized with a solution of 0.05% saponine in 10 mM PBS/20 mM glycine. After 10 min, the cells were blocked with a 1% bovine serum albumin solution in 10 mM PBS/20 mM glycine for 20 min and then incubated with various specific antibodies and dyes (phalloidin-TRITC, 1:2000; and DAPI, 1:500) for 1 h at 37 °C. The phalloidin-TRICT was used to stain actin filaments of the cytoskeleton, and DAPI was used to dye the cells' nuclei. The samples were rinsed and mounted on slides with Mowiol mounting media (Calbiochem) and observed in a Leica TCS40 confocal microscope.

3.3. Results

3.3.1. Thermal characterization

The thermal characteristics of PLA and PLA/PEG samples both before and after processing are shown in Table 3.2. DSC analysis showed that the addition of $5\%_{w/w}$ of PEG into the PLA matrix decreased Tg to 40 °C. It also confirmed that the crystalline fraction of PLA/PEG did not changed significantly when the polymer was processed. Indeed, it varied between 27.48% and 26.51% for the material before and after processing, respectively. Moreover, there were no significant differences between the glass transition temperature values before and after the process.

Material		**Tg (ºC)**	**%Xc**
PLA		59.15±0.16	40.68±0.42
PLA/PEG	Non-processed	40±0.6	27.48±0.72
	Processed	44.61±0.32	26.51±0.19

Table 3. 2. Thermal characteristics of PLA/PEG

3.3.2. Morphological evaluation by SEM and porosity

Fig. 3.2 shows the final ORTH structures for both PLA/PEG and PLA/PEG/G5. Both polymeric and composite scaffolds showed well-defined structures with pore size ≈ 375 ± 25 μm in the axial view and strut width ≈75 ± 5 μm. The total spacing between the struts axes was therefore ≈ 500 μm, according to the nominal design. In the case of the material with G5 glass, a fairly homogeneous distribution of the particles within the matrix was observed. The glass was well incorporated and embedded by the polymer (Fig. 3.2b, d) adding an interesting topography to the scaffold surface.

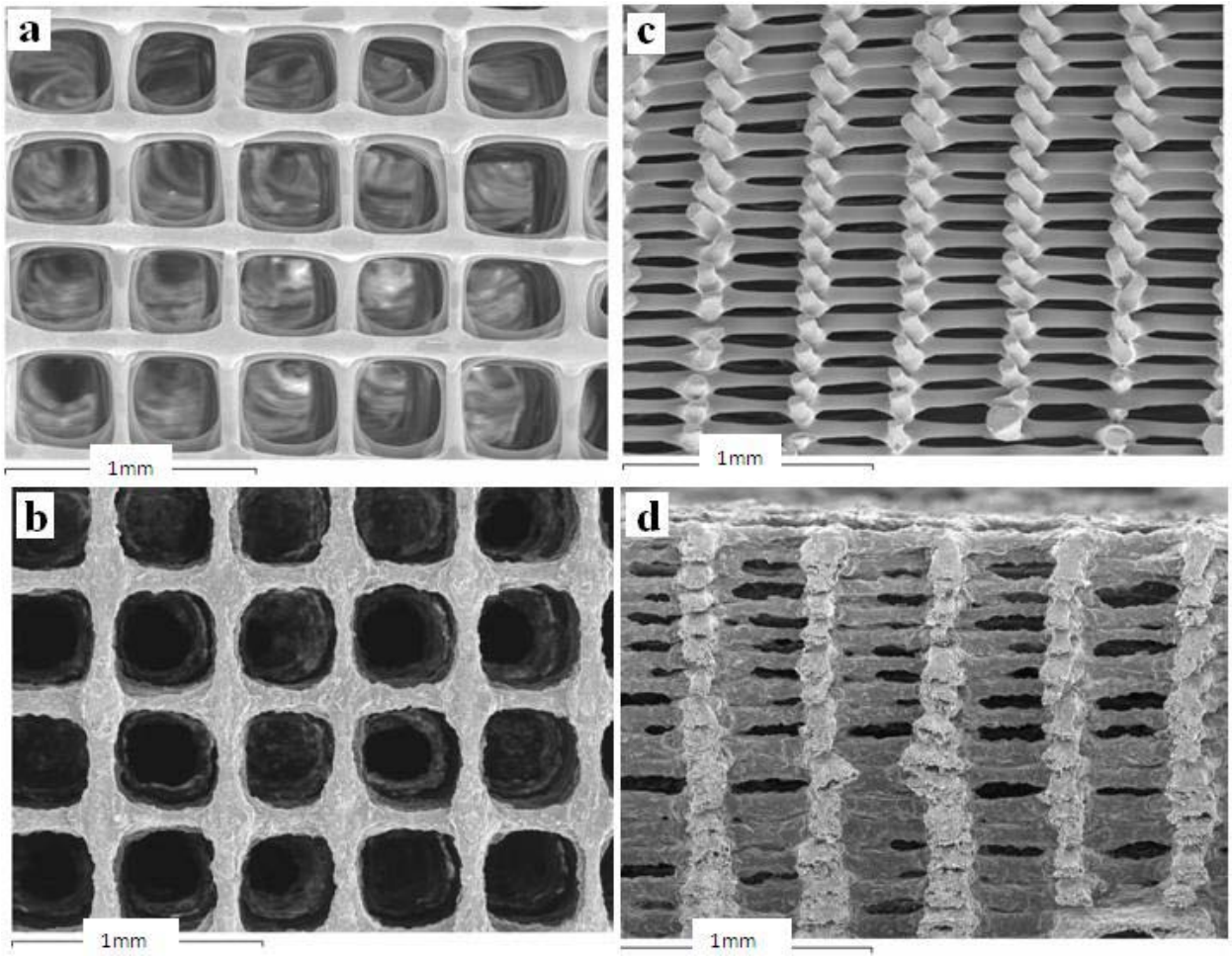

Figure 3. 2. SEM micrographs of 3-D printed scaffolds with ORTH pattern: (a, c) PLA/PEG ; (b, d) PLA/PEG/G5; (a,b) top view; (c,d) cross-section view.

Fig. 3.3 shows the final DISPL structures obtained for PLA/PEG and PLA/PEG/G5. SEM images showed well-defined structures with pores ≈165 ± 5 μm and struts ≈ 75 ± 5 μm. In this case, the pores size in the transversal direction (Fig. 3.3c, d) was improved (double) with respect to the one of the ORTH design. Furthermore, in both cases, these 3-D structures showed a combination of porosities ranging from the macroscale due to the initial designed pore size to the micro and nanoscale due to the presence of glass particles and to the pores left by solvent evaporation (Fig. 3.4c, d).

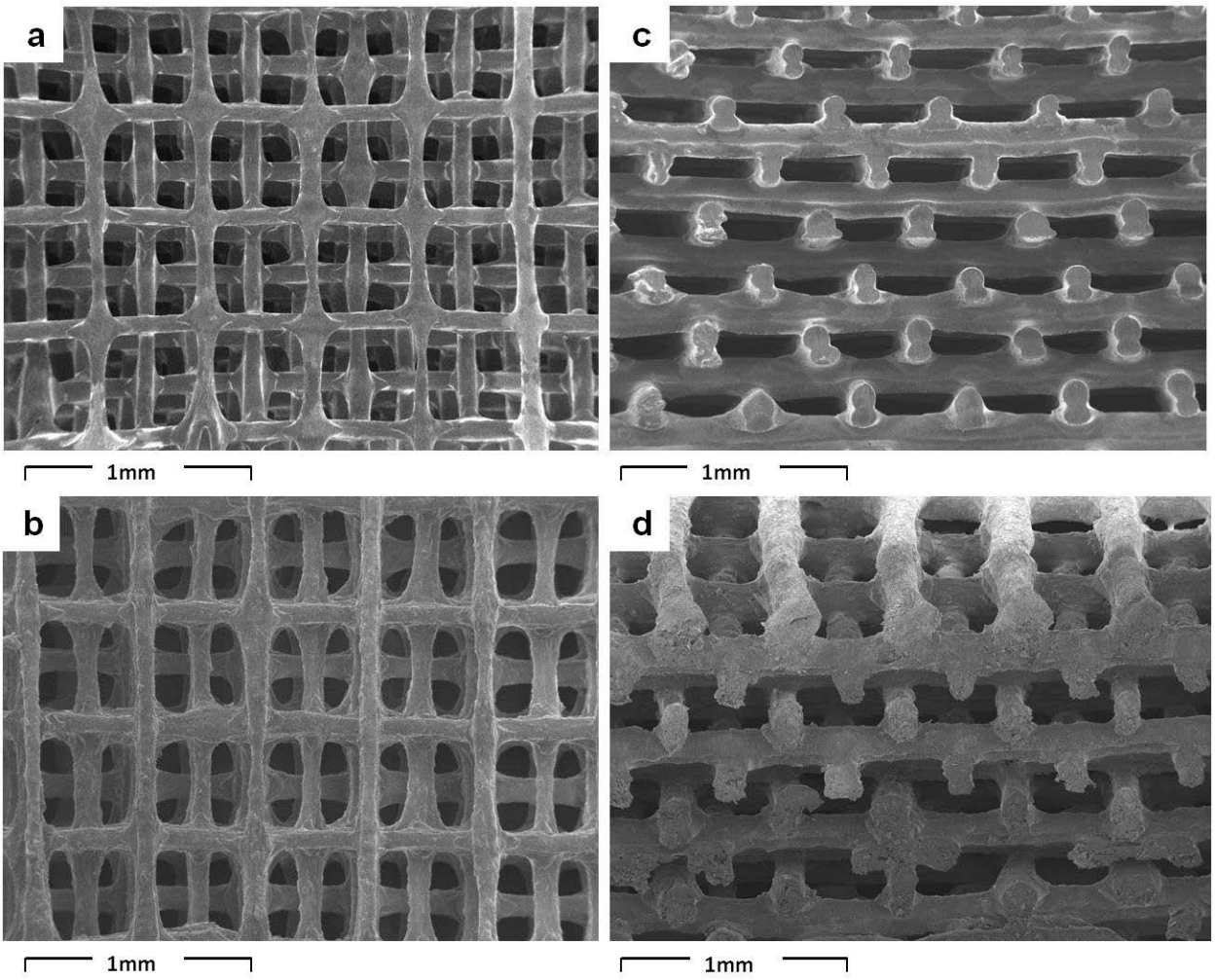

Figure 3. 3. SEM micrographs of 3-D printed scaffolds with DISPL pattern: (a, c) PLA/PEG; (b, d) PLA/PEG/G5; (a,b) top view; (c,d) cross-section view.

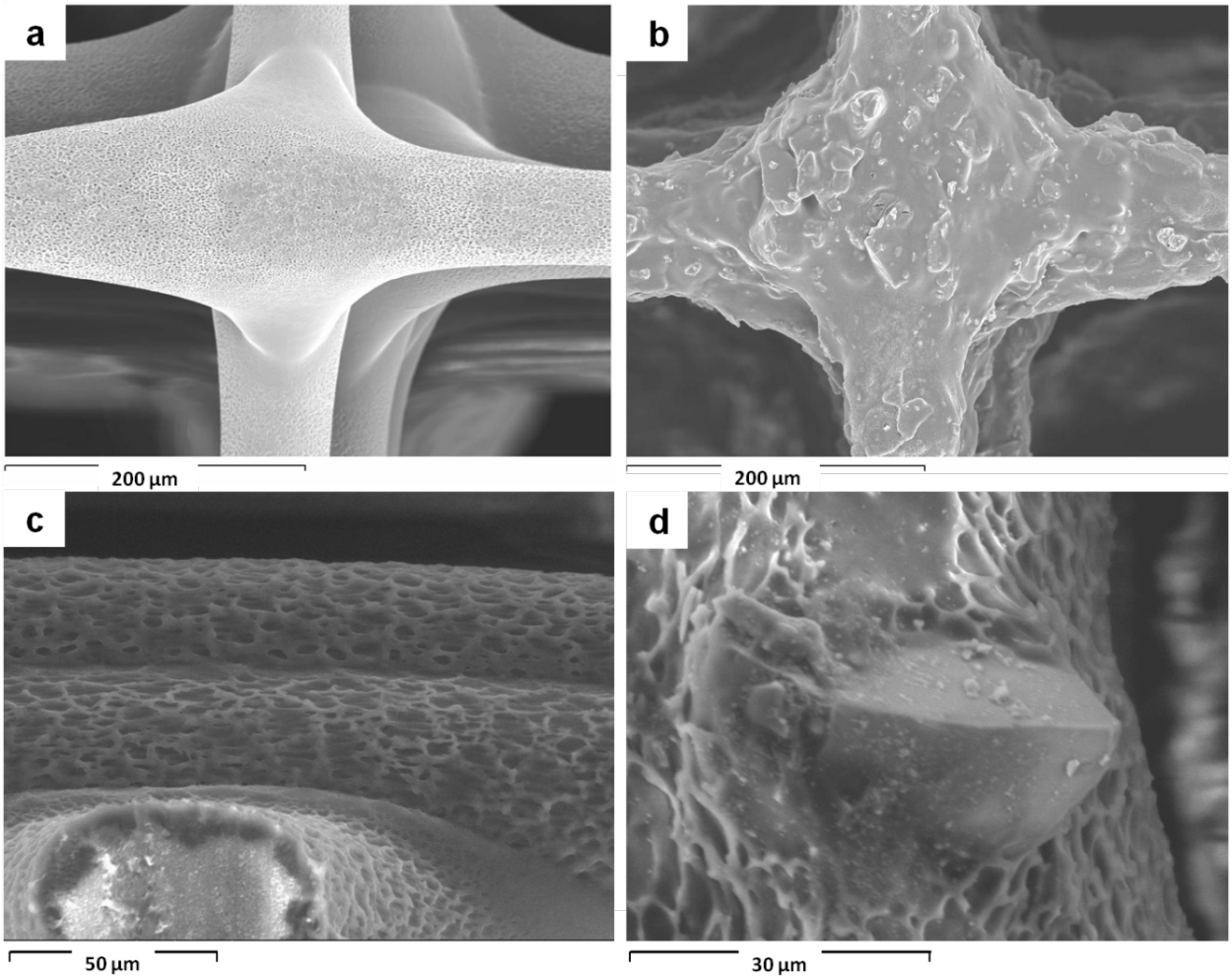

Figure 3. 4. SEM micrographs of (a) PLA/PEG and (b) PLA/PEG/G5 scaffolds surface. Higher magnification of (c) PLA/PEG and (d) PLA/PEG/G5 struts surface showing microporosity due to the evaporation of solvent and presence of glass particles.

3.3.3. Porosity and microstructure characterization by μCT

Theoretical volume porosity percentage ranged between 85.7% and 87.2% (for both materials, ORTH geometry) considering a distance between struts (D) of 400 μm and 350 μm, respectively.

μCT enabled 3-D characterization of RP-fabricated scaffolds. The 3-D reconstructed model for PLA/PEG/G5 scaffold, displayed in Fig. 5a, shows disposition of struts and pores size similar to the SEM image (Fig. 3.5b) of the same structure. Moreover, analogous topography, due to the presence of glass particles embedded by the polymer struts, can be observed in both images.

The evaluation of porosity from the μCT 3-D reconstruction revealed values of 75 ± 0.86% for the PLA/PEG blend scaffold and 70 ± 1.2% for the PLA/PEG/G5 one. A homogeneous distribution of the glass particles throughout the scaffold structure, and full pore interconnectivity were confirmed from the analysis of 3-D reconstruction (Fig. 3.5).

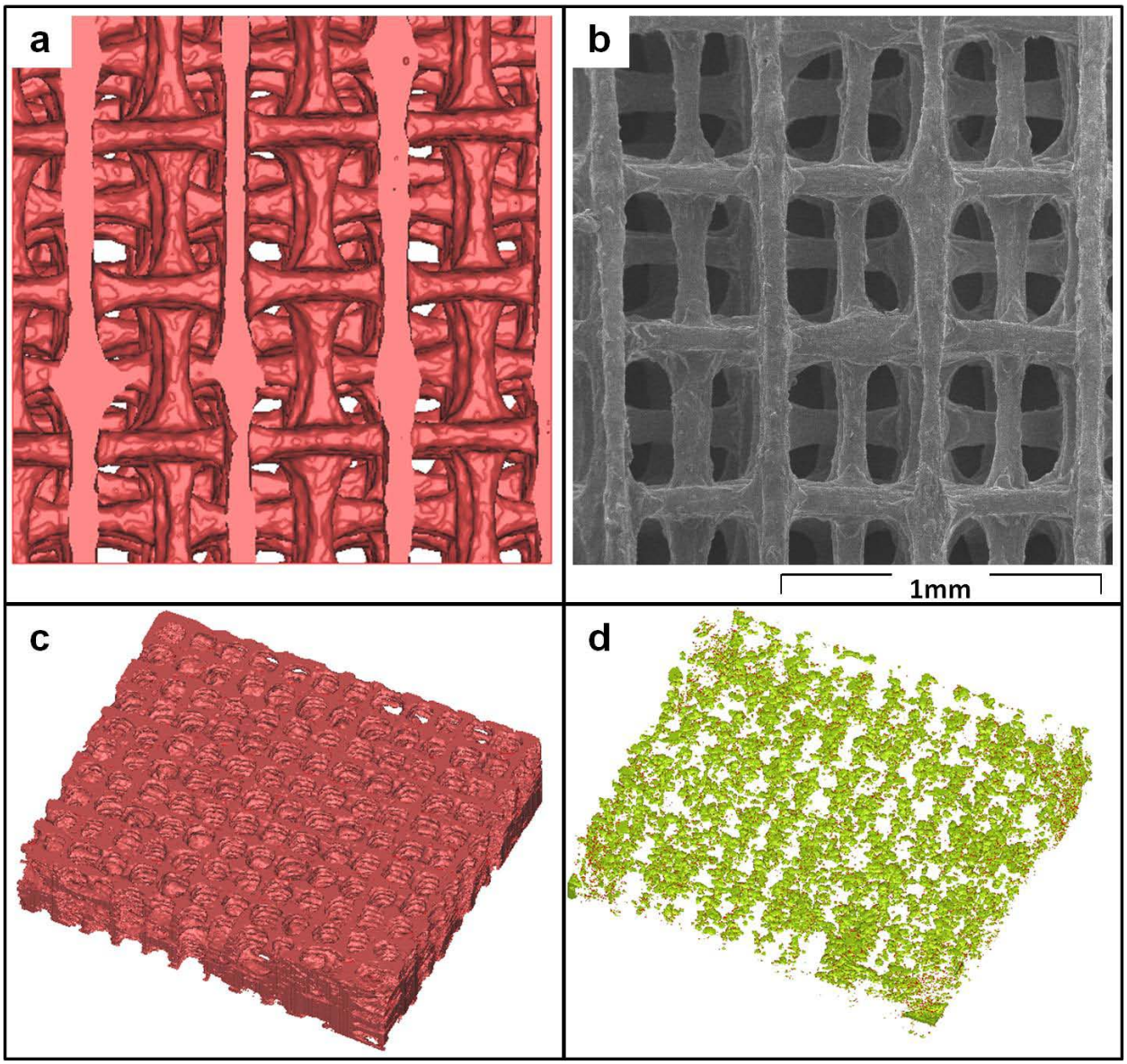

Figure 3. 5. (a) 3-D reconstructed and (b) SEM images of a PLA/PEG/G5 scaffold. Three-dimensional reconstructions of an ORTH scaffold (c) PLA/PEG/G5 scaffold, and (d) G5 particles distribution within the polymeric matrix.

3.3.4. Mechanical evaluation

Fig. 3.6 shows the data corresponding to the compressive modulus for the polymer both with and without glass particles and for both geometries, ORTH and DISPL. The compressive modulus of PLA/PEG scaffolds was found to be 92.32 ± 2.18 MPa for the ORTH design and 28.38 ± 3.99 MPa for the DISPL one, whereas for PLA/PEG/G5 the value increased to 99.81 ± 3.55 MPa for the ORTH and to 44.19 ± 2.67 MPa for the DISPL design.

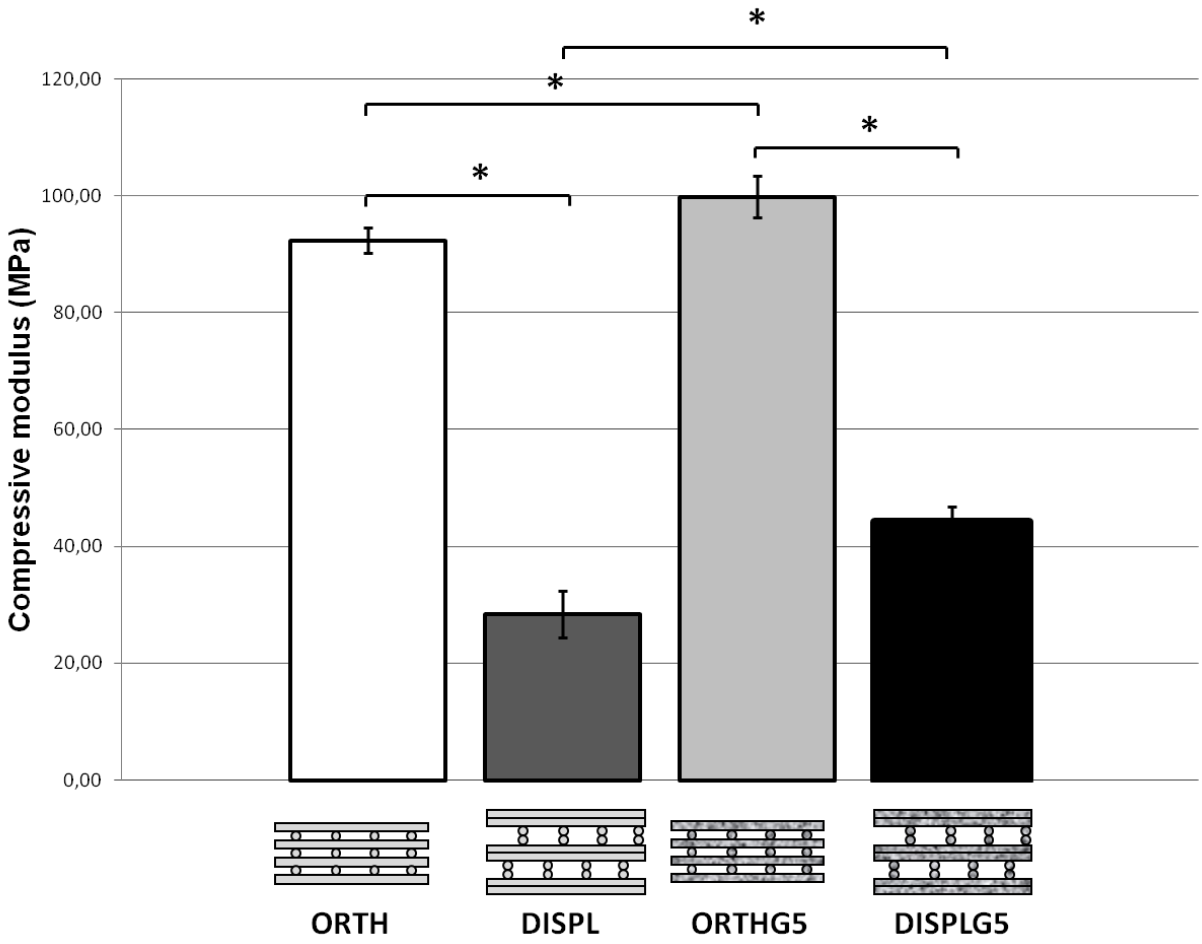

Figure 3. 6. Compressive modulus of PLA/PEG and PLA/PEG/G5 scaffolds with both ORTH and DISPL geometries. The values marked with the asterisk (*) showed statistical significant differences ($p \leq 0.05$).

3.3.5. Topography

Table 3.3 displays the results obtained for the topography study. Interferometry measurements showed that the average roughness of PLA (117.72 ± 60.50 nm) increased significantly with the addition of G5 glass particles and PEG ($S_{aPLA/G5}$ = 1401.81 ± 570.59 nm and $S_{aPLA/PEG/G5}$ = 1003.89 ± 228.45 nm). Additionally, S_{sk} values suggested a higher surface asymmetry when 5% PEG was added to PLA. No statistically significant differences ($p \leq 0.05$) were found for S_{ku} values for the studied materials.

Material	PLA	PLA/PEG	PLA/G5	PLA/PEG/G5
Sa (nm)	117.72±60.50	147.12±29.11	1401.81±570.59	1003.89±228.45
Ssk	0.79±0.66	1.08±0.55	-0.5±0.17	-0.03±0.52
Sku	7.56±5.62*	4.71±0.39*	3.8±1.10*	2.82±0.26*

Table 3. 3. Roughness parameters for the studied materials[a] (value ± SD). [a]Sa = average roughness, Ssk = skewness, Sku = kurtosis. The values marked with the asterisk (*) didn't show statistical significant differences ($p \leq 0.05$).

3.3.6. Contact angle measurement

The contact angle values for the studied materials are showed in Table 3.4. As observed, the presence of G5 increased the wettability of the surface. Moreover, the addition of 5% PEG into the PLA and PLA/G5 materials also led to a decrease in the contact angle.

Material	PLA	PLA/PEG	PLA/G5	PLA/PEG/G5
Distilled and Deionized Water (°)	83.77±0.77*	76.56±1.61**	77.57±7.58*·**	60.33±8.57

Table 3. 4. Contact Angle Values for the studied materials (value ± SD). The values marked with the asterisk (*,**) didn't show statistical significant differences ($p \leq 0.05$).

3.3.7. Cell adhesion

Cell adhesion was assessed from two different points of view. The viability of the cells was evaluated using the WST assay, and the cell morphology was monitored using immunofluorescence staining. Fig. 7a displays the absorbance values after both 4 and 24 h adhesion as measured by the WST assay, and the fluorescence images of the attached cells.

After 4 h of contact with the studied scaffolds, the polystyrene control plate showed the highest absorbance values, and no significant differences ($p \leq 0.05$) were observed between the PLA/PEG and PLA/PEG/G5 samples. After 24 h of culture, no significant differences were observed between the studied samples and, once again, the polystyrene plate showed the highest absorbance values.

Despite the fact that, after 4 h, the WST assay did not display any important difference ($p \leq 0.05$) for both scaffolds (PLA/PEG and PLA/PEG/G5) the immunofluorescence study demonstrated very clear variations in the morphology of the cells. Fig. 3.7b and c shows images of the rMSC adhering to the two different scaffolds after 4 h of contact.

The cells adhering to the surface of the PLA/PEG scaffold showed mostly rounded shapes, and were sparsely spread on the surface. In the case where the glass particles were added, the cells showed a very well-spread morphology with a spread cytoskeleton.

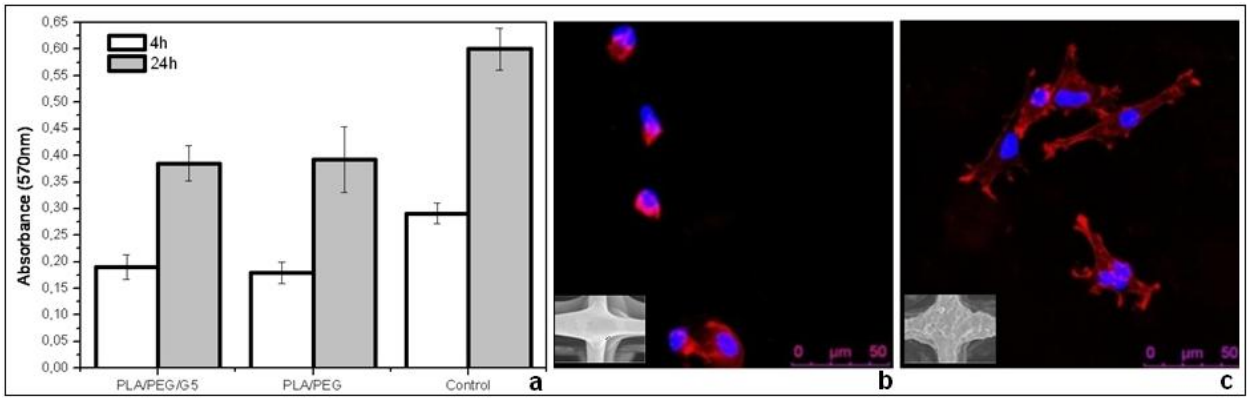

Figure 3. 7. (a) WST assay and fluorescence images of attached cells on (b) PLA/PEG and (c) PLA/PEG/G5 scaffolds.

3.4. Discussion

In this study, the RP method was used to fabricate 3-D polymeric (PLA/PEG) and composite (PLA/PEG/G5) scaffolds for tissue engineering applications. Scaffolds' fabrication parameters were optimized, and the final structures were studied using SEM, μCT, optical interferometry, contact angle, compressive mechanical testing, and DSC to characterize their architecture, the surface topography and wettability, and their mechanical and thermal properties.

It is known that an optimal ''printing'' process involves complex interactions between the hardware, software and material properties [7,23]. Thus, each aspect has to be carefully tuned in order to successfully obtain the right 3-D structures for each particular application. Choosing the right processing conditions guarantees obtaining high quality 3-D structures without harming the material properties; in the case of PLA, processing by nozzle deposition is relatively complex, owing to the combination of parameters affecting the polymer solution, such as solvent evaporation and processing temperature, among others.

In this work, the most advantageous set of parameters for fabricating 3-D scaffolds without degrading or affecting the polymer properties was chosen. In the case of the composite material, a set of parameters and an adequate polymer/solvent concentration were chosen to avoid any segregation phenomenon in the syringe due to the glass particles. In addition, PEG was used as plasticizer to decrease the Tg of the blend and to facilitate the material processing at low temperature. A PEG percentage of $5\%_{w/w}$ was chosen, given that it was the minimal amount for considerably lowering the Tg of the blend (PLA Tg = 59.15 °C; PLA/5% PEG Tg = 40 °C) and for improving the material processing without affecting the physico-chemical properties of the polymer. In fact, DSC results confirmed that the processing parameters used to elaborate the scaffolds did not induce significant changes in terms of polymer Tg and crystallinity (Table 3.2). Thus, the material did not undergo degradation because of possible elevated temperatures or shear forces during material deposition, which in turn could compromise scaffold in vitro and in vivo behaviour.

The selected set of fabrication parameters allowed well-defined porous structures to be obtained, as observed by SEM. According to the morphological analysis, though the struts were thinner than the needle diameter, the distance between axes and the overall structure are very close to the theoretical geometries designed by CAD software. Two different geometries were used in this work, namely orthogonal and displaced geometry. The idea was to decrease the pore size in the axial direction and improve it in the transversal one by changing the printing pattern of the scaffold.

In addition, important information regarding pore and strut dimensions was also retrieved from the SEM analysis. It was observed that the average diameter of the struts was ≈ 75 μm, while pore size ranged between 165 and 375 μm and between 75 and 150 μm in the axial and transversal directions, respectively, depending on the scaffold geometry. These results are in good agreement with those reported in previous investigations of bone ingrowth into porous materials [2,3,24,25]. In addition, large pore size could improve infiltration of new blood vessels into the scaffold enhancing its vascularization and providing

cell survival into the inner part of the scaffold. Moreover, RP scaffolds showed high pore size interconnectivity required to improve permeability, facilitating mass transport within the 3-D construct.

The diameter of the struts of the structures obtained in this study was significantly thinner than the diameter of other polymer RP structures reported in the literature and fabricated by similar nozzle-deposition-based systems [7,26,14]. This ‘‘high-resolution’’ effect was attributed to the interplay between the right printing parameters (pressure, temperature, speed, nozzle diameter and distance between the needle and the substrate), the viscosity of the polymer solution and the evaporation of the solvent that takes place once the material has been deposited. It allowed overall control of the printing process. The solvent found in the polymer solution plays a major role, since it evaporates immediately after the solution flows out from the syringe, leading to an important increase in viscosity, shrinkage of the struts and formation of pores at the scaffold surface.

Differences observed between the nominal diameter of the struts and the experimental are mainly attributed to this solvent evaporation effect. Indeed, in the case of fused deposition systems, where polymers are melted and subsequently extruded without using solvent, this shrinkage phenomenon is not as significant [7,10,14,26].

In general, a reduction in strut diameter confers a higher scaffold resolution though it leads to a reduction in pore size in the transversal direction and increases the fabrication time to obtain a desired volume. Additionally, lower dimension of struts lead to scaffolds with higher specific surface, improving the interaction between the material and the biological environment. In order to double the interconnecting pore size in the cross-section view, the approach adopted was to dispense two equal layers one on top of the other in each direction.

Two different methods were used to measure the scaffolds porosity: theoretical and experimental by μCT. As expected, the theoretical porosity was higher than that obtained by μCT 3-D reconstruction. During the fabrication process, it is possible that some fusion between the struts (of deposited material) and the underlying layers takes place; this is the reason why μCT evaluations of porosity were somewhat lower than the theoretical ones. Moreover, differences between porosity values can be further explained by the fact that the theoretical calculations assume a unit cube as opposed to the actual deposition of struts, which generated edge effects [26]. Despite the structure fabrication defects, porosity evaluation by μCT gives lower values than the theoretical one ($Vol_{theoretical} > Vol_{\mu CT}$) as a consequence of considering fabricated scaffolds. However, 3-D reconstruction allowed a quantitative measurement and examination of morphologies, interconnectivity and the internal architecture of the scaffolds. Composite scaffolds showed a porosity value of 70%, whereas the polymer blend scaffolds with the same geometry showed 75% of porosity. This difference could be attributed to the lower content of polymer per strut in the case of composites. Since the polymer is the shrinkable phase during solvent evaporation, a lower content of polymer could lead to less shrinkage and, therefore, to smaller pores and lower porosity.

It is well known that not only the architecture of the scaffolds, but also their surface properties are of paramount importance for understanding cell/material interactions and developing successful constructs.

Two-dimensional (2-D) solvent-casting films were used to reproduce the surface of the scaffolds' struts and to analyse their topography and wettability. As shown in Fig. 3.5, glass particles were well distributed in the polymer matrix. The presence of G5 particles added an interesting topography to the scaffold surface, as observed in Fig. 3.4. In addition, the surface of the polymer struts showed micro and nanopores left by the evaporation of the solvent. Thus, the final structures presented a combination of porosities ranging from the macroscale due to the pores initially designed to the micro and nanoscale due to solvent evaporation. According to the interferometry results, the addition of both glass particles and PEG significantly increased the average roughness (S_a) of the surface in comparison with PLA. In the case of PLA/PEG samples, incorporation of PEG increased Sa values because of its plasticizing effect, which accelerated the spherulite growth and formation rate of PLA [27,28]. The fast spherulites formation in PLA/PEG led to higher values of skewness (S_{sk}) showing a higher asymmetry of the surface about the mean plane in comparison with PLA. Nonetheless, in the case of PLA/PEG/G5 material, the good plasticizing properties of PEG led to a better coating and embedment of the glass particles in the polymer matrix, providing a smoother surface and decreasing Sa values. According to the results obtained, both PLA/G5 and PLA/PEG/G5 showed negative Ssk values. This fact indicates that, in these cases, the asymmetry with respect to the mean plane was mainly due to the presence of valleys rather than peaks. These valleys were probably caused by the polymer/glass non-unions. No statistical differences in the values of the kurtosis (S_{ku}) were found. Nevertheless, similarly to the S_{sk} results, S_{ku} values for the materials with G5 suggested some differences with respect to PLA and PLA/PEG surfaces. The materials without glass particles showed the spikiest surfaces, probably due to the presence of scratches caused during their manipulation and to the presence of non-randomly distributed spherulites induced by the effect of PEG [28]. Composite materials PLA/G5 and PLA/PEG/G5 showed S_{ku} values ≈ 3 driving to a random distribution of peaks within the surfaces.

With respect to the wettability, the contact angle measurements reported in Table 4 showed important differences on addition of PEG and G5 glass to PLA. It is known that G5 glass has a highly hydrophilic surface (29.8º) [29]. Thus, addition of G5 particles contributed to a decrease in PLA contact angle. PEG is also considered to be a hydrophilic polymer [30]. Therefore, the contact angle obtained for the PLA/PEG/G5 material showed the synergistic contribution of PEG and G5 particles' hydrophilicity.

The mechanical properties of 3-D structures are an important issue to consider in order to fulfil the requirements of the final application of the scaffold. According to the compression test results, changing the scaffold geometry from ORTH to DISPL decreased the scaffold's compressive modulus significantly. This diminution could be caused mainly by two aspects: (1) the separation between layers in the case of the DISPL geometry, and (2) the displaced disposition of the struts. The synergistic effect of both aspects leads to a combination of compressive and flexural stresses in the struts that decrease the mechanical stability of the structure in comparison to the ORTH scaffold. In the case of the ORTH structures, layers are closer and pores are smaller in the transversal direction, leading to a more dense and solid structure in the direction where compressive forces are applied during the mechanical test. Conversely, the displaced

disposition of the struts in the case of the DISPL structures led to a higher pore size in the transversal direction, and the discontinuous arrangement of the vertical struts increased the bending effect of the horizontal struts under the compressive forces, resulting in lower compressive modulus values.

It was also observed that, independently of the geometry, the addition of G5 particles increased the compressive modulus of the scaffolds, being more remarkable in the case of the DISPL structures. More specifically, the compressive modulus of the DISPL structures increased ≈ 35%, whereas ORTH ones showed an increase of 8%. In general, the structures obtained in this study showed compressive modulus values considerably higher than those reported in the literature for other RP structures with similar geometry and similar porosity percentages [7,14].

With respect to the biological evaluation, the WST test results, in combination with the images obtained from the immunofluorescence study, showed an interesting picture of the cells' behavior in contact with the studied surfaces after short periods of time. The addition of G5 glass particles into the polymer matrix strongly influenced the cell response in terms of morphology at early culture times. According to the WST results, though there was a general increase of the number of cells after 24 h of culture, there were no statistical significant differences ($p \leq 0.05$) between PLA/PEG and PLA/PEG/G5. It is worth mentioning that the substantially higher absorbance values obtained in the case of the control polystyrene plate were due to some extent to the fact that, after each culture time point, scaffolds were removed from the plate and replaced in a new plate to quantify only the amount of viable cells attached to the structure, leaving behind the ones attached in the bottom of the polystyrene wells. However, cells cultured on the 2-D control material were quantified directly in the same wells and the cell density was higher.

In spite of the WST results obtained after 4 and 24 h, remarkable differences were observed in the cells' morphology on comparing both types of scaffolds. After 4 h of adhesion, immunofluorescence images showed clear differences in the morphology of the cells, depending on what substrate was used (see Fig. 3.7b, c). In the case of PLA/PEG, cells showed a relatively rounded morphology with a clear nucleus, and no signs of cytoskeleton spreading as observed by the phalloidin stained actin fibres. In the case of the material with glass particles, cells spread very well, with a clear cytoskeleton extending along the scaffolds struts. Moreover, a higher intensity of the phalloidin staining was concentrated toward the edges of the extended filopodia. Surface characterization indicated remarkable differences between materials both with and without glass particles in terms of their wettability and roughness. Thus, the information obtained from the surface analysis together with cell results suggest that both topography and chemistry changes owing to the presence of the glass particles in the surface of the scaffolds' struts strongly affect cell response at early contact times.

These results are in full agreement with previous work showing how other cell types preferentially attach and spread when in contact with G5 glass [16,29]. Moreover, it has been reported recently that the biological effect of G5 glass is attributed mainly to the contribution of the chemotactic effect of the Ca ions released by the particles (mediated through the calcium sensing receptor, CaRS) and the material stiffness (mediated through NMII cytoskeletal contraction and signaling) [31].

3.5. Conclusion

RP, in particular the nozzle-based deposition system used in the present work, is suitable for fabricating 3-D composite scaffolds based on PLA and glass (G5). The addition of 5% PEG to the PLA matrix in combination with the chosen processing parameters allowed high-resolution 3-D scaffolds to be obtained without affecting the polymer blend properties. The technique also permitted the fabrication of highly porous scaffolds with mechanical properties considerably higher than other methods commonly used to fabricate 3-D polymer scaffolds, such as solvent-casting and phase separation.

The addition of the soluble G5 glass particles (and PEG) to the PLA matrix changed both the morphology and the physico-chemical properties of the surface of the materials. These surface changes affected cell behavior. Both types of scaffolds showed positive biological response; however, only the scaffolds with G5 displayed well-spread cells. In general, the technique/materials combination used in this work led to the fabrication of promising fully degradable, mechanically stable, bioactive and biocompatible composite scaffolds with well-defined architectures valuable for tissue engineering applications.

3.6. References

[1] Hutmacher DW. Scaffolds in tissue engineering bone and cartilage. Biomaterials 2000;21:2529–43.

[2] Hutmacher DW, Schantz JT, Lam CXF, Tan KC, Lim TC. State of the art and future directions of scaffold-based bone engineering from a biomaterials perspective. J Tissue Eng Regen Med 2007;1:245–60.

[3] Hollister SJ. Porous scaffold design for tissue engineering. Nat Mater 2005;4:518–24.

[4] Moroni L, Elisseeff J. Biomaterials engineered for integration. Mater Today 2008;11:44–51.

ller R. Structural and material approaches to bone tissue engineering in powder-based threedimensional printing. Acta Biomater 2011;7:907–20.

[6] Yeong WY, Chua CK, Leong KF, Chandrasekaran M. Rapid prototyping in tissue engineering: challenges and potential. Trends Biotechnol 2004;22:643–52.

[7] Zein I, Hutmacher DW, Tan KC, Teoh SH. Fused deposition modeling of novel scaffold architectures for tissue engineering applications. Biomaterials 2002;23:1169–85.

[8] Taboas JM, Maddox RD, Krebsbach PH, Hollister SJ. Indirect solid free form fabrication of local and global porous, biomimetic and composite 3D polymer– ceramic scaffolds. Biomaterials 2003;24:181–94.

[9] Geng L, Feng W, Hutmacher DW, Wong YS, Loh HT, Fuh JYH. Direct writing of chitosan scaffolds using a robotic system. Rapid Prototyping J 2005;11(2):90–7.

[10] Moroni L, de Wijn JR, van Blitterswijk CA. 3D fiber-deposited scaffolds for tissue engineering: Influence of pores geometry and architecture on dynamic mechanical properties. Biomaterials 2006;27:974–85.

[11] Seal BL, Otero TC, Panitch A. Polymeric biomaterials for tissue and organ regeneration. Mater Sci Eng R Rep 2001;34:147–230.

[12] Melchels FP, Feijen J, Grijpma DW. A poly(D,L-lactide) resin for the preparation of tissue engineering scaffolds by stereolithography. Biomaterials 2009;30:3801–9.

[13] Xiong Z, Yan Y, Wang S, Zhang R, Zhang C. Fabrication of porous scaffolds for bone tissue engineering via low-temperature deposition, Scripta Mater 2002; 46 (11):771–776.

.eri S, Wen X, Gandhi M, Sun W. Fabrication of three-dimensional polycaprolactone/hydroxyapatite tissue scaffolds and osteoblast–scaffold interactions in vitro. Biomaterials 2007;28:5291–7.

[15] Charles-Harris M, del Valle S, Hentges E, Bleuet P, Lacroix D, Planell JA. Mechanical and structural characterisation of completely degradable polylactic acid/calcium phosphate glass scaffolds. Biomaterials 2007;28:4429–38.

[16] Charles-Harris M, Koch MA, Navarro M, Lacroix D, Engel E, Planell JA. A PLA/ calcium phosphate degradable composite material for bone tissue engineering: an in vitro study. J Mater Sci Mater Med 2008;19:1503–13.

[17] Rezwan K, Chen QZ, Blaker JJ, Boccaccini AR. Biodegradable and bioactive porous polymer/inorganic composite scaffolds for bone tissue engineering. Biomaterials 2006;27:3413–31.

[18] Navarro M, Ginebra MP, Clement J, Martinez S, Avila G, Planell JA. Physicochemical degradation of resorbable phosphate glasses stabilized with TiO2. J Am Ceram Soc 2003;86:1345–52.

[19] Navarro M, Ginebra MP, Planell JA. Cellular response to calcium phosphate glasses with controlled solubility. J Biomed Mater Res 2003;67:1009–15.

[20] Sanzana ES, Navarro M, Macule F, Suso S, Planell JA, Ginebra MP. Of the in vivo behaviour of calcium phosphate cements and glasses as bone substitutes. Acta Biomater 2008;4:1924–33.

[21] Li B, Church KH, Clark PA. Robust direct-write dispensing tool and solutions for micro/meso-scale manufacturing and packaging. In: Proceedings of the ASME International Manufacturing Science and Engineering Conference; 2007. p.715–721.

[22] Puppi D, Mota C, Gazzarri M, Dinucci D, Gloria A, Myrzabekova M, Ambrosio L, Chiellini F. Additive manufacturing of wet-spun polymeric scaffolds for bone tissue engineering. Biomed Microdevices; 2012 Jul 6.

[23] Comb JW, Priedeman WR, Turley PW. Layered manufacturing control parameters and material selection criteria'. Manuf Sci Eng ASME Production Eng Division. 1994;68:547–56.

[24] Karageorgiou V, Kaplan D. Porosity of 3D biomaterial scaffolds and osteogenesis. Biomaterials 2005;26:5474–91.

[25] Lu JX, Flautre B, Anselme K, Hardouin P, Gallur A, Descamps M, et al. Descamps. Role of interconnections in porous bioceramics on bone recolonization in vitro and in vivo. J Mater Sci Mater Med 1999;10:111–20.

[26] Woodfield TB, Malda J, de Wijn J, Péters F, Riesle J, van Blitterswijk CA. Design of porous scaffolds for cartilage tissue engineering using a three-dimensional fiber-deposition technique. Biomaterials 2004;25:4149–61.

[27] Hu Y, Hu YS, Topolkaraev V, Hiltner A, Baer E. Crystallization and phase separation in blends of high stereoregular poly(lactide) with poly(ethylene glycol). Polymer 2003;44:5681–9.

[28] Kulinski Z, Piorkowska E. Crystallization, structure and properties of plasticized poly(L-lactide). Polymer 2005;46:10290–300.

[29] Navarro M, Engel E, Planell JA, Amaral I, Barbosa M, Ginebra MP. Surface characterization and cell response of a PLA/CaP glass biodegradable composite material. J Biomed Mater Res A 2008;85:477–86.

[30] Annunziata O, Asherie N, Lomakin A, Pande J, Ogun O, Benedek GB. Effect of polyethylene glycol on the liquid–liquid phase transition in aqueous protein solutions. Proc Natl Acad Sci USA 2002;99:14165–70.

[31] Aguirre A, González A, Navarro M, Castaño O, Planell JA, Engel E. Control of microenvironmental cues with a smart biomaterial composite promotes endothelial progenitor cell angiogenesis. Eur Cell Mater 2012;24:90–106.

Chapter 4 - Impact of 3-D printed PLA- and chitosan-based scaffolds on human monocyte/macrophage responses: Unraveling the effect of 3-D structures on inflammation

Implants success is highly dependent on the inflammatory response and subsequent foreign body reaction. In fact, cell response triggered immediately after material implantation may activate either the regenerative pathway or implant rejection. Therefore, understanding the effect of scaffolds properties (pore size, chemistry, surface among others) on inflammation is of paramount importance to design a new generation of materials and scaffolds able to provide the right signals to the biological environment and modulate the inflammatory response towards the regenerative side.

The previous chapters focused on the development, physico-chemical characterization and optimization of RP 3D structures with well defined geometries. This chapter focuses on a more biological approach; it studies the impact of the developed structures on human monocytes/macrophages in order to assess their *in vitro* inflammatory response and also to help unraveling the effect of 3D scaffolds´features on inflammation. To this end, not only PLA-based scaffolds developed in chapter 2 and 3 were used but also new Chitosan structures in order to introduce two new parameters namely chemistry and geometry.

4.1. Introduction

Implantation of a biomaterial elicits an inflammatory reaction, which influences the behavior of different cell populations involved in the regenerative process determining implant success [1]. The emerging view is that activation of the inflammatory process can lead to implant rejection, but is also key for efficient tissue regeneration and repair [2,3]. Having the capacity to modulate the inflammatory response will lead to more effective tissue engineering (TE) strategies. Indeed, it has been recently shown that materials modified with inflammatory molecules can impact on human natural killer cell behavior, and lead to increased mesenchymal stem/stromal cell (MSC) recruitment [4].

Inflammation is an extremely complex, multistage process involving numerous cell types and mediator signals. Macrophages are dominant infiltrating cells that respond rapidly to biomaterial implantation and play a crucial role in regulating the inflammatory response and tissue remodeling, by secreting large amounts of bioactive mediators that can initiate inflammation, cell migration and differentiation, tissue remodeling and blood vessel formation [1,2]. The mediators secreted will depend on the material properties, and will direct subsequent inflammation and/or tissue repair. If macrophages fail to phagocytose a certain material or foreign body, cells may fuse and form multinucleated giant cells (MGC), which have thus been related with the foreign body response. It is generally believed that macrophages can polarize towards either a proinflammatory or anti-inflammatory phenotype, exhibiting regulatory, pro-regenerative and angiogenic functions [5].

Monocyte/macrophage activation and cytokine secretion are affected by surface chemistry and topography [6–8]. Additionally, porous structures promote faster healing and form a thinner fibrous capsule than dense solid implants [9,10], suggesting that the implant architecture can play a role in foreign body reaction. Thus, not only the intrinsic material properties but also the geometry/architecture and surface cues of the 3-D scaffolds may be of importance in the design of new surfaces and scaffolds that can tailor macrophage activation towards a regenerative pathway.

Polylactic acid (PLA) and chitosan (Ch) are two well-known biodegradable polymers that are widely used in scaffolds for TE purposes. Both materials possess distinct chemical, physical and biological properties that may affect the inflammatory response. The inflammatory impact of the US Food and Drug Administration (FDA) approved PLA has been mainly reported in terms of the effect of its acidic degradation by-products upon implantation [11].

Though there is some literature on the PLA inflammatory response in vitro, only a few works have tackled the behavior of cells in 3-D structures [12,13]. As for Ch, some contradictory results have been reported on the inflammatory response elicited when the polymer was presented in different forms [14,15]. Recently, it was shown that 2-D Ch surfaces drive polarization of human macrophages towards an anti-inflammatory phenotype and dendritic cells towards a pro-inflammatory profile [16]. However, the effect of PLA and Ch 3-D scaffolds on primary human monocyte/macrophage responses has not been fully established.

Rapid prototyping (RP) is an emergent tool in the biomaterials field that enables fabrication of 3-D structures with well-defined and reproducible geometries and architectures. By combining polymers together with RP, it is possible to build 3-D scaffolds with different characteristics and well-distinguished geometric and physico-chemical features, allowing the study of the effect of these factors on inflammatory cell responses.

The hypothesis behind this work was that both the chemical composition and the architecture of 3-D scaffolds affect macrophage responses. We hypothesized that the geometry of pores could affect macrophage behavior and, in particular, cytokine secretion, as it has already been shown for other cells, particularly for MSCs, that differentiation depends on the geometry of the substrate (in two dimensions), by affecting the curvature of the cytoskeleton actin fibers [17]. Thus, here we set out to determine which impacted on macrophage behavior the most: the chemical composition or the geometry of the scaffold. Therefore, this work aims at: (i) the controlled fabrication of novel 3-D platforms of PLA and Ch using RP, and (ii) the study of the macrophage morphology and cytokine profile in these matrices. To this end, Ch scaffolds with two different geometries (orthogonal and diagonal) and PLA-based orthogonal scaffolds made of PLA and a combination of PLA and a biodegradable calcium phosphate glass (G5) were fabricated. Fabrication of Ch scaffolds with two defined geometries allowed us to evaluate the effect of scaffolds architecture while keeping the surface properties and material chemistry constant. In contrast, by adding G5 glass to PLA scaffolds, the effect of the surface topography/chemistry was investigated, while enhancing both the biological and mechanical performance of the scaffolds [18,19], due to G5's

bioactive properties [20]. The impact of these 3-D scaffolds on the secretion of the cytokines tumor necrosis factor (TNF)-α, interleukin (IL)-6, IL-10, IL-12/23(p40) and tumor growth factor (TGF)-β1 was analyzed. TNF-α and IL-6 are pro-inflammatory cytokines commonly analyzed when studying the inflammatory response induced by different biomaterials. Timely production of the appropriate amounts of TNF-α and IL-6 is critical for the efficient repair of, for example, bone [3], and macrophages usually associated with an inflammatory M1 or a regenerative M2b phenotype produce increased amounts of these two cytokines [21]. We also quantified the amounts of p40, thus detecting the monomer p40 and the heterodimeric cytokines IL-12 or IL-23, which consist of p40 bound to either p35 or p19 chains, respectively. These two pro-inflammatory cytokines of the same family can be produced at high levels by M1 macrophages and stimulate the differentiation of proinflammatory TH1 and TH17 cells [22]. Regarding cytokines with anti-inflammatory properties, we analyzed IL-10 and TGF-β. IL-10 is one of the most studied anti-inflammatory cytokines, as it regulates many steps of an immune response, being crucial in restraining inflammation [23]. TGF-β has a role in controlling immune homeostasis [23] and is also an important player in regulating bone repair [3].

4.2. Materials and methods

4.2.1. Materials

The materials used for the fabrication of the PLA-based scaffolds have been described in chapter 3 (3.2.1). Endotoxin-free Ch powder (Chitosan 123, France-Chitine), with M_W = 324 ± 27 × 10^3 and 11–12% of N-acetylation [4], was purified as previously described [25]. Ch solution ($3\%_{W/V}$) was prepared by hydrating Ch overnight in MilliQ water, dissolving in acetic acid (2%, Sigma) overnight at 4 °C under constant stirring and centrifuging for 5 min at 800g.

4.2.2. Scaffolds fabrication

Scaffold fabrication has been conducted following the methodology described in chapter 2 (2.2.2). Two different architectures were designed and fabricated (Fig. 4.1): (i) an orthogonal displaced doubled layer (orthogonal) configuration, with distance between struts D = 1 mm and 500 μm for Ch and PLA-based scaffolds, respectively; and (ii) an orthogonal–diagonal double layer design (diagonal) with distance D1 = 1 mm between the struts axes of the orthogonal layers and D2 = 700 μm between the struts axes of the diagonal layers. In the case of the PLA-based scaffolds, the orthogonal design was used. In the case of Ch, scaffolds were produced in two different geometries: ChO, with orthogonal struts, and ChD, with diagonal and orthogonal struts. Three-dimensional structures were built by layer-by-layer deposition. In the case of PLA-based scaffolds, a printing pressure between 40 – 80 psi, a motor speed of 3mm s^{-1} and a G27 (200 μm) nozzle were used. The syringe temperature was 40 ± 5 °C, and room temperature was 25 ± 2 °C. In the case of Ch scaffolds, a printing pressure around 40 psi, a motor speed of 7 mm s^{-1}, and a

Teflon tip with diameter of 150 µm were used. Additionally, NaOH ($8\%_{W/V}$) in ethanol (70%) was dispensed drop by drop on top of the printed struts to cross-link the polymer structure during the fabrication process [26]. Ch scaffolds were kept protected from light overnight at room temperature in NaOH ($8\%_{W/V}$) and washed three times for 5 min each with MilliQ water. Ch scaffolds were kept hydrated at 4 °C until use. Endotoxin levels were measured in water extracts prepared by incubating scaffolds in endotoxin-free water (40 ml g^{-1} material) for 24 h at 50 °C while shaking (250 rpm), and measured using the Limulus Amebocyte Lysate (LAL) QCL-1000 test (Lonza), as described elsewhere [27]. All extracts revealed endotoxin levels lower than the recommended FDA limit (0.5 EU ml^{-1}). Table 4.1 shows the different scaffolds according to their composition and geometry. Henceforth, PLA-based polymeric and composite scaffolds containing 5% (w/w) of PEG will be named PLA and PLA/G5 rispectively.

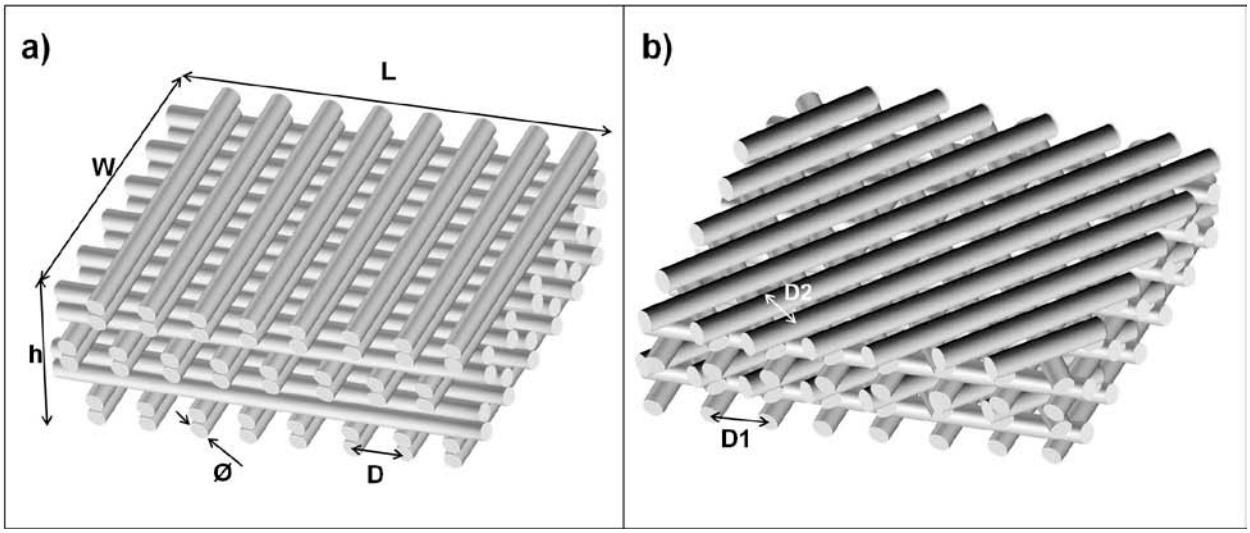

Figure 4. 1. 3-D view of the theoretical 3-D structures of (a) orthogonal and (b) diagonal scaffolds. D = 1 mm; D1 =1mm; D2 = 700 µm; w = scaffold width, h = scaffold height, L = scaffold length, Ø = 200 µm and 150 µm for PLA and Ch, respectively.

Scaffold code	Material Composition (w/w %)				Geometry	Porosity (%)	Strut size (µm ± SD)
	Polymer matrix			Glass particles			
	PLA	PEG	Ch	G5			
PLA	95	5			Orthogonal	85.7	75 ± 5
PLA/G5[a]	95	5		50	Orthogonal	85.7	75 ± 5
ChO			100		Orthogonal	75.6	250 ± 30
ChD			100		Diagonal	79.1	250 ± 30

Table 4. 1. Composition and geometry of the studied scaffolds. [a] The percentages shown for the polymer matrix of the PLA/G5 scaffolds correspond to 50% of the total weight of the scaffold.

4.2.3. Scaffold characterization

Morphological analysis of the structures was carried out by scanning electron microscopy following the procedure described in chapter 2 (2.2.3.1). However, a low vacuum was used to minimize Ch dehydration during the assays. Scaffolds porosity was calculated using the approach explained in chapter 2 (2.2.3.2).

4.2.4. Cell isolation and seeding

Human monocytes were isolated by negative selection from healthy donors buffy coats by using a RosetteSep human monocyte enrichment cocktail (StemCell Technologies), as described elsewhere [16]. Cells were resuspended in complete medium (RPMI 1640 + Glutamax (Invitrogen) supplemented with FBS (10%, Lonza) and penicillin G–streptomycin (1%, Invitrogen)). Prior to cell seeding, scaffolds 4 mm in diameter and 2 mm in height were cut and placed in 96-well culture plates. Scaffolds were disinfected in 70% ethanol, washed with PBS and then incubated in complete medium (200 μl) for at least 1 h at 37 °C/5% CO_2. Medium was removed and 1.6×10^5 cells in complete medium (5 μl) were added on top of each scaffold. As a control, cells were also cultured on tissue culture polystyrene (TCPS). Cells were incubated at 37 °C/5% CO_2 for 3 h and complete medium (200 μl) was added. Negative controls consisting of scaffolds without cells were treated in the same way. Cells were incubated for 3, 7 and 10 days prior to analysis of their metabolic activity, morphology and cytokine secretion.

4.2.5. Determining metabolic activity

Metabolic activity after 3, 7 and 10 days of incubation was assessed with a resazurin assay as described elsewhere [28]. Values obtained with scaffolds incubated in the absence of cells were subtracted in the final analysis. Three replicates for each scaffold were performed.

4.2.6. Actin staining

In order to observe cellular morphology, cells were stained for actin and nuclei. After 10 days of cell differentiation in the scaffolds, cells were washed with PBS and fixed with paraformaldehyde (4%) for 20 min at room temperature, washed with PBS and incubated with PBS/Triton (0.1%) at room temperature for 5 min. Cells were incubated with phalloidin–AlexaFluor 488 (50 μl, Invitrogen) in PBS/Triton (1:40) for 1 h and washed with PBS. Nuclei were then counterstained with 4',6-diamidino-2-phenylindole (100 μg ml^{-1}) for 10 min followed by washing with PBS. Scaffolds were imaged on a laser scanning confocal microscope (Leica TCS SP5 II, model DMI6000B-CS, Bioimaging Center for Biomaterials and Regenerative Therapies, b.IMAGE, Porto). To image the whole diameter of scaffolds, Tile Scan functionality followed by the Mosaic Merge tool were used. Nine fields of view (×10), through a depth of approximately 200 μm, were imaged. More detailed images were obtained with a × 20 water immersion objective. Maximum projection images were visualized with software LAS AF version 2.6.0.7266

(Leica). Cells with three or more nucleus were classified as MGCs and cells with an aspect ratio (major axis/minor axis) higher than 2 were considered to be elongated. A qualitative analysis was performed to compare which scaffolds favored the presence of cells with different morphologies (MGCs, with filopodia-like structures, elongated).

4.2.7. Cytokine secretion

For evaluation of cytokine secretion, supernatants were collected after 3, 7 and 10 days, centrifuged and kept frozen until analysis. TNF-α, IL-6, IL-10, IL-12/23(p40) and TGF-β1 levels were quantified by enzyme-linked immunosorbent assay (ELISA; Legend Max human ELISA kits, BioLegend) according to manufacturer's instructions. Concentrations were determined for three replicates pooled together per condition and values were corrected with the amount determined for scaffolds incubated in the absence of cells. The regulatory effect of different cytokines may depend on the context they will be acting in, but overall, TNF-α, IL-6 and IL-12/23(p40) are considered pro-inflammatory cytokines. IL-12/23 refers to the subunit p40, shared by both IL-12 and IL-23. IL-10 is an anti-inflammatory cytokine and TGF-β is associated with tissue repair.

4.3. Results

4.3.1. Scaffold characterization

Fig. 4.1 shows a schematic representation of the orthogonal and diagonal structures obtained for PLA, PLA/G5 and Ch. SEM images (Fig. 4.2) showed well-defined PLA and PLA/G5 structures, with pores of around 165 ± 5 μm in the axial direction and struts of approximately 75 ± 5 μm. Ch structures showed pores of around 380 ± 60 μm and 600 ± 93 μm for ChD and ChO, respectively, in the axial direction, and struts of around 250 ± 30 μm, which varied depending on the degree of dehydration of the hydrogel sample.

Differences between the two materials were also observed in the transverse porosity. Due to Ch swelling, pores in the transverse direction were more defined and uniform in the PLA-based scaffolds than in the Ch ones. Moreover, in PLA and PLA/G5 scaffolds, a combination of porosities, ranging from the macroscale due to the initial designed pore size to the micro- and nanoscale due to the addition of G5 particles and to the pores left by solvent evaporation, was observed. Conversely, Ch scaffolds showed rather smooth surfaces. The theoretical volume porosity percentage was 85.7% for the PLA and PLA/G5 scaffolds, and between 75.6% and 79.1% for the ChO and ChD scaffolds, respectively. The porosity percentages were calculated considering a distance between struts of 400 μm for orthogonal scaffolds, a distance between orthogonal struts of 1000 μm and a distance between diagonal struts of 700 μm for ChD.

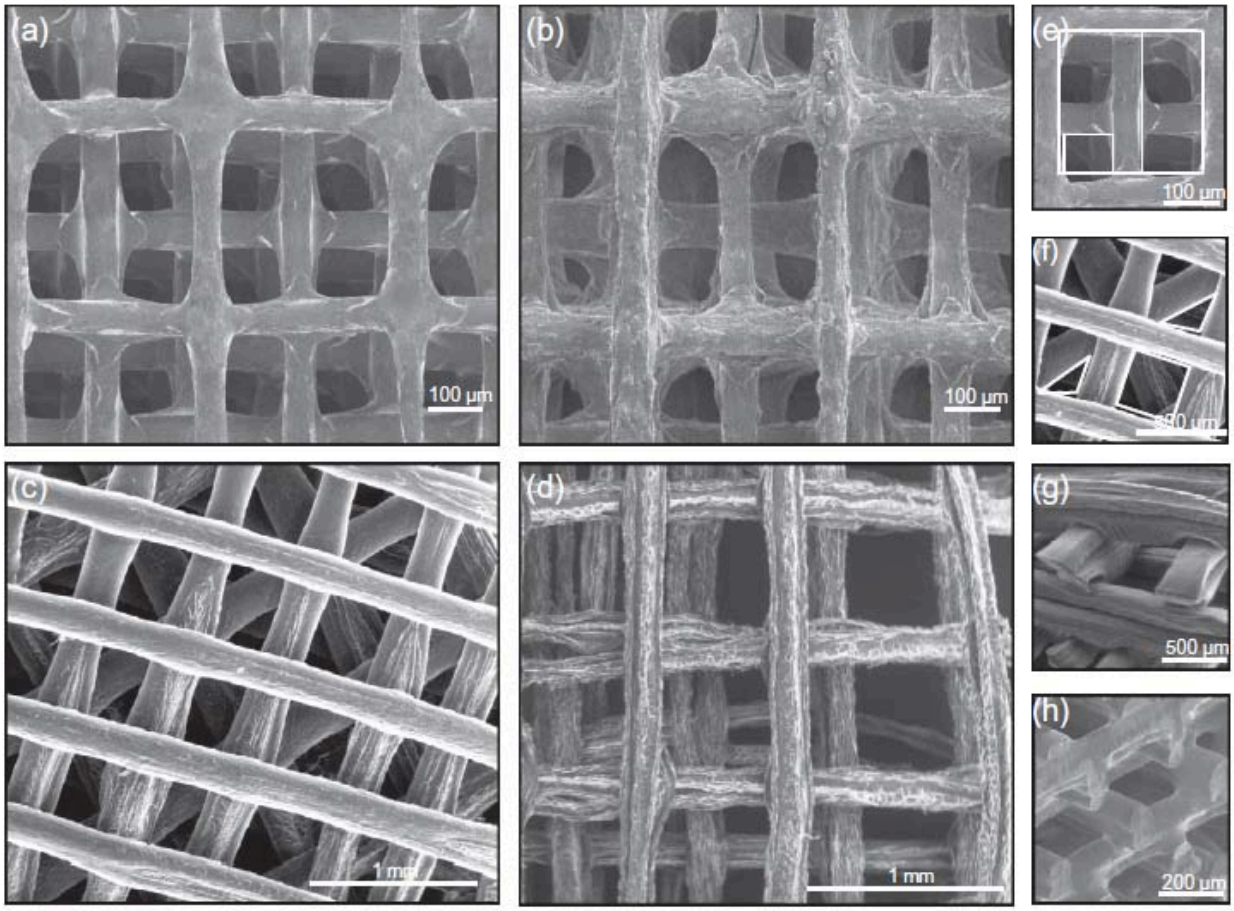

Figure 4. 2. SEM images of the four polymeric platforms. Axial view of the (a) PLA orthogonal structure, (b) PLA/G5 orthogonal structure, (c) ChD structure and (d) ChO structure, (e) pore geometry for orthogonal scaffolds, (f) pore geometry for diagonal scaffolds, (g) cross-section of a ChO scaffold and (h) cross-section of a PLA scaffold.

4.3.2. Metabolic activity

During inflammation, monocytes and not fully differentiated macrophages are recruited from the blood to the implant site, where they can differentiate into macrophages [29].

Thus, studies addressing human macrophage–biomaterial interactions are commonly performed with peripheral blood monocytes that are allowed to differentiate into macrophages [6,7,16]. In this work, cell behavior was evaluated along monocyte to macrophage development by analyzing responses at early (day 3) and late (days 7 and 10) stages of macrophage differentiation.

The metabolic activity of cells incubated on all scaffolds remained on average at around 150% of that of cells cultured for 3 days in TCPS, indicating that the different materials were not cytotoxic (Fig. 4.3). No significant differences in time were found, except for cells incubated on ChO for 7 and 10 days, where there was an increase in relative metabolic activity to an average above 250% and 185%, respectively, and for cells incubated on TCPS, which showed decreased metabolic activity with time.

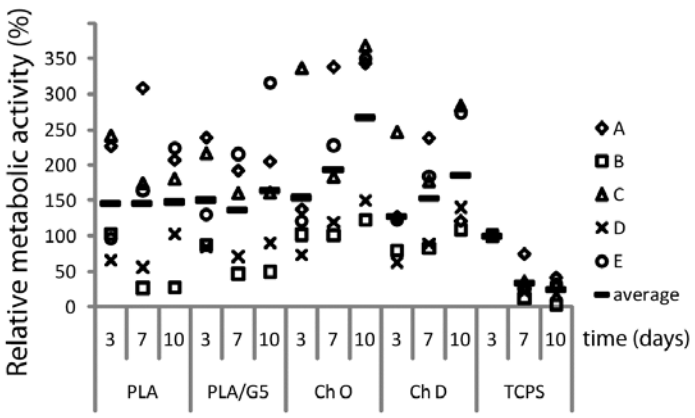

		PLA			PLA/G5			ChO			ChD			TCPS		
		3	7	10	3	7	10	3	7	10	3	7	10	3	7	10
PLA	3		ns	ns	ns	ns	ns	ns	ns	**	ns	ns	ns	ns	**	**
	7			ns	ns	ns	ns	ns	ns	**	ns	ns	ns	ns	*	**
	10				ns	ns	ns	ns	ns	**	ns	ns	ns	ns	**	**
PLA/G5	3					ns	ns	ns	ns	**	ns	ns	ns	ns	**	**
	7						ns	ns	*	**	ns	ns	ns	ns	**	**
	10							ns	ns	*	ns	ns	ns	ns	**	**
ChO	3								*	*	ns	ns	ns	ns	**	**
	7									*	ns	ns	ns	ns	**	**
	10										**	**	ns	**	**	**
ChD	3											ns	ns	ns	**	**
	7												ns	ns	**	**
	10													ns	**	**
TCPS	3														**	**
	7															ns
	10															

Figure 4. 3. Metabolic activity of monocytes/macrophages cultured on different 3-D scaffolds. Primary human monocytes were seeded on PLA, PLA/G5, ChO or ChD scaffolds or on TCPS and metabolic activity was measured by performing a resazurin assay after 3, 7 or 10 days of incubation and normalized relative to the metabolic activity in TCPS after 3 days of culture. Left, each symbol corresponds to the average of three replicas for different donors (A, B, C, D and E). The bar represents the average of the analyzed donors. Right, Mann–Whitney tests were performed for every pair of conditions (*p ≤ 0.05; **p ≤ 0.01; ns, not significant).

4.3.3. Morphological analysis (actin staining)

Actin was stained to observe the morphology of macrophages after 10 days of differentiation in the 3-D scaffolds. Microscopy observation indicated a non-uniform distribution of cells, particularly in Ch scaffolds (data not shown). A more detailed visualization of cells revealed the presence of both round and elongated cells (Fig. 4a). Furthermore, cells exhibited filopodia-like and podosome-like structures, which are involved in cell motility and adhesion, respectively (Fig. 4a). Nanotubes, which may regulate long-distance intercellular communication by allowing vesicle trafficking [30], were also observed (Fig. 4.4a). Crucially, MGCs were found, although no external cytokines were added (Fig. 4.4a). Visual inspection of the different scaffolds revealed very heterogeneous cell populations, but ChO scaffolds seemed to have more MGCs, PLA more cells with many filopodia and ChD showed more elongated cells (Fig. 4.4b).

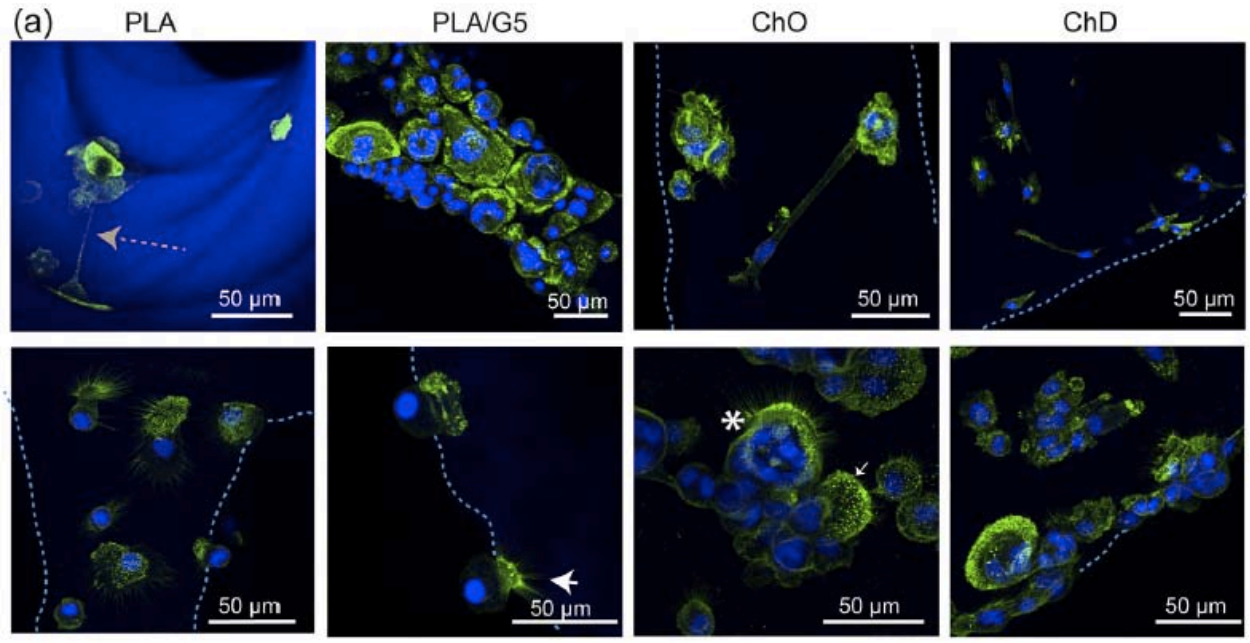

(b)

	Multinucleated Giant Cells				Cells with filopodia				Elongated cells			
	PLA	PLA/G5	ChO	ChD	PLA	PLA/G5	ChO	ChD	PLA	PLA/G5	ChO	ChD
A	+	+	+	-	+	++	+	+	+	-	++	++
B	+	+++	+	-	++	+	+	+	+	-	+	+
C	-	-	++	-	++	+	+	+	++	+	+	++
D	-	-	+	+	++	+	+	++	+	-	+	++
E	+	-	+++	+	+++	+++	++	++	-	-	+	+

Figure 4. 4. Morphology of cells in contact with the different scaffolds. Upon incubation for 10 days in the presence of the indicated scaffolds, cells were fixed and stained for actin (green) and the nuclei (blue) before being visualized by laser scanning confocal microscopy. The scaffolds can be observed in blue due to their autofluorescence. (a) Examples of macrophages and multinucleated giant cells (*) in the indicated scaffolds. Dashed lines indicate the limits of the scaffolds struts. Grey dashed arrow, nanotube. Big arrowhead, cell with filopodia-like structures. Small arrow, cell with podosome-like structures. (b) Table with the relative amounts of multinucleated giant cells, cells with filopodia and elongated cells for five independent cell donors (A–E). +, few cells; ++, some cells; +++, many cells; –, no cells.

4.3.4. Cytokine secretion

To analyze secretion of both pro- and anti-inflammatory cytokines by monocytes/macrophages in contact with scaffolds, supernatants were analyzed for TNF-α, IL-6, IL-12/23, IL-10 and TGF-β levels. Interestingly, despite donor differences, we found that, overall, TNF- α levels (Fig. 5a) were significantly higher for cells incubated on Ch than for cells incubated on PLA, PLA/G5 or TCPS, except for ChO scaffolds after 3 days. No differences were observed when comparing PLA with PLA/G5, which did not elicit any detectable amounts of this cytokine. However, differences were found when comparing Ch scaffolds with the different geometries, with ChO scaffolds leading to higher secretion of TNF- α than ChD for late time points. Also, there were no significant differences with the incubation time for each material, except with ChD, where a decrease could be observed from 7 to 10 days.

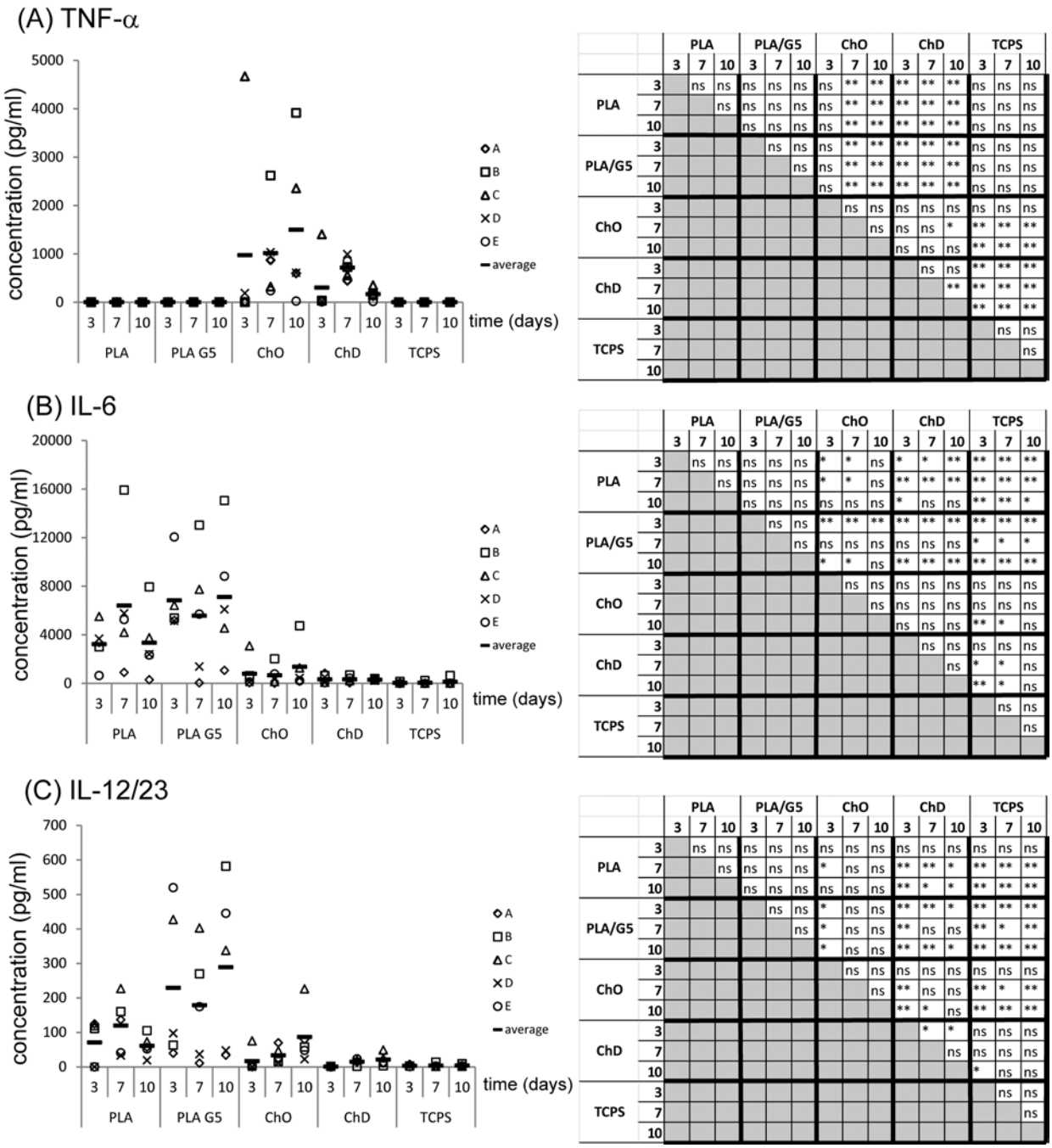

Figure 4. 5. TNF-α, IL-6 and IL-12/23 cytokine secretion pattern of monocytes/macrophages cultured on distinct scaffolds. Cells were cultured for 3, 7 or 10 days on PLA, PLA/G5, ChO or ChD scaffolds or on TCPS and the amounts of (a) TNF-a, (b) IL-6 and (c) IL-12/23 present in the pooled supernatants from three replicas were quantified by ELISA. Left, each symbol corresponds to one donor (from A to E) and the bar represents the average. Right, Mann–Whitney tests were performed for every pair of conditions (*$p \leq 0.05$; **$p \leq 0.01$; ns, not significant).

Remarkably, the analysis of IL-6 secretion revealed a different outcome (Fig. 4.5b). The amount of IL-6 was higher in PLA or PLA/G5 than in Ch scaffolds, where it remained mostly very low. However, for 10

days of incubation with ChO and 7 and 10 days with ChD, values were higher than when cells were incubated on TCPS for 3 and 7 days. No major differences were observed when comparing PLA with PLA/G5, or when comparing Ch scaffolds with different geometries.

The amount of the subunit p40, shared by both IL-12 and IL-23, was in general higher in PLA and PLA/G5 than in Ch scaffolds (with significant differences more evident with diagonal scaffolds) and in TCPS (Fig. 4.5c). No statistically significant differences were found between PLA and PLA/G5, though we observed a tendency for an increase with PLA/G5. Also, there is a trend for an increase in the amount of IL-12/23 produced over time when cells are incubated with Ch scaffolds. Furthermore, a slight but statistically significant increase was found with ChO as opposed to ChD scaffolds. The amount of IL-12/23 was higher on ChO scaffolds than with TCPS for 7 and 10 days, but no major differences were found between cells incubated on ChD or TCPS.

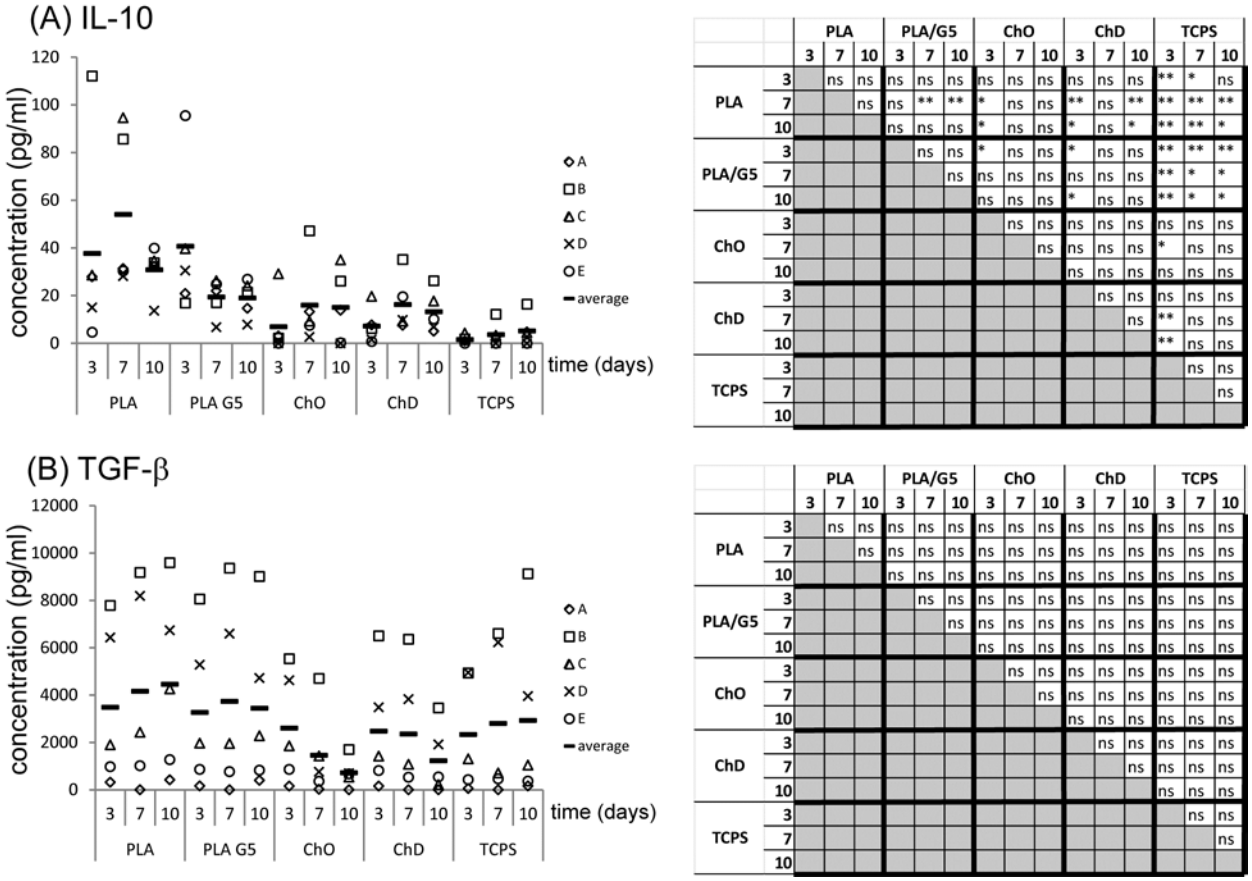

		PLA			PLA/G5			ChO			ChD			TCPS		
		3	7	10	3	7	10	3	7	10	3	7	10	3	7	10
PLA	3		ns	ns	ns	ns	ns	ns	ns	ns	ns	ns	ns	**	*	ns
	7			ns	ns	**	**	*	ns	ns	**	ns	**	**	**	**
	10				ns	ns	ns	*	ns	ns	*	ns	*	**	**	*
PLA/G5	3					ns	ns	*	ns	ns	*	ns	ns	**	**	**
	7						ns	ns	ns	ns	ns	ns	ns	**	*	*
	10							ns	ns	ns	*	ns	ns	**	*	*
ChO	3								ns	ns	ns	ns	ns	ns	ns	ns
	7									ns	ns	ns	ns	*	ns	ns
	10										ns	ns	ns	ns	ns	ns
ChD	3											ns	ns	ns	ns	ns
	7												ns	**	ns	ns
	10													**	ns	ns
TCPS	3														ns	ns
	7															ns
	10															

		PLA			PLA/G5			ChO			ChD			TCPS		
		3	7	10	3	7	10	3	7	10	3	7	10	3	7	10
PLA	3		ns	ns	ns	ns	ns	ns	ns	ns	ns	ns	ns	ns	ns	ns
	7			ns	ns	ns	ns	ns	ns	ns	ns	ns	ns	ns	ns	ns
	10				ns	ns	ns	ns	ns	ns	ns	ns	ns	ns	ns	ns
PLA/G5	3					ns	ns	ns	ns	ns	ns	ns	ns	ns	ns	ns
	7						ns	ns	ns	ns	ns	ns	ns	ns	ns	ns
	10							ns	ns	ns	ns	ns	ns	ns	ns	ns
ChO	3								ns	ns	ns	ns	ns	ns	ns	ns
	7									ns	ns	ns	ns	ns	ns	ns
	10										ns	ns	ns	ns	ns	ns
ChD	3											ns	ns	ns	ns	ns
	7												ns	ns	ns	ns
	10													ns	ns	ns
TCPS	3														ns	ns
	7															ns
	10															

Figure 4. 6. IL-10 and TGF-b cytokine secretion pattern of monocytes/macrophages cultured on distinct scaffolds. Cells were cultured for 3, 7 or 10 days on PLA, PLA/G5, ChO or ChD scaffolds or on TCPS and the amounts of (a) IL-10 and (b) TGF-β present in the supernatant were quantified by ELISA. Left, each symbol corresponds to one donor (from A to E) and the bar represents the average. Right, Mann–Whitney tests were performed for every pair of conditions (*$p \leq 0.05$; **$p \leq 0.01$; ns, not significant).

Interestingly, there was a tendency for IL-10 levels to be higher with PLA than with other scaffolds (Fig. 6a). Significant differences were found when comparing cells cultured on PLA or PLA/G5 with cells

cultured on TCPS. Cells seeded on PLA (cultured for 7 and 10 days) or PLA/G5 (3 days) showed significantly higher values than cells seeded on ChO (3 days) and ChD (3 and 10 days) scaffolds and on TCPS (3, 7 and 10 days). Also, IL-10 levels were significantly higher on cells cultured on PLA for 7 days than on PLA/G5 (7 and 10 days). Though the amount of secreted IL-10 was slightly higher for cells cultured on Ch scaffolds than on TCPS, no significant differences were found. Finally, no significant differences were found for secretion of TGF-β in the presence of the different scaffolds (Fig. 4.6b).

4.4. Discussion

New approaches elucidating the role of inflammation and of macrophages in particular, in tissue repair/regeneration are attracting more and more attention within the field of regenerative medicine. Though the role of the inflammatory response to implantable biomaterials has long been recognized, the impact of 3-D scaffolds on human immune cells has not been properly examined and described. Many studies are currently done with murine models, and caution should be taken when extrapolating data to the human system, as a direct comparison between the human and murine immune responses remains controversial [31]. Here, striking differences in the cytokine secretion profile of human macrophages interacting with 3-D structures with different architectures and surface properties were revealed. To study the response of macrophages to differences in scaffold geometry and surface properties (mainly chemistry), we chose to study four platforms: two based on PLA (PLA and PLA/G5) and two based on Ch (ChO and ChD). PLA, PLA/G5 and ChO allowed us to study differences in surface chemistry and topography while keeping the same architecture, whereas ChD and ChO allowed us to evaluate differences due to architecture while keeping the same chemistry/topography. As far as we are aware, this is the first study where the specific impact of materials with precisely defined 3-D structures on macrophage responses was analyzed (as opposed to 2-D materials with different topographies or comparisons between 3-D materials with disorganized and random porous and non-porous structures).

Rapid prototyping was used to fabricate structures with a well-defined and reproducible geometry. PLA (thermostable polymer) and Ch (hydrogel) require completely different fabrication approaches. Thus, the fabrication parameters were optimized and carefully tuned for the fabrication of both PLA- and Ch-based scaffolds. In the case of PLA-based scaffolds, the right interplay between temperature/plasticizer/printing parameters and the post-processing shrinkage of the struts was achieved to obtain scaffolds with struts with significantly smaller diameter than the nominal ones [18]. For Ch, the right concentration and dispensing rate of the NaOH solution to neutralize and cross-link Ch and keep the scaffolds' integrity were optimized.

Though PLA is a well-known polymer in the biomedical field, its use in the fabrication of rapid prototyping scaffolds, in particular by nozzle-based printing systems, has been limited. Currently, most of the work done with PLA and 3-D printing require the molecular modification of the PLA matrix, or the use of high temperatures to melt the polymer [32–34]. Thus, as reported in chapter 3 [18], fabrication of PLA-based scaffolds, like the ones reported in this work, with higher resolution than the ones obtained

with other currently used methods is a novelty. Also, in addition to the high resolution achieved, having the possibility of adding up to 50% (w/w) of glass particles (< 40 μm) distributed well within the scaffold, as well as tuning other properties, such as the mechanical properties or surface topography, by controlling the solvent and glass concentrations, are advantages over current PLA RP scaffolds.

Chitosan scaffolds with orthogonal geometry have been previously developed by a rapid prototyping robotic system [26,35], by hybrid system coupling nozzle deposition and by freeze-drying processes [36]. However, the present study allowed the development of two different designs: a displaced double-layer design (ChO) and an orthogonal–diagonal one (ChD). Moreover, the scaffolds developed in this study have achieved a structural integrity that allows them to be used without being lyophilized. Most of the studies found in the literature performed biological assessment on freeze-dried scaffolds.

Ch swells when in contact with aqueous media and thus structures with significantly larger struts diameter than the predefined one were obtained. Observation of hydrated Ch scaffolds by SEM has rarely been reported. Here, a low vacuum protocol was chosen to reduce the vacuum effect and analyze the Ch structures. According to SEM analysis, despite the struts' thickness differences in comparison to predefined structures, the predetermined geometry and the distance between theoretical axes were successfully reproduced. The remarkable difference in diameter between PLA and Ch scaffolds was translated into a higher surface area of PLA and PLA/G5 structures in comparison to Ch ones. With respect to porosity, all structures presented pores between 150 and 600 μm, which are in the accepted range for cell growth, migration and vascularization [37,38]. With Ch, the sizes of struts and pores were highly dependent on the degree of hydration of the sample. Ch swelling also led to differences in the transverse porosity, pores in the Ch scaffolds being considerably smaller than those in the PLA and PLA/G5 counterparts. Relevant differences in the axial porosity of ChD and ChO were also observed. ChD displayed smaller pores and a different pore geometry due to the presence of diagonal struts, which led to the formation of triangular pores and decreased the pore size in comparison to the orthogonal design.

These four scaffolds (PLA, PLA/G5, ChO and ChD) were then used to determine whether and how these properties might affect human monocytes/macrophages responses.

Analysis of the cells metabolic activity revealed small differences between the different structures, while the values for metabolic activity in TCPS were found to be low. This implies that scaffolds supported adhesion and development of monocyte/macrophages. Visualization of cells upon actin staining showed that cells could indeed adhere to all of the scaffolds analyzed. Furthermore, observations of cellular morphology indicate that cells interacting with scaffolds adhere, communicate with each other and can adopt varied morphologies, showing a heterogeneous profile in all scaffolds. Cell morphology was analyzed by imaging up to 200 μm, as confocal imaging did not allow imaging deeper in the scaffold. In our previous studies with MSCs, scaffolds were cut into slices and cells were found to be distributed throughout the scaffold, with no significant differences between the surface and the inner scaffold (data not shown). Also, scaffolds used in this work had pore sizes that should allow cells to migrate easily.

Thus, it is reasonable to assume that no major differences will be found between different layers of these scaffolds.

Interestingly, observation of MGCs was more evident in ChO. The presence of MGCs correlated with a higher secretion of TNFa, which is one of the main cytokines related to MGCs, being involved in granuloma formation [39]. Elongated cells were observed mainly in ChD scaffolds, whereas rounded cells with filopodia-like structures were mainly present in PLA scaffolds. The effect of both surface chemistry and topography on cell morphology has been widely documented [40–42]. The structures used in this study presented somewhat different surface properties. Previous surface characterization of these materials revealed contact angles of 76.6° for PLA (PLA/PEG), 60.3° for PLA/G5 (PLA/PEG/G5) and 87.2° for Ch; and roughness values (S_a) of 147.12 nm for PLA, 1003.89 nm for PLA/G5 and 1.50 nm for Ch [18,43]. Though these values were obtained from polymer films, it is most likely that they are also valid for the studied 3-D structures since the fabrication process of both films and 3-D scaffolds is similar. Here, elongated cells were more evident in both Ch scaffolds, specifically in ChD. Given that almost no elongated cells were seen in PLA/G5, which are the rougher scaffolds, these results suggest that macrophages have a tendency to adopt an elongated configuration when in contact with flatter/smooth surfaces, in agreement with others, who showed an increase in cell elongation with decreasing roughness [41]. The more rounded cells with filopodia-like structures, found mainly on PLA and PLA/G5, seemed to prefer rougher surfaces. Similar macrophage morphology has been reported by other studies both in vitro and in vivo [1,40]. On the other hand, as experiments reported here were performed in the presence of serum, it is also possible that scaffolds with a different chemical composition affect macrophage behavior indirectly, due to differences in protein adsorption on their surface. Indeed, protein adsorption to surfaces with different chemistries has been shown to affect macrophage adhesion and morphology [42]. Paracrine effects between cells adhering to the scaffolds or to the plastic surface, which may regulate subsequent cell behavior, cannot be excluded.

A major goal of this work was to determine a cytokine profile of monocyte/macrophages when in contact with different 3-D scaffolds. The impacts of the 3-D PLA and Ch scaffolds on the macrophage cytokine profile are substantially different (Fig. 4.7). Clearly, the PLA and PLA/G5 scaffolds lead to a secretion profile distinct from that of Ch, with the former eliciting higher secretion of IL-6, IL-12/23 and IL-10. Strikingly, Ch scaffolds stimulated production of large amounts of TNF-α, which remained high through the incubation time, and small amounts of IL-10 that did not increase with time, with no differences in the amount of TGF-β being secreted. The results presented here are thus somewhat different from what has been found with 2-D Ch films, where production of pro-inflammatory cytokines decreased with time and production of IL-10 and TGF-β increased [16]. Different outcomes on macrophage behavior in the presence of 2-D or 3-D substrates have also been reported by others [44] and attest to the importance of studying the impact of 3-D scaffolds on inflammatory responses for TE approaches.

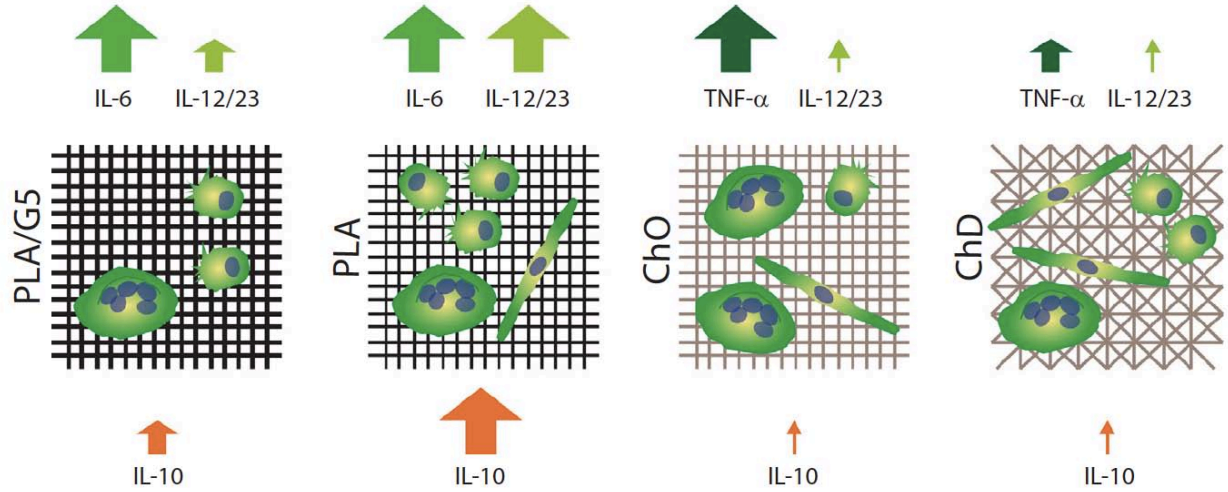

Figure 4. 7. Scheme summarizing the effect of each scaffold on macrophage cytokine profile. The overall tendency for cytokine secretion levels by macrophages cultured with the analyzed scaffolds is represented by arrows of different sizes. Red and green arrows represent anti- and pro-inflammatory cytokines, respectively. MGCs, elongated cells and cells with filopodia-like structures are also represented. Not to scale.

As for the impact of scaffold geometry, some differences were found when comparing ChO with ChD scaffolds, with the orthogonal scaffolds stimulating higher levels of TNF-α and IL-12/23, particularly for late time points, correlating with an increase in the metabolic activity. This correlation between the amounts of TNF-α and IL-12/23 with the cells' metabolic activity is most likely not due to an increase in cell number, as otherwise the secreted amounts of IL-10 and TGF-β would also have increased with time and also macrophages are unlikely to proliferate. Here we used a resazurin assay to estimate the metabolic activity of macrophages, which more specifically measures the cells redox metabolism. Interestingly, it has been suggested that the cells redox metabolism may contribute to macrophage polarization, and that proinflammatory cells are associated with a ''reductive state'' [45,46]. This correlates well with the fact that scaffolds leading to increased metabolic activity (ChO) also lead to increase production of the pro-inflammatory cytokines TNF-α and IL-12/23.

Interestingly, more MGCs existed in the presence of orthogonal scaffolds while diagonal scaffolds had more elongated cells. Taken together, these data seem to suggest that an orthogonal geometry is correlated with a stronger inflammatory reaction than a diagonal geometry, where cells may adopt more elongated morphologies upon adhesion to struts that form tighter angles and smaller pores. In line with this hypothesis, substrate shape can indeed affect cellular behavior, as seen, for example, with MSC differentiation [17] and proliferation of pre-osteoblastic cells [47].

Some studies have focused on analyzing whether macrophages polarize towards an M1 or an M2 phenotype, which have been correlated with a pro-inflammatory and a pro-regenerative function, respectively, by analyzing the production of a number of soluble factors and the expression of cell surface markers [2,16,21]. Here, we focused on characterizing a cytokine secretion profile that is a crucial functional readout, rather than analyzing in detail the polarization of cells into M1 or M2. Thus, we

quantified the secretion of the cytokines TNF-α, IL-6, IL-12/23, IL-10 and TGF-β, which are commonly analyzed with biomaterials and have a role in regulating tissue repair/regeneration. Interestingly, for each scaffold we describe a profile that is not typical of either a classic M1 or M2 phenotype. The heterogeneity of monocyte/macrophage populations implicates difficulties in classify them within any of these two types. Macrophage plasticity implies that cells may shift from one profile to the other [5], and it has even been suggested that this plasticity allows cells to transdifferentiate [48]. Others have also found that culturing macrophages in 3-D nanofibers induced the expression of surface markers characteristic of M1 macrophages, accompanied by secretion of pro-angiogenic factors and decreased production of pro-inflammatory cytokines, which usually characterizes M2 polarization [44]. Furthermore, it has been suggested that, at least in a pathogenic scenario, macrophages can exhibit a heterogeneous profile, expressing both M1 and M2 markers at the same time [49]. Therefore, more than classifying cells as being M1 or M2, it is important to understand which functional responses will be stimulated by different biomaterials, cytokines being crucial players in driving subsequent cellular responses.

4.5. Conclusions

Building the right 3-D platforms with parameters that are tunable on demand is of paramount importance to analyzing and deciphering the monocyte/macrophage response to different materials/structures. Rapid prototyping has been demonstrated to be a valuable tool for the fabrication of such platforms. This work shows that the impact of four different 3-D platforms on macrophage morphology and cytokine profile is distinct, with macrophages being mostly affected by material properties and slightly by scaffold features such as pore geometry. More specifically, PLA-based scaffolds induced higher production of IL-6, IL-12/23 and IL-10, while Ch led to increased secretion of TNF-α, with the scaffold geometry impacting on the amounts of TNF-α and IL-12/23 secreted. Thus, we believe that it is important to select biomaterials based on the right chemistry, surface properties and geometry. However, the ideal response and cytokine environment still remain uncertain, and more complex studies (e.g. with co-cultures with other cell types, testing more surface features) are required.

4.6. References

[1]. Anderson JM, Rodriguez A, Chang DT. Foreign body reaction to biomaterials. Semin Immunol 2008;20:86–100.

[2]. Brown BN, Ratner BD, Goodman SB, Amar S, Badylak SF. Macrophage polarization: an opportunity for improved outcomes in biomaterials and regenerative medicine. Biomaterials 2012;33:3792–802.

[3]. Mountziaris PM, Spicer PP, Kasper FK, Mikos AG. Harnessing and modulating inflammation in strategies for bone regeneration. Tissue Eng Part B Rev 2011;17:393–402.

[4]. Almeida CR, Vasconcelos DP, Gonçalves RM, Barbosa MA. Enhanced mesenchymal stromal cell recruitment via natural killer cells by incorporation of inflammatory signals in biomaterials. J R Soc Interface 2012;9:261–71.

[5]. Porcheray F, Viaud S, Rimaniol AC, Leone C, Samah B, Dereuddre-Bosquet N, et al. Macrophage activation switching: an asset for the resolution of inflammation. Clin Exp Immunol 2005;142:481–9.

[6]. Bota PCS, Collie AMB, Puolakkainen P, Vernon RB, Sage EH, Ratner BD, et al. Biomaterial topography alters healing in vivo and monocyte/macrophage activation in vitro. J Biomed Mater Res 2010;95A:649–57.

[7]. DeFife KM, Colton E, Nakayama Y, Matsuda T, Anderson JM. Spatial regulation and surface chemistry control of monocyte/macrophage adhesion and foreign body giant cell formation by photochemically micropatterned surfaces. J Biomed Mater Res 1999;45:148–54.

[8]. Waterfield JD, Ali TA, Nahid F, Kusano K, Brunette DM. The effect of surface topography on early NFjB signaling in macrophages. J Biomed Mater Res 2010;95A:837–47.

[9]. Hulbert SF, Morrison SJ, Klawitter JJ. Tissue reaction to three ceramics of porous and non-porous structures. J Biomed Mater Res 1972;6:347–74.

[10]. Ward WK, Slobodzian EP, Tiekotter KL, Wood MD. The effect of microgeometry, implant thickness and polyurethane chemistry on the foreign body response to subcutaneous implants. Biomaterials 2002;23:4185–92.

[11]. Turvey TA, Proffit WP, Phillips C. Biodegradable fixation for craniomaxillofacial surgery: a 10-year experience involving 761 operations and 745 patients. Int J Oral Surg 2011;40:244–9.

[12]. Saino E, Focarete ML, Gualandi C, Emanuele E, Cornaglia AI, Imbriani M, et al. Effect of electrospun fiber diameter and alignment on macrophage activation and secretion of proinflammatory cytokines and chemokines. Biomacromolecules 2011;12:1900–11.

[13]. Pan H, Jiang H, Kantharia S, Chen W. A fibroblast/macrophage co-culture model to evaluate the biocompatibility of an electrospun dextran/PLGA scaffold and its potential to induce inflammatory responses. Biomed Mater 2011;6:065002.

[14]. Barbosa JN, Amaral IF, Aguas AP, Barbosa MA. Evaluation of the effect of the degree of acetylation on the inflammatory response to 3D porous chitosan scaffolds. J Biomed Mater Res 2010;93A:20–8.

[15]. Guzmán-Morales J, Ariganello MB, Hammami I, Thibault M, Jolicoeur M, Hoemann CD. Biodegradable chitosan particles induce chemokine release and negligible arginase-1 activity compared to IL-4 in murine bone marrow-derived macrophages. Biochem Biophys Res Commun 2011;405:538–44.

[16]. Oliveira MI, Santos SG, Oliveira MJ, Torres AL, Barbosa MA. Chitosan drives anti-inflammatory macrophage polarisation and pro-inflammatory dendritic cell stimulation. Eur Cells Mater 2012;24:136–52. discussion 52–3.

[17].Kilian KA, Bugarija B, Lahn BT, Mrksich M. Geometric cues for directing the differentiation of mesenchymal stem cells. Proc Natl Acad Sci U S A 2010;107:4872–7.

[18].Serra T, Planell JA, Navarro M. High-resolution PLA-based composite scaffolds via 3-D printing technology. Acta Biomater 2013;9:5521–30.

[19].Navarro M, Aparicio C, Charles-Harris M, Ginebra MP, Engel E, Planell JA. Development of a biodegradable composite scaffold for bone tissue engineering: physicochemical, topographical, mechanical, degradation, and biological properties. Adv Polym Sci 2006;200:209–31.

[20].Navarro M, Ginebra MP, Planell JA. Cellular response to calcium phosphate glasses with controlled solubility. J Biomed Mater Res 2003;67A:1009–15.

[21].Mantovani A, Sica A, Sozzani S, Allavena P, Vecchi A, Locati M. The chemokine system in diverse forms of macrophage activation and polarization. Trends Immunol 2004;25:677–86.

[22].Vignali DA, Kuchroo VK. IL-12 family cytokines: immunological playmakers. Nat Immunol 2012;13:722–8.

[23].Banchereau J, Pascual V, O'Garra A. From IL-2 to IL-37: the expanding spectrum of anti-inflammatory cytokines. Nat Immunol 2012;13:925–31.

[24].Navarro M, Ginebra MP, Clement J, Martinez S, Avila G, Planell JA. Physicochemical degradation of titania-stabilized soluble phosphate glasses for medical applications. J Am Ceram Soc 2003;86:1345–52.

[25].Antunes JC, Pereira CL, Molinos M, Ferreira-da-Silva F, Dessı` M, Gloria A, et al. Layer-by-layer self-assembly of chitosan and poly(c-glutamic acid) into polyelectrolyte complexes. Biomacromolecules 2011;12:4183–95.

[26].Geng L, Feng W, Hutmacher DW, Wong YS, Loh HT, Fuh JYH. Direct writing of chitosan scaffolds using a robotic system. Rapid Prototyping J 2005;11: 90–7.

[27].Santos SG, Lamghari M, Almeida CR, Oliveira MI, Neves N, Ribeiro AC, et al. Adsorbed fibrinogen leads to improved bone regeneration and correlates with differences in the systemic immune response. Acta Biomater 2013;9: 7209–17.

[28].Bidarra SJ, Barrias CC, Barbosa MA, Soares R, Granja PL. Immobilization of human mesenchymal stem cells within RGD-grafted alginate microspheres and assessment of their angiogenic potential. Biomacromolecules 2010;11: 1956–64.

[29].Franz S, Rammelt S, Scharnweber D, Simon JC. Immune responses to implants – a review of the implications for the design of immunomodulatory biomaterials. Biomaterials 2011;32:6692–709.

[30].Önfelt B, Nedvetzki S, Benninger RKP, Purbhoo MA, Sowinski S, Hume AN, et al. Structurally distinct membrane nanotubes between human macrophages support long-distance vesicular traffic or surfing of bacteria. J Immunol 2006;177:8476–83.

[31].Mestas J, Hughes CC. Of mice and not men: differences between mouse and human immunology. J Immunol 2004;172:2731–8.

[32].Melchels FPW, Feijen J, Grijpma DW. A poly(D, L-lactide) resin for the preparation of tissue engineering scaffolds by stereolithography. Biomaterials 2009;30:3801–9.

[33].Xiong Z, Yan YN, Wang SG, Zhang RJ, Zhang C. Fabrication of porous scaffolds for bone tissue engineering via low-temperature deposition. Scripta Mater 2002;46:771–6.

[34].Taboas JM, Maddox RD, Krebsbach PH, Hollister SJ. Indirect solid free form fabrication of local and global porous, biomimetic and composite 3D polymer– ceramic scaffolds. Biomaterials 2003;24:181–94.

[35].Ang TH, Sultana FSA, Hutmacher DW, Wong YS, Fuh JYH, Mo XM, et al. Fabrication of 3D chitosan–hydroxyapatite scaffolds using a robotic dispensing system. Mater Sci Eng C 2002;20:35–42.

[36].Liu L, Xiong Z, Yan YN, Zhang RJ, Wang XH, Jin L. Multinozzle low-temperature deposition system for construction of gradient tissue engineering scaffolds. J Biomed Mater Res B 2009;88B:254–63.

[37].Hollister SJ. Porous scaffold design for tissue engineering. Nat Mater 2005;4:518–24.

[38].Karageorgiou V, Kaplan D. Porosity of 3D biomaterial scaffolds and osteogenesis. Biomaterials 2005;26:5474–91.

[39].Hernandez-Pando R, Bornstein QL, Aguilar Leon D, Orozco EH, Madrigal VK, Martinez Cordero E. Inflammatory cytokine production by immunological and foreign body multinucleated giant cells. Immunology 2000;100:352–8.

[40].Lee HS, Stachelek SJ, Tomczyk N, Finley MJ, Composto RJ, Eckmann DM. Correlating macrophage morphology and cytokine production resulting frombiomaterial contact. J Biomed Mater Res 2013;101:203–12.

[41].Chen S, Jones JA, Xu Y, Low HY, Anderson JM, Leong KW. Characterization of topographical effects on macrophage behavior in a foreign body response model. Biomaterials 2010;31:3479–91.

[42].Maciel J, Oliveira MI, Gonçalves RM, Barbosa MA. The effect of adsorbed fibronectin and osteopontin on macrophage adhesion and morphology on hydrophilic and hydrophobic model surfaces. Acta Biomater 2012;8:3669–77.

[43].Amaral IF, Granja PL, Melo LV, Saramago B, Barbosa MA. Functionalization of chitosan membranes through phosphorylation: atomic force microscopy, wettability, and cytotoxicity studies. J Appl Polym Sci 2006;102:276–84.

[44].Bartneck M, Heffels KH, Pan Y, Bovi M, Zwadlo-Klarwasser G, Groll J. Inducing healing-like human primary macrophage phenotypes by 3D hydrogel coated nanofibres. Biomaterials 2012;33:4136–46.

[45].Biswas SK, Mantovani A. Orchestration of metabolism by macrophages. Cell Metab 2012;15:432–7.

[46].Murata Y, Shimamura T, Hamuro J. The polarization of Th1/Th2 balance is dependent on the intracellular thiol redox status of macrophages due to the distinctive cytokine production. Int Immunol 2002;14:201–12.

[47].Bidan CM, Kommareddy KP, Rumpler M, Kollmannsberger P, Fratzl P, Dunlop JW. Geometry as a factor for tissue growth: towards shape optimization of tissue engineering scaffolds. Adv Healthcare Mater 2012;2:186–94.

[48].Mooney JE, Rolfe BE, Osborne GW, Sester DP, van Rooijen N, Campbell GR, et al. Cellular plasticity of inflammatory myeloid cells in the peritoneal foreign body response. Am J Pathol 2010;176:369–80.

[49].Pettersen JS, Fuentes-Duculan J, Suarez-Farinas M, Pierson KC, Pitts-Kiefer A, Fan L, et al. Tumor-associated macrophages in the cutaneous SCC microenvironment are heterogeneously activated. J Invest Dermatol 2011;131:1322–30.

Chapter 5 - PLA and PLA/CaP glass 3D scaffolds for Guided Bone Regeneration (GBR) devices: An *in vivo* study

Chapter 4 showed how materials, geometries and morphological features affect the *in vitro* inflammatory response to different 3D-printed scaffolds. Moreover, the important role of biomaterials on monocytes/macrophages morphology and cytokines profile was observed. In addition to surface properties and geometrical features, scaffolds degradation rate also play an important role in the inflammatory response.

Given the known relation between inflammation and regeneration, and the effect of scaffolds properties on inflammatory cells, the present chapter aims to develop and characterize a novel scaffold, a 3D biphasic PLA - PLA/G5 scaffold for Guided Bone Regeneration (GBR). The study involves an *in vitro* degradation evaluation of the scaffolds together with *in vivo* testing.

Combining the previous *in vitro* analysis with the study of *in vivo* response will allow a better understanding of the role of scaffold design parameters with the final goal of modulating inflammation and improving tissue regeneration.

5.1. Introduction

The search of novel and suitable bone grafts for the treatment of osseous defects is strongly required. Bone defects may originate as a result of dental and periodontal infections, traumatic injuries, tumor surgery, congenital diseases or developmental disorders, among others.

For instance, periodontal disease is due to chronic inflammation and bacterial infection of the gum that diffuse to the ligaments and alveolar bone that support the teeth. If it is not adequately threated can provoke the reduction of bone level at the zone surrounding the teeth with consequently loss.

Among the strategies to increase the rate of bone formation and to expand the bone volume, guided bone regeneration (GBR) represents one of the most promising approaches. The main fundamentals of GBR have had origin during the eighties with the guided tissue regeneration strategies (GTR) developed by Nyman and Karring [1]. Since then, GBR methods have been used to enhance bone tissue in the site with lack of bone volume for the fixation of endosseous dental implants. GTR process is based on the principle of guiding the proliferation and regrowth of the different components of the periodontal tissue. GTR strategies have also been applied for the regeneration of other areas such as bone loss due to dental trauma or maxillofacial injuries that need plastic surgery procedures.

Basically, the main concept of GBR is that the cells migrating in a defined zone establish the tissue regenerating in that zone. In order to guarantee the augmentation of bone volume, a mechanism to stop the fast moving epithelia tissue is required. Therefore, the development of barrier-systems enabling the exclusion of endothelial and gingival connective tissue cells from the resorbed bone area is a good

option. Such systems could allow the periodontal ligament cells and bone cells to repopulate the area and regenerate new bone.

More specifically, it would be desirable to develop scaffolds/membranes that act as a) initial barrier that becomes integrated by the tissue afterwards, and b) stimulates transmembrane vascularization with the end of supplying oxygen and nutrient to the inner zone for promoting bone development. Indeed, vascularization of the implanted material is a fundamental aspect for its integration and degradation, and therefore the tissue growth [2].

Up to now, a number of membrane systems have been adopted both in experimental and clinical studies for GBR. Different no resorbable materials have been successfully used such as polytetrafluoroethylene (PTFE) [3], titanium [4]. In spite of their high performance in GBR, such materials have a clear limitation to be non resorbable and, therefore, have to be removed with a second surgical procedure. This procedure can also damage the tissue and affect patients' morbidity. Thus, the aim of recent research in guided bone regeneration is the development of resorbable barriers for clinical application. A number of biodegradable materials have been used such as freeze-dried collagen [5], silk fibroin [6], polylactic-co-glycolic acid [7] among others. Moreover, novel studies have been conducted by using membrane guides in conjunction with preformed porous scaffolds or a particulate osteoconductive material in order to enhance bone regeneration [8]. Several approaches such as growth factors, or antibiotics have been used for the activation of vascularization through scaffolds and to avoid infections in the implanted site [9,10]. Among others, a more typical tissue engineering strategy has been adopted by Gomez and colleagues [11] applying a cell sheet technique for cementum-periodontal regeneration. However, the implantation of such fragile *in vitro* developed extracellular matrix sheet has been always coupled with a support of synthetic membranes that eventually need a second operation to be extracted. To increase implant stability and avoid the membrane extraction step, Vaquette and colleagues proposed a cell-engineering construct in which different cells where previously *in vitro* seeded on a biodegradable scaffold obtained coupling rapid prototyping with electrospum fibers to regenerate bone and periodontal ligament respectively [12]. Nevertheless, the advantages of using cell-free scaffolds have been already mentioned in the introduction of this thesis, and are strongly required for GBR applications.

In this scenario, the development of biphasic cell-free scaffolds composed by PLA and PLA/G5 could be a good option to regenerate the soft tissue and the bone compartment respectively. The G5 angiogenic effect [13,14] could contribute to the transmembrane vascularization that selectively will form new bone and soft tissue. Moreover, the use of 3D-printing technique allows the fabrication of biphasic scaffold in a controllable and reproducible way with a precise spatial deposition of materials. In addition, it permits evaluating the role of both PLA and PLA/G5 while keeping same structural/geometrical properties.

Recent works indicate that macrophages and multinucleated giant cells (MGCs), both starring actors of the inflammatory response and foreign body reaction are not only involved in the degradation process of implanted biomaterial scaffolds but also on the production of angiogenic signaling molecules, such as

VEGF that could also contribute significantly to scaffold vascularization [6,15]. In particular, it has been shown that the penetration of host inflammatory cells, specifically macrophages, into a fibroin scaffold play a key role in the vascularization process by their production of pro-angiogenic growth factors [6].

Moreover, it has been reported that the host tissue reaction is in some way related to the material degradation rate, being macrophages and multinucleated giant cells involved in the degradation of scaffolds [6,16]. Thus, from this point of view, it is important to understand the degradation behavior of the material and its relation to MGCs formation in order to develop suitable scaffolds for guided tissue regeneration. In this chapter, various experiments have been performed to determine the impact of the developed scaffolds on monocytes and further MGCs fusion and stimulation due to materials degradation. Furthermore, the pro-angiogenic effect of G5 together with the presence of MGCs is also evaluated.

The aims of this work are: a) the design, fabrication, and characterization of new biphasic scaffolds composed by PLA and PLA/G5 phases, b) evaluation of the in vitro degradation behavior of PLA and PLA/G5 scaffolds, and c) the assessment of the *in vivo* response of the studied scaffolds in terms of inflammation and vascularization in order to evaluate their potential for GBR applications.

5.2. Materials and Methods

5.2.1. Materials

The materials used have been described in chapter 2 (2.2.1) and combined according to the compositions shown in Table 5.1.

Scaffold	**Polymer matrix (w/w %)**		**G5 particles (w/w%)**
	PLA	PEG	
PLA	95	5	-
PLA/ G5[a]	95	5	50
Biphasic[b]	95	5	-
	95	5	50

Table 5. 1. Composition of the studied materials. [a] The percentage shown for the polymer matrix of the PLA/G5 scaffolds correspond to 50% of the total weight of the scaffold. [b] Biphasic scaffolds are a combination of both PLA and PLA/G5 phases as shown in Figure 1.

5.2.2. Scaffolds fabrication

Scaffold fabrication has been conducted following the protocol described in chapter 2 (2.2.2). A displaced double layer design shown in Figure 5.1 was adopted to fabricate the polymeric (PLA), composite (PLA/G5) and biphasic (composed by PLA and PLA/G5 phases) three-dimensional

structures described in Figure 5.1. For this, polymer and composite blends (Table 5.1) were dispensed through a G27 (200µm) nozzle at a pressure ranging between 40-80 psi and a motor speed of 7 mm s^{-1}. Polymer and composite inks were kept at 40 ± 5ºC during the printing process by using a heating jacket. Room temperature was kept at 25 ± 2 ºC. Finally, cylindrical scaffolds (4 mm diameter x 4 mm height) were cored from larger 3D printed pieces and used in the degradation studies and *in vivo* implantation.

5.2.3. Degradation study in simulated body fluid (SBF)

In vitro degradation studies were performed by immersing the scaffolds in simulated body fluid (SBF) as described in chapter 2 (2.2.4). Samples were immersed in SBF at 37ºC during 8 weeks. Materials degradation was evaluated in terms of weight loss, molecular weight and morphological variations along the immersion time. Aging studies were only conducted with PLA and PLA/G5 scaffolds.

5.2.4. Morphological SEM study

Morphological analysis of the 3D structures was carried out by scanning electron microscopy (as mentioned in 2.2.3.1) to visualize and evaluate: the architecture of the 3D scaffolds, surface morphology of the deposited struts, and the distribution and exposure of the glass particles. Moreover, SEM observation was used to visualize any degradation sign appearing at the material surface after 8 weeks of immersion in SBF.

In order to check if the glass particles were exposed on the struts surface of the PLA/G5 scaffolds, an Alizarin Red S assay (ARS) (Millipore, Billerica, MA), which stains calcium into a red color, was performed.

5.2.5. Weight loss

Scaffolds' weight loss during immersion in SBF was measured by recording the weight changes of the dry specimen after the specified incubation time periods (4 and 8 weeks). The percentage of weight loss was computed using the same approach described in chapter 2 (2.2.4.1).

5.2.6. GPC analysis

Weight average molecular weight (Mw) of PLA/PEG 95/5 and PLA/PEG/G5 composite scaffolds along degradation was determined by gel permeation chromatography (GPC) using a modular system, composed of an isocratic pump, a vacuum degasser, and refractive index detector (Waters Alliance 2414). Separations were performed in column PSS PFG Analytical 10^3 Å (Dimensions: 300 x 8.00 mm, particle size: 7 µm). Narrow poly(methyl methacrylate) standards (Fluka) were used for calibration. Analysis were performed at 30°C, using 50mM in hexafluoroisopropanol as solvent and filtered (0.22

µm) before injection with a flow-rate of 0.8 ml/min. Acquisition and treatment of chromatographic data was carried out by Empower GPC Software.

5.2.7. Mechanical properties of scaffolds

The evaluation of the mechanical properties of the scaffolds has been conducted using the procedure described in chapter 3 (3.2.3.5). Compressive modulus of PLA and PLA/G5 scaffolds has been measured before and after 8 weeks of incubation in SBF.

5.2.8. Experimental study design and subcutaneous implantation

For these experiments 60 female, 6-8 week-old CD-1 mice (Charles River Laboratories, Germany) were coincidentally divided into four study groups. Thereby each of the first three study groups contained 16 animals, which obtained subcutaneous implantation of the three different scaffolds for four study time points, i.e. 3, 10, 15 and 30 days, with n = 4 animals per experimental group and time point.
A fourth group ("control") underwent the operation without biomaterial insertion to analyze comparatively the tissue reaction to the surgical procedure. Therefore 12 animals were used in this group for the above-mentioned study time points (n = 3 animals per time point).
The subcutaneous implantation was conducted following the protocol described by Ghanaati and collegues [17,18]. In brief, the animals were anesthetized via an intraperitoneal injection (10 ml ketamine [50 mg/ml] with 1.6 ml Xylazine [2%]). After shaving and disinfection of the rostral subscapular region, a horizontal incision down to the subcutaneous tissue was made and a subcutaneous pocket was built, in which the biomaterials were inserted. Finally the wounds were sutured.
Animal housing was conducted at the *in vivo* Laboratory Animal Unit of the Institute of Pathology. Thereby the animals were kept under standard conditions (water *ad libitum*, artificial light and regular rat pellet (Laboratory Rodent Chow, Altromin, Germany)) and a pre- and postoperative care was accomplished. The described *in vivo* experiments were previously authorized by the Committee on the Use of Live Animals in Teaching and Research of the State of Rhineland-Palatinate, Germany.

5.2.9. Explantation and histological workup

After the course of the experiments the animals were euthanized with an overdose of the above-described anesthetics and a subsequent thorax opening. Immediately afterwards the implanted biomaterials and the surrounding tissue or the area of the control incision were explanted. The histological workup was conducted as previously described by Ghanaati and colleagues [18]. Thereby the explanted tissue was fixed using a 4% formalin solution for 24 hours and afterwards the explants were cut into in three segments of identical dimensions including the left margin, the centre and the right margin of the biomaterial. Subsequently a dehydratation via a series of increasing alcohol concentrations and a final xylol exposure was performed before paraffin embedding. After that 3-5 µm

thick slides were made using a rotation microtome (Leica, Wetzlar, Germany) and primarily stained with with haematoxylin and eosin (H&E) to choose the best of the three tissue blocks per animal. Following this, five further slides were cut from every tissue block.

After these preparation steps the following stains were made for quantitative and qualitative analyses of the tissue reactions: Haematoxylin and eosin-staining (H&E) (nuclei and cytoplasm), Azan-staining (nuclei and collagen), Movat Pentachrome-staining (collagen), Tartrate-resistant acid phosphatase (TRAP) (osteoclast-like cells and multinucleated giant cells) staining as well as an immunohistochemical CD31-staining (endothelial cells, blood vessel, identification of angiogenesis), which included a respective control slide, according to methods described by Ghanaati et al. [18].

5.2.10. Histological analyses

The histological analyses, which involved the outcome of the tissue-biomaterial-interactions within the implantation beds of he scaffolds and their surrounding tissue, were conducted using an Eclipse 80i histological microscope (Nikon, Tokyo, Japan). Thereby special focus was on the evaluation of the following parameters within the framework of the early and the late tissue response related to the implants: Fibrosis, haemorrhage, necrosis, vascularization and the presence of neutrophils, lymphocytes, plasma cells, macrophages, multinucleated giant cells and TRAP-positive, osteoclast-like cells.

Finally microphotographs were made via a Nikon DS-Fi1 digital camera and a DS-L2 digital sight control unit (both: Nikon, Tokyo, Japan) connected to the microscope.

5.2.11. Histomorphometrical analyses

The histomorphometrical analyses included the comparative measurements of the vascularization (vessel density and percent vascularization) as well as the measurement of the extent of material-related multinucleated giant cells as described in [18]. In brief, so-called “total scans” were generated with aid of an specialized scanning microscope, which consists of an Eclipse 80i histological microscope combined with a DS-Fi1 digital camera and an automatic scanning table (Prior Scientific, Rockland, MA) connected to an PC system running the NIS-Elements software (all: Nikon, Tokyo, Japan). The resulting images were composed of 100 to 120 single images with a 100x magnification in a resolution of 2500x1200 pixels and contain the complete biomaterial area as well as the peri-implant tissue. For conduction of this study the Azan slides as well as the CD-31 stains were digitized. These images allowed to analyze the tissue reactions to the biomaterials with the use of the NIS-Elements software.

For measurement of the vascularization the complete area of the biomaterial was measured with the “area tool” within the digitized CD-31 stains at first. After that the vessels were manually marked also using this tool. For calculation of the vessel density (vessels/mm^2) the number of counted vessels per slide was related to one millimeter of the implant area, while the measurements of the percent

vascularization were realized by calculating the percent amount of the vascularized implant area based on the summarized vessel areas and the total implant area.
Additionally for measurement of the extents of the material-related multinucleated giant cells, the amounts of these cells were manually counted using the "count tool" of the NIS-Elements software and related to the total implant area (giant cells/mm^2).

5.2.12. Statistical analyses

Quantitative data are shown as mean ± standard deviation after an analysis of variance (ANOVA) followed by LSD post hoc assessment, which enabled to compare the data from the study groups via the GraphPad Prism 6.0 software (GraphPad Software Inc., La Jolla, USA). Thereby statistical differences were marked as significant if p-values were less than 0.05 ($*p \leq 0.05$), and highly significant if p-values were less than 0.01 ($**p \leq 0.01$).

5.3. Results

5.3.1. SEM observation

Figure 5.1 summarizes the structures of the studied scaffolds namely PLA, PLA/G5 and biphasic ones. As observed, the 3D printed scaffolds reproduced very well the predesigned structures (Figure 5.1a,e,i). Structures with struts diameters of approximately 75 ± 5 μm and pores of 165 ± 5 μm respectively were obtained, as the scaffolds described in chapters 3 and 4. In the case of biphasic scaffolds a clear transition from the polymer phase to the composite one was observed. Both SEM observation and alizarin red staining (Figure 5.1b-d, f-h, j-l) confirmed the presence and exposure of glass particles well distributed in the surface and inner part of the struts.

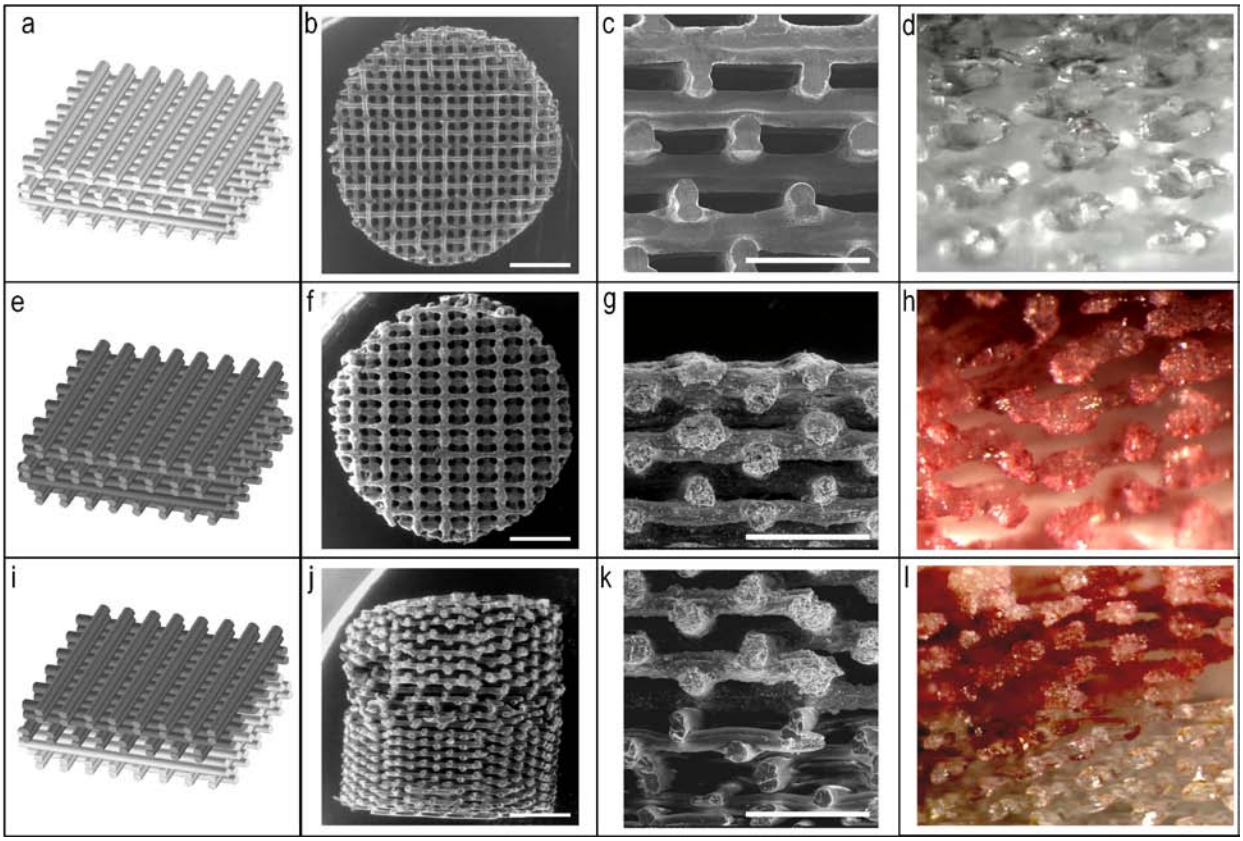

Figure 5. 1. Structures of the studied scaffolds. (a,e,i) Design of the scaffols, (b,f,j) axial and (c,g,k) cross-sectional SEM micrographs, and (d,h,l) alizarin red staining images of the PLA, PLA/G5 and biphasic scaffold respectively.

Figure 5.2 displays the surfaces of both PLA and PLA/G5 scaffolds before and after the degradation time. Figures 5.2a,b show PLA scaffolds before immersion in SBF whereas Figures 5.2c and d show PLA/G5 ones. In the case of PLA scaffolds a rather smooth and continuous surface is observed. In the case of the PLA/G5 composite scaffolds a significantly rough surface with irregularities and protuberances due to the presence of the glass particles is seen. Figures 5.2e,f and 5.2 g-k reveal clearly eroded surfaces after 8 weeks of immersion in SBF. Degradation signs were more visible in the case of PLA/G5 scaffolds than in PLA ones. PLA/G5 scaffolds exhibited the formation of cracks as well as an increased exposure of the glass particles and a rougher PLA matrix.

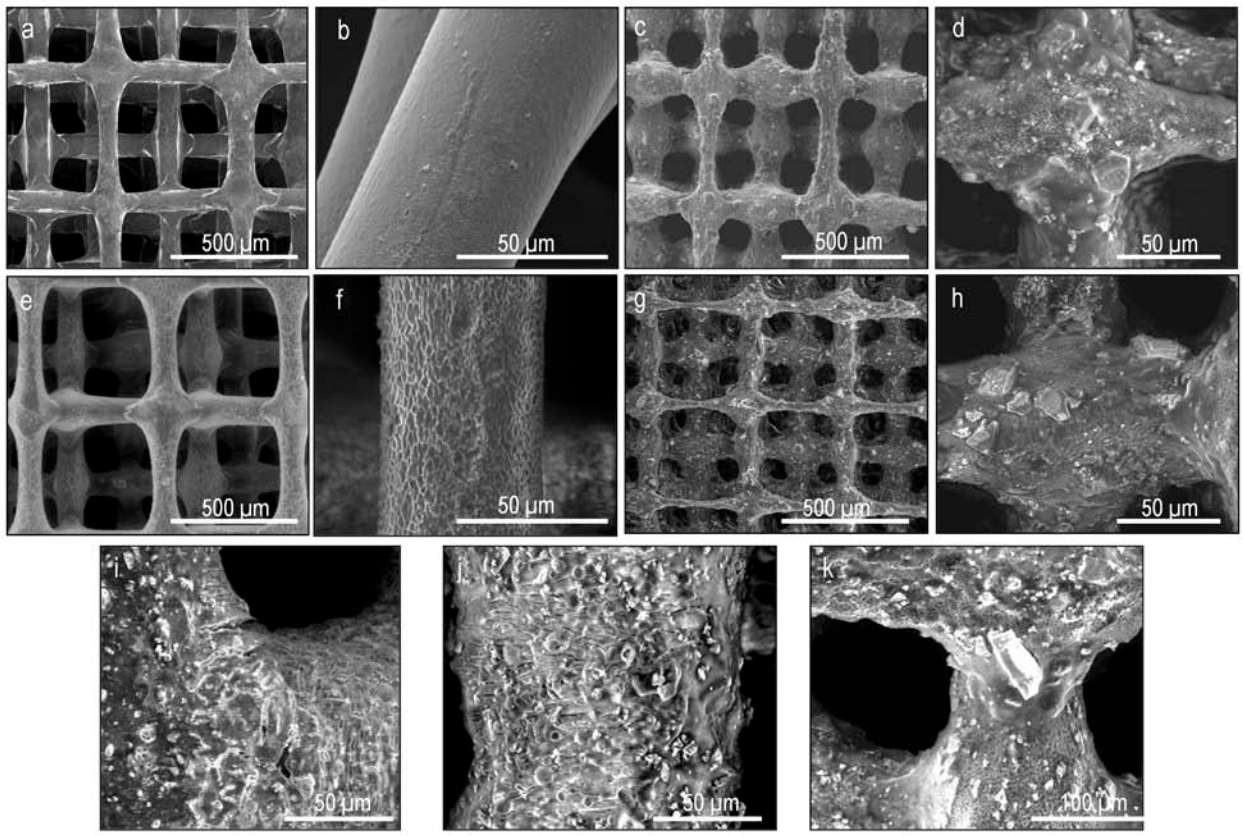

Figure 5. 2. SEM micrographs indicating surface morphology of PLA and PLA/G5 scaffolds before and after the degradation. In particular: (a,e) PLA and (b,f) PLA/G5 scaffolds before degradation; (c,g) PLA and (d,h,) PLA/G5 after degradation. In addition, in (i,j,k) higher magnification images of the PLA/G5 scaffolds after degradation are shown.

5.3.2.Weight loss

The evolution of the physical and chemical properties of the studied scaffolds over an 8-week aging period is shown in Figure 5.3. Figure 5.3a shows the weight variation of the PLA and PLA/G5 scaffolds during the aging period. According to the graph, both types of scaffolds underwent an increasing mass loss; however, each material showed a different behavior. PLA/G5 scaffolds displayed an increasing weight loss since the first weeks of immersion in SBF, whereas, in the case of PLA scaffolds mass loss started after the second week of aging. Though PLA/G5 revealed an initial faster weight loss in comparison to PLA, PLA scaffolds showed a steeper trend, loosing up to 8% of its mass after 8 weeks of degradation.

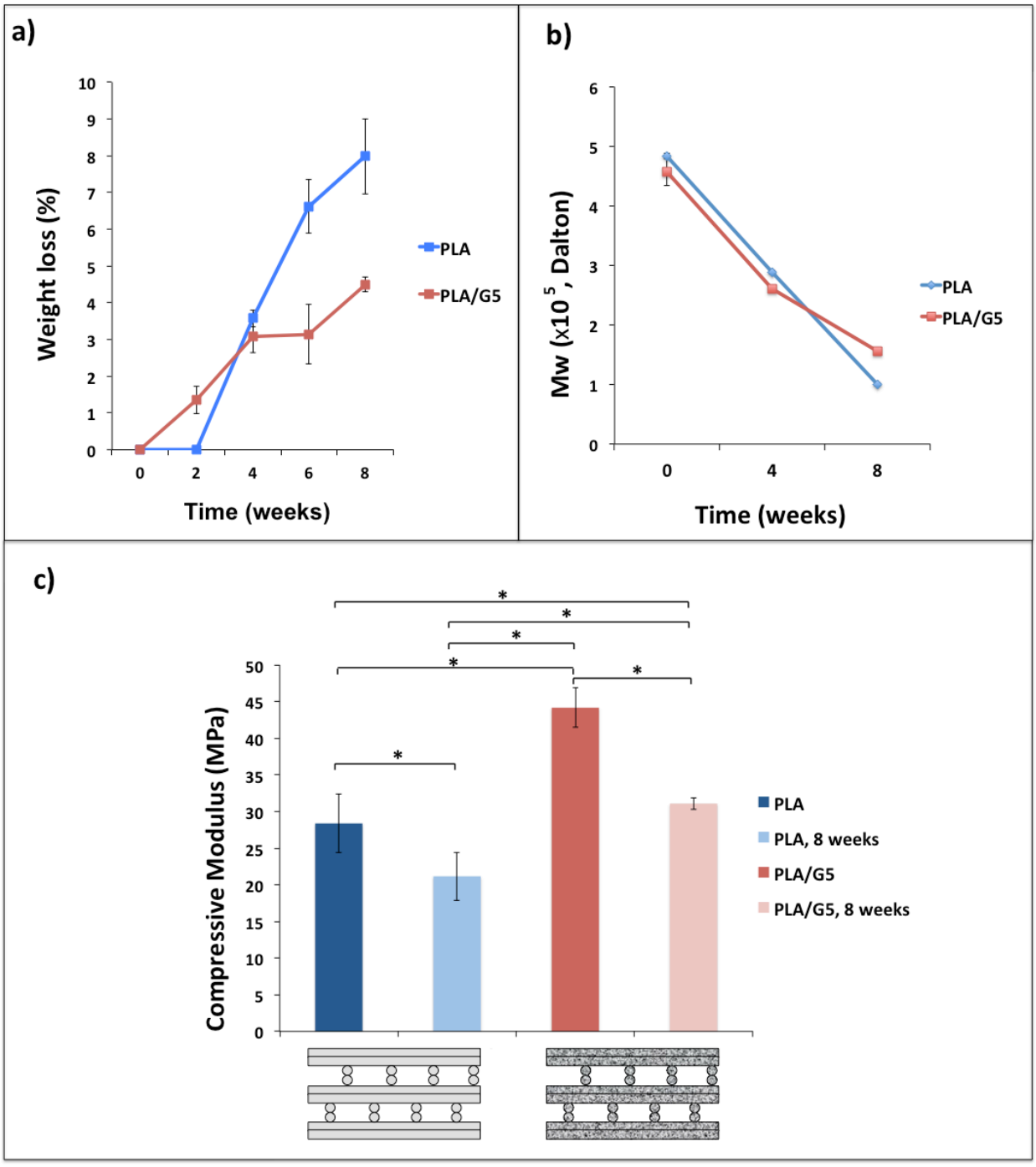

Figure 5. 3. (a) Weight loss, (b) molecular weight evolution, and (c) mechanical test of PLA and PLA/G5 scaffolds over an 8-weeks aging period. The values marked with asterisk (*) showed statistical significant differences ($p \leq 0.05$).

5.3.3. Evolution of the molecular weight

The molecular weight (Mw) of the polymer samples was analyzed by GPC, the obtained results are shown in Figure 5.3b. A significant reduction of around 50% of the initial weight average molecular weight was observed for both materials after 4 weeks of study. Moreover, PEG and PLA/G5 scaffolds showed a Mw decrease around 80% and 66% respectively after 8 weeks of immersion in the fluid.

5.3.4. Mechanical test

Figure 5.3c displays the variation of the compressive strength of PLA and PLA/G5 scaffolds after 8 weeks of degradation. As expected, there was an initial increase of the compressive strength with the addition of glass particles. In fact, PLA scaffolds showed compressive modulus around 28 MPa while PLA/G5 showed values around 44 MPa. As observed in the graph, immersion in SBF affected significantly the mechanical stability of the scaffolds. The compressive modulus decreased to 21 MPa in the case of the polymer scaffolds and to 31 MPa for the composite ones.

5.3.5. Qualitative histological results

The histological analyses revealed that the implantation of the scaffolds of each study group did not show any signs of necrosis, implant loss or exaggerated inflammatory reactions at any of the study time points (Fig. 5.4a, 5.5a and 5.6a).

At day 3 after implantation a mixture of fibrin and connective tissue fibers combined with a low extent of mononuclear cells were observed within the implantation bed of all scaffolds, i.e. the PLA scaffolds (Fig. 5.4b), the PLA/G5 scaffolds (Fig. 5.5b) as well as the biphasic scaffolds (Fig. 5.6b). No signs of ingrowth of complex tissue, vessels or multinucleated giant cells were observable at this early time point.

At day 10 after implantation the scaffolds of each study group were integrated within a connective / granulation tissue (Fig. 5.4c, 5.5c and 5.6c). Thereby the composition of the surrounding tissue as well as the occurrence and the amounts of the material-adherent cells differed between the three different scaffolds.

The peri-implant tissue of the PLA scaffolds showed signs of a low-grade manifestation of a material-induced inflammatory reaction as it showed a fibre-rich composition without a high amount of cells and blood vessels (Fig. 5.4c). A high amount of mononuclear cells were detectable at the surfaces of the PLA biomaterial, while only a few multinucleated giant cells were found (Fig. 5.4c).

In contrast, the peri-implant tissue of the PLA/G5 scaffolds showed a high amount of cells and blood vessels at this study time point in combination with high extents of multinucleated giant cells and low numbers of mononuclear cells at their material-tissue-interfaces (Fig. 5.5c).

The histological observation of the mixture of both material classes, i.e. the biphasic scaffolds, showed that this material induced a high number of adherent multinucleated giant cells (Fig. 5.6c). The peri-implant tissue of this group did also contain of a high number of cells and vessels (Fig. 5.6c).

At day 15 and day 30 after implantation the histological analyses furthermore revealed comparable results as described for day 10. Altogether the PLA materials induced also at these study time points the lowest amount of material-adherent multinucleated giant cells combined with high amounts of mononuclear cells as well as the lowest amount of vascularization of the implantation bed (Fig. 5.4d and e). The observation revealed furthermore that the PLA/G5 materials evoke the highest extents of multinucleated giant cells and vessels, while mononuclear cells were only involved to a minor degree within the tissue reaction (Fig. 5.5d and e). At these study time points the biphasic materials showed an intermediate extent of both the amount of material-induced multinucleated giant cells as well as vascularization of the implantation bed (Fig. 5.6d and e).

Additionally, the histological analysis of the TRAP expression also showed that the amount of TRAP-positive multinucleated giant cells at all study time points was lowest in the PLA study group and highest in the PLA/G5 group, while the group of the biphasic scaffolds showed an middle-grade extent of TRAP-positive giant cells (Fig. 5.7).

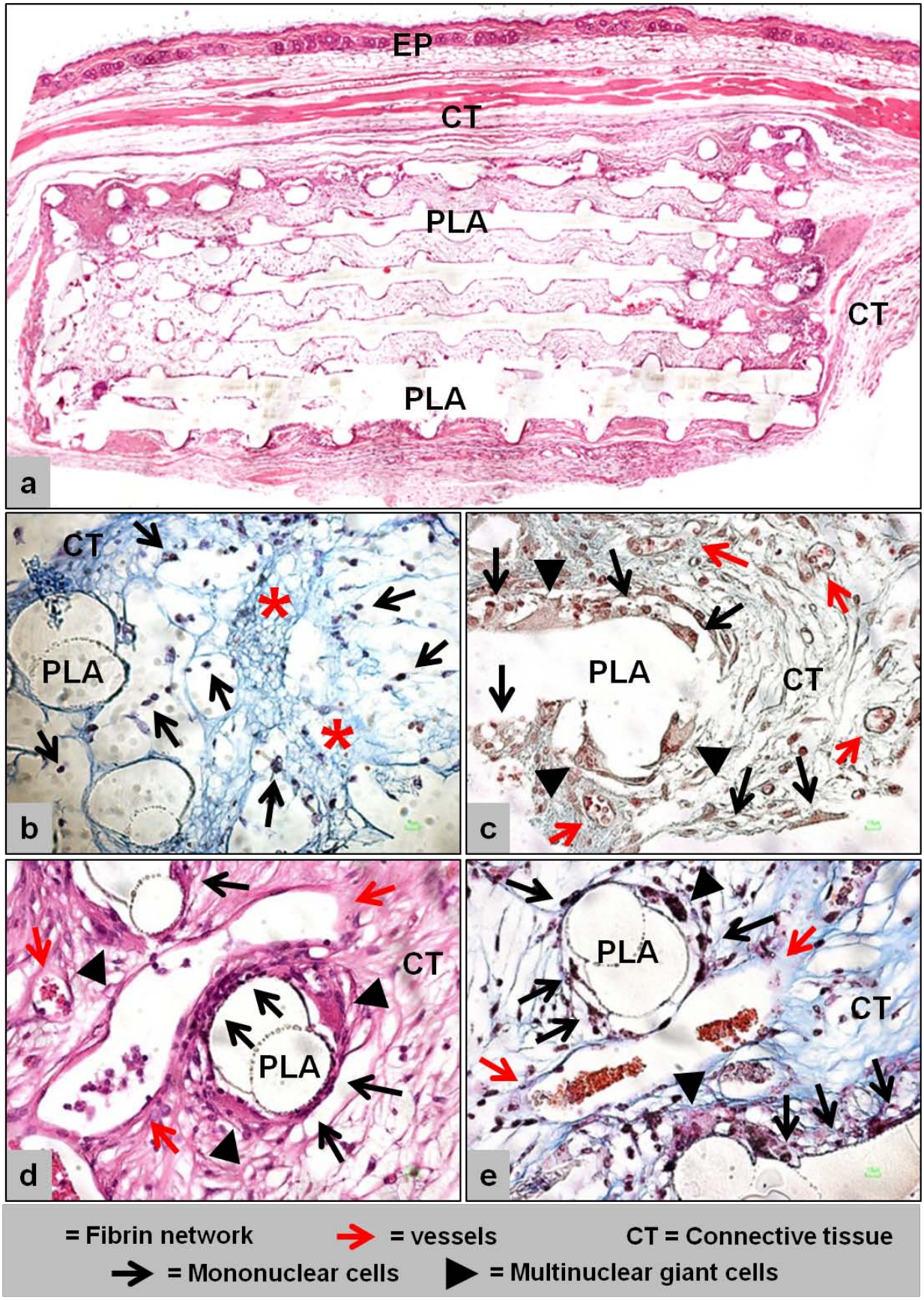

Figure 5. 4. Histological images of PLA scaffold. (a) A total scan of the implant region did not show any signs of necrosis, implant loss or exaggerated inflammatory reactions. At (b) day 3, (c) day 10, (d) day 15 and (e) day 30 after implantation.

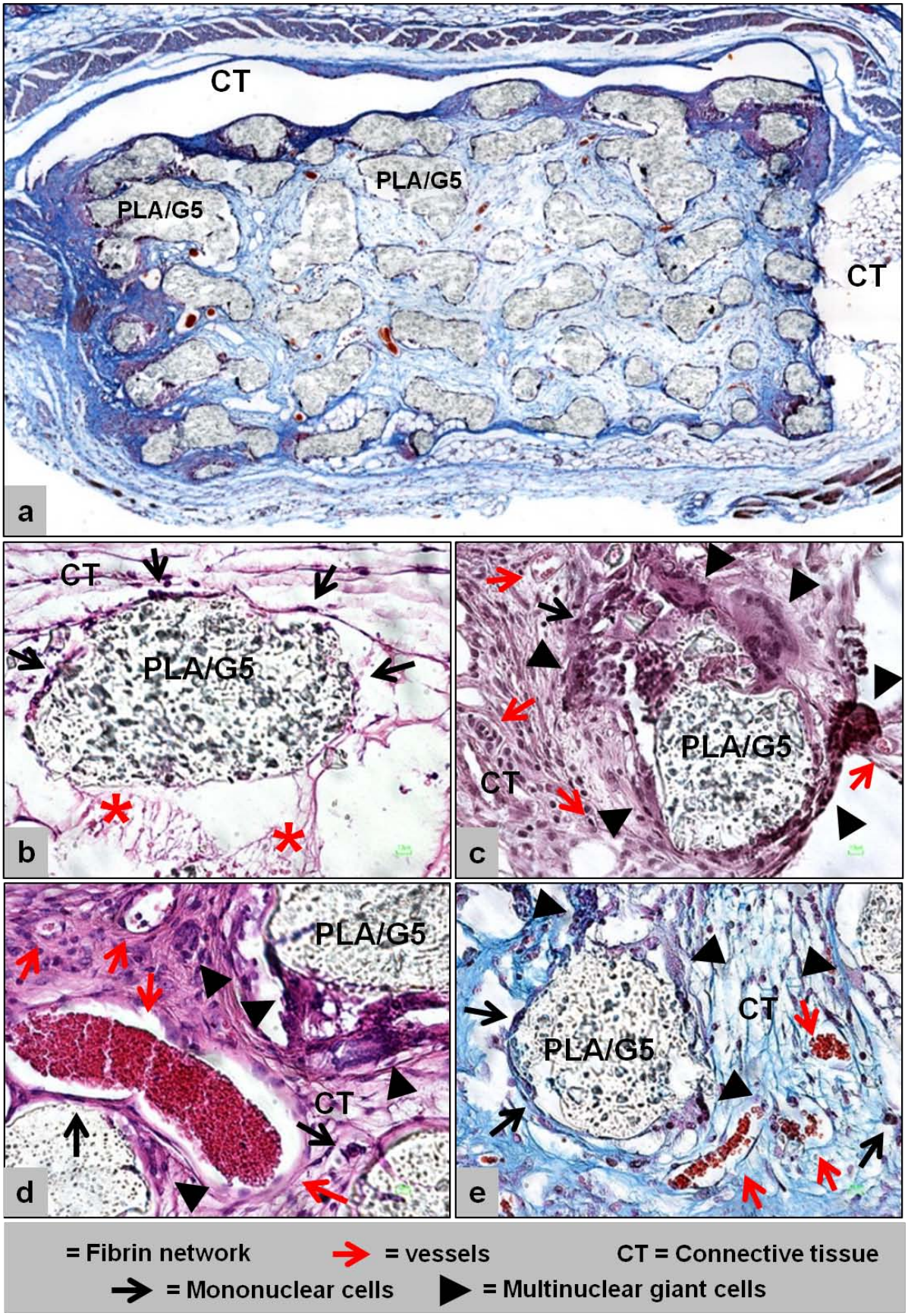

Figure 5. 5. Histological images of PLA/G5 scaffold. (a) A total scan of the implant region did not show any signs of necrosis, implant loss or exaggerated inflammatory reactions. At (b) day 3, (c) day 10, (d) day 15 and (e) day 30 after implantation.

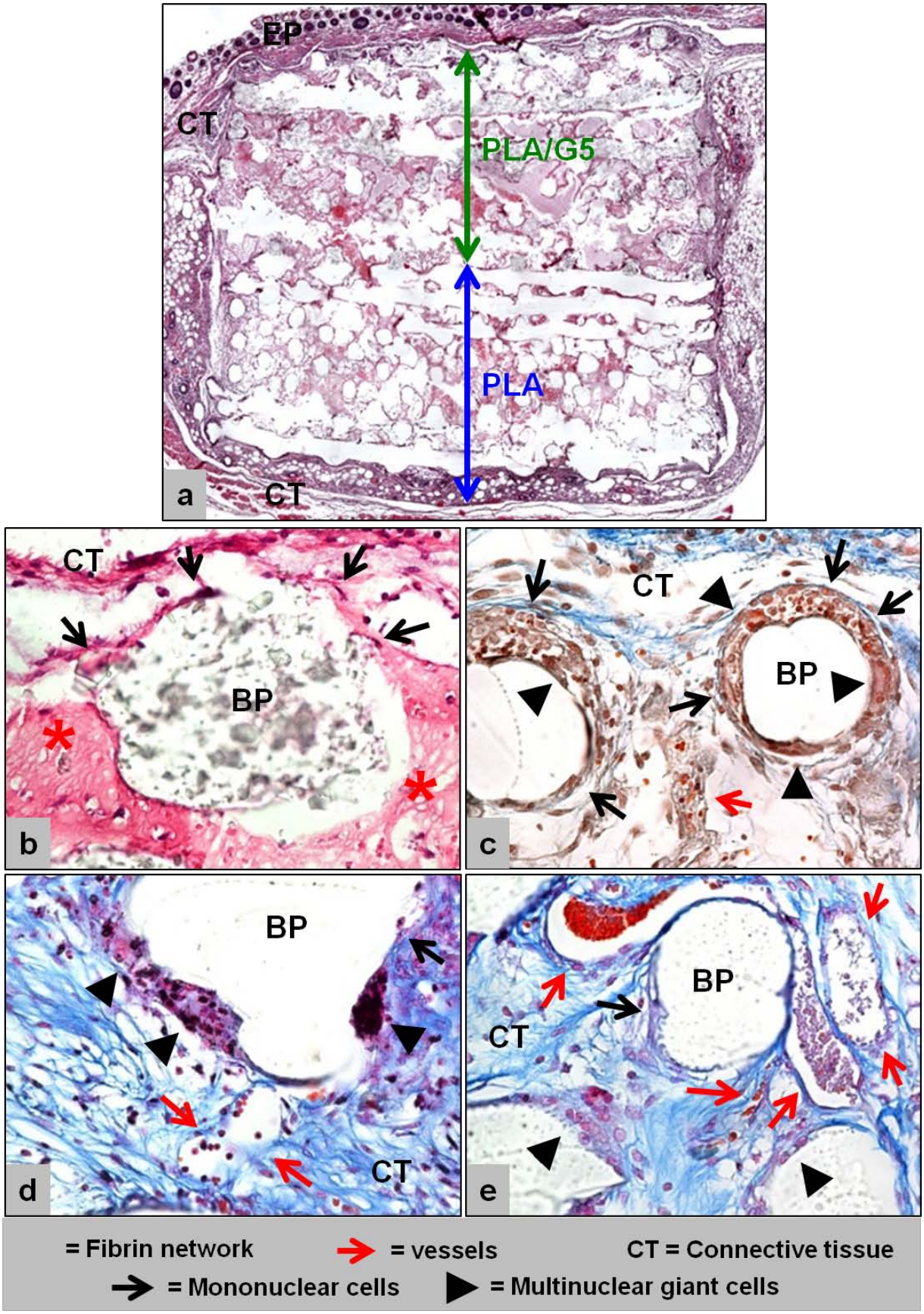

Figure 5. 6. Histological images of Biphasic scaffold. (a) A total scan of the implant region did not show any signs of necrosis, implant loss or exaggerated inflammatory reactions. At (b) day 3, (c) day 10, (d) day 15 and (e) day 30 after implantation.

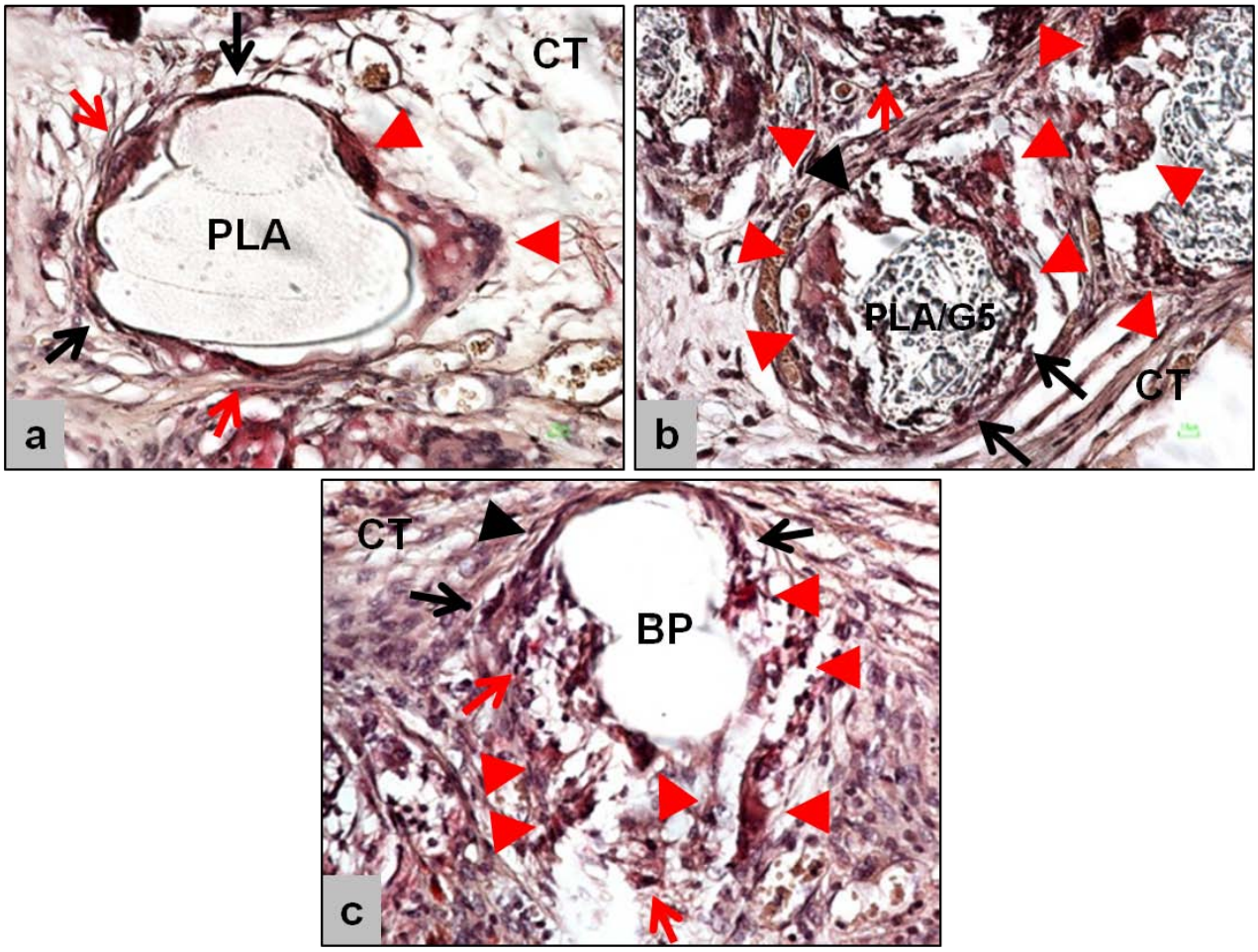

Figure 5. 7. ***In vivo*** **data comparative TRAP activity after 30 days** for (a) PLA, (b) PLA/G5, and (c) Biphasic scaffolds (TRAP staining, red triangles, 200× magnification).

5.3.6. Quantitative histomorphometrical results

5.3.6.1 Results of the vascularization measurements

The comparative measurements of the vessel density showed that within none of the implantation bed of the three scaffold types any signs of vessel ingrowth were findable. In contrast, the control group showed a moderate amount of vessel ingrowth that has therefore high significant higher values compared to the three study groups (** $p \leq 0.01$) (Fig. 5.8a). At day 10 after implantation the analyses revealed that the PLA/G5 group showed the highest vessel density that was significantly higher than PLA and the control group, but not in comparison to the biphasic scaffolds (** $p \leq 0.01$) (Fig. 5.8a). Additionally, there were no significant differences between the PLA group, the biphasic group and the control group.

The histomorphometrical results furthermore showed that the PLA/G5 group induced a significantly higher amount of vessels compared to the PLA group and the control group at day 15 after implantation

(** $p \leq 0.01$), while no differences were measurable in comparison to the biphasic study group (Fig. 5.8a). In addition, the biphasic study group showed significantly higher amounts of vessels compared to the PLA group and the control group (** $p \leq 0.01$) (Fig. 5.8a). No significant differences were measured between the PLA group and the control group (Fig. 5.8a).

At day 30 after implantation the measurements revealed that the PLA/G5 group again induced significantly higher amounts of vessel in comparison to the PLA group and the control group (** $p \leq 0.01$), while no differences were measurbable compared to the biphasic study group (Fig. 5.8a). Furthermore, the vessel density of the biphasic group showed significantly higher values in comparison to the PLA and the control group (* $p \leq 0.05$), while no differences were identifiable between the PLA and the control group (Fig. 5.8a).

The histomorphometrical analyses of the percent vascularization showed that at day 3 after implantation the control group has high significant higher values compared to the other three study groups (** $p \leq 0.01$), whose values did not differ (Fig. 5.8b).

At day 10 after implantation the PLA/G5 group showed the highest values that were (high) significant greater compared to the biphasic group, the PLA group and the control group (* $p \leq 0.05$ / ** $p \leq 0.01$ / *** $p \leq 0.001$) (Fig. 5.8b). The biphasic study group additionally showed (high) significant more vascularization percent compared to the PLA group and the control group (* $p \leq 0.05$ / ** $p \leq 0.01$) (Fig. 8b). The PLA group showed significantly higher vascularization percentage compared to the control group at this time point (* $p \leq 0.05$) (Fig. 5.8b).

At day 15 after implantation the PLA/G5 group furthermore showed significantly higher vascularization percentage compared to the PLA group and the control group (** $p \leq 0.01$ / *** $p \leq 0.001$), while no differences in comparison to the biphasic group were measurable (Fig. 5.8b). The biphasic group showed also significantly higher values in comparison to both groups (** $p \leq 0.01$) (Fig. 5.8b). In addition, the PLA group showed a significantly higher vascularization percentage compared to the control group (* $p \leq 0.05$) (Fig. 5.8b).

The analyses revealed that at day 30 after implantation the PLA/G5 group again showed significantly higher values of vascularization in comparison to the PLA group and the control group (** $p \leq 0.01$ / *** $p \leq 0.001$), while no differences compared to the biphasic group were found (Fig. 8b). Additionally, the biphasic group had significantly higher percentage of vascularization compared to the control group (** $p \leq 0.01$) and also no significant differences compared to the PLA group were measured (Fig. 5.8b). The PLA group had again significantly higher vascularization compared to the control group (* $p \leq 0.05$) (Fig. 5.8b).

5.3.6.2. Results of the giant cell measurements

The histomorphometrical analysis of the extent of material-induced multinucleated giant cells showed that the implantation beds of all study groups did not exhibit cells of this lineage at day 3 after implantation (Fig. 5.8c). Therefore, no significant differences were measured.

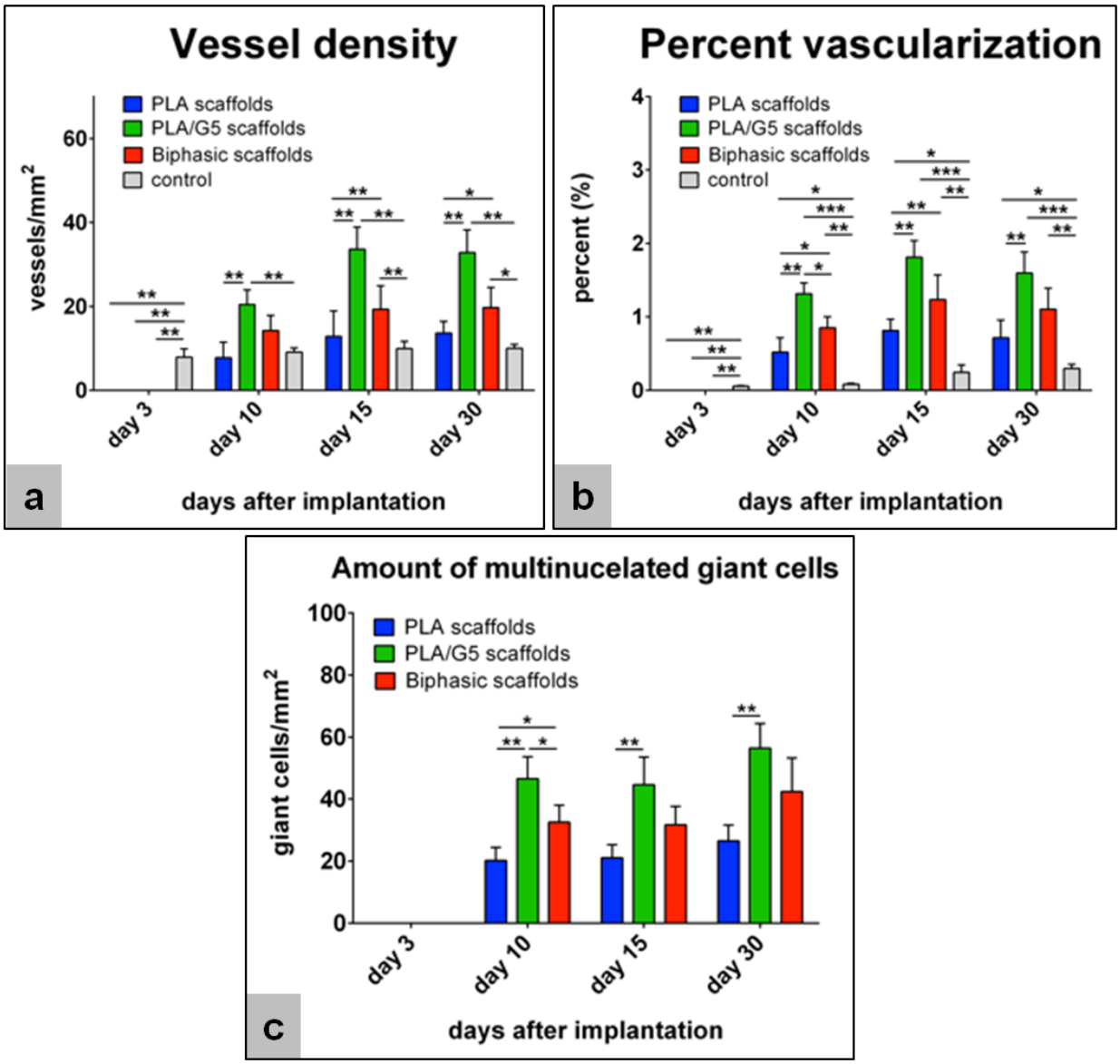

Figure 5. 8. Quantitative histomorphometrical *in vivo* data for PLA, PLA/G5, and Biphasic scaffolds. (a) vessel density, (b) vascularization percentage, and (c) amount of multinucleated giant cells.

At day 10 after implantation the analyses revealed that the PLA/G5 group showed the highest amount of multinucleated giants cells, which significantly differed in comparison to the two other study groups (* $p \leq 0.05$ / ** $p \leq 0.01$) (Fig. 5.8c). The biphasic study group also induced significantly more giant cells compared to the PLA group at this time point (* $p \leq 0.05$) (Fig. 5.8c).

At day 15 and day 30 after implantation no significant differences of the amount of multinucleated giant cells were measurable between the PLA/G5 group and the biphasic study group as well as between the PLA group and the biphasic study group, while the PLA/G5 group induced a significant higher amount of giant cells compared to the PLA group at both time points (** $p \leq 0.01$) (Fig. 5.8c).

5.4. Discussion

This study has explored a novel therapeutic approach to guided bone regeneration by using a biphasic PLA-based scaffold developed via 3-D printing technique. The *in vivo* implantation of PLA-based devices has been largely reported and the degradation time is in the order of several years [19,20]. Moreover, it is generally noted that *in vivo* degradation is faster than the *in vitro* one [21,22], and many are the limitations to re-create the *in vivo* microenvironment in order to carry on these experiments. In addition, a main limitation in conducting *in vivo* degradation measurements of implanted 3D porous structures consists in the presence of the new tissue entrapped into the pores. This tissue is hardly removed from the pores and hinders the appropriate evaluation of scaffold degradation [22,23]. For this reason, only few studies have been done to assess the degradation of PLA-based scaffolds *in vivo* [22, 24].

In this work a dual approach, both *in vitro / in vivo* has been used to study the evolution of the scaffold properties. The use of an additive manufacturing technique, allowing the fabrication of precise and reproducible geometries, improved the assessment of the mechanical and morphological properties. Such approach could lead to less confused conclusions than the ones obtained by using random architectures with high variability among the samples [23].

The *in vitro* degradation study conducted up to 8 weeks, allowed the observation of the changes in morphology, weight loss, molecular weight, and mechanical properties. At this early stage of degradation, 3D structures maintain structural stability without completely losing the initial architecture and strength. It allows comparing morphological and mechanical properties with the ones of the initial scaffolds.

Figure 5.1 shows the results of the scaffolds design and fabrication from a morphological point of view. The development of three different scaffolds: polymeric (Fig. 5.1a, b, c, d), composite (Fig. 5.1e, f, g, h), and biphasic (Fig. 5.1i, j, k, l) was achieved. Interestingly, the cross-section view (indicated in Fig. 5.1c, g, k) evidenced the different morphologies of the structures. As explained in previous chapters, the PLA/PEG scaffolds (Fig 5.1c) presented struts with smoother surface than the composite ones (Fig. 5.1g). A clear discontinuity in terms of morphology could be observed in the case of the biphasic structure in Figure 5.1k. Finally, alizarin red assay was an additional method to elucidate the presence of the two phases in biphasic scaffolds. Figure 5.1l highlights the different phases due to the polymeric and composite layers.

The changes in morphology of the polymeric and composite scaffolds after 8 weeks of immersion in SBF solution are shown in Fig. 5.2. An increase of surface roughness was observed for both types of samples. In the case of the polymeric scaffolds, the increase of roughness was mostly attributed to an enlargment of the micro and nanopores already present in the surface of the strut due to the fabrication process as described in chapter 3 [25].

In the case of the composite structures, higher surface erosion was noticed after 8 weeks. The struts containing G5 glass particles were slightly thinner than before degradation and showed superficial

cracks that were observed at higher magnifications (Figure 5.2i, j, k). This phenomenon could be attributed to an easier penetration of fluid at the interface between the polymeric matrix and the hydrophilic G5 particles. It led to an acceleration of the hydrolytic degradation of the polymer matrix, and the formation of cracks at the struts surface [26]. As a consequence, glass particles were more exposed to the surface.

Interestingly, the weight loss studies showed significant differences between both types of scaffolds. PLA/G5 exhibited a higher and progressive weight loss during the first two weeks of degradation in SBF. However, between weeks 4 to 6 the degradation rate decreased significantly. Finally, after 8 weeks, the composite scaffold showed a weight loss of about 4.5% (Figure 5.3a). On the contrary, PLA weight loss started only after two weeks of immersion overtaking the PLA/G5 at 4 weeks and reaching the 8% of weight loss after 8 weeks. As mentioned before, the weak interface between polymer and glass particles could be the driving agent of the faster weight loss in composite scaffolds at the initial weeks. Since the fourth week to the end of the immersion period the weight loss evolution was influenced by other two events strictly related with the incorporation of G5 particles. The first one consisted in the possible formation of CaP precipitates on the surface of the composite (PLA/G5) scaffolds as observed by Navarro et al. in a previous study on similar materials [26]. To explain the second event it is important to remark that PLA generates acidic products (mostly lactic acid) that can lower down the pH of the surrounding solution accelerating the degradation in an autocatalytic way [27]. Thus, in the case of the composite (PLA/G5) scaffolds, G5 particles acted as a buffer agent for the surrounding solution mitigating the degradation process. Both phenomena acted synergistically to slow down the composite scaffolds weight loss, which became lower than the polymeric one after 8 weeks.

However, it is interesting to observe that, excluding the brief sprint of the composite material at the early steps, weight loss curves for the 3D scaffolds were quite similar to the one shown by 2D PLA/G5 films reported in chapter 2. Final weight loss percentages were between 4.5 and 8% for both materials in 2D and 3D. As mentioned in chapter 2, the presence of PEG domains strongly influenced the degradation rate of the 2D materials. In this chapter, same amount of PEG (5%) was used for the development of both polymeric and composite scaffolds. The effect of hydrophilic PEG, enhancing the fluid erosion at the interface between polymer and G5 particles, led to a faster degradation of the PLA/G5 scaffolds during the first weeks of immersion. Furthermore, PEG showed a more determinant effect in the degradation process of the polymeric (PLA) scaffolds leading to higher weight loss after 8 weeks.

To confirm the degradation of the scaffolds, GPC analysis was carried out. Figure 5.3b shows the data obtained from GPC analysis. It displays a continuous decrease in molecular weight values due to the progressive cleavage of the polymeric chains. In particular, it seems that the PLA/PEG/G5 reduction of molecular weight was less than for the PLA/PEG one. This result was in good agreement with the weight loss analysis previously described. It could be explained by the higher concentration of PEG in

the PLA scaffold in comparison to the composiste one (PLA/G5) where 50% (w/w) is composed by glass particles.

It is known that an ideal scaffold should gradually transfer the load to the new forming bone during degradation [23,28]. Thus, a suitable choice of materials and designs in order to tune both degradation rate and mechanical properties should be done. In this study, the values of compressive modulus diminished for both scaffolds after 8 weeks of immersion in SBF. Furthermore, diminutions of 25% and 30% were observed for the PLA and the PLA/G5 scaffolds respectively. Thus, the composite scaffold became weaker than the polymeric one. A possible reason could be found observing the SEM micrographs (Fig. 5.2). As previously written, PLA/G5 surface was mainly subjected to liquid erosion because of the fluid penetration at the interface between polymer and glass particles. The formation of fractures together with the weakening of polymer-glass adhesion led to the reduction of its mechanical properties. Nevertheless, even after the studied degradation process, composite scaffolds presented higher modulus than the one shown by the polymeric scaffold before degradation.

As already mentioned in the introduction, the general aim of this chapter was the assessment of novel biphasic PLA-PLA/G5 scaffolds as temporary supports for GTR and GBR in maxillofacial applications. In this in vivo evaluation, the tissue reaction to the biphasic, PLA and PLA/G5 scaffolds was examined. Special focus was placed on the integration and degradation of its two morphologically distinct surfaces. Results were compared to the ones obtained with pure PLA and PLA/G5 scaffolds to observe whether the biphasic material induced two well differentiated responses similar to the ones obtained with PLA and PLA/G5 scaffolds or a new combined reaction.

According to the results, there was neither an acute inflammatory response nor signs of necrosis or capsule formation at any of the studied time points for any of the studied materials. After the first 3 days of implantation the biological response was similar for the three types of scaffolds, only a mix of fibrin and connective tissue with a low content of mononuclear cells was observed. However, after 10 days and up to 30 days of implantation the studied materials led different tissue reactions. Basically, PLA scaffolds induced mainly the formation of a fiber-rich tissue with numerous mononuclear cells; PLA/G5 scaffolds showed the presence of a significant amount of blood vessels and multinucleated giant cells; and the biphasic scaffold presented both responses depending on the scaffold side. Thus, it is clear that the presence of both the multinucleated giant cells and the formation of blood vessels is related to the presence of G5 glass particles.

In fact, in previous studies it has been reported that G5 possesses pro-angiogenic potential both in vivo and in vitro [13,29]. It is believed that the angiogenic potential of this glass is due to the chemotactic effect of the Ca ions released by the glass together with the material stiffness [13].

Moreover, it has also been stated that there is a close relationship between inflammation and vascularization. In particular, a study carried out by Ghanaati et al [6] demonstrated that inflammatory cells specifically, multinucleated giant cells are known to promote angiogenesis through the production of vascular endothelial growth factor, which is a known promoter of angiogenesis [30]. In this context,

biodegradable biomaterials are of special interest since their degradation process may facilitate triggering angiogenesis by activating and recruiting inflammatory cells. These inflammatory cells are usually partially activated by the degradation products of these materials and participate in the degradation process of the material as well as in the secretion of certain cytokines and factors that promote vascularization.

It is clear from the obtained results that scaffolds containing glass particles induced a significantly higher amount of multinucleated giant cells. In general, the presence of multinucleated giant cells on the surface of the material seems to be the result of cells trying to mediate the cellular and enzymatic degradation of the material [30]. According to Figure 5.2 PLA/G5 scaffolds showed a faster degradation than PLA structures during the first two weeks of immersion in SBF. Thus, this faster degradation could be related to the activation of the formation of a higher amount of multinucleated giant cells. Moreover, it is known that giant cell formation is dependent on biomaterial surface properties, requiring the adsorption of a specific spectrum of proteins in order to trigger fusion of adherent mononuclear cells into multinucleated giant cells [31]. In the present work, it is possible that besides the degradation process of the composite material, the glass particles themselves induced this fusion of mononuclear cells into multinucleated giant ones. In fact, in previous chapters it has been described how the presence of glass particles affects surface properties, and consequently cell response.

It has been reported that the host multinucleated giant cells and tissue reaction is, in certain way, related to both the easiness with which the material is degraded and the generated degradation by-products. Indeed, it has been observed that the immune response and formation of multinucleated giant cells with further vascularization is highly dependent on the polymer origin (synthetic or natural) [31]. Also, it has been seen that variables such as scaffold thickness, porosity, chemical cross-linking, source, and purification method of a same polymer affect tissue reaction significantly. Thus, in addition to G5 angiogenic potential, differences in the degradation rate between PLA and PLA/G5 could also be responsible of the formation of multinucleated giant cells and vascularization in the case of the composite scaffolds.

Differences in vascularization were clearly observed after vessels quantification. Again, materials with G5 glass displayed a significantly higher percentage of vessels (Figure 5.8). Furthermore, TRAP staining also showed a higher presence of TRAP positive cells when G5 glass particles were present. TRAP is recognized to be expressed by osteoclasts, macrophages, lymphocytes, granulocytes and multinucleated giant cells [32]. The data shown in this work demonstrated that the PLA-based scaffolds used here, in particular the ones containing G5 glass induced a higher amount of TRAP positive cells in comparison to PLA. It has been reported that materials that induce TRAP-positive macrophages and the fusion of these cells to multinucleated giant cells might undergo greater vascularization than materials that induce a TRAP-negative mononuclear cellular inflammatory response [30].

As already mentioned the ideal material for GBR/GTR should on one hand, act as a tissue barrier membrane for an extended period of time and then become integrated by the surrounding soft tissue,

and on the other hand, should trigger tissue vascularization and bone regeneration. In this context, the developed biphasic scaffolds combines both characteristics in a satisfactory way. The PLA side acts as a temporary barrier while the PLA/G5 side enhances vascularization and therefore contributes to regenerate bone tissue.

This study not only sheds lights on the use of these biphasic scaffolds for GTR/GBR applications but also brings up a relevant question on the effect of G5 glass on osteoclast-like cells. Finally, this study together with the previous chapter reinforces the possibility to tune the immune cell response by modifying materials chemistry, degradation rate, and porosity among other to guide scaffold vascularization.

5.5. Conclusion

In this study, a novel approach to guided bone regeneration has been explored. A biphasic scaffold composed by two different compartments: PLA and PLA/G5 has been fabricated and characterized. An 8 weeks long *in vitro* degradation showed that scaffolds kept their structural stability while changes in morphology were observed, specifically for the PLA/G5 scaffold. Weight loss was higher for the polymeric scaffold, confirming the important effect of PEG in the degradation process. Mechanical properties decreased along degradation; nevertheless the PLA/G5 scaffolds presented higher compressive modulus than PLA ones, confirming the reinforcing effect of G5 even after immersion time. Finally, *in vivo* evaluation showed prevalence of mononucleated cells in PLA scaffold that did not experience relevant vascularization. On the contrary, PLA/G5 showed an elevated number of multinucleated giant cells and higher vascularization. The use of such biphasic scaffold represents a suitable platform to study the influence of multinucleated giant cells and G5 particles in inducing vascularization, and a valuable option for guided bone regeneration therapies.

5. 6. References

[1]. Karring T, Nyman S, Lindhe J. Healing following implantation of periodontitis affected roots into bone tissue. J Clin Periodontol 1980: 7: 96-105.

[2]. Kirkpatrick CJ, Unger RE, Krump-Konvalinkova V, Peters K, Schmidt H, Kamp G. Experimental approaches to study vascularization in tissue engineering and biomaterial applications. J Mater Sci Mater Med. 2003 Aug;14(8):677-81.

[3]. Gotfredsen K, Nimb L, Buser D, Hjørting-Hansen E. Evaluation of guided bone regeneration around implants placed into fresh extraction sockets. An experimental study in dogs. J Oral Maxillofac Surg 1993: 51: 879–884.

[4]. Watzinger F, Luksch J, Millesi W, Schopper C, Neugebauer J, Moser D, Ewers R. Guided bone regeneration with titanium membranes: a clinical study. Br J Oral Maxillofac Surg. 2000 Aug;38(4):312-5.

[5]. Javed F, Hussain HA, Romanos GE. Re-stability of dental implants following treatment of peri-implantitis. Interv Med Appl Sci. 2013 Sep;5(3):116-21.

[6]. Ghanaati S, Unger RE, Webber MJ, Barbeck M, Orth C, Kirkpatrick JA, Booms P, Motta A, Migliaresi C, Sader RA, Kirkpatrick CJ. Scaffold vascularization in vivo driven by primary human osteoblasts in concert with host inflammatory cells. Biomaterials. 2011 Nov;32(32):8150-60.

[7]. Chen G, Xia Y, Lu X, Zhou X, Zhang F, Gu N. Effects of surface functionalization of PLGA membranes for guided bone regeneration on proliferation and behavior of osteoblasts. J Biomed Mater Res A. 2013 Jan;101(1):44-53.

[8]. Guda T, Walker JA, Singleton BM, Hernandez JW, Son JS, Kim SG, Oh DS, Appleford MR, Ong JL, Wenke JC. Guided bone regeneration in long-bone defects with a structural hydroxyapatite graft and collagen membrane. Tissue Eng Part A. 2013 Sep;19(17-18):1879-88.

[9]. Srouji S, Ben-David D, Kohler T, Müller R, Zussman E, Livne E. A model for tissue engineering applications: femoral critical size defect in immunodeficient mice. Tissue Eng Part C Methods. 2011 May;17(5):597-606.

[10]. Kenawy E, Bowlin GL, Mansfield K, Layman J, Simpson DG, Sanders EH, et al. Release of tetracycline hydrochloride from electrospun poly(ethylene-co-vinylacetate), poly(lactic acid), and a blend. J Control Release 2002;81: 57-64.

[11]. Gomez Flores M, Hasegawa M, Yamato M, Takagi R, Okano T, Ishikawa I. Cementum-periodontal ligament complex regeneration using the cell sheet technique. J Periodontal Res 2008;43:364-71.

[12]. Vaquette C, Fan W, Xiao Y, Hamlet S, Hutmacher DW, Ivanovski S. A biphasic scaffold design combined with cell sheet technology for simultaneous regeneration of alveolar bone/periodontal ligament complex. Biomaterials. 2012 Aug;33(22):5560-73.

[13]. Aguirre A, Gonz.lez A, Navarro M, Castaño O, Planell JA, Engel E. Control of microenvironmental cues with a smart biomaterial composite promotes endothelial progenitor cell angiogenesis. Eur Cell Mater 2012; 24:90-106, discussion 106.

[14]. Vila OF, Bag. JR, Navarro M, Alieva M, Aguilar E, Engel E, Planell JA, Rubio N, Blanco J. Calcium phosphate glass improves angiogenesis capacity of poly(lactic acid) scaffolds and stimulates differentiation of adipose tissue-derived mesenchymal stromal cells to the endothelial lineage. J Biomed Mater Res A 2013; 101:932-41.

[15]. Ghanaati S, Barbeck M, Orth C, Willershausen I, Thimm BW, Hoffmann C, et al. Influence of beta-tricalcium phosphate granule size and morphology on tissue reaction in vivo. Acta Biomater 2010;6:4476-87.

[16]. Ghanaati S, Orth C, Unger RE, Barbeck M, Webber MJ, Motta A, Migliaresi C, James Kirkpatrick C. Fine-Tuning scaffolds for tissue regeneration: effects of formic acid processing on tissue reaction to silk fibroin. J Tissue Eng Regen Med. 2010 Aug;4(6):464-72.

[17]. Ghanaati SM, Thimm BW, Unger RE, Orth C, Kohler T, Barbeck M, Müller R, Kirkpatrick CJ. Collagen-embedded hydroxylapatite–beta-tricalcium phosphate–silicon dioxide bone substitute granules assist rapid vascularization and promote cell growth. Biomed Mater. 2010 Apr;5(2):25004.

[18]. Ghanaati S, Orth C, Barbeck M, Willershausen I, Thimm BW, Booms P, Stübinger S, Landes C, Sader RA, Kirkpatrick CJ. Histological and histomorphometrical analysis of a silica matrix embedded nanocrystalline hydroxyapatite bone substitute using the subcutaneous implantation model in Wistar rats. Biomed Mater. 2010 May 11;5(3):035005.

[19]. Bergsma JE, de Bruijn WC, Rozema FR, Bos RR, Boering G. Late degradation tissue response to poly(L-lactide) bone plates and screws. Biomaterials 1995;16:25–31.

[20]. Barber FA, Dockery WD. Long-term absorption of poly-L-lactic acid interference screws. Arthroscopy 2006;22:820–6.

[21]. Sung HJ, Meredith C, Johnson C, Galis ZS. The effect of scaffold degradation rate on three-dimensional cell growth and angiogenesis. Biomaterials 2004;25:5735–42.

[22]. Liao SS, Cui FZ. In vitro and in vivo degradation of mineralized collagen-based composite scaffold: nanohydroxyapatite/collagen/poly(L-lactide). Tissue Eng 2004;10:73–80.

[23]. Saito E, Liu Y, Migneco F, Hollister SJ. Strut size and surface area effects on long-term in vivo degradation in computer designed poly(L-lactic acid) three-dimensional porous scaffolds. Acta Biomater. 2012 Jul;8(7):2568-77.

[24]. Gong Y, Zhou Q, Gao C, Shen J. In vitro and in vivo degradability and cytocompatibility of poly(L-lactic acid) scaffold fabricated by a gelatin particle leaching method. Acta Biomater 2007;3:531–40.

[25]. Serra T, Planell JA, Navarro M. High-resolution PLA-based composite scaffolds via 3-D printing technology. Acta Biomater. 2013 Mar;9(3):5521-30.

[26]. Navarro M, Ginebra MP, Planell JA, Barrias CC, Barbosa MA. In vitro degradation behavior of a novel bioresorbable composite material based on PLA and a soluble CaP glass. Acta Biomater. 2005 Jul;1(4):411-9.

[27]. Zhou H, Lawrence JG, Bhaduri SB. Fabrication aspects of PLA-CaP/PLGA-CaP composites for orthopedic applications: a review. Acta Biomater. 2012 Jul;8(6):1999-2016.

[28]. Hutmacher DW, Schantz JT, Lam CX, Tan KC, Lim TC. State of the art and future directions of scaffold-based bone engineering from a biomaterials perspective. J Tissue Eng Regen Med. 2007 Jul-Aug;1(4):245-60.

[29]. Sanzana ES, Navarro M, Macule F, Suso S, Planell JA, Ginebra MP. Of the in vivo behaviour of calcium phosphate cements and glasses as bone substitutes. Acta Biomater 2008;4:1924–33.

[30]. Ghanaati S. Non-cross-linked porcine-based collagen I-III membranes do not require high vascularization rates for their integration within the implantation bed: a paradigm shift. Acta Biomater. 2012 Aug;8(8):3061-72.

[31]. Ghanaati S, Schlee M, Webber MJ, Willershausen I, Barbeck M, Balic E, Görlach C, Stupp SI, Sader RA, Kirkpatrick CJ. Evaluation of the tissue reaction to a new bilayered collagen matrix in vivo and its translation to the clinic. Biomed Mater. 2011 Feb;6(1):015010.

[32]. Hayman AR. Tartrate-resistant acid phosphatase (TRAP) and the osteoclast/immune cell dichotomy. Autoimmunity. 2008 Apr;41(3):218-23.

Chapter 6 - Conclusions

This thesis is an extensive study on development and characterization of scaffolds for tissue engineering applications. An additive manufacturing technique has been used to fabricate 3D structures, specifically a low temperature nozzle-based 3-D printer. The starting materials were polylactic acid (PLA) and a soluble calcium phosphate glass.

- A full-scale study on the effect of PEG in the PLA-blends has been carried out with the aim of developing a novel PLA-based blend, containing PEG as plasticizer, ensuring materials printability and thermal stability. Such optimization of the materials and printing condition allowed the fabrication of 3D-printed PLA-based scaffolds with various PEG concentrations (5, 10, 20%$_{w/w}$).
  Structural, surface, and mechanical characterization has been conducted on both film (2D) and scaffolds (3D); in addition, an *in vitro* degradation study has been performed. It has been shown that the presence of PEG led to non-uniform geometries, decreased the glass transition temperature and the mechanical properties of the scaffolds. Moreover, PEG increased surface roughness, wettability and degradation rate of the PLA-blends. Finally, addition of 5% PEG to the PLA-blend, in combination with the chosen processing parameters, allowed the fabrication of PLA-based 3D scaffolds at low temperature without affecting the polymer blend properties.

- PLA and PLA/G5 scaffolds were fabricated by using two different designs: orthogonal (Orth) and a Displaced double layer design (Displ). Displ design allowed decreasing the pore size in the axial direction and increase in the transversal direction. Indeed, Orth geometry showed pore size around 375 μm while for Displ geometry was around 165 μm.
  The achieved 3D-printed scaffolds presented higher-resolution and thinner struts ($\Phi \approx 75$ μm) with respect to the other nozzle-based fabrication systems reported in litterature (250 μm < Φ < 1000 μm). Furthermore, this was a suitable direct-printing method in order to tune both surface and bulk properties of the scaffolds. Indeed, an interesting strut's topography due to a) the pores left by the evaporation of the solvent during the process and b) the presence of G5 particles exposed on the surface was achieved. MicroCT reconstruction of the 3D scaffolds showed fully interconnected structures with porosity ranging between 75 and 70% for the polymeric and composite scaffold respectively. Moreover glass particles were homogeneously dispersed into the matrix with a percentage close to the theorical one that we chose.
  The mechanical properties were considerably higher than conventional fabrication methods such as solvent casting (300 kPa) and thermally induced phase separation (4.72 MPa). The compressive modulus of PLA scaffolds was found to be 92.32 ± 2.18 MPa for the ORTH design and 28.38 ± 3.99 MPa for the DISPL one, whereas for PLA/G5 the value increased to 99.81 ± 3.55 MPa for the ORTH

and to 44.19 ± 2.67 MPa for the DISPL design. Moreover, addition of G5 particles enhanced the mechanical properties of the scaffolds. Such increase was dependent on the scaffolds' design.

In vitro biological evaluation demonstrated that the presence of G5, adding bio-chemical and bio-physical cues, had a positive effect on cell adhesion.

An optimal set of parameters for the pumping equipment was selected: printing pressure in a range between 40 and 80 psi, deposition speed of 3-7 mm/s, and needle diameter of 200 μm (G27). The syringe temperature was set at 40-45 ºC while ambient temperature was 25 ± 2ºC.

The technique/materials combination used in this thesis led to the fabrication of promising fully degradable, mechanically stable, bioactive and biocompatible composite scaffolds with well-defined architectures valuable for Tissue Engineering applications.

- 3D-printing technique has demonstrated to be a valuable tool to fabricate 3D platforms for *in vitro* study, specifically to analyze and unravel the monocyte/macrophage response to different materials/structures. A new setup for the fabrication of 3D-printed Chitosan scaffolds was done and two geometries were achieved: orthogonal displaced double layer (O) and orthogonal-diagonal (D) scaffolds.

  Metabolic activity of monocytes/macrophages incubated in all scaffolds remained high along time, contrarily to cells incubated in TCPS, indicating that the different materials were not cytotoxic.

  Analysis of the cytokines released by macrophages was carried out. PLA-based scaffolds induced higher production of IL-6, IL-12/23 (pro-inflammatory cytokines) and IL-10 (anti-inflammatory cytokine). Chitosan scaffolds elicited increased secretion of TNF-α (pro-inflammatory cytokine), with the geometry of scaffolds impacting on production of TNF-α. However, cytokine profile was mostly affected by material properties and slightly by scaffold properties such as pore geometry.

  Morphological evaluation of the monocytes/macrophages showed: a) rounded cells with filopodia-like structures, mainly found on PLA and PLA/G5 scaffolds, confirming that this kind of cells prefer rough surface; b) multinucleated giant cells (MGCs), more present on ChO, confirming that high TNF-α levels are strongly related to granuloma formation; c) elongated cells, more evident in chitosan scaffolds, specifically in ChD confirming that they prefer smooth surface.

- A novel therapeutic approach to guided bone regeneration (GBR) by using novel biphasic 3-D printed scaffolds has been investigated. Firstly, the design, fabrication, and *in vitro* degradation of new biphasic scaffolds composed by two PLA and PLA/G5 phases were achieved. Structural and morphological evaluation showed that the scaffolds maintained structural integrity after 8 weeks of degradation. However, changes in morphology are observed at higher magnification due to the G5 particles more exposed on the surface. Higher weight loss was detected for the polymeric scaffold, confirming the important effect of PEG in the degradation process. The mechanical properties of the scaffolds decreased along the degradation process. The compressive modulus decreased from 28 to 21 MPa for PLA scaffolds, while from 44 to 31 MPa for PLA/G5 ones. Such decrease was higher for

PLA/G5 scaffolds (30%) than for PLA ones. Anyhow, the reinforcing effect of glass particles was observed after the degradation process, when PLA/G5 compressive modulus was still higher than the one of the polymeric scaffold.

In vivo study showed that PLA scaffolds mainly induced mononuclear cells and does not undergo a high vascularization. However, the addition of G5 particles enhanced the MGCs formation and accordingly enhanced the vascularization of the scaffolds.

The combination of the two materials (PLA and PLA/G5) by implanting biphasic scaffolds can contribute to generate the "ideal" material for GBR/GTR. Indeed, the PLA-side acts as barrier, while the PLA/G5 one contributes to enhance vascularization and tissue regeneration.

Appendix A - Additive manufacturing technique

Technical specifications

The 3D-printing tool used in this study is developed and commercialized by “nScrypt, Inc”. This machine (Tissue Engineering 3D-300 series) is able to print 3D scaffolds from different materials (such as polymer, ceramic, composites and living cell solutions) with large range of viscosities from 1 to 1,000,000 cps (centipoises). It is connected with a CAD (Computer Aided Design) tool, which allows the development of the design. The material can be deposited using one of the three different pumps (Figure A.1).

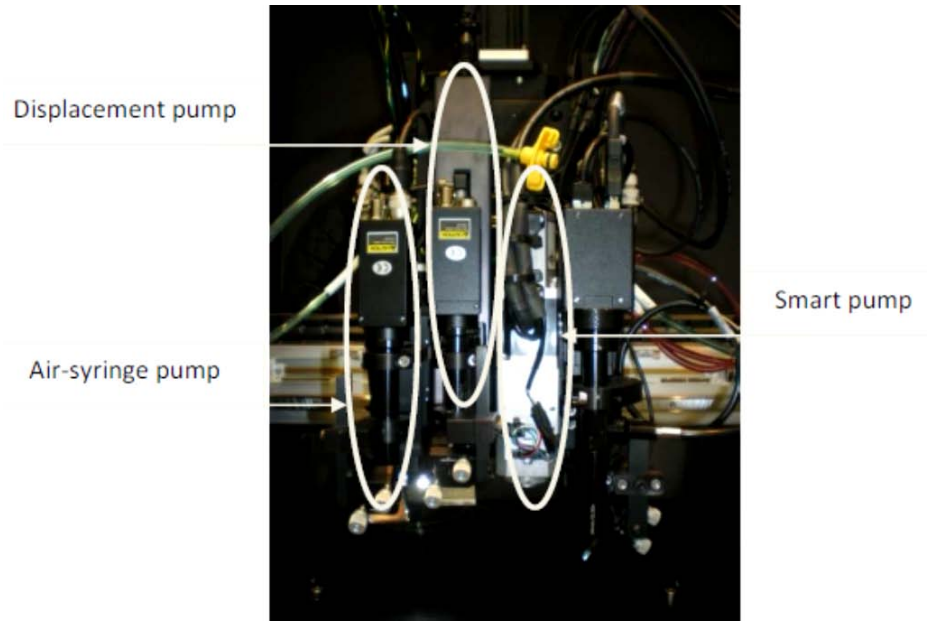

Figure A. 1. Digital picture of the deposition molding machine.

Pumps specifications

Air-syringe pump: Also known as Air pressure pump. The air pressure is injected in a syringe containing the depositing solution. The syringe is fixed to the motion system, and can be plugged to a wide range of needles. Then, due to the pressure, the depositing solution is flowing via the needles, and printed on the substrate.

Displacement pump: Also known as positive displacement pump. In this case, a piston is plugged inside the syringe and presses the material solution out of the needle.

Smart Pump: This is the most important and clever pump of the machine. It is capable of dispensing material with a wide range from 1 to 1,000,000 cps (centipoises) precisely with accurately controlled air pressure, timing, valve opening and dispensing height. The valve is moving in z direction. To understand the process of the smart pump, here is a sketch, which describes the mechanism of operation (Figure A.2):

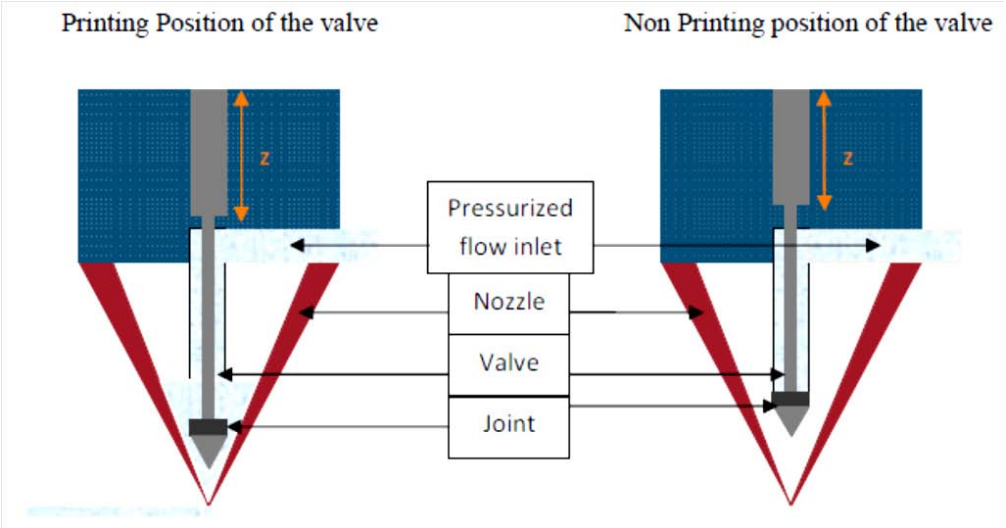

Figure A. 2. Schematic representation of the smart pump.

This valve technology creates a backpressure when the dispensing process finishes, causing the material to be pulled back into the print nozzle. This removes the material on the tip and creates a fresh start for the next print session.

CAD tool

The CAD tool is a software that helps the user to create the desired design. Once it has been created, the design is sent to the RP machine and creates the desired structure. This is a very useful tool that allows the printing of very complex 3D shapes. Three steps are involved in the process for producing a scaffold: (i) Draw the design; (ii) Configuration of the machine; (iii) Launch of the RP.

i. This is the very first step of the process. We have to draw the desired design (Figure A.3) with a special software. It is like programming, a code is required to create the required 3D design.
ii. The machine configuration is done by the “Resource Control panel” (Figure A.4). This panel is the interface between the machine, the design software and the user.
iii. Once the machine is configured and the design ready. The “RunForm” panel is opened, and the “Cycle Start” button pressed. The program then will compile the data for a while and start the printing.

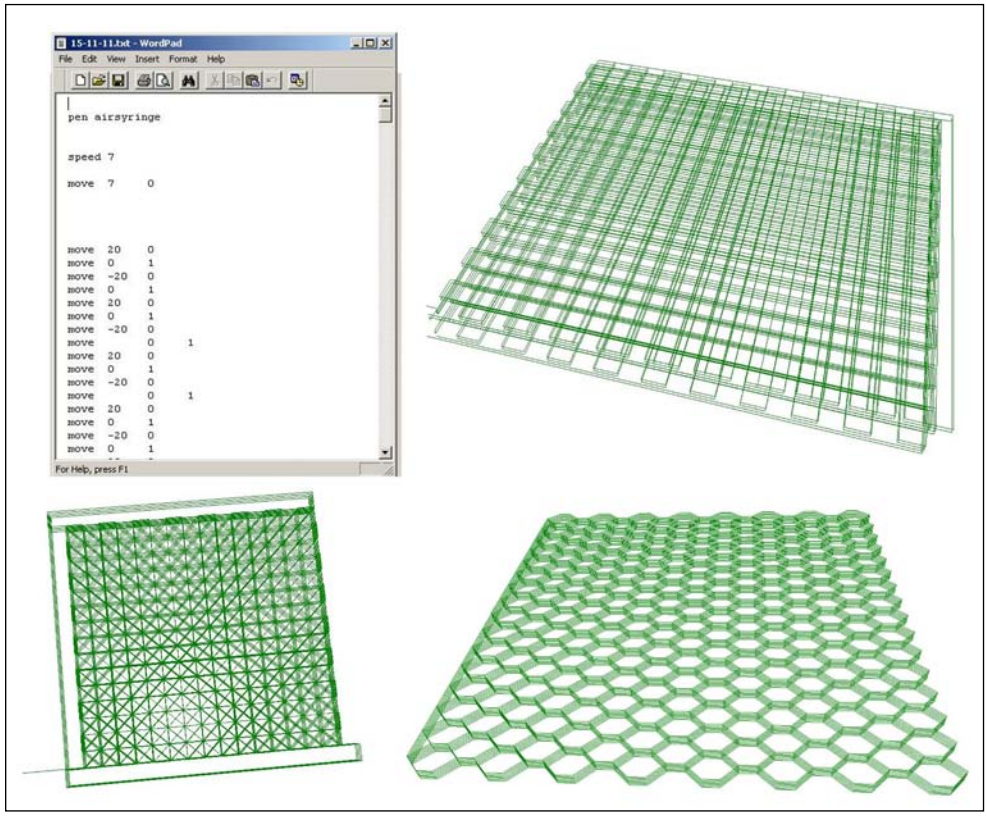

Figure A. 3. Draw the design

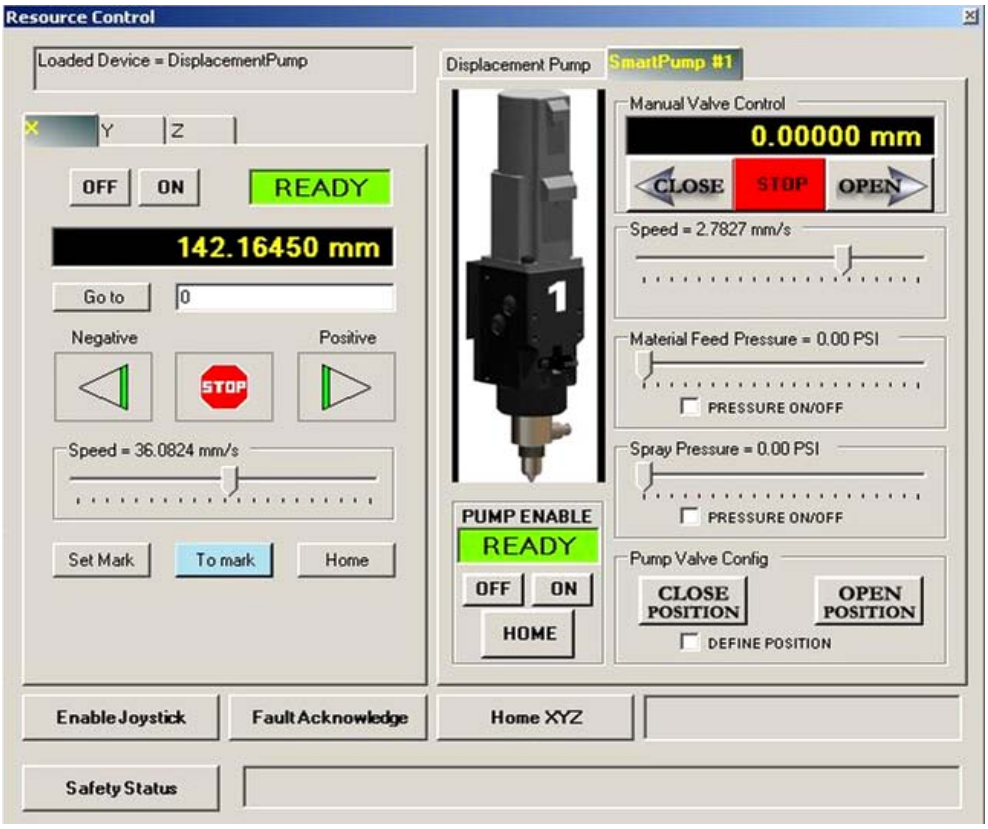

Figure A. 4. Resource control panel.

Appendix B - Optimization of printing parameters

Prior to fabrication, standard "calibration curves" for the polymer and composite solutions were generated by depositing material lines at various speeds and pressures to establish the range of line widths obtainable for a given tip diameter. Different PEG concentrations (5-10-20%$_{W/W}$) were mixed with PLA and G5 in order to evaluate the effect of PEG in the material processing. Two sets of two-dimensional structures composed of parallel lines were created: one by fixing the deposition rate at 3 mm s^{-1} and varying the extrusion pressure between 10 and 100 psi, the second by keeping the pressure constant at 50 psi and varying the deposition rate between 1 and 10 m s^{-1}. For each value of pressure and deposition speed, three lines were deposited and their widths were measured using a profilometer (Dektak 6M, Veeco) (Figure B.1). The calibration lines of the system were obtained for all polymer solutions and were used to establish the optimal printing parameters.

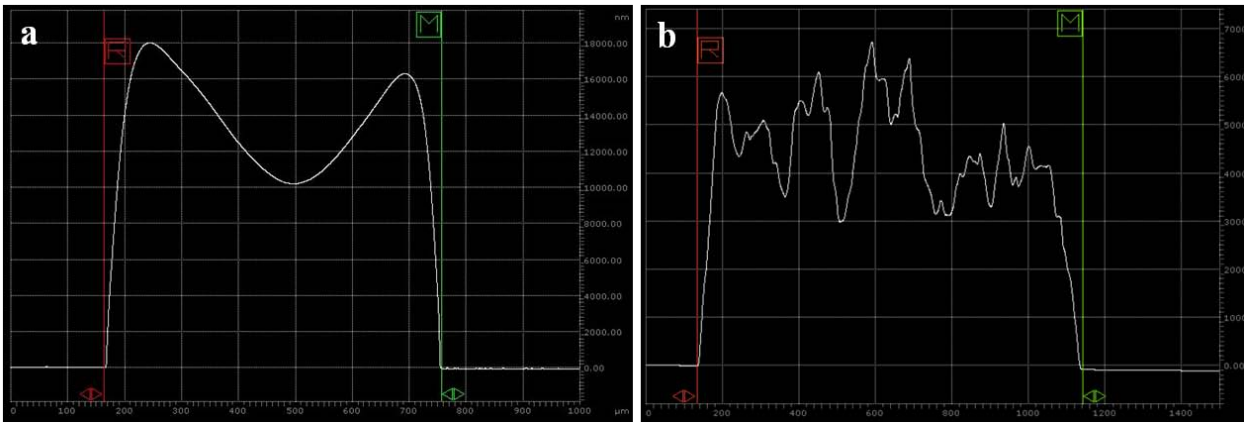

Figure B. 1. Typical shape of (a) polymeric and (b) composite struts obtained by profilometer measurements.

Results

Optimization of deposition parameters ("calibration curves")

Figure B.2 shows the measured line widths of solutions of PLA/PEG blend at different concentrations (20%, 10% and 5% w/w of PEG) and PLA/PEG/G5, respectively, as a function of the applied pressure. It is observed that in general, the lines width increases linearly as the applied pressure increases. Furthermore, for the same value of pressure, the width increases slightly by decreasing PEG concentration (and increasing PLA concentration) while G5 introduction had a more significant effect.

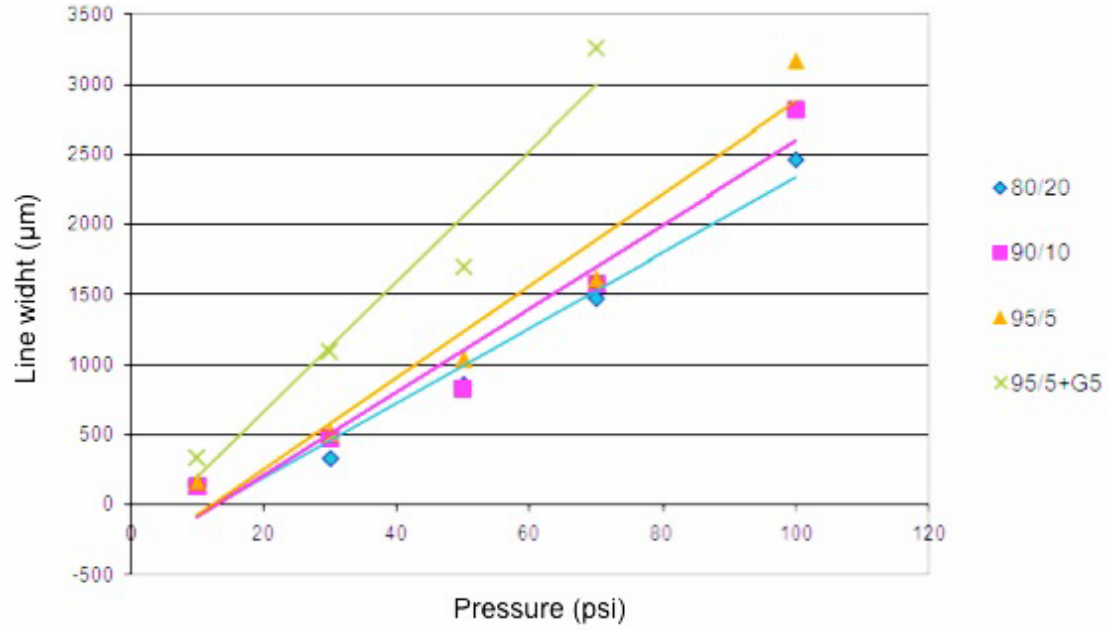

Figure B. 2. Line widths of PLA/PEG blend at different concentrations and PLA/PEG/G5 as a function of applied pressure. Deposition speed: 3 mm s^{-1}; needle diameter: 200 µm.

Figure B.3 shows line widths as a function of the deposition rate for the same set of solutions. It is observed that the lines width decreases remarkably as deposition speed increases. The blends with 20 and 10 % of PEG (PLA/PEG 80/20 and 90/10) showed similar behaviours. The blend with 5% PEG (PLA/PEG 95/5) displayed a remarkable increase in line width in comparison to the other compositions. A similar behaviour was observed when G5 glass was added to the polymer blend.

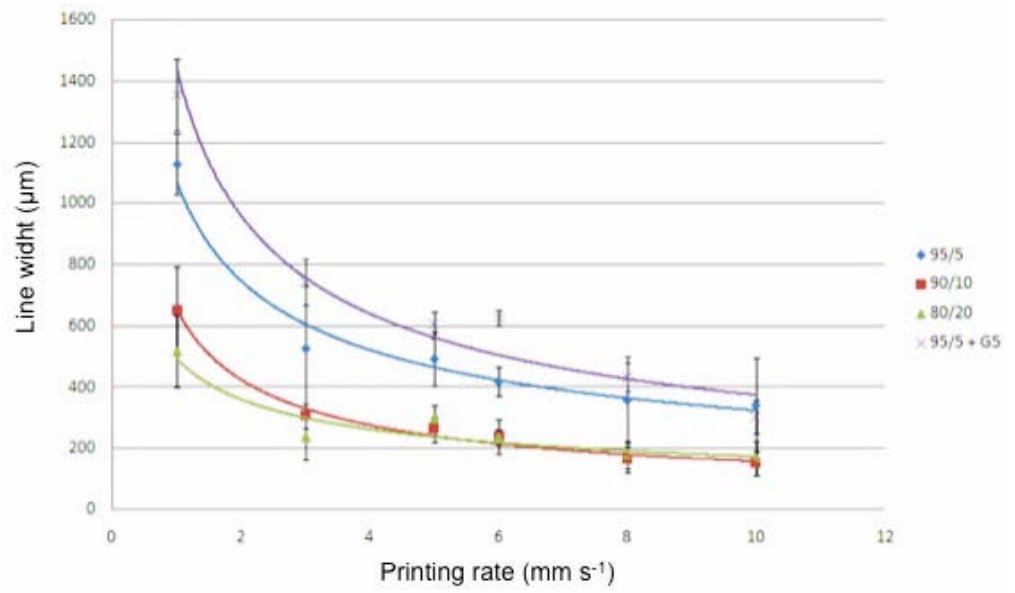

Figure B. 3. Line width of PLA/PEG blend at different concentrations as a function of the deposition speed. The points refer to experimental data Driving pressures: 50 psi; needle diameters: 200 µm

Dispensing pressure	40 - 80 psi
Temperature	40 - 45 ºC
Printing rate	3 mm/s
Nozzle size	200 μm

Table B. 1. Detailed processing parameters for the fabrication of scaffolds

An optimal set of parameters for the pumping equipment was selected from the obtained results, i.e. a printing pressure in a range between 40 and 80 psi and a deposition speed of 3 mm/s. Such combination of parameters was used with a G27 (200μm) nozzle (Table B.1). The syringe temperature was set at 40-45 ºC while ambient temperature was 25 ± 2ºC.

Appendix C - 3D printed PLA-based scaffolds: a versatile tool in regenerative medicine

Rapid prototyping (RP), also known as additive manufacturing (AM), has been well received and adopted in the biomedical field. The capacity of this family of techniques to fabricate customized 3D structures with complex geometries and excellent reproducibility has revolutionized implantology and regenerative medicine. In particular, nozzle-based systems allow the fabrication of high-resolution polylactic acid (PLA) structures that are of interest in regenerative medicine. These 3D structures find interesting applications in the regenerative medicine field where promising applications including biodegradable templates for tissue regeneration purposes, 3D in vitro platforms for studying cell response to different scaffolds conditions and for drug screening are considered among others. Scaffolds functionality depends not only on the fabrication technique, but also on the material used to build the 3D structure, the geometry and inner architecture of the structure, and the final surface properties. All being crucial parameters affecting scaffolds success. This Commentary emphasizes the importance of these parameters in scaffolds' fabrication and also draws the attention toward the versatility of these PLA scaffolds as a potential tool in regenerative medicine and other medical fields.

1. Introduction

Additive manufacturing techniques have been welcome in the biomaterials field. This family of techniques also known as Rapid prototyping (RP) has become part of the set of techniques currently used in the development of new implants and 3D scaffolds for tissue engineering [1-4]. Owing to their capacity to build custom-made 3D structures, RP techniques have arisen special interest within the regenerative medicine community. In addition to revolutionize implantology and regenerative therapies by introducing new possibilities to reconstruct and regenerate tissues in a patient-specific manner, RP also provides a tremendous tool to fabricate scaffolds on demand to obtain in vitro platforms for studying the effect of various parameters such as scaffolds architecture, pore size, geometry, topography, wettability, and mechanical properties among others, on cells behavior including inflammatory response.

Within the additive manufacturing techniques family, nozzle-depositionbased ones have shown great versatility. The approach consisting in a controlled dispensing system integrated with pumping technology and a CAD/CAM system allows the precise and reproducible fabrication of 3D structures with well-defined predetermined geometries. In particular, the use of this technique to fabricate "high-resolution" polylactic acid (PLA) 3D structures has been recently reported by us [5]. In that work we describe the fabrication of PLA based scaffolds with different geometries and provide valuable information on the importance of the different fabrication parameters on both bulk and surface properties, and their impact on cell adhesion. In brief, both PLA and PLA/glass scaffolds were 3D-printed using the

nozzle-deposition based system (Tissue Engineering 3-Dn-300, Sciperio/nScrypt Inc., available in the Rapid Prototyping service of the Biomedical Networking Center, CIBERBBN, and IBEC www.ibecbarcelona.eu/biomaterials). Homogeneous polymer and polymer/glass solutions in chloroform (5% w/v) were prepared and printed at 3mm/s and a pressure between 40–80 psi, through a G27 (200 μm) nozzle. Structures with two different architectures were fabricated: a) orthogonal structures (Fig. C.1a) with distance between struts axes (~500μ m) and struts diameter around ~70 μm, and b) displaced double-layer structures (Fig. C.1d) with a distance between struts axes of ~250 μm and two layers dispensed in each direction [5]. Structural, mechanical and surface properties of the developed scaffolds were studied as well as in vitro cell adhesion. Results shown in that work illustrate and highlight the significance of factors such as: (1) the material used to fabricate the 3D structure, (2) the geometry and architecture of the final structure, and (3) surface properties of the scaffolds.

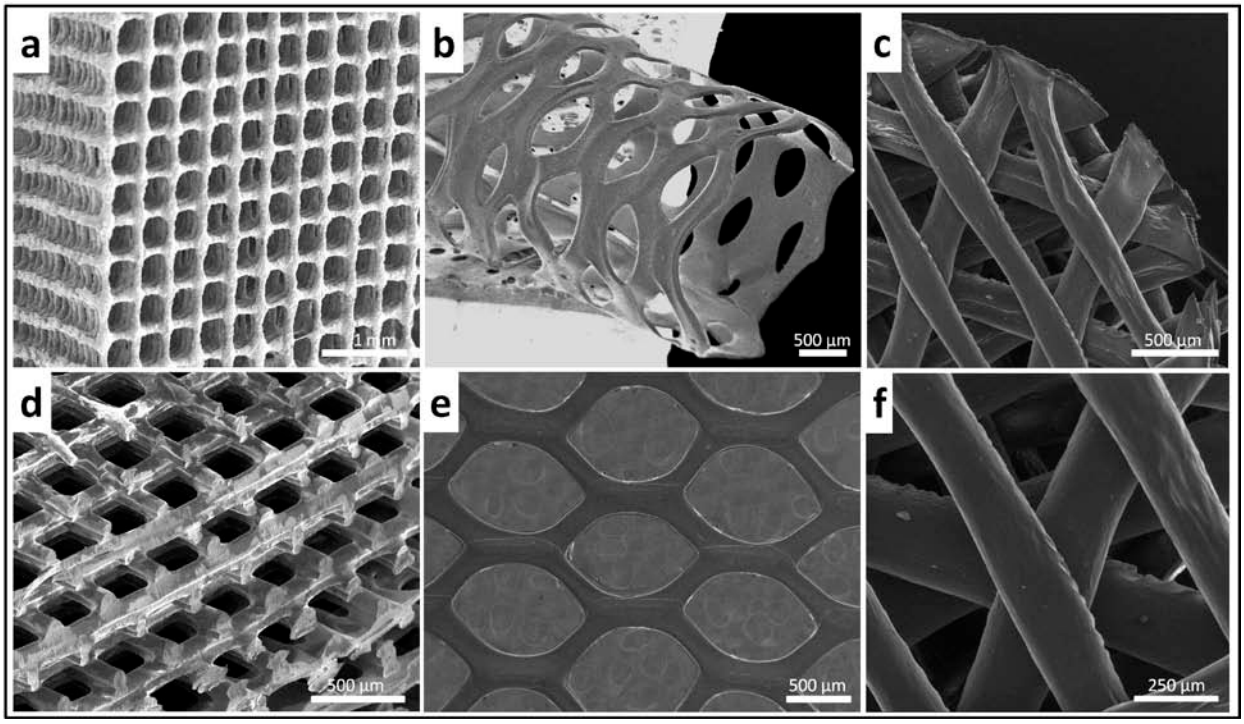

Figure C. 1. SEM images of biodegradable 3D structures with various materials, geometries and architectures, (a) PLA/CaP glass composite orthogonal structure; (b) PLA tubular hexagonal mesh; (c,f) Chitosan orthogonal-diagonal structure; (d) PLA orthogonal-displaced structure, (e) PLA hexagonal mesh.

2. Importance of materials in 3-d printing

Choosing the right material is crucial to achieve functional 3D structures. Materials' intrinsic properties may affect both surface and bulk properties of the final structure. Moreover, materials' properties have a

direct effect on the attainment of certain predetermined geometries. All these aspects affect the mechanical properties and the overall performance of the 3D scaffold.

In the case of PLA, processing with the already mentioned 3D printing tool allows obtaining highly precise structures with better resolution than the ones obtained with other currently used methods [6,7]. This improvement in resolution is due to a particular interplay between a set of temperature/plasticizer/printing parameters and the post-processing shrinkage of the struts due to solvent evaporation that must be carefully tuned in order to obtain such structures [5]. However, if a completely different material such as a hydrogel or a PLA/glass composite material is used, results are completely different. This is the case of chitosan scaffolds; chitosan is a natural hydrogel that requires in situ cross-linking to keep the scaffold structural integrity. Moreover, chitosan swells when in contact with aqueous media. Thus, structures with significantly larger struts diameter than the pre-defined ones are obtained.

In the case of composite materials such as PLA/glass particles, though the overall structural results are the same as with PLA, the increase of viscosity due to the addition of glass particles in the printing solution implies some changes in the printing parameters and the morphology of the final structures. Furthermore, from the morphological point of view, incorporation of glass particles in the polymer matrix has a significant effect on surface topography. In addition, the presence of glass particles in the scaffold affects the mechanical behavior of the structure and its degradation rate [8,9]. In fact, when 50% of glass particles (< 40 μ m) are blended in the polymer solution, the elastic modulus of the structures increases substantially (PLA = 28.38 ± 3.99 MPa, PLA/glass = 44.19 ± 2.67 MPa; n = 3) [5]. Therefore, it is clear that materials' properties have to be carefully considered since each material requires different and specific processing conditions, and each material leads to different structures.

3. Design and architecture of 3D scaffolds

Design and inner architecture of the 3D structure strongly depends on its final application; in this sense, a wide variety of geometries can be developed as the ones depicted in Figure C.1. An important parameter affecting cell response is the scaffold geometry including pores size, shape, and struts size and orientation among others. Scaffolds architecture not only affects their mechanical performance but also affects their permeability, nutrients diffusion and cell response [10]. Indeed, it has been reported that mesenchymal stem cells (MSCs) differentiation and proliferation of pre-osteoblastic cells is highly affected by the geometry of individual pores within the scaffold [11,12].

Also, it has been published that the separation between struts as well as the morphology of pores and the angle formed between struts affect macrophages reponse [13]. In fact, we have recently confirmed that the variation of scaffold geometry from an orthogonal configuration (squared pores) to a diagonal configuration (triangular pores) (see Fig. C.1) affects both macrophages morphology and cytokine expression. Furthermore, orthogonal scaffolds promoted the presence of rounded multinucleated giant cells, whereas diagonal ones lead to elongated macrophages.

Moreover, the distribution of struts and their thickness may also affect significantly on the mechanical properties of the final scaffolds. As a matter of fact, it has been shown that by modifying scaffolds geometry from an orthogonal design to a displaced or shifted one (Fig. C.1a and d), there is a substantial variation on the compressive modulus of both scaffolds ($E_{orthogonal}$ = 93.32 ± 2.18; $E_{displaced}$ = 28.38 ± 3.99MPa; n = 3) as described by us [5]. Thus, depending on the mechanical requirements of the final application, the right material/design combination has to be chosen in order to get the most adequate structures.

Additionally to struts' orientation and conformation, struts' thickness plays an important role. Thinner rods contribute to increasing the specific area of the scaffolds considerably and therefore the contact area between material and cells increases. However, diminishing struts diameter implies that the number of rods required to build a specific volume increases and therefore longer fabrication times are required. Nonetheless, higher scaffolds resolution is a valuable asset as pointed by Hollister et al. [14] who stated that one of the technical constraints of currently used solid free form techniques in order to fulfill scaffolds translation to clinic is their limitation in terms of feature size resolution to the hundreds of micron scale. Albeit this is the case in most of the work published in this area, the work reported by us reveals that high resolution structures with features below the hundreds of microns are possible with nozzle-based printing technology [5].

4. Enhancing cell response by controlling surface properties

Overall, the success of a biomaterial strongly depends on its interaction with the biological environment. There are applications where a direct and tight contact between the tissue and the material is required while there are other applications where a rather antifouling behavior

is needed. Hence, it is clear that biomaterials surfaces are crucial to enhance and control the biological response of scaffolds and implantable devices. Both surface chemistry and surface topography are the most important features affecting biomaterials biological response.

Modification of surface chemistry is the most direct way to influence protein adsorption and therefore cell behavior. By tailoring functional groups available at the material surface it is possible to modify its surface properties, and consequently its wettability, surface electrical charges, and free energy are also changed. As a result, the affinity of some proteins and cellular response for a particular substrate is altered. Nowadays, different techniques aimed to modify scaffolds' surface have been developed [15–18], among them surface functionalization with proteins or peptide sequences as well as the incorporation of an inorganic bioactive phase that triggers specific cell events have been successfully achieved.

4.1. Surface functionalization with bioactive molecules

Coupling functional groups, or specific biomolecules such as functional peptides to the surface by means of chemical treatments is one the most currently studied methods for improving biomaterials bioactivity.

In this context, surface functionalization of the already mentioned PLA 3D printed scaffolds with collagen has been investigated. Both, physisorbed and covalently bonded collagen surface coatings have been achieved. In the case of physical absorption, the scaffolds were directly immersed in a solution containing collagen, whereas to achieve covalent bonding the surface was previously treated with NaOH + EDC/NHS in order to activate the accessible functional groups and subsequently immersed in the collagen solution (100 μg/ml in PBS, 24h at room temperature). Both types of samples were evaluated and characterized by CBQCA and Micro BCA assays to evaluate the amount and distribution of the biomolecule on the surface of the scaffolds. The experiment was performed in triplicate. As observed in Figure C.2, fully and homogeneously collagen covered scaffolds were obtained (Fig. C.2a). In addition, a higher protein density was quantified on the covalently functionalized scaffolds (Fig. C.2c). Also, a cell viability assay was performed to measure cell adhesion on both non-functionalized and functionalized (covalently attached collagen) scaffolds. Mesenchymal stem cells (3×10^5 cells/scaffold) were seeded in the scaffolds, polystyrene microplate wells were used as control. Cell adhesion was studied at 4 and 24 h using a LDH assay kit. Results shown in Figure C.2d are expressed as the average absorbance levels of three samples (Fig. C.2d). An ANOVA analysis was performed to establish possible statistical significant differences ($p \leq 0.05$) in the absorbance values. Cell studies showed a positive cell response in the functionalized scaffolds. In fact, after 72 h of culture, mesenchymal stem cells were very well spread and completely covering the scaffold surface (Fig. C.2b).

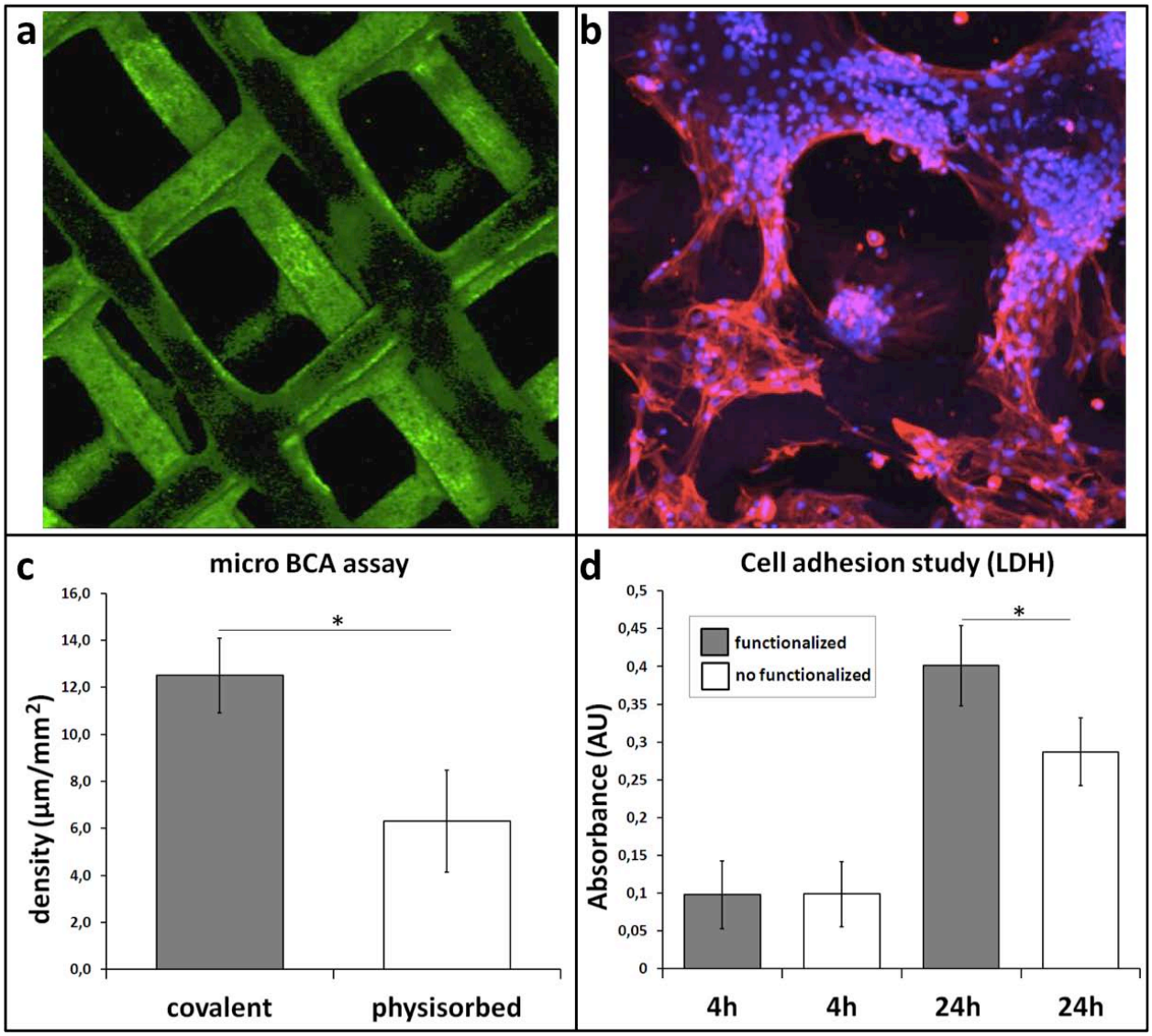

Figure C. 2. Surface functionalization of PLA 3D scaffolds: (a) Fully and homogeneously collagen covered scaffold; (b) rMSCs cultured on the functionalized scaffolds after 72 h; (c) Quantification of the amount of collagen on the scaffolds surface. Covalently functionalized scaffolds showed a significantly higher protein density than physisorbed ones; (d) LDH assay of adhered rMS Cs after 4 and 24h of culture on both covalently- and non-functionalized PLA scaffolds. Functionalized scaffolds showed a higher number of viable cells after 24h. The values marked with asterisk (*) showed statistical significant differences ($p \leq 0.05$).

4.2. Improving surface bioactivity by adding inorganic particles

As previously mentioned, other method for modifying surface chemistry is by adding bioactive inorganic particles to the PLA matrix. In this line, addition of a soluble, bioactive CaP glass, known as G5 [19,20], in particles shape to reinforce and improve bioactivity of PLA scaffolds has been explored [9]. It is known that G5 glass is highly hydrophilic (contact angle = 29.8°) [21]. Thus, addition of G5 particles contributes to decrease PLA contact angle. Previous studies have demonstrated a preferential attachment and spreading of cells on G5 glass particles than in the polymer matrix [10,21]. This soluble glass

degrades along time while releasing different ions to the surrounding media [19]. It has been demonstrated that the presence of G5 glass particles not only increases cell attachment and spreading but also triggers angiogenesis and bone formation owing the Ca^{2+} release and stiffness of the glass [22,23]. Indeed, several studies have demonstrated the relevant role of ions on tissue regeneration [24,25]. Given that the glass particles incorporated into the polymer scaffold are partially exposed in the surface, as demonstrated by an alizarin red assay (where only the calcified inorganic phase is stained in red color, Fig. 3b), their presence contribute both to modify surface chemistry and surface topography.

Addition of G5 particles into the polymer matrix introduced an interesting topography to the scaffold surface as observed in Figure 3a and c. In addition, the surface of the polymer struts showed micro and nanopores left by the evaporation of the solvent (see Fig. 3d). Thus, the final structures presented a combination of porosities and other topography features ranging from the macroscale due to the pores initially designed to the micro and nanoscale due to solvent evaporation and the presence of glass particles. According to the interferometry results, the addition of glass particles significantly increased the average roughness (S_a) of the surface in comparison to PLA (PLA = 117.72 ± 60.50 nm, PLA/glass = 1003.89 ± 228.45 nm; n = 9) [5]. It is known that both surface micro and nanoporosity play important roles in protein adhesion and therefore on cell response [26]. Surface nanoporosity not only increases the contact surface area between the material and biological entities but also generates nanoscale topographical cues affecting cell behavior. In fact, enhancement of cell interaction due to nanotopography has been reported [27,28]. Cells do not interact directly with biomaterials, but with an absorbed protein layer that provides anchoring sequences to cells. Protein adsorption is highly dependent on surface properties; in particular, it is believed that since the dimensions of surface nanofeatures are closer to proteins, their interaction is stronger. Thus, controlled nanoporosity might play an important role in biological interactions.

We reported on the results of rMSCs response to PLA and PLA/CaP glass scaffolds with similar architecture at short periods of time. Cell viability (WST assay, n = 3) and morphology (confocal microscopy observation upon nuclei and cytoskeleton staining) were evaluated after 4 and 24 h of adhesion in contact with the materials. Results revealed that although both materials displayed similar cell viability results, noteworthy differences were observed in cells' morphology when comparing both types of scaffolds. After 4 h, immunofluorescence images showed well spread cells with extended cytoskeleton on the scaffolds with CaP glass particles and relatively rounded cells on the PLA scaffolds. Thus, the obtained results suggested clear early cell morphological differences due to topographical and chemical changes [5].

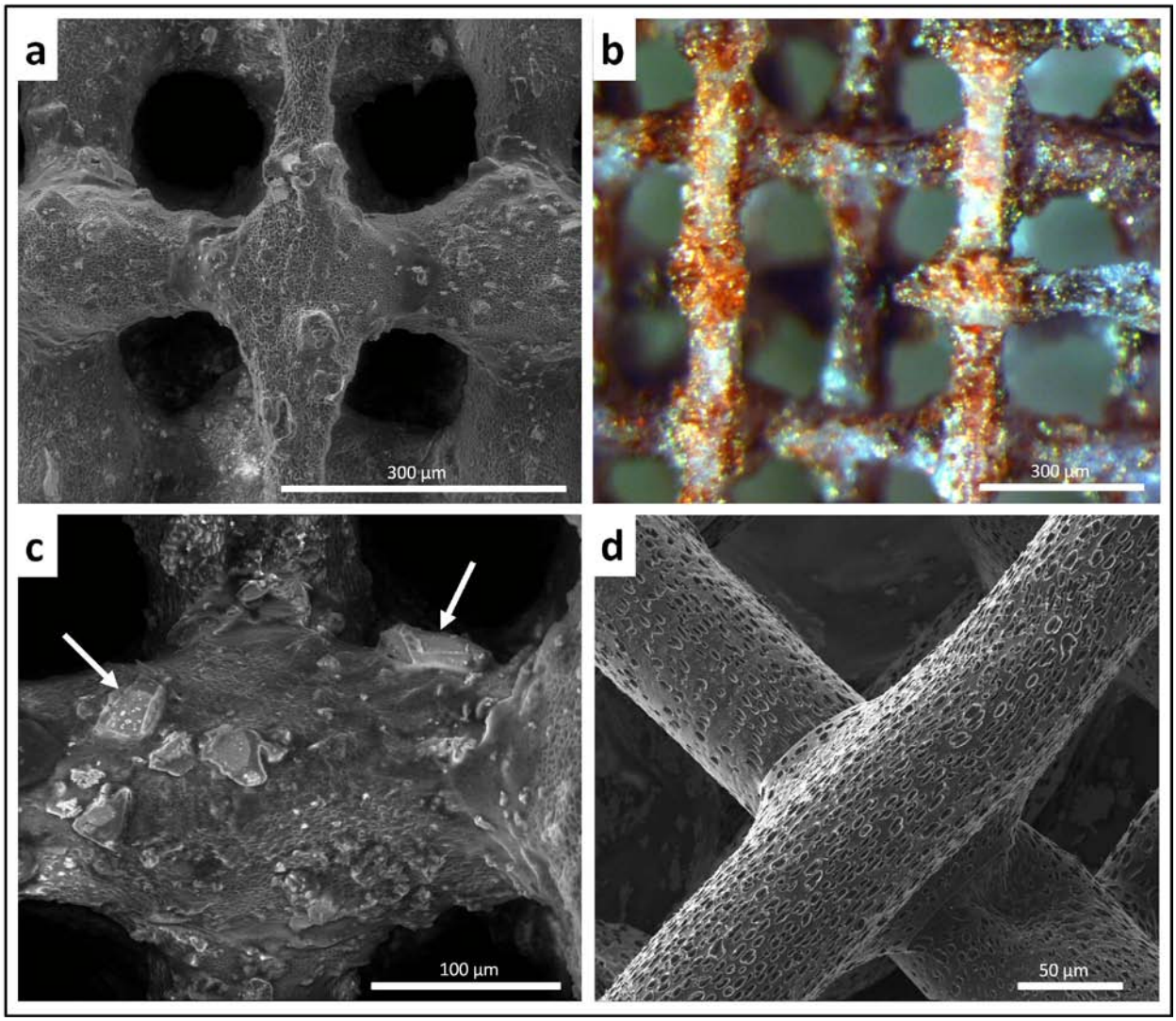

Figure C. 3. SEM images of (a and c) PLA/CaP glass composite scaffolds showing glass distribution and glass/polymer interface, white arrows indicate glass particles; (d) Struts of a PLA scaffold showing the micro and nanoporosity left after solvent evaporation; (b) PLA/CaP glass scaffold after Alizarin red staining. Red colored areas denote the CaP inorganic phase indicating the glass particles exposed on the scaffold surface.

5. Conclusions

Data reported by us is a glimpse that opens new possibilities to produce novel PLA-based scaffolds with finely tuned architectures at a higher resolution than currently used methods. As described in the previous sections, the success of 3D scaffolds depends on the combination of the appropriate materials with the right design and the right fabrication technique and fabrication conditions that lead to the attainment of tailored 3D structures adapted to specific needs. Current fabrication tools allow obtaining tridimensional structures with complex architectures and surface properties on demand. In this sense, the possibility to build customized scaffolds combining various bulk and surface properties is of main interest not only in the tissue/organs engineering field, where the aim is to obtain temporal templates with properties adapted to the tissue to be regenerated; but also, in drug screening and in certain malignancies therapeutics such as in cancer [29]. Three-dimensional scaffolds provide an environment able to recapitulate *in vivo* conditions

in a more resembling way than traditional 2D in vitro cell culture systems. In particular, in the case of cancer, it has been reported that tumor phenotype is governed by the 3D tumor microenvironment. Thus, 3D scaffolds seem to be a good option to mimic tumor architecture and the in vivo scenario.

In the same direction, it could be expected that in a near future advances in the fabrication techniques and development of 3D structures will provide scaffolds that allow a better replica of the in vivo milieu. Having templates that better mimic the in vivo microenvironment could lead to both, better scaffolds for tissue regeneration and more accelerated drug screening systems with a significant reduction on animal testing.

6. References

[1]. Hollister SJ. Porous scaffold design for tissue engineering. Nat Mater 2005; 4:518-24.

[2]. Hutmacher DW, Schantz JT, Lam CXF, Tan KC, Lim TC. State of the art and future directions of scaffold-based bone engineering from a biomaterials perspective. J Tissue Eng Regen Med 2007; 1:245-60.

[3]. Moroni L, Elisseeff J. Biomaterials engineered for integration. Mater Today 2008; 11:44-51.

[4]. Yeong WY, Chua CK, Leong KF, Chandrasekaran M. Rapid prototyping in tissue engineering: challenges and potential. Trends Biotechnol 2004; 22:643- 52.

[5]. Serra T, Planell JA, Navarro M. High-resolution PLA-based composite scaffolds via 3-D printing technology. Acta Biomater 2013; 9:5521-30.

[6]. Melchels FP, Feijen J, Grijpma DW. A poly(D,Llactide) resin for the preparation of tissue engineering scaffolds by stereolithography. Biomaterials 2009; 30:3801-9.

[7]. Xiong Z, Yan Y, Wang S, Zhang R, Zhang C. Fabrication of porous scaffolds for bone tissue engineering via low-temperature deposition. Scr Mater 2002; 46:771-6.

[8]. Navarro M, Ginebra MP, Planell JA, Barrias CC, Barbosa MA. In vitro degradation behavior of a novel bioresorbable composite material based on PLA and a soluble CaP glass. Acta Biomater 2005; 1:411-9.

[9]. Navarro M, Aparicio C, Charles-Harris M, Ginebra MP, Engel E, Planell JA. Development of a biodegrdable composite scaffold for bone tissue engineering: physicochemical, topographical, mechanical, degradation, and biological properties. Adv Polym Sci 2006; 200:209-31.

[10].Charles-Harris M, Koch MA, Navarro M, Lacroix D, Engel E, Planell JAA. A PLA/calcium phosphate degradable composite material for bone tissue engineering: an in vitro study. J Mater Sci Mater Med 2008; 19:1503-13.

[11].Bidan CM, Kommareddy KP, Rumpler M, Kollmannsberger P, Fratzl P, Dunlop JW. Geometry as a factor for tissue growth: towards shape optimization of tissue engineering scaffolds. Adv Healthc Mater 2013; 2:186-94.

[12].Kilian KA, Bugarija B, Lahn BT, Mrksich M. Geometric cues for directing the differentiation of mesenchymal stem cells. Proc Natl Acad Sci U S A 2010; 107:4872-7.

[13].Saino E, Focarete ML, Gualandi C, Emanuele E, Cornaglia AI, Imbriani M, Visai L. Effect of electrospun fiber diameter and alignment on macrophage activation and secretion of proinflammatory cytokines and chemokines. Biomacromolecules 2011; 12:1900-11.

[14].Hollister SJ, Murphy WL. Scaffold translation: barriers between concept and clinic. Tissue Eng Part B Rev 2011; 17:459-74.

[15].Yoshida M, Langer R, Lendlein A, Lahann J. From advanced biomedical coatings to multi-functionalized biomaterials. Pol Rev 2006; 46:347-75.

[16].Kim JE, Lee EJ, Kim HE, Koh YH, Jang JH. The impact of immobilization of BMP-2 on PDO membrane for bone regeneration. J Biomed Mater Res A 2012; 100:1488-93.

[17].Miyagi Y, Chiu LL, Cimini M, Weisel RD, Radisic M, Li RK. Biodegradable collagen patch with covalently immobilized VEGF for myocardial repair. Biomaterials 2011; 32:1280-90.

[18].Chung HJ, Park TG. Surface engineered and drug releasing pre-fabricated scaffolds for tissue engineering. Adv Drug Deliv Rev 2007; 59:249-62.

[19].Navarro M, Ginebra MP, Clement J, Martinez S, Avila G, Planell JA. Physico-chemical degradation of resorbable phosphate glasses stabilized with TiO2. J Am Ceram Soc 2003; 86:1345-52.

[20].Navarro M, Ginebra MP, Planell JA. Cellular response to calcium phosphate glasses with controlled solubility. J Biomed Mater Res A 2003; 67:1009- 15.

[21].Navarro M, Engel E, Planell JA, Amaral I, Barbosa M, Ginebra MP. Surface characterization and cell response of a PLA/CaP glass biodegradable composite material. J Biomed Mater Res A 2008; 85:477- 86.

[22].Aguirre A, Gonz.lez A, Navarro M, Castaño O, Planell JA, Engel E. Control of microenvironmental cues with a smart biomaterial composite promotes endothelial progenitor cell angiogenesis. Eur Cell Mater 2012; 24:90-106, discussion 106.

[23].Vila OF, Bag. JR, Navarro M, Alieva M, Aguilar E, Engel E, Planell JA, Rubio N, Blanco J. Calcium phosphate glass improves angiogenesis capacity of poly(lactic acid) scaffolds and stimulates differentiation of adipose tissue-derived mesenchymal stromal cells to the endothelial lineage. J Biomed Mater Res A 2013; 101:932-41.

[24].Mouri.o V, Cattalini JP, Boccaccini AR. Metallic ions as therapeutic agents in tissue engineering scaffolds: an overview of their biological applications and strategies for new developments. J R Soc Interface 2012; 9:401-19.

[25].Martin RA, Yne S, Hanna JV, Lee PD, Newport RJ, Smith ME, Jones JR. Characterizing the hierarchical structures of bioactive sol-gel silicate glass and hybrid scaffolds for bone regeneration. Philos Transct A Math Phys Eng Sci 2012; 370:1422-43.

[26].Biggs MJP, Richards RG, McFarlane S, Wilkinson CDW, Oreffo ROC, Dalby MJ. Adhesion formation of primary human osteoblasts and the functional response of mesenchymal stem cells to 330nm deep microgrooves. J R Soc Interface 2008; 5:1231-42.

[27].Dalby MJ, Gadegaard N, Tare R, Andar A, Riehle MO, Herzyk P, Wilkinson CDW, Oreffo ROC. The control of human mesenchymal cell differentiation using nanoscale symmetry and disorder. Nat Mater 2007; 6:997-1003.

[28].McMurray RJ, Gadegaard N, Tsimbouri PM, Burgess KV, McNamara LE, Tare R, Murawski K, Kingham E, Oreffo ROC, Dalby MJ. Nanoscale surfaces for the long-term maintenance of mesenchymal stem cell phenotype and multipotency. Nat Mater 2011; 10:637-44.

[29].Fong EL, Lamhamedi-Cherradi SE, Burdett E, Ramamoorthy V, Lazar AJ, Kasper FK, Farach-Carson MC, Vishwamitra D, Demicco EG, Menegaz BA, et al. Modeling Ewing sarcoma tumors in vitro with 3D scaffolds. Proc Natl Acad Sci U S A 2013; 110:6500-5.

Publications

- **Serra T**, Navarro M, Planell JA. Fabrication and characterization of biodegradable composite scaffolds for Tissue Engineering. In *Innovative Developments in Virtual and Physical Prototyping. Proceedings of the 5th International Conference on Advanced Research in Virtual and Rapid Prototyping, Leiria, Portugal.* P 67–72. Taylor and Francis Group, London. **2012**

- **Serra T**, Planell JA, Navarro M. High-resolution PLA-based composite scaffolds via 3-D printing technology. Acta Biomater. **2013** Mar;9(3):5521-30.

- **Serra T**, Mateos MA, Planell JA, Navarro M. 3D printed PLA-based scaffolds: A versatile tool in regenerative medicine. Organogenesis. **2013** Aug 19;9(4).

- Almeida CR, **Serra T**, Oliveira MI, Planell JA, Barbosa MA, Navarro M. Impact of 3-D printed PLA- and chitosan-based scaffolds on human monocyte/macrophage responses: Unraveling the effect of 3-D structures on inflammation. Acta Biomater. **2014** Feb;10(2):613-22.

- **Serra T**, Ortiz M, Engel E, Planell JA, Navarro M. Relevance of PEG in PLA-based blends for Tissue Engineering 3D-printed scaffolds. Mater Sci Eng: C **2014**. May;38(1):55–62.

- PLA and PLA/CaP glass 3D scaffolds for Guided Bone Regeneration (GBR) devices: An *in vivo* study. *In preparation.*